GEOCHIMICA ET COSMOCHIMICA ACTA

UNIVERSITY OF HAWAII
LIBRARY
AUG 9 '57

JOURNAL OF THE GEOCHEMICAL SOCIETY

EDITORIAL ADVISORY BOARD

T. BARTH–OSLO · A. F. BUDDINGTON–PRINCETON, N.J. · L. CAPDECOMME–TOULOUSE
E. J. CONWAY–DUBLIN · P. ESKOLA–HELSINKI · P. GALLITELLI–MODENA
D. GUIMARÃES–BELO HORIZONTE · A. HADDING–LUND · O. HAHN–GÖTTINGEN
H. W. HARVEY–PLYMOUTH · F. HEIDE–JENA · A. HOLMES–EDINBURGH
G. E. HUTCHINSON–NEW HAVEN, CONN. · W. Q. KENNEDY–LEEDS · PH. H. KUENEN–GRONINGEN · S. LANDERGREN–STOCKHOLM · F. MACHATSCHKI–VIENNA
B. H. MASON–NEW YORK · A. MUIR–HARPENDEN · J. ORCEL–PARIS · E. RAGUIN–PARIS · K. RANKAMA–HELSINKI · E. REINHARD–BASLE · TH. G. SAHAMA–HELSINKI
C. E. TILLEY–CAMBRIDGE · T. VOGT–TRONDHEIM · W. WAHL–HELSINKI
T. WATANABE–TOKYO · F. WHIPPLE–CAMBRIDGE, MASS.
R. WILDT–NEW HAVEN, CONN.

EDITORS

L. H. AHRENS
CAPETOWN

C. W. CORRENS
GÖTTINGEN

E. INGERSON
WASHINGTON

S. R. NOCKOLDS
CAMBRIDGE

F. A. PANETH
MAINZ

H. C. UREY
CHICAGO

JOHN VERHOOGEN
BERKELEY, CALIF.

A. P. VINOGRADOV
MOSCOW

L. R. WAGER
OXFORD

F. E. WICKMAN
STOCKHOLM

VOLUME 11 No. 4

1957

PERGAMON PRESS LONDON · NEW YORK · PARIS

Geochim. et Cosmochim. Acta
QE 351
C 415

GEOCHIMICA ET COSMOCHIMICA ACTA

EDITORS

PROF. L. H. AHRENS, *Department of Chemistry, University of Capetown, Rondebosch, Cape Province, South Africa.*

PROF. C. W. CORRENS, *Sedimentpetrographisches Institut der Universitat, Lotzestr.* 13, *Göttingen, Germany.*

DR. E. INGERSON, *Geochemistry and Petrology Branch, U.S. Geological Survey, Washington* 25, *D.C., U.S.A.*

DR. S. R. NOCKOLDS, *Department of Mineralogy and Petrology, The University, Cambridge, England.*

PROF. F. A. PANETH, F.R.S., *Max-Planck-Institut für Chemie, Mainz, Saarstrasse* 23, *Germany.*

PROF. H. C. UREY, For. Mem. R.S., *The Enrico Fermi Institute for Nuclear Studies, University of Chicago, Illinois, U.S.A.*

DR. JOHN VERHOOGEN, *Department of Geology, University of California, Berkeley, California, U.S.A.*

PROF. A. P. VINOGRADOV, *The Academy of Sciences of the U.S.S.R., Moscow, U.S.S.R.*

PROF. L. R. WAGER, F.R.S., *Department of Geology and Mineralogy, The University, Oxford, England.*

PROF. F. E. WICKMAN, *Naturhistoriska Riksmuseets, Mineralogiska Avdelning, Stockholm* 50, *Sweden.*

VOLUME 11, No. 4 1957

CONTENTS

PAGE

L. H. AHRENS: Lognormal-type distributions—III 205

R. D. RUSSELL and L. H. AHRENS: Additional regularities among discordant lead-uranium ages 213

HERBERT L. VOLCHOK and J. LAURANCE KULP: The ionium method of age determination 219

ROBERT A. CHALMERS and E. S. PAGE: The reporting of chemical analyses of silicate rocks 247

E. L. FIREMAN and D. SCHWARZER: Measurement of Li^6, He^3, and H^3 in meteorites and its relation to cosmic radiation 252

JOHN F. LOVERING, WALTER NICHIPORUK, ARTHUR CHODOS, and HARRISON BROWN: The distribution of gallium, germanium, cobalt, chromium, and copper in iron and stony-iron meteorites in relation to nickel content and structure 263

HEINZ DEGENHARDT: Untersuchungen zur geochemischen Verteilung des Zirkoniums in der Lithosphäre 279

JULIAN R. GOLDSMITH and DONALD L. GRAF: The system CaO—MnO—CO_2: Solid-solution and decomposition relations 310

THOMAS W. STORM and HEINRICH D. HOLLAND: The distribution of nickel in the Lambertville diabase 335

Books received 348

Publishing Offices: Pergamon Press Ltd., 4 & 5 Fitzroy Square, London W.1. (EUS 4455)

Subscription per volume (including postage) (A) £6 (U.S.A. $17.00); (B) For individual subscribers certifying that the journal is for their private use, £3 10s. (U.S.A. $9.80). Members of the Geochemical Society are entitled to purchase the Journal at the rate of $10.00 *per annum.*

Back numbers, £7 ($19.60) per volume

Distributors: I. R. Maxwell & Co., Ltd., 4 & 5 Fitzroy Square, London W.1
and Pergamon Press, Inc., 122 East 55th Street, New York 22, N.Y.

PERGAMON PRESS

4 & 5 FITZROY SQUARE, LONDON W.1 122 EAST 55TH STREET, NEW YORK 22, N.Y.

24 RUE DES ÉCOLES, PARIS Ve

PRINTED IN NORTHERN IRELAND AT THE UNIVERSITIES PRESS, BELFAST

Geochimica et Cosmochimica Acta, 1957, Vol. 11, pp. 205 to 212. Pergamon Press Ltd., London

Lognormal-type distributions—III

L. H. Ahrens
Department of Chemistry, University of Cape Town

(*Received* 2 *August* 1956)

Abstract—Aspects of recent papers by Miller and Goldberg, and by Aubrey, are discussed, and further examples of lognormal-type distributions are given. There is now a large body of evidence to show that lognormal-type distributions are very common indeed.

Attention is drawn to extreme positive skewness in a histogram of grain-size distribution of pyroxene from the Merensky Reef, Bushveld Igneous Complex.

Introduction

Two recent papers (Miller and Goldberg, 1955; Aubrey, 1956) discuss frequency distributions of elements in specific geological materials. Both criticize the general conclusion of lognormality arrived at by Ahrens (1954a) in his first paper on lognormal distributions, but neither discusses the second (Ahrens, 1954b)—apart from reference—which was written partly in a response to a criticism by Chayes (1954) so as to set out more clearly the meaning and purpose of the so-called lognormal "law." The second paper also gave further examples of distributions approaching lognormality and discussed other aspects of the application of statistics to geochemistry. The present paper is written partly as a reply to some of the criticisms in the papers of Miller and Goldberg, and Aubrey, and partly to provide further examples of lognormal-type distributions. In the discussions which follow we consider first aspects of Edwards and Goldberg's paper and, after examining some new examples of frequency distribution discuss aspects of Aubrey's paper.

Discussion

(1) *Aspects of the Paper by Miller and Goldberg*

Miller and Goldberg tested the analytical data used by Ahrens (1954a) and also some on meteorites and sediments. Concerning Ahrens' general observation about lognormality, they conclude that, though some of the observations could be lognormal, others could not (their Table 1). At the same time (p. 58), but unfortunately as a footnote only, they make an important statement;

> "In fact, it should be made clear that great difficulties are involved in showing that any set of empirical data is *precisely* described by a specific function. Thus the search for specific functions to describe universes in nature seems fruitless. On the other hand, if a universe is approximately described by a particular function, statements of prediction and comparison can be made. Herein lies the usefulness of such investigations!"

The italics and exclamation mark are Miller and Goldberg's and give correct emphasis; their statement may be compared with that given by Ahrens (1954b,

pp. 124–125) but which appeared after Miller and Goldberg had written their paper:

> "We seek to find a distribution which fits the various sets of observation (several elements) reasonably well and which may therefore be used for the geochemical purpose of comparison and prediction. The lognormal distribution fits all sets of observations examined thus far reasonably well, and this conclusion has been expressed in the form of a geochemical law; but in so doing, it is not meant to imply that exact fit is to be expected in any particular case, that some other distribution might sometimes show slightly better fit, or that on very rare occasions a really serious exception will be found."

With very few slight exceptions, all observations considered so far (Ahrens, 1954a and b), together with those to be considered, are approximately described by a lognormal distribution, and accordingly, for the purpose of comparison and prediction, overall lognormality may be assumed. The same certainly could not be said of an overall assumption of normality, even if we stretch the term "approximate".

We may now consider further data on the distribution of the concentration of elements in specific geological materials. The fresh data will, where possible, be presented in the form of frequency-distribution diagrams. As before (Ahrens, 1954a, b), their shape will be used as the main guide as to whether the observations approximate closely or not to either a normal or a lognormal distribution. A more rigorous test of whether the observations conform *precisely* or not to one of these distributions will not be attempted, for reasons given before (Ahrens, 1954b); see also the first two sentences in Miller and Goldberg's statement above.

(2) *Further Examples of Distributions Approaching Lognormality*

(a) *Phosphorus in igneous rocks*

Goldschmidt (1954, pp. 457–458) refers to the frequency distribution of phosphorous in different igneous rocks; basalt, andesite, rhyolite, gabbro, diorite, syenite, and granite. The number of observations ranges from 83 for rhyolite to 342 in basalt. All histograms are reported as very asymmetric and positively skewed, and accordingly the arithmetic mean (abundance) in each of the seven rock types is usually found to be far greater than the mode, the most frequent concentration. The ratio of arithmetic mean to mode in six of the seven types is from about ~2–3; in one (granite) it is 1·2. (For discussion of the relationship between the ratio arithmetic mean/geometric mean and dispersion in lognormal distributions, see Ahrens, 1954a, b). The original data are unfortunately not available for detailed examination, but, provided analytical error (see below) is not excessive, they lead to the firm conclusion of +ve skewness in each example, and distributions presumably approach lognormality.

In the Fairbairn *et al.* study on the accuracy of conventional methods of chemical analysis, the relative deviation for phosphorus is given as 39% and 33% respectively for granite G-1 and diabase W-1 (Fairbairn, 1953). This is

quite an appreciable error and may in fact amount to a third or so—occasionally possibly more—of the spread reported by GOLDSCHMIDT (see his Table LXXIV), where relative deviations usually lie between 70% and 105%. Nevertheless, as the observed dispersion is quite considerably greater than what seems to be a fair estimate of analytical error, we may assume that the histograms do reflect reasonably well the actual distribution of phosphorus in these igneous-rock types.

It is of interest to note that GOLDSCHMIDT (1954, p. 458) raises the question as to which quantity should be used, arithmetic mean or median, when comparing the phosphorus content of various rock types (see also AHRENS, 1954c). On the same page it is also stated that the high phosphorus values in the asymmetric histogram may be regarded as anomalies; this is not so, as these high values are found in almost every example of large dispersion examined so far, and are merely confirming evidence that distribution is not approximately normal but of a positively skewed lognormal or related type.

(b) *Molybdenum in basalt + diabase, and in gabbros and ultramafics*

The distribution of Mo in granite (KURODA and SANDELL, 1954) has been discussed (AHRENS, 1954a) and is considered a good example of a lognormal-type distribution (see Fig. 16 of that paper). Here we consider the distribution of Mo in other igneous rocks and again use the data of KURODA and SANDELL. Eighty-four specimens of basalt + diabase have been analysed, and Fig.1(a) shows a distribution curve similar to that shown by KURODA and SANDELL. Extreme positive skewness is again evident. The distribution of Mo becomes fairly symmetrical and bell-shaped when a geometric interval is used (Fig. 2a). A fitted curve has been drawn. We note that the distribution is not perfect, and particularly a deficiency in the 0·2–0·4-p.p.m. interval and an excess in the 0·4–0·8-p.p.m. interval is apparent. Such irregularity is not regarded as serious when taking into consideration the problem of sampling and the possibility of significant analytical error (values given by KURODA and SANDELL are to within 0·1 p.p.m. Mo, which at, say, 0·1–0·4 p.p.m. is a large tolerance); fit is quite good and, for the geochemical purposes outlined before, a lognormal distribution may be assumed.

A much smaller number of observations is available for gabbros and ultramafics, but the data are quite sufficient to indicate that distribution is markedly positively skew in both rock types (see Fig. 1 of KURODA and SANDELL).

(c) *Arsenic in igneous rocks*

ONISHI and SANDELL (1955) have determined As in a large number of igneous rocks. Inspection of their frequency-distribution diagrams (see their Fig. 1) shows that decided positive skewness is present in each type except volcanic glass + felsite and rhyolite, which were considered as one group. By far the largest number of observations were made on granite and basalt + diabase and the distribution of As in these two types will be considered further. Part of their Fig. 1 (granitic rocks and basalts + diabase) is redrawn here as Figs. 1(b) and 1(c), together with two histograms using a geometric interval (Figs. 2b and 2c). In each of these two examples, extreme positive skewness has been strongly

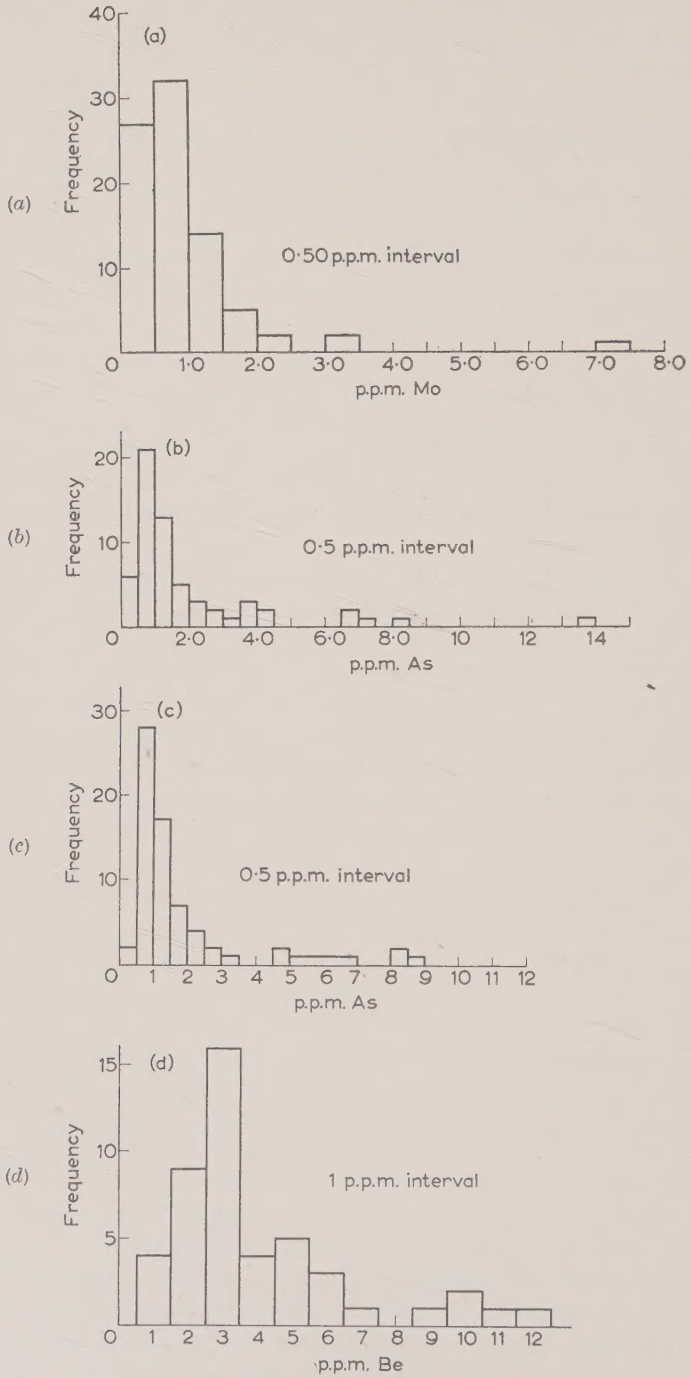

Fig. 1. Frequency distribution diagrams of (*a*) Mo in 84 specimens of basalt + diabase (data of KURODA and SANDELL, 1954), (*b*) as in 57 specimens of granite (data of ONISHI and SANDELL, 1955), (*c*) as in 67 specimens of basalt and diabase (data of ONISHI and SANDELL, 1955), and (*d*) of Be in granitic rocks (data of HAMAGUCHI, KURODA and GORAI, 1955). Positive skewness is well developed in each example. Compare with Fig. 2.

reduced by the use of a geometric interval. A slight positive skewness remains, however; in As in granite, a comparison of the fitted curve with the observed distribution shows this tendency as very slight indeed, but it is somewhat greater in the distribution curve of As in basalt + diabase. In this example a fitted curve has not been drawn. Although the one example in particular shows some distinct departure from lognormality, prediction and comparison of dispersion on the basis of assumed lognormality would not be seriously in error. Gross distortion would, however, result if normality were to be assumed, leading in these two examples, as in many others, to predictions of negative concentrations of elements in granite and in basalt + diabase.

Onishi and Sandell (1955) have discussed the occasional strong enrichment of arsenic in igneous rocks. They draw attention to the presence of secondary sulphide,* as in the specimen from Cook County (their Table 5), and suggest secondary mineralization as a cause for high As enrichment. This may be the reason for the presence of some skewness in Figs. 2 and 3 and illustrates a typical difficulty which is encountered when examining the distribution of an element in a specific geological material.

(d) *Beryllium and boron in Japanese granites*

Hamaguchi, Kuroda, and Gorai (1955) have determined Be in forty-six Japanese rocks which they describe as intrusive-type granitic rocks. Their histogram, copied here as Fig. 1(d) shows decided positive skewness; this may be compared with Fig. 2(d), in which a geometric interval has been used. The curve as drawn fits the observed distribution reasonably well and, for the purpose of prediction and comparison, a lognormal distribution may be assumed.

The distribution of boron in Japanese intrusive granitic rocks is also positively skewed (see Hamaguchi, Kuroda, and Goria, 1955). The boron concentration is, however, below the detection limit in eight specimens, and this example will not be examined in detail.

(e) *Fluorine in Japanese igneous rocks*

One example of a positively skewed lognormal-type distribution given in the first paper (Ahrens, 1954a) was that of fluorine in granite (Canadian and New England). Kokubu (1956) has determined fluorine in Japanese igneous rocks and draws attention to the asymmetry (positively skewed) of the distribution of fluorine in ninety-nine rocks grouped under "volcanic rocks" (his Fig. 1). The arithmetic mean is almost twice the most frequent concentration.

(3) *Aspects of the Paper by Aubrey*

Aubrey (1956) raises the question of a negatively skewed distribution. He shows theoretically, considering first a two-component system and then a system with more components, that if the distribution of concentration of one or more of the major components is positively skewed, the distribution of the others will be negatively skewed. Further, that there will be minor elements associated

* As was low in magmatic sulphides.

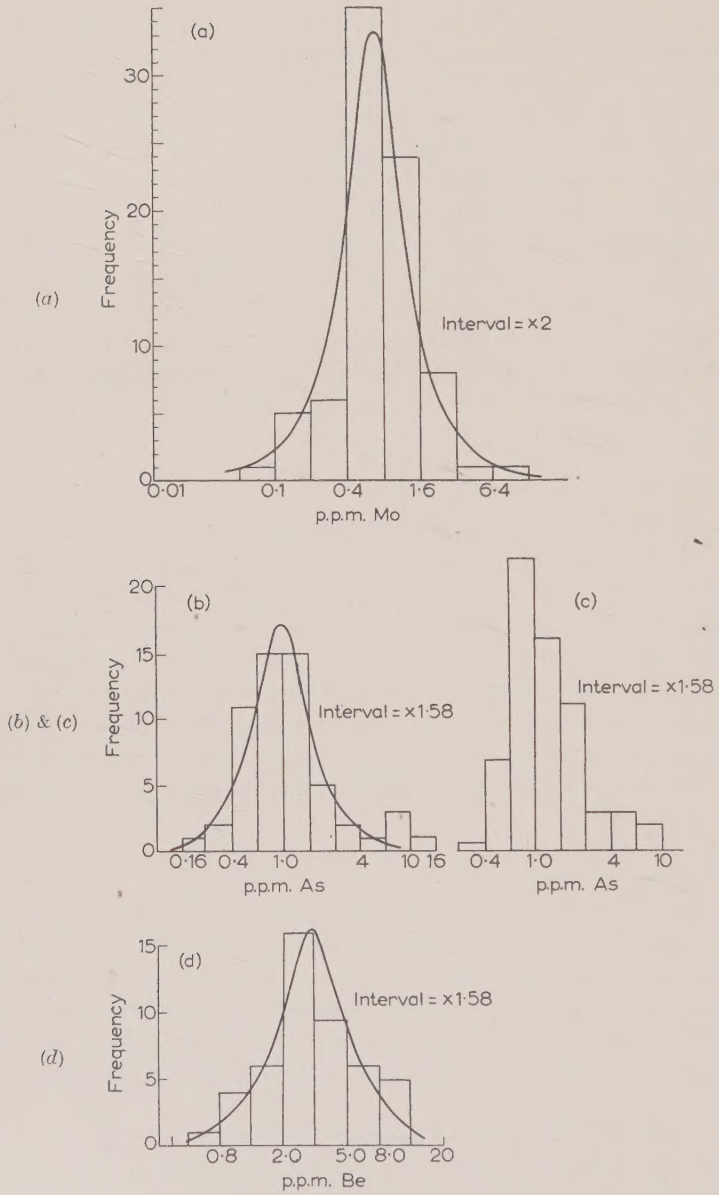

Fig. 2. Frequency distribution diagrams as in Fig. 1, but using a geometric interval. The power factor is indicated in each case. [(*a*) = Mo in granite; (*b*) = As in granite; (*c*) = As in basalt + diabase; and (*d*) = Be in granite.]

with the negatively skewed major elements and hence departure from a positively skewed lognormal-type distribution will not be rare.

Distinct evidence of this interesting predicted possibility has yet to be found. *Slight* tendencies of negative skewness have been pointed out by AUBREY (1956) in the distribution curves of Sc (*d*), K (gr), Rb (gr), and Co (*d*) given by AHRENS (1954a). Dispersion in these examples is very small and, unfortunately therefore,

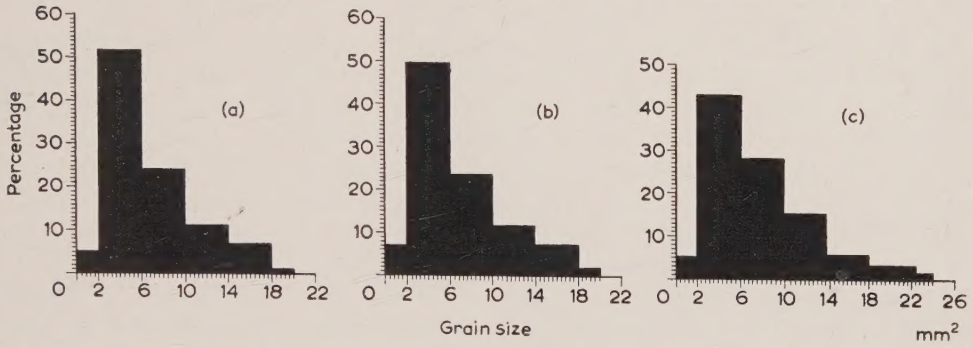

Fig. 3. Frequency distribution diagrams of grain size of orthopyroxenes from three localities in the Merensky Reef (Bushveld Igneous Complex). After SCHMIDT (1952).

analytical error makes a fairly significant contribution to the total spread of observations. (This possibility was not discussed earlier (AHRENS 1954a and b, because main emphasis was on the elements with moderate to large dispersion; for those with small dispersion, it matters little as a rule, for the purpose of comparison and prediction, whether distribution is assumed to be normal or lognormal.) This does not, however, rule out the possibility that the distributions of Sc, K, Rb, and Co are slightly negatively skewed, as pointed out by AUBREY, but significant analytical error introduces a complicating factor; compare with the example of phosphorus above. If the theoretical considerations of AUBREY do apply to natural environments, it is not clear why distinct examples of negative skewness have not yet been found. The possible examples of Sc and Co may provide a clue as to where negatively skewed examples might be found. These two elements, together with Ni, are usually associated with Fe and Mg in ferromagnesian minerals, and the distribution of Fe, Mg, and Ni in a selected suite of diabases and related rocks may be instructive. For further discussion in this respect, see AUBREY (1956).

The fresh data given in the present paper, together with that given before, provides a large body of evidence that positively skewed lognormal-type distributions are very common indeed, and leads to the conclusion that, if examples of distinct negative skewness are found, their proportion is likely to be small.

(4) *Note on Grain Size of Orthopyroxenes from the Merensky Reef, Bushveld Complex*

Related to the general problem of the statistical nature of the distribution of concentration of an element in specific igneous rocks and minerals, is that of the statistical nature of crystal grain-size distribution of minerals in igneous

rocks. It is not the purpose here to consider this problem in detail, but merely to draw attention to one example of an exhaustive study of grain-size distribution of a mineral from igneous rocks. Whereas grain-size distribution in sediments has been studied extensively for some time, the writer is not aware of exhaustive studies of grain-size distribution of minerals in igneous rocks except for the example discussed briefly here.

Schmidt (1954) has examined grain-size distribution of orthopyroxene crystals from the Merensky Reef. Measurements were made in c″ section, in which Schmidt points out grain size is larger and far more equidimensional than in a″ and b″ sections. Fig. 6 shows histograms (after Schmidt, 1954) of pyroxene grain size (in mm^2) from three localities; for details see original paper. In each example, distribution is decidedly positively skewed and regular, with the result that average grain size is much larger than the most frequent grain size. A fairly large number of measurements have been made (200 to 300 grains), but unfortunately the original measurements are not available to test whether the distributions approach lognormality *very* closely. The distribution of grain elongation is also positively skewed (see Schmidt, 1954); this observation may be compared with that of Wyatt (1954), who found that the distribution of grain-size elongation of zircon from Moine granite and porphyritic aplite was also positively skewed.

References

Ahrens L. H. (1954a) *Geochim Cosmochim. Acta* **5,** 49.
Ahrens L. H. (1954b) *Geochim. Cosmochim. Acta* **6,** 121.
Ahrens L. H. (1954c) *Geochim. Cosmochim. Acta* **6,** 155 (Book review).
Aubrey K. V. (1956) *Geochim. Cosmochim. Acta* **9,** 83.
Chayes F. (1954) *Geochim. Cosmochim. Acta* **6,** 119.
Fairbairn H. W. (1953) *Geochim. Cosmochim. Acta* **4,** 143.
Goldschmidt V. M. (1954) *Geochemistry* Oxford University Press.
Hamaguchi H., Kuroda R., and Gorai M. (1955) *J. Chem. Soc. Japan* **76,** 919.
Kuroda P.K. and Sandell E. B. (1954) *Geochim. Cosmochim. Acta* **6,** 35.
Onishi H. and Sandell E. B. (1955) *Geochim. Cosmochim. Acta* **7,** 1.
Miller R. L. and Goldberg E. D. (1955) *Geochim. Cosmochim. Acta* **8,** 53.
Schmidt E. R. (1952) *Trans. Geol. Soc. S. Afr.* **LV,** 233.
Wyatt M. (1954) *American Mineral* **39,** 983.

Geochimica et Cosmochimica Acta, 1957, Vol. 11, pp. 213 to 218. Pergamon Press Ltd., London

Additional regularities among discordant lead-uranium ages

R. D. Russell* and L. H. Ahrens†

(*Received* 20 *July* 1956)

Abstract—The ratios N_{206}/N_{238} and N_{207}/N_{235} are linearly related in twelve samples of pitchblende from the west ore body of the Ace Mine, Goldfields, Saskatchewan. A similar relationship has been noted before (Ahrens, 1955b) in monazites and uraninites mainly from southern Africa. Wetherill (1956a and b) has shown that such linearity could be explained by a chemical removal of lead from the mineral at some single time subsequent to its formation. It is pointed out that such an explanation leads to an apparent relationship between the time of chemical removal of lead and the age of the mineral. There appears to be a preferential deficiency (9%) of Pb^{207} over Pb^{206} in specimens participating in the linear relationships. This suggests physical control of lead escape rather than chemical. One possible process involves recoil of atoms following alpha-particle emission. Whatever the correct explanation, we find a convergent age of 1800 m.y. for the west ore body of the Ace Mine.

Two earlier papers (Ahrens 1955a and b) showed the presence of well developed regularities in some Pre-Cambrian lead age data. Probably the most significant relationship was that between N_{207}/N_{235} and N_{206}/N_{238} which was found to be linear in three Rhodesian monazites. In addition, the corresponding ratios for

Table 1. Pitchblendes from Ace Mine, Saskatchewan.
(Representing samples taken across a single ore body.)

Toronto number	Chemical analysis		Isotopic analysis				Age		
	%Pb	%U	$\%Pb^{204}$	$\%Pb^{206}$	$\%Pb^{207}$	$\%Pb^{208}$	206/238	207/235	207/206
348	3·18	16·5	0·055	87·90	9·89	2·15	1140	1350	1710
349	9·70	40·3	0·014	89·50	9·87	0·60	1430	1580	1790
352	1·04	11·0	0·089	86·64	9·99	3·29	590	830	1630
354	6·80	33·8	0·03	89·55	9·43	0·99	1210	1380	1660
355	5·87	30·1	0·034	89·53	9·73	0·70	1180	1370	1700

monazite from Antsirabe, Madagascar and uraninite from Manitoba appeared to fit the same straight line, whereas ratios for seven uraninite concentrates from Witwatersrand and related sediments showed a less perfect fit to a second line of smaller slope. Neither of these lines passes through the origin ($N_{207}/N_{235} = N_{207}/N_{238} = 0$) and therefore cannot be explained by errors in chemical analysis.

A suite of five pitchblende samples from the west ore body of the Ace Mine, Saskatchewan, has since been analysed (Table 1). Uranium and lead were determined by Dr S. C. Robinson and R. Trail of the Geological Survey of Canada, using an X-ray fluorescent method; Dr R. M. Farquhar carried out the isotope

* Department of Physics, University of Toronto.
† Department of Geology and Mineralogy, Oxford University. Now at Department of Chemistry, University of Cape Town.

analyses at the University of Toronto. Fig. 1 relates N_{207}/N_{235} to N_{206}/N_{238} and again the relationship is linear and cannot be ascribed to analytical error. Fig. 2 shows the relationship of this line to the others already published (Ahrens, 1955b). On Fig. 1 we have also plotted ratios calculated from analyses reported by Eckelman and Kulp (1956) for other samples from the west ore body of the Ace Mine. These ratios also fit the same straight line that was found for the Ottawa-Toronto analyses.

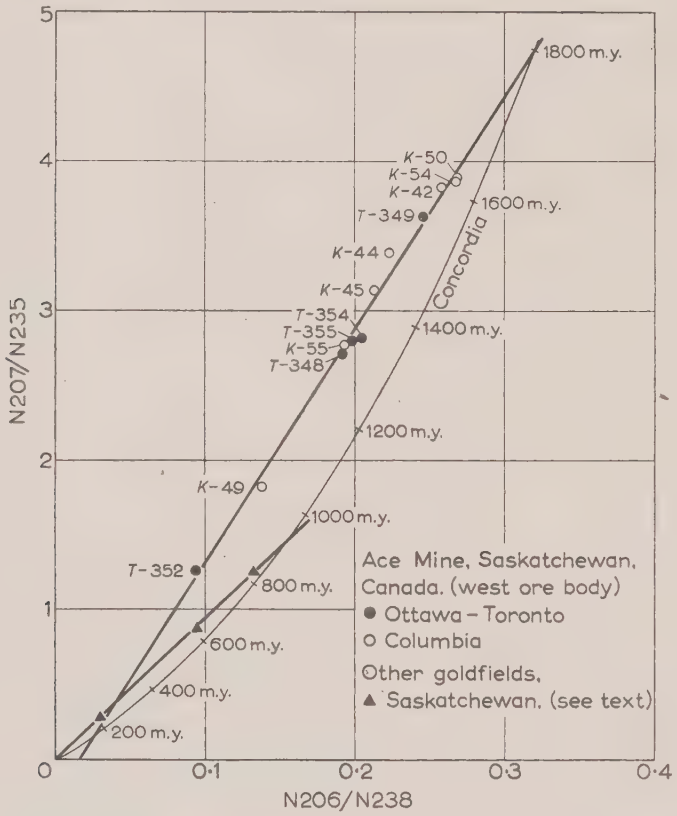

Fig. 1. Parent-daughter isotope relationships of pitchblendes from the west ore body of the Ace Mine, Goldfields, Saskatchewan, Canada.

Wetherill (1956a and b) has been able to show that such linear relationships would result if minerals of given age were to lose some proportion of their lead at some single episode during their history. The rigorous mathematical proof of this theorem given by Wetherill (1956b) is long and complex, but the result can easily be shown to be true. If a curve "concordia" be drawn on a N_{207}/N_{235} vs N_{206}/N_{238} plot so that it relates pairs of ratios yielding identical ages, any sample which has retained all the lead will have ratios lying on that curve. Analytical errors or very recent removal of Pb (or U) from the mineral would displace the point from concordia along a straight line to (or away from) the origin, provided that significant fractionation of lead or uranium isotopes does

not occur. If this same graph had been plotted in the past, the origin would be moved backward along concordia to the point corresponding to that time. Removal of Pb (or U) at that time would then displace a point representing an "unaltered"* sample along a line to the new origin. Thus the removal of lead at time T_1 from a sample of true age T_0, must be represented by a point on the straight line through the points T_1 and T_0 on concordia. Similarly any sample represented by a point not on concordia (and therefore already deficient

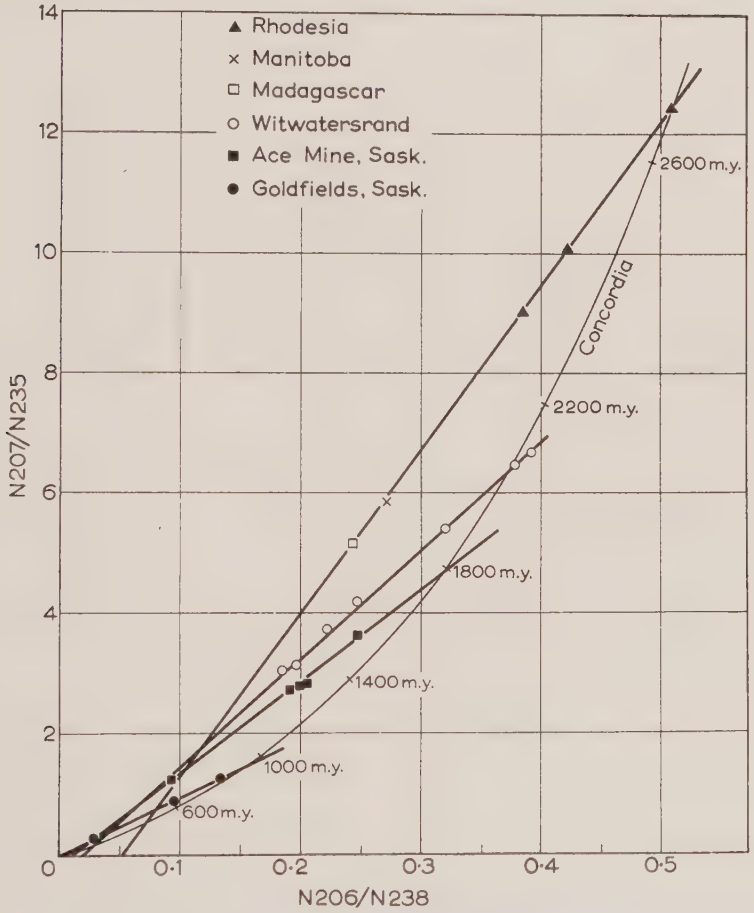

Fig. 2. A comparison of the regularities noted for the Saskatchewan pitchblendes with those previously described by Ahrens (1955b) for very old uraninites and monazites.

in lead or uranium) gives, as the result of subsequent further loss of lead at T_1, a point along the line to T_1 on concordia.

This theorem at first seems to provide an immediate explanation to the relationships shown in Fig. 2. Thus, interpreting these straight lines as indicating a single episode of lead removal, we find for the Rhodesia group (three Rhodesian

* In this paper we use the word "unaltered" to describe any sample having concordant lead-uranium ages, *not* in any other mineralogical sense.

monazites, one Madagascan monazite, and one Manitoban uraninite), selected Witwatersrand concentrates and Saskatchewan pitchblendes, ages ($\times 10^6$ years) of 2680, 2040, and 1800 respectively with corresponding times (also $\times 10^6$ years) of lead removal of 500, 300, and 150.

While at first glance this seems a straightforward and reasonable explanation for these discordant lead-uranium ages, a closer inspection reveals several remarkable coincidences. In the first place, it seems extraordinary that the minerals

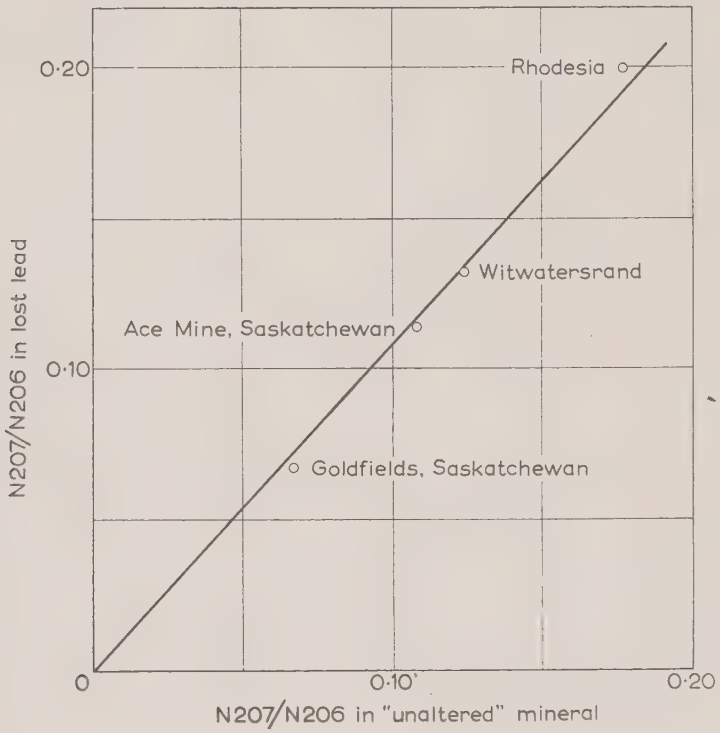

Fig. 3. A plot of the lead isotope ratios in the lead apparently deficient against that calculated for the "unaltered" mineral, showing lead-207 to be deficient approximately nine per cent in excess of the lead-206 deficiency.

have existed thousands of millions of years without losing lead, only to be grossly altered and lose a proportion of their lead a few hundred million years ago. Chemical alteration would seem much more reasonable if such a process had taken place very recently, as it could then perhaps be caused by surface weathering. The coincidence becomes very much more remarkable when it is noted that there is apparently a direct correlation between the age of the mineral and the time at which it apparently lost its lead.

Fig. 3 relates, as ordinate, N_{207}/N_{206} in lead which has been lost from a mineral to the value of this ratio in the lead from a mineral of the same age which, however, has retained all its lead. (The ordinate values come from the slopes of the straight lines in Fig. 2 and the abscissal values from the intercepts of these straight lines with concordia.)

Though not ideal, the regularity is at least closely linear and suggests that the lead removed from minerals is enriched some 9% in Pb^{207} over that which should be present in the unaltered minerals, regardless of their age. It will be recalled that for participants of the Rhodesia age pattern AHRENS (1955b) has shown that the deficiency of Pb^{207} was greater than that of Pb^{206}, despite the fact that $t(207/235) > t(206/238)$.

In an attempt to extend our investigation to even younger minerals, we have plotted on Figs. 1, 2, and 3 data from COLLINS *et al.* (1954) for three samples from the Goldfields region in Saskatchewan. It is well known that the pitchblendes from the Goldfields represent more than a single generation so that their relationships may be complex and we do not consider these points as valuable as the others. However the measured ratios N_{207}/N_{235} and N_{206}/N_{238} again show an excellent linearity, and the slope with the calculated lead ratios for the "unaltered" mineral gives a point that fits fairly well the line on Fig. 3. Thus we find the observed relationships to hold for minerals 940 m.y., 1800 m.y., 2040 m.y. and 2680 m.y. and having indicated ages from 190 m.y. to 2700 m.y.

If these regularities are real and do not represent a series of coincidences, they cannot easily be explained by ordinary chemical extraction of lead from the mineral. A relationship between the time of lead removal and the age of the mineral seems highly improbable and there seems to be no process that would alter each mineral chemically in very *recent times* and provide a 9% fractionation of the lead isotopes. Therefore we consider these additional data to support a previous suggestion (AHRENS, 1955b) that some distinctly physical process, rather than chemical, is involved in the apparent deficiency of lead.

One possible nuclear process is the ejection of members of the decay series into microfissures by the recoil energy from alpha-particle emission, followed by the removal of these members or their descendents by diffusion, leaching or any other process. The loss in each series would be roughly proportional to the sum of the recoil distances of the products concerned. If the recoil distance of the recoiling atom is proportional to the alpha particle range (i.e. proportional to the cube of the recoil velocity), it is easily calculated that a partial loss by recoil of all members immediately following an alpha decay results in loss of lead enriched in Pb^{207} by 4%. If only the recoil of the gaseous emanations is important, the enrichment would be 11%, and if only those members above the emanations are lost when they decay to the emanations, the enrichment would be 30%. Thus the loss of intermediate products by recoil following alpha decay provides a possible mechanism for the loss of lead which would fractionate the lead isotopes in the direction indicated by Fig. 3. It would also account for the radon which has been observed escaping from radioactive minerals.

We do not suggest that this is the only possible mechanism for discordance, or that all discordant ages are caused by a single process. There are cases in which uranium has apparently been leached from the minerals, and in which thorium lead has been selectively removed; a few minerals have clearly been involved in more than one period of mineralization. We also do not exclude the possibility that the N_{207}/N_{235} vs. N_{206}/N_{238} regularities could have been caused by some wholly unforeseen process. However, in those cases in which discordant ages

suggest a simple lead deficiency, the process responsible may be primarily physical, rather than chemical, and may be rather more regular than is often supposed. Until more detailed studies of single deposits have been made, it will be impossible to say whether Wetherill's explanation or a mechanism such as is suggested here is more nearly correct.

Acknowledgements—One of us (R. D. R.) wishes to acknowledge receipt of a grant from the Alfred P. Sloan Foundation Inc., part of which made possible a visit to Oxford University.

References

Ahrens L. H. (1955a) The convergent lead ages of the oldest monazites, and uraninites. *Geochim. et Cosmochim. Acta* **1,** 294–300.

Ahrens L. H. (1955b) Implications of the Rhodesian age pattern. *Geochim. et Cosmochim. Acta* **8,** 1–15.

Collins C. B., Farquhar R. M., and Russell R. D. (1954) The isotopic constitution of radiogenic leads and the measurement of geological time. *Bull. Geol. Soc. Amer.* **65,** 1–22.

Eckelman W. R. and Kulp J. L. (1956) Uranium lead method of age determination. Part I: Lake Athabasca problem. *Bull. Geol. Soc. Amer.* **67,** 35–55.

Wetherill G. W. (1956a) An interpretation of the Rhodesian and Witwatersrand age patterns. *Geochim. et Cosmochim. Acta* **9,** 290–292.

Wetherill G. W. (1956b) Discordant uranium-lead ages—I. *Trans. Amer. Geophys. Un.* (In press).

Geochimica et Cosmochimica Acta, 1957, Vol. 11, pp. 219 to 246. Pergamon Press Ltd., London

The ionium method of age determination*

Herbert L. Volchok† and J. Laurance Kulp
Lamont Geological Observatory, Columbia University, Palisades, New York

(*Received* 28 *September* 1955, *in final form* 11 *June* 1956)

Abstract—The ionium method of age determination, potentially applicable to deep sea sediments over the past 400,000 years, has been studied in an attempt to define its validity and limitations. In order for the method to apply, a chronologically undisturbed sediment column must be present and the sediment must be homogeneous with regard to chemisorption potential. The experimental techniques which were employed on a number of deep-ocean cores from the Atlantic and Pacific Oceans and the Caribbean Sea included total radium and gas-phase radon measurement with a low-level ionization chamber, total alpha emission by scintillation counting and absolute surface area determination by gas adsorption.

A complete age analysis was carried out on two cases: one, a red-clay core from the Pacific and the other, a globigerina-ooze core from the Caribbean. This analysis shows the sources of error. For those cores that meet the geological requirements, the accuracy of the dates is largely dependent on the accuracy of the radium determination and the frequency with which the samples are taken along the core.

From these two cores rates of sedimentation can be calculated with fair precision. From 200,000–300,000 years ago until 30,000–40,000 the rates of sedimentation were apparently constant for the red clay at one locality at $0{\cdot}15 \pm 0{\cdot}05$ cm/1000 years and for the globigerina ooze at another locality at $0{\cdot}60 \pm 0{\cdot}20$ cm/1000 years. At the close of the Wisconsin the rates of sedimentation for both sediment types increased by factors of 2–4.

The ionium method holds some promise as a dating technique for restricted areas of the deep ocean floor. Determination of ages in one core by the independent ionium and carbon-14 methods exhibited satisfactory agreement.

Introduction

In theory, the ionium method of age determination based on the inequilibrium relationships of the radioelements of the uranium-235 series is applicable to deep-sea sediments in the time span from the present to about 300,000 years ago. Unlike some of the other available dating methods which measure the ratio of final products to the long-lived parent in equilibrium decay, this method depends upon the decay of ionium to equilibrium with its parent. Such a quantitative dating method specifically applicable to oceanic sediments over the last one-half million years could do a great deal to clarify several important geological problems such as the exact time for the subdivisions of the Pleistocene period, the time for a continental glacier to grow and decay, and the rate of sediment accumulation in the ocean basins.

Historical development

Since early in this century it has been known that certain deep-sea sediments near the surface of the ocean floor contain abnormally high concentrations of radium.

Joly (1908) suggested direct precipitation of radium or a radium compound from ocean water unsupported by any of its long-lived parent radioelements.

* Lamont Geological Observatory Contribution No. 217. This research was supported by the Office of Naval Research.

† The research described in this paper was submitted in partial fulfillment of the requirements for the Ph.D. degree in the Faculty of Pure Science at Columbia University. Present address: Isotopes Inc., Westwood, N.J.

This seemed unlikely because of the relatively short half-life of radium. In later studies the high-radium concentrations were explained as being uranium supported; that is, that the uranium series are in radioactive equilibrium (Joly, 1908a; Piggot, 1933). For this explanation to be valid, however, uranium concentrations in deep-sea sediments would have to be higher than those observed by approximately a factor of 100. Further, on this hypothesis, it would be expected that the radium content would remain essentially constant at the high value through much greater depths than the 50 to 200 centimetres observed, since the uranium half-life is so large (about 5×10^9 years).

H. Petterson (1930, 1938, 1953) studied the radium and uranium concentrations of ocean-water samples and found that the relative concentrations of the two elements in sea water are far from being in radioactive equilibrium. On comparing the relative concentrations of thorium in continental rocks and sea water, Pettersson found it to be greatly depleted in the ocean (i.e. 3 : 1 in rocks to 0·01 : 1 for sea water, Koczy, 1949). On the basis of these data, Pettersson suggested that an ocean-wide precipitation of the mother isotope of radium (ionium, Th 230; half-life 83,000 years) was the significant cause of radium enrichment in the deep-sea sediments.

C. S. Piggot and W. D. Urry studied the radium concentration of deep-ocean sediments from several cores and observed a characteristic behaviour with depth (Piggot and Urry, 1939, 1941, 1942; Urry and Piggot, 1942). If radium concentration is plotted against depth, the curve (Fig. 2) ideally showed a peak in radium content a short distance below the top of the core which smoothly diminished with depth. On the basis of these data they proposed the age-determination method based on the relative concentrations of uranium, ionium and radium in deep-ocean cores. (Piggot and Urry, 1942a; Urry, 1942, 1948, 1948a, 1949).

Holland and Kulp (1954) studied the mechanism of removal of ionium and radium from ocean water. Using short-lived radioisotopes of thorium and radium, they showed that base exchange plays an important rôle in the removal of ionium and radium from ocean waters on the surface of deep-ocean sediments. In the concentration of the elements existing in sea water, ionium was selectively adsorbed on deep-sea sediments leaving the uranium behind. Radium was not absorbed sufficiently to be in equilibrium with the ionium but was more strongly adsorbed than uranium. They concluded that the ionium Method of Age Determination is applicable only to core samples having equivalent base-exchange properties.

The present research was initated to examine a representative number of North Atlantic cores with a view to defining more closely the limitations of the ionium method.

Theory

Ions of the radioelements of the uranium-238 series dissolved in sea water are adsorbed on the surfaces of ocean-floor sediments. These muds are made up of particles of rock flour, clay minerals, and microscopic shells. The ratios of the concentrations of these ions on the surfaces at the time of deposition differ greatly

from the fixed ratios at radioactive equilibrium, due to the different base-exchange capacities of the ions. Ionium (Th^{230}) is found on the surface in great excess of that necessary for equilibrium with the radium, while much less uranium is present than is required for equilibrium with either the radium or ionium. The buildup and decrease of radium content through the length of the core, is a function of time as established by the laws of radioactive disintegration, and is dependent

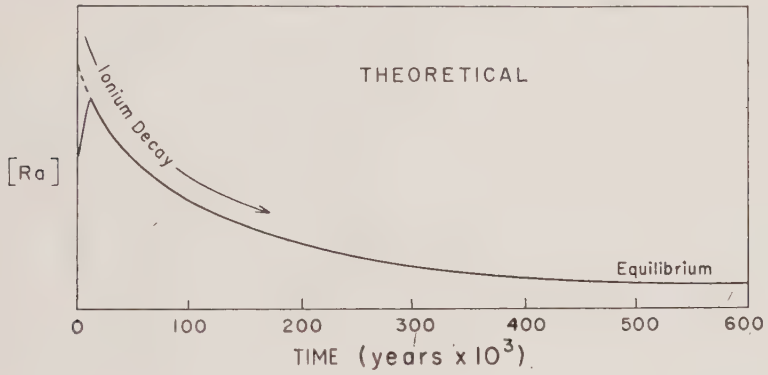

Fig. 1.

upon the initial amounts of uranium, ionium and radium present on the surface of the particles. Therefore, the linear measure of depth in the core is a function of time in some complicated way. Fig. 1 illustrates the theoretical plot of radium content versus time rather than depth, and indicates the various regions of the curve.

The experimental curves obtained by Piggot and Urry are thus explained in the following way. The initial increase in radium content is due to the production of radium by ionium at a rate in excess of the rate at which radium is decaying. Once equilibrium between ionium and radium has been achieved, the radium concentration is controlled by the decay of the ionium. The decreasing ionium concentration with depth in the core occurs because of insufficient uranium to support it. Finally radioactive equilibrium between all three elements is established when the uranium present is producing the same number of atoms of ionium as are disintegrating.

The theoretical treatment of the experimental data primarily aims at converting units of depth in the core to time intervals. The mathematical treatment of accomplishing this conversion has been given by Urry (1942)

The equation may be written:

$$\frac{Ra_t}{Ra_0} = \theta_2 + \frac{\lambda_{Ra}(\theta_1 - \theta_2)e^{-\lambda_I t}}{\lambda_{Ra} - \lambda_I} + \frac{\lambda_{Ra}(1 - \theta_1) - \lambda_I(1 - \theta_2)\, e^{-\lambda_{Ra} t}}{\lambda_{Ra} - \lambda_I} \qquad (1)$$

where:

Ra_t = Radium content at a time t as represented in the core,

Ra_0 = Radium content at the present time t_0 as represented at the top of the core,

λ_U = Decay constant of uranium,

λ_I = Decay constant of ionium,

λ_{Ra} = Decay constant of radium,

$\theta_1 = I_0\lambda_I/Ra_0\lambda_{Ra}$

$\theta_2 = U_0\lambda_U/Ra_0\lambda_{Ra}$

Experimental Techniques

Four types of measurements were carried out in the course of this study: Gas-phase and solid-phase radon, thick-source alpha counting and absolute surface area. Descriptions of the apparatus and procedure used in these measurements have been previously described. In order to determine the radon content within sedimentary grains, dried, powdered (< 60 mesh) samples of the sediment are weighed and then completely fused in a high-vacuum graphite resistance furnace modified after those used earlier (Evans, 1935; Urry and Piggot, 1941). The emanating gases are dried and conveyed to an ionization chamber which is brought to one atmosphere pressure with nitrogen. The counting system used in this study has already been described. (Bate, Volchok, and Kulp, 1954).

To determine the radon in the gas phase, no preparation of the sample is necessary other than drying at 110°C. Once dried the samples are stored in sealed glass tubes for at least thirty days, allowing equilibrium between radium and radon to be established. For measurement the tubes are cracked in a closed system and the accumulated radon is removed and flushed into the ionization chamber.

To measure the alpha activity dried, powdered (< 60 mesh) samples of the core material were counted in a scintillation-counting system. (Kulp, Holland, and Volchok, 1952). The extremely low levels of α activity encountered in these samples made it necessary to employ thick sources, thereby virtually eliminating the possibility of obtaining absolute disintegration rates. The thick-counting procedure is simple and yields excellent reproducibility.

Absolute surface-area measurements of many of the core samples were carried out using the argon-adsorption method (Kulp and Carr, 1952). Best results were obtained where the sediment was not powdered since powdering causes loss of the fine dust fraction.

Results

In the course of this study a total of eight ocean cores were analysed by some or all of the experimental techniques described in the previous section. These particular cores were chosen as a representative suite to illustrate the limiting conditions of the ionium method of age determination.

Pacific ocean core N-2

Through the kind co-operation of J. L. Hough, of the University of Illinois, essentially half of core N-2 was made available for this study. The core was obtained by Dr. Hough on board the USCGC *Northwind*, as part of the US Navy Antarctic Expedition of 1946-1947. The core was secured from 1980 fathoms of water, at Latitude 32° 21′. Longitude 105° 55′.

This core is composed of a red clay of uniform colour and texture. It was analysed by Urry, (1949), for total radium content. The data are plotted in Fig. 2. The curve drawn through the points is the interpretation of Urry and illustrates the characteristics predicted by the theory. The relative radium concentrations, apparently smooth variation of radium content, time span involved and availability of sufficient core material, all make this core exceedingly

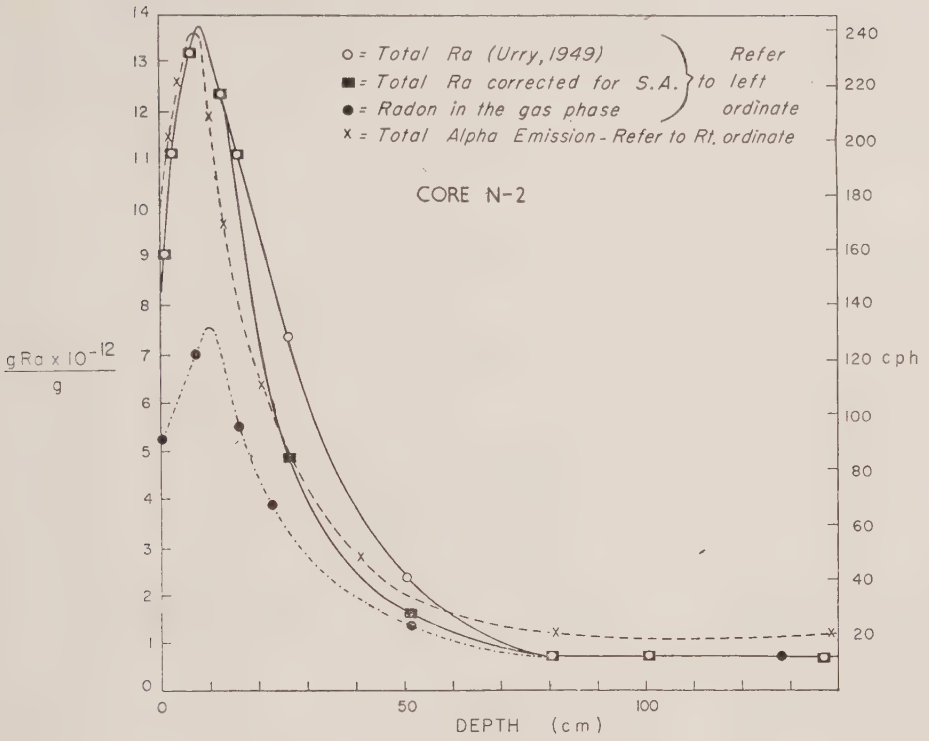

Fig. 2.

valuable for testing the procedures and hypotheses, involved in the ionium method.

Surface-area measurements made on this core are listed in Table 1, along with the radium concentrations obtained by URRY. The surface area is essentially constant except for two points. The largest spread of radium concentration between the points at 6 centimetres and 100 centimetres is a factor of about 17. No corresponding spread in the surface areas of these two points can be seen;

Table 1. Surface area and radium content of core N-2

Depth (cm)	Ra (g Ra $\times 10^{-12}$/g) (URRY, 1949)	Surface area (m^2/g)
0–0·5	9·08	30·6
2–2·5	11·09	31·4
6–6·5	13·19	32·9
11·8–12·5	12·33	32·1
16–16·5	11·16	31·0
25–26	7·30	51·5
50–51	2·35	57·4
80–81	0·72	32·5
100–101	0·76	32·9
137–end	0·69	26·7

in fact they differ by only about 0·1%, well within the limit of experimental error. The two surface-area values which are higher than the other eight by about a factor of 2 probably can be correlated with a minor difference in chemical or physical composition of the material at those points. If it is assumed that the radium concentration is directly proportional to the surface area, the radium versus depth curve may be corrected for differences in surface area. Fig. 2 also illustrates these data so corrected. It can be seen that although the surface areas of two of the points differed from the mean by almost a factor of two, the resulting curve of radium versus depth is still smooth. The apparent age at these depths will, of course, be affected. Measurements of the thick-source alpha emission and gas-phase radon were also made on this core. The results are also plotted in Fig. 2. The problems connected with the interpretation of the gas phase measurements are given in appendix A.

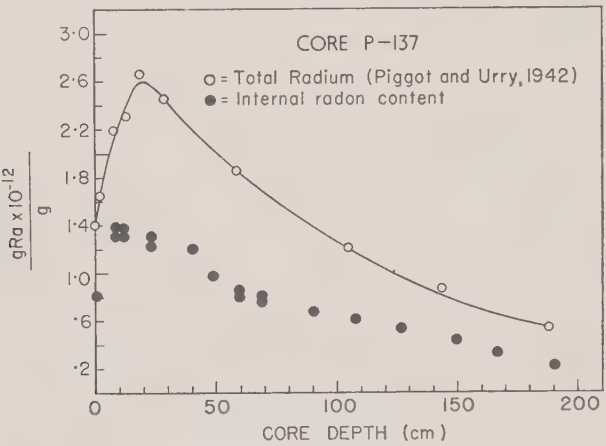

Fig. 3.

Caribbean sea core P-137

Core P-137 was taken by C. S. Piggot in 1937 aboard the research ketch *Atlantis* of the Woods Hole Oceanographic Institution from a point well down on the north slope of the Bartlett Deep in the Caribbean Sea. This core, composed of a rather homogeneous globigerina ooze, was one of the earliest used by Piggot and Urry in studies leading to the formulation of the age method (Piggot and Urry, 1942). The remaining samples of the core were kindly provided by Dr. Urry as a means of interchecking between laboratories.

Piggot and Urry measured the total radium content of about ten depths in this core. Their results are plotted in Fig. 3. The curve shown is the interpretation of Piggot and Urry. This curve, like the one for N-2 illustrates the radium variation with depth in the core predicted by the theory, except that insufficient time has elapsed for complete equilibrium.

At this laboratory samples of this core obtained from Dr. Urry were measured for internal radon content. The results of these measurements are also plotted on Fig. 3 to illustrate the difference in total and internal radon content.

Atlantic ocean cores

Six cores from the North Atlantic Ocean were chosen for study from the extensive core collection at Lamont Geological Observatory. Fig. 4 and Table 2 describe the locations and depths of these along with core Kelvin No. 5, analysed by Piggot and Urry (1942a). Fig. 5 has plotted the total alpha-emission rates of the five cores. Table 3 lists surface-area measurements on samples of these cores.

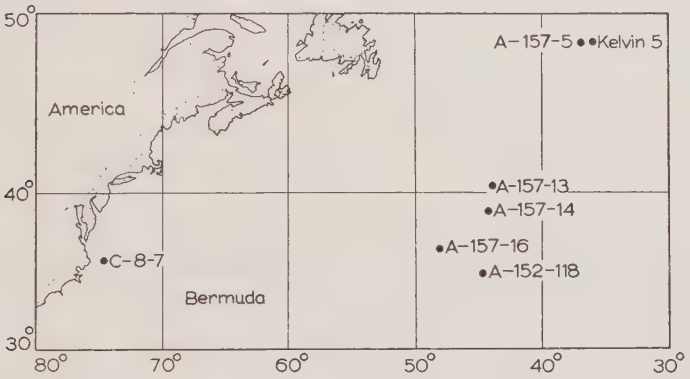

Fig. 4.

Core C-8-7. Lithologically this core is a typical of continental-shelf deposit. Both the total α activity and surface area measurements along the length of this core proved to be quite constant, as compared to the other N Atlantic samples. This is in substantial agreement with the constant radium content found by Urry (1949).

Table 2

Core No.	Lat. (N)	Long. (W)	Depth (m)	Length (cm)
C-8-7	35° 56′	74° 41′	1370	495
A-157 5	48° 35′	36° 51′	4500	320
A-157 13	40° 30′	43° 50′	4680	720
A-157 14	39° 00′	44° 15′	4775	490
A-157 16	36° 45′	48° 05′	5230	317
A-152-118	35° 07′	44° 40′	4340	645

Core A-152-118. Both the total alpha emission and surface area measurements on this core vary rather widely and in no apparent systematic way.

Studies of the lithologic units in this core by D. B. Ericson indicated that a large portion of this core was deposited in other than the normal way. Thus at his suggestion, radiocarbon measurements were carried out on selected samples Fig. 6 illustrates the results. Approximately 50% of the entire core material has been deposited by slumping or turbidity currents. This has thoroughly

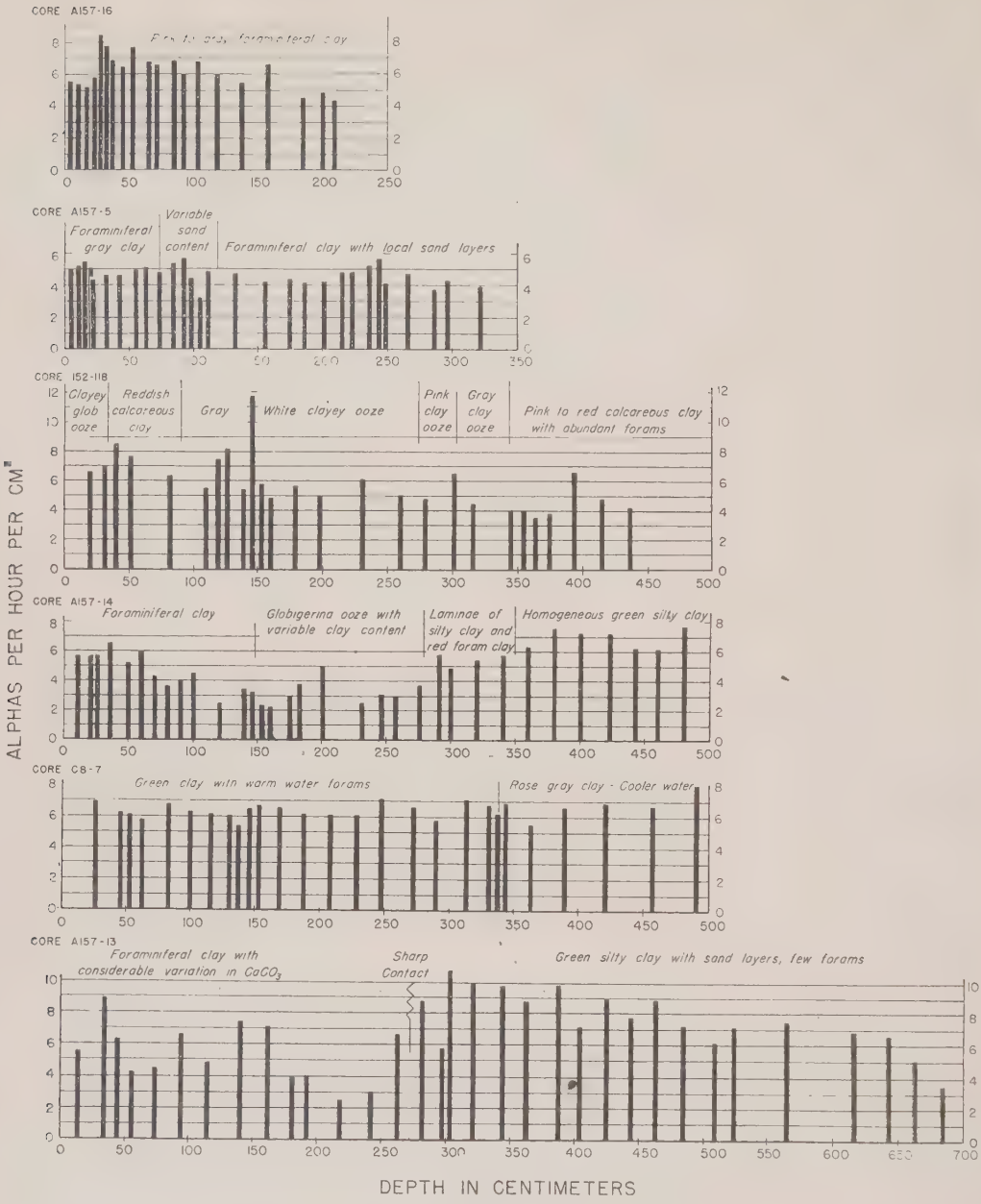

Fig. 5.

destroyed the chronologic sequence of the core, which explains the irregular pattern of the radioactivity and surface-area data.

Core A-157 No. 16. This core is lithologically rather homogeneous beyond the break at 30 cm. The α activity data clearly reflect the lithologic change at that point and the very rough downward trend beyond 30 cm suggest ionium decay but without the peak no absolute age analysis is possible.

Table 3. Surface-area measurements on North Atlantic cores

Depth (cm)	Surface area (m^2/gm)	Description	Depth (cm)	Surface area (m^2/gm)	Description
Core C-8-7			Core		
26	10·5 ± 0·4	Green clay	A-152-118		
53	12·7 ± 0·5		128	25·2	Clayey
99	12·1 ± 0·5		147	23·3	globigerina
130	11·7 ± 0·5		150	21.6	ooze
145	12·5 ± 0·5		181	21·7	
188	10·3 ± 0·5		200	23·7	
227	11·1 ± 0·4		210	24·8	
330	14·0 ± 0·5		234	25·0	
340	15·5 ± 0·5	Rose-grey clay	263	25·3	
343	10·7 ± 0·4		285	22·1	Pink to grey
361	17·3 ± 0·5		305	18·0	clayey ooze
487	12·6 ± 0·5		360	15·8	Pink to red clay
			380	18·8	with abundant
Core A-157-5			400	30·1	foraminifera
10	18·8	Foraminiferal	407	24·2	
23	27·8	grey clay	410	24·8	
43	22·5		420	26·2	
63	24·5		442	27·6	
84	28·8	Grey and tan glacial marine	539	24·4	
112	32·7	Clay with varied			
155	18·3	sand content			
186	14·2		10–11	14·97	Inhomogeneous
222	31·1		19–20	20·07	foraminiferal
248	17·8		30–31	22·34	clay with
			35–36	27·48	considerable
Core			42–43	25·90	variation
A-152-118			49–50	28·78	in $CaCO_3$
11	13·4	Light pink	55–56	22·20	
25	17·9	globigerina ooze	59–60	14·89	
			73–74	21·50	
30	34·1	Calcareous red	80–81	22·12	
40	29·7	clay	99–100	18·60	
52	27·1		140–141	24·33	
75	32·5		215–216	17·64	
110	21·9	Greyish-white clay	240–241	18·58	

Core A-157 No. 5. Core A-157-5 was expressly chosen for its proximity to core Kelvin 5, analysed by Piggot and Urry (1942a). The total α count curve even modified quantitatively by the surface-area measurements does not suggest regular ionium decay. To further enable comparison with Kelvin 5, internal radon determinations were made on A157-5 but no obvious correlation was obtained. This core does not appear to be datable by the ionium method.

Core A-157 No. 13. This core is the longest of all the six Atlantic cores (~720 cm) and is of interest because of the very abrupt change in colour at a depth of 273 cm, suggesting an unconformity.

The thick source total alpha rate, shown in the last graph on Fig. 5, clearly reflects the contact by a sudden increase in alpha activity. From the top of the core to the contact at 273 centimetres the points seem to vary randomly, and no real hint of an ionium decay curve can be found.

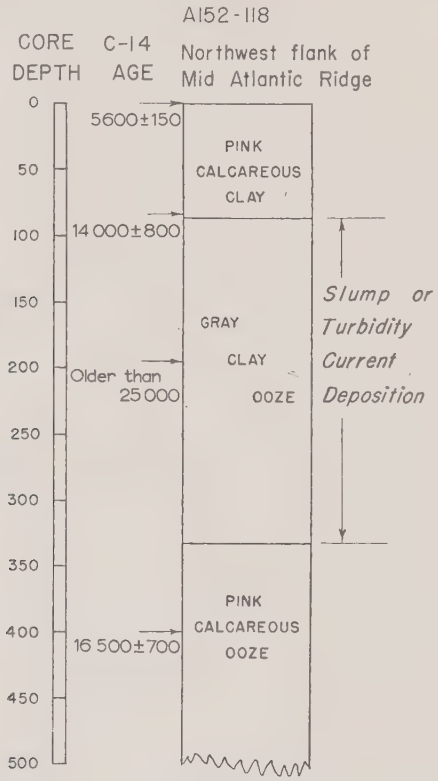

Fig. 6.

The internal radon content of this core was also measured. The data are plotted as a function of depth in Fig. 7. A well-defined ionium decay curve is not present. However, the last seven points before the sedimentary break suggest the approach of equilibrium of ionium with uranium. The low concentrations in the upper few centimetres of the core, and the very high value at 30–50 centimetres, also tend to suggest that in this core the enrichment was not entirely obliterated by other factors.

Numerous surface-area measurements were also made on this core. These values of surface area vary considerably. An analysis of these values shows a very direct correlation with radium content point by point along the length of the core (Fig. 7) down to 100 cm suggesting that these variations may be due to differences in sediment type.

Geological Theory

The foregoing results show that most of the cores under investigation from the deep Atlantic Ocean floor cannot be dated by the ionium method. To obtain a sedimentary column containing the radioactive relations dictated by the theory it appears that there are rather definite restrictions on the environment. For the ionium method to be valid, four geological conditions must be fulfilled.

Condition 1—*The ionium concentration of the ocean must have been constant for at least the last four hundred thousand years*

The concentration of ionium (Th 230) in ocean water is dependent primarily on the uranium concentration and the total rate of sedimentation. Practically all of the ionium in ocean water comes from the decay of dissolved uranium, since thorium carried by rivers to the sea is largely precipitated on the continental shelf.

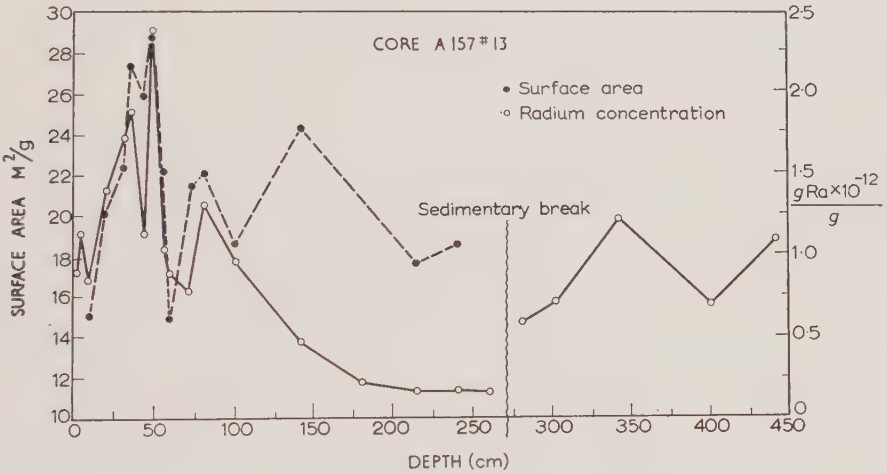

Fig. 7.

If the value of the ionium concentration in sea water calculated by Holland and Kulp (1954) is accepted (i.e. 3×10^{-15} g/cc) along with the uranium concentration of about 1×10^{-9} g/cc determined by Foyn *et al.* (1939) and Koczy (1950) it is clear that these radioelements are not in equilibrium, ionium being low by a factor of 5–10.* This suggests that most of the ionium is removed physically in sedimentation rather than by radioactive decay. On this basis it would appear that the ionium concentration in ocean water of constant uranium content, would be affected by the rate of sedimentation. This effect might, however, be directly offset, since an increased sedimentation rate implies an increased rate of weathering, and in turn an increased uranium concentration of the water. Thus it appears that a balance may exist between rate of erosion and

* Preliminary experimental measurements of the ionium concentration in sea water by Koczy, Picciotto, Poulaert, and Wilgain (private communication from Dr. Koczy) indicate less than 2×10^{-16}g/cc. This would mean that ionium in sea water is out of equilibrium with uranium by at least a factor of 100.

rate of deposition, erosion tending to build up ionium concentration through an increased uranium concentration, and deposition tending to deplete ionium in the sea through adsorption. This balance while probably not quantitative, may serve to hold the ionium concentration of ocean water relatively constant.

From measurements of the apparent age of ocean water by the carbon-14 method made in this laboratory, it seems that the ocean is well mixed at least on the scale of a few thousand years and that the bottom water is circulated on the scale of hundreds of years. Since the freshly deposited sediment particles are in contact with this bottom water, possible differences in ionium concentration of this sediment due to short-term variations in ionium concentration of the sea-water column should be smoothed out. Only long-term variations in the ionium content of sea water should be reflected in the sediment.

It is concluded that condition 1 may be adequately fulfilled over the time span for the ionium method.

Condition 2—Apart from the uppermost few centimetres in which the radium content is increasing with depth, radioactive equilibrium between ionium and radium should prevail

For the specific purpose of determining the validity of this condition, N. Issac and E. Picciotto of the Centre de Physique Nucleaire de Bruxelles, have evolved a method for the direct determination of ionium in sediments (Issac and Picciotto, 1953).

Up to the present the data on only five samples have been published. These data, while indicating no large departure from equilibrium, are not in themselves sufficient either to substantiate or invalidate condition 2. In a private communication Dr. H. Pettersson has advised the authors that several later measurements by Issac and Picciotto indicate the general condition of equilibrium between radium and ionium in the sediments.

If inequilibrium between ionium and radium were a general condition due to migration in the cores, curves such as obtained with N-2 and P-137 would be most difficult to interpret. Migration in a homogeneous core should tend to even out differences in radium concentration, rather than leave a large single peak as obtained in N-2.

Condition 3—Only "normal" sedimentation processes must have been responsible for the emplacement of the material of the core, and no subsequent external factors have influenced or disturbed the original sediment column

The existence of eroding and depositing bottom currents, turbidity currents, and submarine slumps, has been realized for some time. Their nature and effects are being actively studied by the Geophysics and Oceanography group at the Lamont Observatory, under the direction of Professor M. Ewing (Ericson, Ewing, and Heezen, 1951; Heezen, Ewing, and Ericson, 1951; Ericson, Ewing, and Heezen, 1952; Heezen and Ewing, 1952). These workers studied a large number of deep-ocean cores from a variety of locations in the Atlantic Ocean including the Hudson Submarine Canyon, Bahamas, Bermuda, Caribbean, Puerto Rico trough and the North American Basin. Among their conclusions, they state, "in the

North Atlantic, most of the samples taken from the floors of the main basins will have a large proportion of sediment deposited by turbidity currents." Although they believe that Pacific Ocean sediments are probably affected much less by this agent, because of its size and its being bordered by effective sediment traps, " . . . one must not overlook the possibility that a specific sample may contain a serious amount of reworked material."

It is clear that condition (3) must be strictly satisfied if the ionium method is to be applicable to a given core. This condition was not met in most of the Atlantic Ocean cores in this study and hence they could not be dated. Fig. 8 is a bathymetric sketch of the western North Atlantic Ocean modified after Heezen, Ewing, and Ericson (1955) showing the locations of these cores. It can be seen that although none fall within the Abyssal Plains they are all in areas somewhat susceptible to sedimentation disturbances. Core A-152-118 as described earlier clearly was affected by slumping. Core A-157-16 was probably affected by much the same type of disturbance, and the two cores from flanks of the Southeast Newfoundland Ridge (A-157-13, A-157-14) contain evidence of submarine erosion and slumping. Core A-157-5 might very possibly have been disturbed by a turbidity current from the slopes of the Mid-Atlantic Ridge.

The other two cores studied, P-137, from the Caribbean Sea; and N-2 from the Pacific Ocean do not show lithologic evidence of abnormal deposition. The radium versus depth plot for these two cores yields a smooth single-peaked curve indicative of inequilibrium relationships predicted by the theory. Apparently condition (3) was therefore satisfied and the method is applicable.

It seems evident therefore that the ocean-bottom topography is quite critical in deciding where to take cores that may be suitable for ionium dating. Fig. 8 is a precision depth profile modified after Heezen, Ewing, and Ericson (1955). The traverse of this section is indicated on the map, Fig. 9. From the available data on ocean-floor topography it appears that condition 3 may be satisfied for only small areas in the Atlantic but for sizable areas in the Pacific.

Condition 4—The sedimentary material must be homogeneous throughout the length of the core, in so far as its chemisorption properties are concerned

The two factors which control the effectiveness of chemisorption or base-exchange capacity of a sediment are its mineral composition and its surface area. Variations in either of these factors would produce discontinuities in the radium versus depth curve.

The validity of condition (4) in particular cores may be tested by means of surface-area measurements and mineralogical studies, of the material along the length of the cores. Most of the cores used in this study were analysed in this way, as described in the section on experimental results. Averaging the data by sediment type, the following values of surface area have been found:

Continental slope, green clay	12·6 m^2/g
Globigerina ooze, foraminiferal green to grey clay	21·9 m^2/g
Red clay	32·8 m^2/g

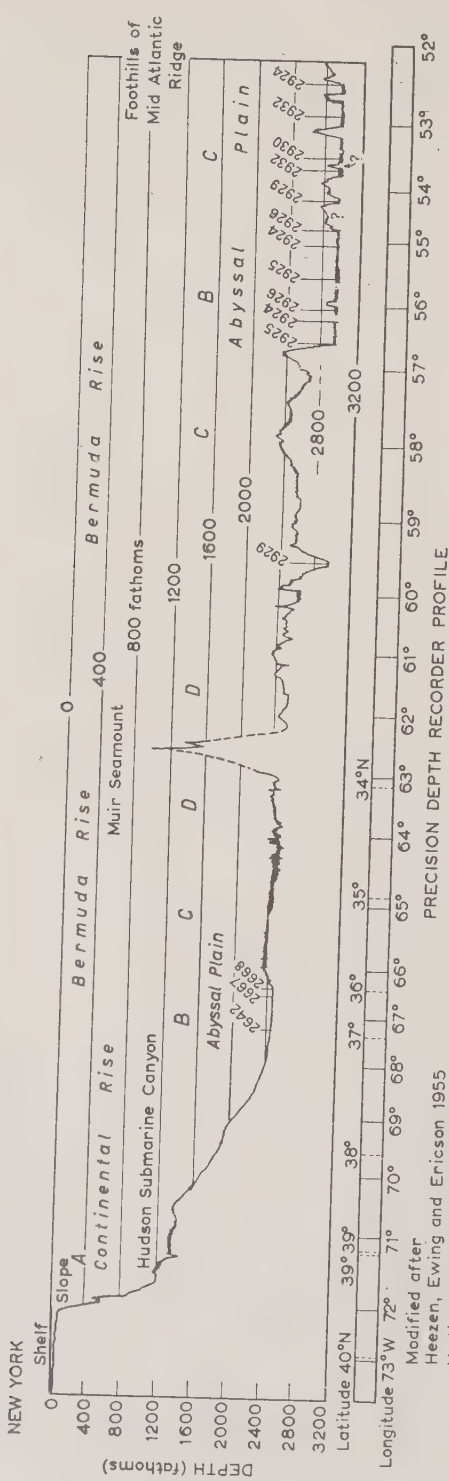
NEW YORK
Shelf
Slope
A
Continental Rise
Hudson Submarine Canyon
B
C
D
Abyssal Plain
Bermuda Rise
Muir Seamount
800 fathoms
Bermuda Rise
Foothills of Mid Atlantic Ridge
Abyssal Plain
DEPTH (fathoms)
0
400
800
1200
1600
2000
2400
2800
3200
Latitude 40°N 39° 39° 38° 37° 36° 35° 34°N
Longitude 73°W 72° 71° 70° 69° 68° 67° 66° 65° 64° 63° 62° 61° 60° 59° 58° 57° 56° 55° 54° 53° 52°
2669
2667
2642
2929
2925
2924
2926
2924
2925
2926
2924
2929
2928
2930
2932
2932
2924
PRECISION DEPTH RECORDER PROFILE
Western Mid Atlantic Ridge to New York
Modified after
Heezen, Ewing and Ericson 1955
Vertical exaggeration 40:1 – 50:1

Fig. 8.

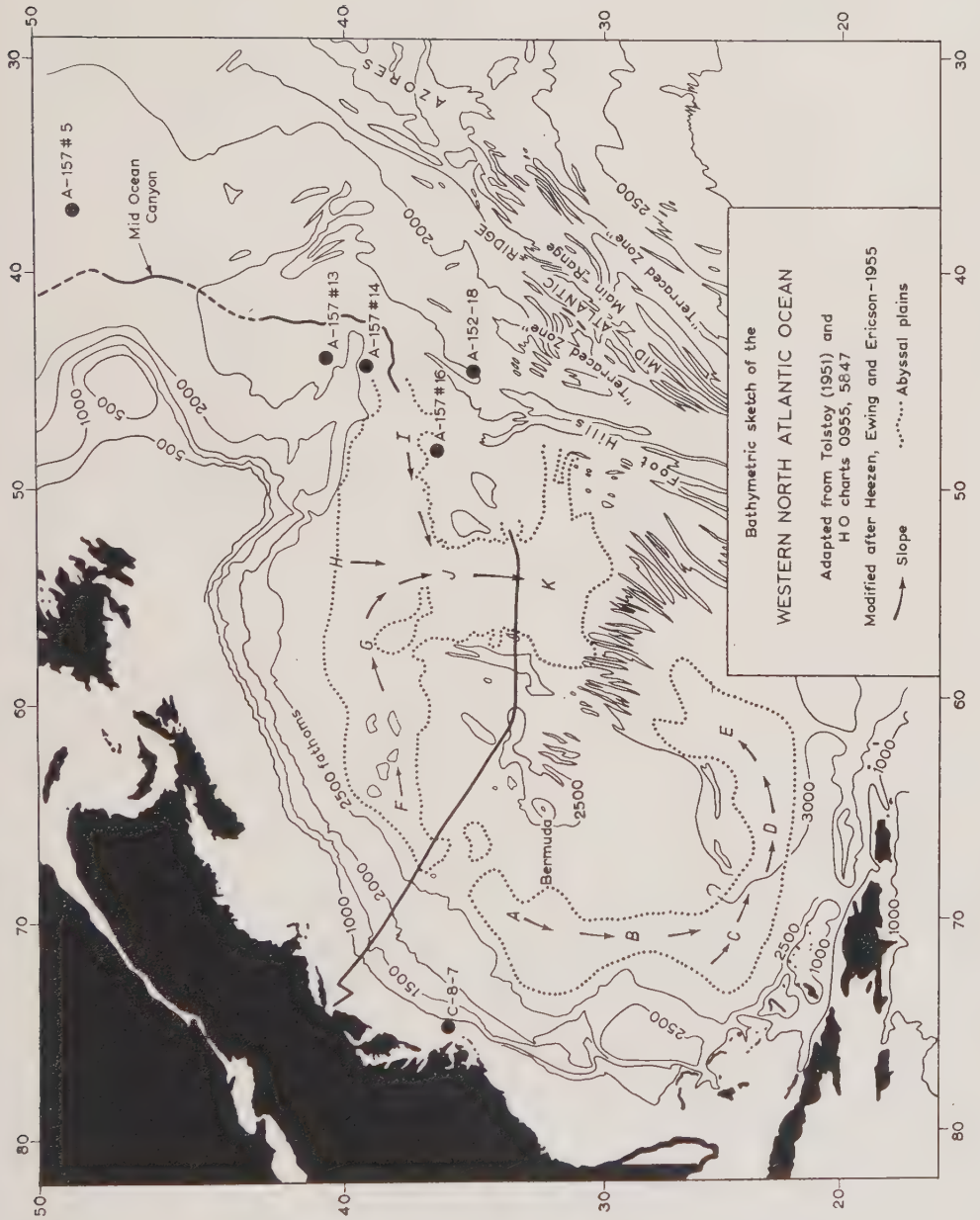
Bathymetric sketch of the
WESTERN NORTH ATLANTIC OCEAN
Adapted from Tolstoy (1951) and
H O charts 0955, 5847
Modified after Heezen, Ewing and Ericson-1955
Slope
Abyssal plains
A-157 # 5
Mid Ocean Canyon
A-157 #13
A-157 #14
A-157 #16
A-152-18
C-8-7
Bermuda
AZORES
RIDGE
Mid Atlantic Ridge
"Terraced Zone"
Hills
Fgot
2500 fathoms
A
B
C
D
E
F
G
H
I
J
K

Fig. 9.

Clearly variations of the concentration of any of these major constituents will directly affect the surface area of a specific sample.

Where only condition (4) is violated as a result of normally fluctuating-sedimentation conditions, it is still theoretically possible to employ the ionium method. If surface area alone is changing, this factor can be measured experimentally, and the curve normalized to constant surface area. If well-defined lithologic layering occurred, the homogeneous layers could be dated independently of the intervening portions. This situation has not been encountered in any of the cores of this study, but a similar analysis was attempted by Urry (1949) and Hough (1953) on one of the Pacific cores exhibiting fluctuating lithology.

The importance of condition (4) is borne out by the results presented in tne previous section. The Pacific core N-2 exhibited lithologic uniformity and the surface-area measurements as described earlier were essentially constant. The radium and total alpha-activity data yield smooth single peaked curves when plotted against depth in accordance with the theory of the method. This is in contrast to the Atlantic Ocean cores studied which varied considerably in sediment type along the core length, lacked consistency in surface area and gave erratic radium data.

It appears, therefore, that of the four necessary conditions upon which the ionium method is based, only conditions (3) and (4) are apt to be violated in deep ocean cores. Since the relative fulfillment of these conditions can be defined either by a careful lithologic study or surface area measurements of the core material, it should be possible to select suitable material prior to extensive radium analysis.

Age Analysis

To define the precision that may be obtained by the use of the ionium method, the data from cores N-2 and P-137 have been studied in detail. These cores were chosen for this purpose because they have yielded radium versus depth curves which are seemingly consistent with the theory. Following the age analysis, attention will be given to the ultimate source of errors.

Core N-2. The apparent ages for core N-2, were never published although the calculated rate of deposition did appear (Urry, 1948). A complete age analysis was made on the original radium data (Urry, 1949). Because of the difficulty of extrapolating the radium curve to the ordinate, θ_1 was obtained by the alternative mathematical method. The values of the two constants were found to be $\theta_1 = 1{\cdot}72$, $\theta_2 = 0{\cdot}086$. Since by definition these constants are respectively the initial amounts of uranium and ionium, expressed as ratios of the amounts which would be in equilibrium with the initial amount of radium, they are in effect each composed of two other constants. To simplify the symbols, let:

Ra_0 = Radium content at t_0

Ra_U = Amount of radium in equilibrium with the uranium content at t_0

Ra_I = Amount of radium in equilibrium with the ionium content at t_0

Then:

$$\theta_1 = \mathrm{Ra}_I/\mathrm{Ra}_0$$

$$\theta_2 = \mathrm{Ra}_U/\mathrm{Ra}_0$$

In the case of core N-2, the constants Ra_0 and Ra_U could be read off the curve of experimental data quite accurately; Ra_0 from the youngest radium content, and Ra_U from the average radium content of the deep end of the core where the ionium content had reached

equilibrium with the uranium. The Ra_I constant, however, is not easy to find because it requires extrapolating the up-swinging curve to zero depth. Despite this difficulty, Ra_I can be calculated since θ_I may be found mathematically, and Ra_0 is known. Due to the uncertainty in the constant Ra_I brought about by the lack of definition of the peaks of the radium curve, the calculated age may be off by as much as a factor of two in the range 2–10,000 years (Table 4). Beyond 50,000 years the disagreement due to this cause becomes trivial. This difficulty may be overcome by a series of closely spaced radium measurements to accurately define the peak, and Ra_I.

A further correction may be applied by normalizing the radium curve to constant surface area (see Fig. 2) and recalculating the ages.

Table 4 lists the ages obtained for points in core N-2 with the possible corrections.

Table 4. Ages in core N-2 (years $\times 10^3$)

Depth (cm)	Peak drawn at		Corrected for surface area
	Maximum depth	Minimum depth	
1·0	0·5	0·6	—
2·0	1·8	1·1	—
3·0	2·3	1·6	—
4·0	3·7	2·4	—
5·0	7·0	3·3	—
6·0	8·2	4·7	—
7·0	10·6	6·5	—
8·0	12·1	9·5	—
9·0	14·2	11·2	—
10·0	15·3	15·0	—
15·0	27	35	27
20·0	55	60	62
25·0	81	87	145
30·0	113	116	208
35·0	143	146	254
40·0	180	182	293
45·0	214	214	337
50·0	247	252	400
60·0	338	350	400

Core P-137. Although an actual set of ages has never been published, a diagram showing the rate of deposition for this core was contained in a later paper by Urry (1948). For core P-137 the experimental data defines the curve in much greater detail than in the case of core N-2, especially in the very critical area of the peak. An analysis similar to the one made on core N-2 has been carried out for this core.

The constants necessary for the age analysis were obtained as follows: Ra_0 is well defined by the experimental data of Urry and is taken as $1{\cdot}40 \times 10^{-12}$g Ra/g. Ra_U was found by directly measuring the uranium concentration at several points in the core. Urry (1941) made three measurements at depth of 0, 19, and 188 centimetres. The maximum spread of these data was about 50%, within the experimental error of his measuring technique. The average value expressed as equilibrium radium concentration is found to be $0{\cdot}30 \times 10^{-12}$ g Ra/g. Qualitatively this is in good agreement with the value obtained by smoothly extrapolating the original data of Fig. 3 to depth in the core. Ra_I was obtained by the mathematical method of finding θ_I as described by Urry (1942). Although the peak area in the radium curve of this core is much better defined than in core N-2, the data are still not sufficient to pinpoint it precisely. Thus the analysis was made on this core following the method used for core N-2,

i.e., choosing a maximum and minimum depth for the occurrence of the peak, based on the available experimental data. The two peaks fall respectively at 20 and 15 centimetres. It may be pointed out that again the peak used by Urry is almost equal to the maximum depth position. Table 5 lists the ages of various depths in core P-137, based on the peak at maximum and minimum depth respectively.

As in the case for core N-2, the correction in ages due to replotting of the radium peak appreciably affects only portions younger than about 40,000 years. For this core, however, the deviations are not as great as found in N-2, this being due to the much better definition of the curve by the data. Here only sections between about 3000 and 20,000 years are affected by more than 10%.

Errors

The absolute accuracy of dating by the ionium method is subject to a variety of possible errors. These may be listed as due to:

(1) accuracy of radium measurements,

(2) loss of surface material from the top of core in handling; and particularly for determining rate of deposition,

(3) distortion of the core due to friction in the coring tube,

(4) compaction of the sediment by overlying material on the ocean floor.

The errors in the absolute accuracy of radium measurements have been discussed in the section on procedures. It is concluded that with the techniques now employed, radium measurements may be made rather routinely with an accuracy of better than 2%.

Loss of material from the top of the core may in some cases place a rather serious limit on the validity of any ages obtained. Because of the very fluid state of the top few centimetres of the sediment column in many areas it will run or slump out of the coring tube unless extreme care is taken in handling. Thus the point of zero depth for these cases is unknown and an age analysis is uncertain. It has been estimated by D. B. Ericson (private communication) that as much as 8 to 10 centimetres of the tops of many cores have been lost in this way. The chief cause of this loss is the swinging of the core to the horizontal position as it is pulled on to the ship. This is necessitated by the extreme lengths of core now being taken. Mr. Ericson pointed out, however, that if the core were kept vertical and if liners were employed, the top of the column would probably be kept intact. The two cores discussed in detail in the first part of this chapter, P-137 and N-2, were probably not subject to this error. They were relatively short cores apparently handled with considerable care and were taken in plastic liners. Thus it is believed that in both of these cases the tops are reasonably well-defined.

The effect of the coring mechanism on the material of the core has been discussed by Piggot and Urry (1942) and Urry (1948). Experiments carried out with the Piggot-core sampler in varved clay pits near Hartford, Connecticut, demonstrated that the shift of the peak in the radium versus depth curve due to this effect is negligible. The only important correction is a reduction in the slope of the ionium decay curve below this peak, i.e., an increase in the apparent rate of deposition. Urry further points out that for the particular cores under consideration i.e., P-137 and N-2, "the effect of distortion is negligible . . . for the upper six-tenths of the total core length." In core P-137, the effect below 0·6 of the core length increases to a maximum error of about 50% in rate of deposition at the very bottom of the core. This effect is insignificant in considering the other sources of error at that depth in the core.

D. B. Ericson (private communication) suggests that with the use of the piston corer now being employed by the staff of the Lamont Geological Observatory, distortion is negligible throughout the entire length of the core. This conclusion is based upon his very careful studies of the condition, positioning and shape of such features as bedding planes appear concave downward in the coring tube, and elongate the normally round burrows common in many cores.

The effect of compaction of the core material due to load likewise appears to be unimportant in evaluating the errors in rate of deposition. Piggot and Urry (1942) measured the specific gravity of numerous samples from core P-137 to a depth of about 200 centimetres. The results

showed no regular increase with depth as would be predicted for a homogeneous core if compaction were appreciable. The values appear to change randomly with the maximum variation of about 15%.

D. B. Ericson (private communication) has measured the specific gravity and porosity of a number of Atlantic cores obtained recently by the Lamont Observatory group. Some increase in specific gravity and decrease of porosity seems to occur with depth but never seems to exceed about 20%.

On the basis of the foregoing discussion it appears that the absolute accuracy of dating by the ionium method is limited ultimately by the errors in measurement of the radium concentrations. The effect of these errors on the ages obtained in an analysis is summarized in

Table 5. Age of samples from core P-137 (years $\times 10^3$)

Depth (cm)	Peak drawn at	
	Maximum depth	Minimum depth
1	0·1	0·1
3	0·5	0·5
5	1·0	1·0
7	1·7	1·7
9	2·6	2·6
11	3·5	3·7
12	4·0	3·8
13	4·6	4·2
14	5·7	4·8
15	8·0	5·4
16	9·2	5·9
17	9·8	7·0
18	10·3	7·3
19	10·6	7·5
20	10·8	8·0
23	12·5	10·5
30	19·6	17·8
50	44	43
80	85	84
100	116	114
120	140	140
140	166	166
160	204	204
180	253	253

Table 6. This table has been compiled for the data of core P-137 since it most closely approaches the ideal case of any of the cores studied. It has been further assumed in preparing this table that the peak in the radium curve is very well defined at the minimum possible depth, i.e. that the parameter θ_1 is closely known. Thus Table 6 represents the best case obtainable with the presently available techniques.

It should be pointed out that in dating by the ionium-method ages are determined solely on an absolute scale, based on the decay characteristics of the radioelements and the length of the core. There is no single error aside from the half-life of ionium which could make all of the ages older or younger either by a fixed or proportional amount. Thus relative ages cannot be more accurate than absolute ages for this method.

Accuracy of dating by the ionium method may be materially improved by greater precision

in the absolute measurement of radium. However, there is some question as to whether this is worthwhile, because few, if any, cores will meet the necessary conditions previously established under "geological theory."

Applications

Rate of deep-sea sedimentation

The indirect methods to estimate the sedimentation rate in the deep sea are outlined in *The Oceans* (Sverdrup, Johnson and Fleming, 1942). These methods fall into two general categories, the supply method and the stratigraphic method.

Kuenen (1937), considering erosion since the Cambrian, and supply from terrestrial volcanoes, estimated total deep sea deposition at a rate of about 0·33 centimetres per thousand years. In a later revision, Kuenen (1941), reduced his estimate to 0·1 cm per thousand years for red clay and 0·2 cm per thousand years for globigerina ooze.

Other estimates based on the supply method by Lohmann (1909) gave values

Table 6. Errors in absolute ages, core P-137

Age of sample (years)	Error	
	± (years)	± (%)
2,000	~100	~5
4,000	~200	~5
6,000	600	10
7,000	1000	14
8,000	1900	24
10,000	1700	17
12,000	1500	12
15,000	1500	10
20,000	1400	7·0
30,000	1400	4·6
40,000	1300	3·3
60,000	1400	2·4
100,000	1500	1·5
150,000	1500	1·0
200,000	2000	1·0
250,000	2500	1·0
300,000	3000	1·0

of 0·1 to 1·2 cm/thousand years and by Revelle and Shepard (1939) of 0·25 cm/thousand years.

Schott (1939) calculated the rate of accumulation of globigerina ooze, blue mud, and red clay in the equatorial Atlantic Ocean, by assuming that certain foraminiferal forms were deposited only since the last glacial period, 20,000 years ago. The corrected values are:

Blue mud	0·59 cm/thousand years
Globigerina ooze	0·40 cm/thousand years
Red clay	0·29 cm/thousand years

The actual end of the glacial period occurred close to 10,000 years ago which would double the results above. Other values for mean sedimentation rates have been published (Moore, 1931; Strom, 1936) for restricted localities.

Estimation of the rate of deposition of deep sea sediment by use of the ionium method is of course limited in accuracy by the validity of ages obtained by the method. Urry (1948) discussed in detail these deposition rates for all of the core studied at the Geophysical Laboratory. His chief conclusions were (a) deposition in most of the cores is more rapid at present than the average of the last half million years, (b) the general rate of deposition was not appreciably affected by the repeated climatic changes of the ice age, and (c) the average rates of deposition are in general agreement with the estimates made earlier by other methods.

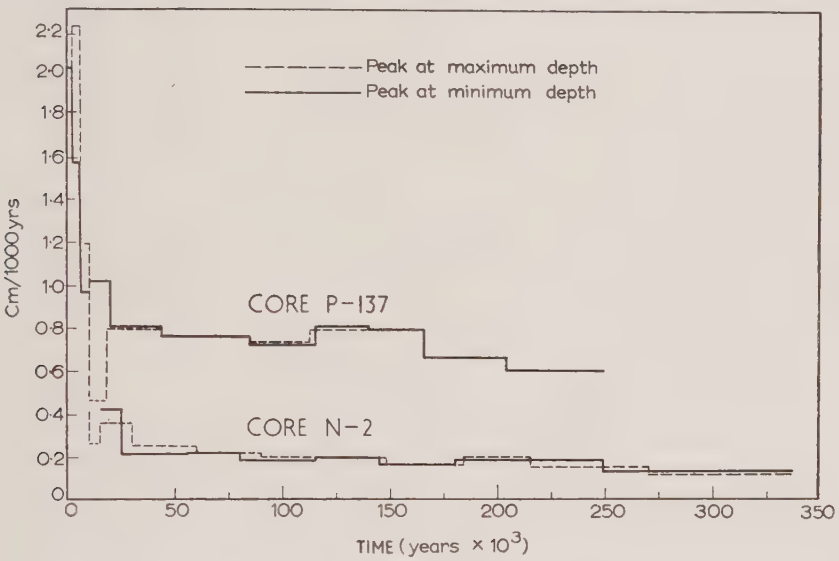

Fig. 10.

Utilizing the ages obtained previously, rates of deposition for red clay (core N-2) and globigerina ooze (core P-137) may be determined for these specific localities.

An average rate for this sediment type can be approximated from restricted localities since by its lithologic properties the material from these localities is representative of a much larger sample of the ocean floor.

Red clay

It may be recalled that in analysing the data of core N-2 the spread in the ages was due to the paucity of the experimental data. Fig. 10 illustrates the rate of deposition of the material of core N-2 for each of the two limiting cases. It is clear that no appreciable difference in the apparent rate of deposition over most of the core is found due to the assumptions made in the age analysis. The average rate of deposition for more than 90% of this red-clay core is about $0{\cdot}15 \pm 0{\cdot}05$ cm/1000 years. This value is in substantial agreement with the

estimates of red-clay accumulation by both the supply (0·1–0·2 cm/1000 years) and stratigraphic (0·29 cm/1000 years) methods.

The rate of deposition of red clay appears to increase at the end of the Wisconsin by a factor of three. According to Urry's treatment of the data this would have occurred in the last 5,000 years (4–5 cm) but in the treatment above it would occur about 12,000 years (8–9 cm) ago.

Globigerina ooze

The rate of deposition of the material of core P-137 is also illustrated in Fig. 10. The calculation was based on the ages developed in the last section. It is seen that no appreciable differences occur due to the various assumptions in the age analysis. The average rate of deposition for more than 90% of the material of this core is $0{\cdot}6 \pm 0{\cdot}2$ cm/1000 years. This value is somewhat higher than Kuenen's 0·2 cm/1000 years for globigerina ooze estimated by the supply method, and Schott's 0·40 cm/1000 years obtained from stratigraphic considerations. However, the rate obtained from the ionium method may be the most quantitative in that it is based on radioactive decay and permits assignment of a numerical error.

Again as in the red clay core N-2, the rate of deposition appears to have increased at the end of the Wisconsin, i.e., about 10,000 years (15 cm) ago, in this case also by about a factor of three.

The increase in the apparent rate of deposition of both red clay and globigerina ooze in the general interval 5000–15,000 years ago cannot be explained by either a compaction phenomenon or systematic experimental error as noted earlier. Thus it appears necessary to accept these high rates and explain them on geological grounds.

The most obvious world-wide event centred on this time is the termination of the Wisconsin glaciation. The world-wide retreat of the Wisconsin ice-sheet began about 11,000 years ago (Ericson *et al.*, 1956) and was extremely rapid. The rate of sedimentation as measured on several deep sea cones by the natural radiocarbon method was fairly constant during the Wisconsin but shows a sudden increase at about 11,000 years. The C^{14} data yields much greater precision in the last few thousand years than the ionium method and shows a rapid decrease of the rate of sedimentation after the surge at 11,000 years ago so that at present the rate is actually below that observed during the Wisconsin. The sedimentation rate curves based on the ionium method are too inaccurate in the past 5000 years, hence, although an increase is indicated at the end of the Wisconsin, the ionium method does not give definite results for most recent time. With retreat of the ice sheet, the resulting increased erosion rate due to the greater volume of water feeding to the seas and the excess rock debris produced by moving rock, would tend to increase the deposition rate of the inorganic red-clay sediment. Simultaneously, the general rise in mean world temperature would bring about an increase in population of organic life in the oceans, leading to higher rates of deposition of organic remains in the globigerina-ooze sediments. It thus appears plausible to explain the measured high rates of deposition at the close of the Wisconsin as due to the changes associated with the retreat of the ice.

On this hypothesis, however, similar increased deposition rates should be in evidence for the time of retreat of the Iowan and Illinoian glacial ice. The absence of any large change in the rate of sedimentation curve may be more experimental than real. Not only is the ionium decay curve relatively insensitive to such changes beyond 70,000 years ago, but also the absence of closely spaced radium analyses make it impossible to recognize such changes. None of the cores studied to the present have been analysed this closely.

In future measurements of cores by the ionium method careful attention should be given to the spacing of the samples if detailed interpretations of depositional rates are desired. It is unlikely that there is a considerable variation in the average sedimentation rate for different cores thus a considerable number must be dated in order to get some notion of the worldwide effect.

Finally, the apparent rate of sedimentation derived from this work and other methods for the Wisconsin and post-Wisconsin period is a factor of ten higher than the average rate for geologic history which must be close to 0·02 cm/1000 based on an average area-floor sediment thickness of one kilometre.

Pleistocene geochronology

Ocean cores taken from the great depths may reveal a detailed record of lithologic changes which in turn may reflect world-wide climatic changes. Since the ionium method of age determination is applicable in principle over the last one-half million years, the existence of this method makes it possible to define the broad phases of the Pleistocene period. In practice this is no simple affair, for not only must cores be obtained that fit the criteria discussed earlier but the definition of a glacial marine deposit from its lithology is not always unambiguous. Further, the most homogeneous cores which may yield smooth ionium decay curves are least interesting in terms of showing climatic changes; whereas the cores which contain layers of glacial marine deposits seldom yield ionium curves that can be interpreted with certainty. Probably the most satisfactory application is through examination of the pelagic microfauna by means of the oxygen thermometer ($0^{18}/10^{16}$) in a homogeneous core which yields a smooth ionium curve.

Some preliminary attempts to read Pleistocene history from ionium method analyses of deep-sea cores have been made. Piggot and Urry (1942) discussed the chronology of three cores from the North Atlantic and one from the Caribbean Sea. They concluded "(1) the effects of glaciation on the continents are contemporaneous with equivalent effects on the type of deposit in the ocean bottom; and (2) that the effects of glaciation on the type of ocean sediment are widespread, extending in the northern hemisphere at least to the Caribbean Sea." It should be pointed out that in the interpretation of the data upon which these conclusions were based no cognizance was taken of the errors outlined previously. Considering (a) the general location of three of these cores, i.e., from areas of the North Atlantic Ocean highly susceptible to bottom disturbances; (b) the extremely inhomogeneous nature of the sedimentary material comprising the three North Atlantic cores; and (c) the errors inherent in the radium determinations, it seems that the conclusions may have been premature.

Hough (1953) described in great detail the "Pleistocene climatic record in a Pacific Ocean core sample." The core (N-1) analysed by Hough in this paper was obtained from the southeastern Pacific Ocean during the same expedition in which core N-2 was taken. The core was analysed by Urry (1949) but the time-depth curve was not published. Lithologically the core exhibited alternate layering of red clay and globigerina ooze. In this core Urry had hoped to obtain two radium vs. depth curves, i.e., one for each sediment type, which would be independently analysed for time. However, the distribution of the material was such that red clay predominated in the upper 30 centimetres and globigerina ooze was found mainly below 20 centimetres in depth. Thus it was impossible to date the two materials independently. It should be pointed out that there were several samples which were considered mixtures of red clay and globigerina

Table 7. Comparison of ionium and C^{14} ages on selected core samples

Core No.	Ionium Age	C^{14} Age
P-130-28	1,100 ± 400	1,500 ± 500
P-130-118	7,000 ± 1000	8,200 ± 800
P-130-185	15,000 ± 1000	14,000 ± 2100
P-126-24	16,000 ± 1000	17,500 ± 2000

ooze. The data for N-1 yield a suggestion of the predicted decay curve, especially in the lower portion of the core. On the basis of the earlier discussions of errors and age analysis, however, it does not seem possible to arrive at anything more than some qualitative estimates of ages for N-1. This means that none of the dates in years tabulated by Hough along the length of core N-1 possess quantitative significance. Unfortunately, in Hough's paper the entire interpretation of geologic and climatic events occuring during the Pleistocene is based on these unreliable dates.

Thus, although the ionium method may make a major contribution to Pleistocene chronology in the future, a satisfactory test case has not been made.

Comparison with C-14 ages

A series of samples from cores which appeared to satisfy the conditions of the ionium method were dated also by the carbon-14 method (Table 8). Since these two dating methods are based on completely independent assumptions, no single systematic error could influence both determinations. The results of this comparison have been published earlier (Kulp and Volchok, 1953) but are pertinent here to emphasize the quantitative intercalibration.

Conclusions

A detailed study of the ionium method of age determination has been carried out. Emphasis has been placed on an examination of the assumptions and limiting conditions upon which the method is based. A number of deep-ocean cores from the Atlantic and Pacific Oceans and Caribbean Sea were measured for internal

radium content, radon in the gas phase, total alpha activity and surface area. Age analyses on the two cores applicable for dating were carried out along with an evaluation of the errors involved in this method. Based on the results of the age analyses certain geological interpretations have been made.

The main conclusions drawn from this investigation may be listed as follows:

(1) Application of ionium method dating is limited to cores possessing certain favourable characteristics:

(a) A chronologically undisturbed sediment column;

(b) Homogeneity with regard to adsorption potential.

(2) The accuracy of dates obtained by the ionium method is limited by:

(a) The accuracy of the radium determinations;

(b) The frequency of samples chosen along the length of the core, for radium determination.

(3) The average rates of deposition of red clay core from the Pacific Ocean and a globigerina ooze core from the Caribbean Sea were determined. For a time interval of at least 200,000 years, except for the most recent 10,000 years, these rates were essentially constant with values of

Red clay	$0{\cdot}15 \pm 0{\cdot}05$ cm/1000 years
Globigerina ooze	$0{\cdot}60 \pm 0{\cdot}20$ cm/1000 years

(4) the high rate of deposition at the end of the Wisconsin exhibited by both of the cores mentioned above may be explained as due to the increased erosion rate and rapid worldwide temperature rise.

The lack of evidence of similar sedimentation rate increases in Iowan and Illinoian time is probably due to the insensitivity of the method to changes in rate of sedimentation for relatively short intervals occurring at times greater than 70,000 years ago.

An intercomparison of the carbon-14 and ionium methods was made on a few selected cores. The agreement supports the assumptions involved in both methods.

The ionium method holds considerable promise for quantitative geochronometry if the conditions and restrictions on its application are understood. With an improved coring apparatus of much larger diameter, e.g., 6–8 inches, selective choosing of coring sites based on studies of ocean-bottom topography, careful studies of lithology and micropaleontology in the laboratory and greatest possible accuracy in radium measurement, valuable information on the detailed chronology of the Pleistocene period, rates of deposition of oceanic sediments, and further clarification of cosmic-ray flux variations in the past may be obtained.

Appendix A

Emission of radon to the gas phase from deep sea sediments

A fraction of the radium of deep-sea sediments originates from the ionium adsorbed on the particle surfaces during sedimentation. This fraction may be close to 100% in the upper layers of certain types of sediments, but for those older than 500,000 years it is negligible. If in the decay sequence from ionium through radium to radon it is assumed that none of the atoms are driven into the grains, and further, if no radon originating within the grain leaks out, then all of the radon derived from the surface ionium would be in the gas phase. In this case measurement of the gas phase radon would be a direct indication of the adsorbed ionium content. If, on the other hand, all the radon atoms end up within the grains, as a result of the recoil

due to the ionium and radium alpha emission, no radon would be present in the gas phase. The actual situation does not correspond to either of these simple cases. Some of the gas-phase radon is derived from ionium originally within the grains. Radium and radon from ionium originally adsorbed on the surface of a grain may be driven into that grain or any adjacent grains by recoil, or may end up in the gas phase. The problem is to estimate the significance of each of these possibilities in an effort to define the source of radon in the gas phase.

The leakage of radon from samples of deep-sea sediments is high compared to leakage from ordinary rocks and minerals. Cryptocrystalline pitchblende shows from <1 to 16% leakage at room temperature (GILETTI and KULP, 1955). Other minerals of high uranium content show much lower leakage, but the deep-sea sediments seem to leak some 30–60% of their radon.

A calculation of the expected leakage of radon from radium within these sedimentary materials may be made. Using the theoretical development of FLUGGE and ZIMENS (1939), the fraction of radon atoms emitted from a spherical grain due to the recoil may be expressed:

$$Fr = (3/4)R/r_0 - \frac{1}{12}(R/r_0)^3 \quad \text{for } 2r_0 \geq R \tag{2}$$

where R = recoil range and r_0 = radius of the grain.

Using a typical surface area for these sedimentary materials of about 20 m^2/g (KULP and CARR, 1950) and an average density of 3 g/cm^3, the grain radius r_0 may be found by

$$r_0 = 3/\text{density} \times \text{surface area}$$

and is found to be 5×10^{-6} cm.

The range of the recoiling radon atom R may be calculated by the use of some approximations. Using the available data (BEHARREL, 1949) on alpha recoil distances, it is found that the ratio R_α/R = range of alpha particle in air/range of recoil atoms in air is rather constant for atoms of similar alpha energies. This ratio indicates that the recoil atom will travel about 3×10^{-3} as far as the alpha particle associated with it. Thus the range of the radium alpha particle in sediment must be determined. Using the Bragg Kleeman rule a value of $1{\cdot}7 \times 10^{-3}$ cm is found for the range of the radium alpha particle in sediment. Thus the recoiling radon atom is seen to have a range R of 5×10^{-6} cm in the same material. Using these values of R and r_0 in equation (2), the fraction of radon atoms emitted due to recoil is seen to be about 70%. A similar analysis of the radon ultimately derived from surface ionium shows that about 78% of such radon atoms will escape to the gas phase, if it is assumed that none are driven into grains other than the one on which the parent ionium ion was adsorbed. This value of 78% is in effect the per cent of total radon which leaves the environs of the grain particle which adsorbed its parent ionium. Thus 78% represents the maximum radon in the gas phase of deep sea sediment. It is clear that the actual fraction of radon in the gas phase will not be 78%. The sizes of grain particles, the space between these particles, and the relative stopping powers of these media suggest that in the radium decay some fraction of the recoiling radon atoms will be driven into adjacent particles. The effect of reflection of recoiling radon atoms from a particle surface will tend to lessen the fraction trapped in other grains. The magnitude of these effects appears impossible to evaluate by a theoretical calculation because of the many uncertainties of the actual mechanisms involved. However, it is certain that the fraction of radon in the gas phase of these sediments should be considerably less than the theoretical maximum of 78%.

Most important, however, is the observation that for this particle size, the fraction of radon that ends up in the gas phase is similar regardless of whether the ancestral ionium ions were inside the grains, or on the surfaces. This means that the radon content of the gas phase of a given quantity of sediment is proportional to the total radium content. Since measurement of gas-phase radon is much simpler than the fusion method of measuring the total radon, and since the sample is preserved in gas-phase measurement, this result is of considerable practical importance.

It was originally thought that the gas-phase radon measurement might be made up almost entirely of radon from adsorbed ionium, and therefore such a measurement could be used to distinguish adsorbed and total ionium contents. Unfortunately this is not true as the above

analysis indicated. If sediments of much larger grain radii are selected differentiation of the two sources of radon is theoretically possible by this method. A simple calculation using equation (2) shows that to decrease the fraction of leakage from within the grains to 1%, the radius of the grains must increase by a factor of about 100. This increase of radius causes a decrease in surface area per gram by a factor of about 100. Thus such a method would fail because the adsorption on particles of such low surface area would not be measurable by present techniques. Further, it should be pointed out that no deep-sea sediments measured had surface areas differing by more than about a factor of 3 from the 20 m^2/g used in the calculation.

Acknowledgements—Several of the critical core samples were supplied by Drs. W. D. Urry and J. L. Hough. Dr. Urry and Drs. P. M. Hurley and D. R. Carr contributed helpful discussions on various phases of this study. Early in the investigation Dr. Hurley generously permitted the authors to spend some time in his laboratory studying the techniques employed there. Dr. H. D. Holland aided considerably in the early phases of the project. Dr. M. Ewing, Director of the Lamont-Geological Observatory of Columbia University, made available the Lamont core collection and consistently encouraged the project. Mr. D. B. Ericson, micropalaeontologist at the Lamont Observatory, contributed very useful information on the lithologic and stratigraphic details of the cores. Mr. R. D. Janes was responsible for the modification of the counters.

References

Bate G. L., Volchok H. L., and Kulp J. L. (1954) Low-level radon counting system. *Rev. Sci. Instrum.* **25,** 153–158.

Beharrel J. (1949) Absorption of alpha rays in thick sources. *Trans. Amer. Geophys. Un.* **30,** 333–336.

Ericson D. B., Ewing M., and Heezen B. (1951) Deep-sea sands and submarine canyons. *Bull. Geol. Soc. Amer.* **62,** 961.

Ericson D. B., Ewing M., and Heezen B. (1952) Turbidity currents and sediments in North Atlantic. *Bull. A.A.P.G.* **36,** 489–511.

Ericson D. B., Broecker W. S., Kulp J. L., and Wollin G. (1956) Dating the end of the last ice age from ocean sediments. *Science* (in press).

Evans R. D. (1935) Apparatus for the determination of minute quantities of radium, radon and thoron in solids, liquids and gases. *Rev. Sci. Instrum.* **6,** 99–112.

Flügge S. and Zimens K. E. (1939) Die Bestimm von Korngroben und von diffusions Konstanten aus dem Emanierver mögen. *Z. Physik. Chem.* B **42,** 179–220.

Foyn E., Karlik B., Pettersson H., and Rona E. (1939) The radioactivity of seawater. *Goteborgs Kingl, Veten skaps-och Vitterhets-Samhalles Handlinger, Ser. B,* **6,** No. 12.

Giletti B. J. and Kulp J. L. (1955) Radon leakage from radioactive minerals. *Amer. Mineral* **40,** 481–496.

Heezen B. C. and Ewing M. (1952) Turbidity currents and submarine slumps, and the 1929 Grand Banks earthquake. *Amer. J. Sci.* **250,** 849–873.

Heezen B. C., Ewing J., and Ericson D. B. (1951) Deep-sea sands and submarine canyons. *Bull. Geol. Soc. Amer.* **62,** 1407.

Heezen H. D., Ewing J., and Ericson D. B. (1955) Reconnaissance survey of the abyssal plain south of Newfoundland. *Deep Sea Research* Vol. II, No. 2 (in press).

Holland H. D. and Kulp J. L. (1954) The transport and deposition of uranium, ionium and radium in rivers, oceans and ocean sediments. *Geochim. et Cosmochim. Acta* **5,** 197–213.

Hough J. L. (1953) Pleistocene climatic record in a Pacific Ocean core sample. *J. Geol.* 61, no. **3,** 252–262.

Issac N. and Picciotto E. (1953) Ionium determination in deep-sea sediments. *Nature* **171,** 742.

Joly J. (1908) On the radium content of deep-sea sediments. *Phil. Mag.* **6,** 19C.
Joly J. (1908a) On the radium content of deep-sea sediments. *Phil. Mag.* **6,** 196.
Koczy F. (1949) Thorium in sea water and marine sediments. *Geol. Foren. Forhandl.* **1,** 238–242.
Koczy F. (1950) Weitere Uranbestimmung an Meerwasserproben. *Mitt. Inst. Radium* 463.
Kröll V. S. (1954) On the age determination in deep-sea sediments by radium measurements *Deep Sea Res.* **1,** 211–215.
Kuenen P. H. (1937) On the total amount of sedimentation in the deep sea. *Amer. J. Sci.* **34,** 457–468.
Kuenen P. H. (1941) Geochemical calculations concerning the total mass of sediments in the earth. *Amer. J. Sci.* **239,** 611–190.
Kulp J. L. (1952) The Carbon 14 method of age determination. *The Scientific Monthly* LXVV, No. 5.
Kulp J. L. and Volchok, H. L. (1953) Constancy of cosmic ray flux over the past 30,000 years. *Phys. Rev.* **90,** 713–714.
Kulp J. L. and Carr, D. R. (1952) Surface area of deep-sea sediments. *J. Geol.* **60,** 148–159.
Kulp J. L., Holland, H. D., and Volchok, H. L. (1952) Scintillation alpha counting of rocks and minerals. *Trans. Amer. Geophys. Union* **33,** 101–113.
Lohmann F. (1909) Plankton-ablagerungen am bodender tiefsee. *Schr. Naturwiss. Ver. Schl. Holst.* **14,** 399–402.
Moore H. B. (1931) The muds of the Clyde Sea area. Chemical and physical conditions; rate and nature of sedimentations and fauna. *Marine Biol. Assn. U.K. Jour.* **17,** 325–358.
Pettersson H. (1930) Teneur en radium des dépôts de mer profonde. *Campagnes Scient. Monaco* **81.**
Pettersson H. (1938) *Mitt. Inst. Radium* 400a.
Pettersson H. (1953) Radium and the deep sea. *American Scientist* **41,** No. 2, 245–255.
Piggot C. S. (1933) Radium content of ocean-bottom sediments. *Amer. J. Sci.* **XXV,** 229–238.
Piggot C. S. and Urry W. D. (1939) The Radium content of an ocean-bottom core. *J. Wash. Ac. Sci.* **29,** 405–415.
Piggot C. S. and Urry W. D. (1941) Radioactivity of ocean sediments. *Amer. J. Sci.* **239,** 81–91.
Piggot C. S. and Urry W. D. (1942) The radium content of sediments of the Cayman Trough. *Amer. J. Sci.* **240,** 1–12.
Piggot C. S. and Urry W. D. (1942a) Time relations in ocean sediments. *Bull. Geol. Soc. Amer.* **53,** 1187–1210.
Revelle R. and Shepard F. P. (1939) Sediments off the California coast. Trask ed.: *Recent Marine Sediments* A.A.P.G., 245–282.
Schott W. (1939) Deep-sea sediments of the Indian Ocean. Trask ed.: *Recent Marine Sediments* 396–408.
Strom K. M. (1936) Land-locked waters; hydrography and bottom deposits in badly ventilated Norwegian fjords with remarks upon sedimentation under anaerobic conditions. *Norske Vidensk. Akad. i Oslo, Skrifter I. Mat.-Naturv. Klasse no.* **7,** 85.
Sverdrup H., Johnson M. W., and Fleming R. H. (1942) *The Oceans,* Chap. XX, 1036, Prentice.
Urry W. D. (1941) The radioactive determination of small amounts of uranium. *Amer. J. Sci.* **239,** 191–203.
Urry W. D. (1942) The radio-elements in non-equilibrium systems. *Amer. J. Sci.* **240,** 426–436.
Urry W. D. (1948) Radioactivity of ocean sediments. *J. Mar. Res.* **7,** 618–634.
Urry W. D. (1948a) Marine sediments and pleistocene chronology. *Trans. N.Y. Acad. Sci.* **10,** 63–69.
Urry W. D. (1949) Radioactivity of ocean sediments. VI. Concentrations of the radioelements in marine sediments of the Southern Hemisphere. *Amer. J. Sci.* **247,** 257–275.
Urry W. D. and Piggot C. S. (1941) Apparatus for determination of small quantities of radium. *Amer. J. Sci.* **239,** 633–657.
Urry W. D. and Piggot C. S. (1942) Concentration of the radioelements and their significance in red clay. *Amer. J. Sci.* **240,** 93–103.

Geochimica et Cosmochimica Acta, 1957, Vol. 11, pp. 247 to 251. Pergamon Press Ltd., London

The reporting of chemical analyses of silicate rocks

Robert A. Chalmers* and E. S. Page †

(*Received* 7 *August* 1956)

Abstract—An appeal is made to analysts to report analyses in such a way that the degree of precision of the analysis is included in the quoted results. Examples are given of the calculation of the statistical errors in an analysis, and of a method of quoting results.

Introduction

The wide spread of results obtained in two recent investigations of precision and accuracy in silicate rock analysis (Fairbairn *et al.*, 1951; Fairbairn and Schairer, 1952) has caused some concern amongst chemists and petrologists. In the first of these papers it is stated that "The retention of two figures beyond the decimal point, except for very minor constituents, becomes ridiculous for most petrological purposes. The chemist is justified in presenting his results in this way since addition to 100 per cent is a test of his work." The first of these statements is probably true, although Chayes (1953) has advocated retention of the second decimal, on the ground that if it is rounded off it cannot be reconstructed by the user of the analysis, who may wish to know it. Chayes's argument is open to the same objection as is the second of the statements quoted above. First, the analyst quotes his results in terms of various oxides, assuming that the elements he has determined are accompanied in the rock by stoichiometric proportions of oxygen, although this may not be the case. Secondly, as has been pointed out by Schlecht (1953), the errors in chemical separations are likely to be greater than those associated with the instruments used, and are certainly harder to control. Thirdly, even if no non-Daltonian compounds are present, and no chemical or manipulative errors have been made, there will still remain an uncertainty in the results, arising from the statistical error inherent in all observed numerical data. In other words, the errors in even the most painstaking work may be sufficiently large to make the reporting of four significant figures unjustifiable.

Schlecht (1953) has criticized the estimation of errors by calculation of the observational errors in the instruments used, on the grounds that the chemical errors may be greater in magnitude than the observational errors and will not usually be susceptible to calculation. Although this is true, it is rather a negative contribution to the problem of providing a criterion for the number of significant figures to be quoted. It is usually fairly easy to estimate the standard deviation of the observational errors and from this to give limits, which would be exceeded only rarely, for the observational error. If then it is desired, the number of significant figures quoted can be adjusted so that the observational errors can be reasonably expected to have no effect on the figures given. It will in general

* Chemistry Department, University of Aberdeen, Old Aberdeen.
† Department of Mathematics, University of Durham, South Road, Durham.

be preferable to state the data as observed and the estimated standard deviation of the observational error, whether or not the former are truncated in a final or summary statement of the results. In such a summary statement it will usually be found that not more than three significant figures can be justified. Two examples will confirm this and illustrate the method.

Statistical Errors

Consider an analysis conducted by the classical method, and suppose that the analytical balance used has a standard deviation of 0·1 mg at the loads used. That is to say, in about 99 per cent of weighings the error of a single weighing will not exceed 0·26 mg. About a gram of sample is weighed and silica determined in the usual way by fusion with sodium carbonate, dehydration in the presence of hydrochloric acid, filtration, recovery of dissolved silica from the filtrate and recovery of any further dissolved silica by coprecipitation with the ammonia precipitate and further treatment of the mixed oxides. The weight of silica will be determined by measuring the loss in weight when the crude silica ignition products are treated with hydrofluoric and sulphuric acids, and reignited. The possible error arising from statistical fluctuations can now be calculated.

Suppose that in weighing the sample there is an error of x mg in the first weighing and y mg in the second weighing. Then we are implicitly supposing that both x and y are independent random variables following the normal or Gaussian distribution with zero mean and standard deviation 0·1 mg. Then the error in the weight of the sample is $x - y$ mg. This error is again a normally distributed random variable with zero mean, but now it has standard deviation $[(0{\cdot}1)^2 + (0{\cdot}1)^2]^{\frac{1}{2}} = 0{\cdot}14$ mg. [In statistical language we have

$$\text{Variance } (x - y) = \text{Variance } x + \text{Variance } y$$

$$\text{Standard deviation} = (\text{Variance})^{\frac{1}{2}}.]$$

If the silica has been initially separated by dehydration, and the silica that has escaped the initial separations has been recovered from the mixed oxides, as described above, then four weighings will have been made in determining the total weight of silica in the sample. Consequently the standard deviation of this weight will be twice the standard deviation of a single weighing.

The percentage of silica in the rock is then calculated from the ratio of the weight of silica to the weight of sample. Let these weights be X and Y respectively (we are supposing that X and Y are normally distributed random variables with means the true weight $\bar{X}$ of silica and the true weight $\bar{Y}$ of the sample, and standard deviations 2σ and $\sigma\sqrt{2}$ respectively, where σ is the standard deviation of a single weighing). The observed percentage of silica is then $100 \,.\, X/Y$. To the first order

$$\text{Variance of } 100 \,.\, X/Y = 10^4 \left\{ \frac{\text{Variance } X}{\bar{Y}^2} + \frac{\bar{X}^2}{\bar{Y}^4} \,.\, \text{Variance } Y \right\}.$$

Taking the case where $\sigma = 0{\cdot}1$ mg and a sample of about 1 g is taken, and where the sample contains about 60 per cent of silica, we obtain standard deviation

of observed percentage of silica = 0·022 per cent. This is, in 99 per cent of all determinations of silica in this rock by the method described, the observational error will not exceed about 0·06 per cent of the rock total.

It is, however, necessary to modify slightly the reasoning given above, to take account of the fact that in practice ignition products are weighed "to constant weight." That is, heatings and weighings are repeated until two consecutive observations agree within some previously decided limit, say k mg., the observed weight being taken as the mean of the last two observations. Obviously k should not be less than the error reasonably to be expected in a single weighing.

If indeed true constant weight has been reached, the last two weighings are independent observations of the same quantity and the observed mean has, therefore, standard deviation $\sigma/\sqrt{2}$, and mean the true weight. This means that the standard deviation of X is $\sigma\sqrt{2}$. This refinement in calculation, however, makes only a negligible difference to the 99 per cent limits of observational error, 0·06 per cent, already quoted.

If, however, the true weight has not been reached when both weighings are made, the recorded value will be distributed about a mean greater than the true weight. This is clearly a chemical error.

In the case of volumetric determinations it is possible to estimate the observational error in the burette readings, and the error involved in the control of addition of reagent, which determines the error involved in observing the end-point. If the smallest amount of reagent that can conveniently be added is 0·03 ml, then an end-point that occurs within such an addition may be in error by almost the whole of the increment. If the total iron is determined in the mixed oxides from 1 g of rock, by reduction to the ferrous state and titration with ceric sulphate, the observational error can be calculated as follows.

In order to estimate the standard deviation of the volume of reagent added from the burette we need to consider the errors in reading the burette at the beginning and the end of the titration, and the error arising from the actual position of the end-point within the last increment of titrant. Let us suppose that each reading of the burette is accurate to $\pm 0{\cdot}01$ ml, and that the smallest drop of titrant that can be conveniently added is 0·03 ml. The error in the amount of titrant needed lies between −0·02 and +0·05 ml. The standard deviation will, then, be of the order of 0·02 ml.* We are not considering the error arising from drainage in the burette during the titration, an error that may amount to a few hundredths of a millilitre (Kolthoff and Sandell, 1952).

Apart from errors arising from the use of the burette, there is likely to be an error of about 1 part per 1000 in the standardization of the titrant. In the case of 0·0500 N ceric sulphate, 1 ml is equivalent to 3·993 mg of ferric oxide, and the error in standardization is therefore equivalent to an error of about 0·004 mg of ferric oxide per ml of titrant; the standard deviation is then about 0·002 mg/ml. Let x ml be the amount of titrant used, and y mg/ml be the ferric-oxide equivalent of the titrant. Then the observed amount of ferric oxide is

* For these readings there is a good case for supposing the distributions to be rectangular, in which case, however, the standard deviation will not be greatly affected. An analogous example in quite a different context is given by Barnard (1951).

xy mg, and we have to the first order, using bars to denote means as before,

$$\text{Variance } (xy) = \bar{y}^2 \text{ . Variance } x + \bar{x}^2 \text{ . Variance } y.$$

When x is about 20 ml and y is about 4 mg/ml (i.e. a gram of a sample containing about 8 per cent of total ferric oxide is being analysed):

$$\text{Variance in amount of ferric oxide} = 8 \times 10^{-3} \text{ (mg)}^2,$$

i.e. the standard deviation of the amount of ferric oxide is 0·09 mg, and the standard deviation of the percentage of ferric oxide is approximately 0·01 per cent. That is, the 99-per cent limits of error are about $\pm 0{\cdot}026$ per cent. The relative error in the determination of total iron could in this case clearly be about 3 parts per 1000.

In a complete analysis by the classical method some constituents will be determined indirectly by difference. For such a determination the variance will be the sum of the variances of the contributing factors, just as was the case for the determination of the total weight of silica. Thus for an indirect determination of alumina some five or six factors are involved, and the standard deviation is likely to be about twice that given above for the total iron, even neglecting the error arising in weighing any alumina recovered from the filtrate from the ammonia precipitation.

The method of analysis of errors given above may be applied to determine the standard deviation of a determination calculated from observed results using only multiplication and division. Approximate results can be obtained when other functions of the observations are used, from formulae such as

$$\text{Variance } f(x) \approx [f'(x)]^2 \text{ Variance } x$$

(Rao, 1952; Davies, 1947).

Let us return to the presentation of results: it is seen that the 99-per cent limit of error amounts, in cases of major constituents, to several units in the second decimal place of percentage. Therefore it is best that the results be presented in full, i.e. giving two decimal places together with the estimated standard deviation. In this way the accuracy of the results is given, limits on the error can be easily calculated, and the results can be compared with others. It is sometimes necessary in a summary to express each result by one number only. Clearly this can only be achieved with some loss of information, and previously the information on the accuracy has been sacrificed as only the result itself, to the full number of decimals, has been quoted. This method of reporting can impart a misleading impression of the accuracy attained, and so we suggest that if this method of summary presentation is unavoidable, the result should be quoted to such a number of decimal places that variation within the 99-per cent limits of error causes at most a variation of one unit in the last figure quoted. Both methods of presentation are exemplified in Table 1. The observed differences in a duplicate analysis are quoted for comparison with the estimated statistical errors. It is seen that in no case of the summary reporting are we justified in quoting to more than the first decimal place. Indeed, for four of the constituents, FeO, CaO, $H_2O(+)$, and P_2O_5, the statistical error could cause the first decimal to be rounded differently.

Chemical errors, which we have not considered here, would add further to

the doubt felt about the accuracy of the determinations. In general it may be said that inadequate reporting of analytical results limits the value of the information contained in them, and may make them misleading. In particular, it must be stressed that in those cases, such as in petrology, where the results are made the basis for comparisons, it is essential that an estimate of the precision

Table 1

	I	II	III	IV
SiO_2	52·82	0·010	0·02	52·8
Al_2O_3	13·40	0·017	0·20	13·4
Fe_2O_3	1·03	0·013	0·07	1·0
FeO	6·96	0·012	0·05	7·0
TiO_2	0·42	0·005	nil	0·4
CaO	10·25	0·007	nil	10·3
MgO	9·70	0·008	0·07	9·7
K_2O	0·20	0·014	0·04	0·2
Na_2O	0·99	0·020	0·03	1·0
H_2O (−)	0·61	0·008	0·03	0·6
H_2O (+)	3·64	0·016	0·01	3·6
MnO	0·17	0·005	0·03	0·2
P_2O_5	0·05	0·005	nil	0·1
Total	100·24			100·3

I. Mean of duplicate analyses.
II. Estimated standard deviation.
III. Observed difference between duplicate determinations.
IV. Results rounded off to imply estimated error.

and accuracy of the results should be available in order that the significance of differences may be properly assessed. This conclusion has been repeatedly stressed in the literature but unfortunately has been more often ignored than heeded.

References

Barnard G. A. (1951) Statistics applied to assembly processes. *Statistical Method in Industrial Production* p. 57, Royal Statistical Society, London.

Chayes F. (1953) In defence of the second decimal. *Amer. Mineral.* **38,** 784.

Davies O. L. (Ed.) (1947) *Statistical Methods in Research and Production* (2nd edition) p. 37, Oliver and Boyd, London.

Fairbairn H. W. and Schairer J. F. (1952) A test of the accuracy of chemical analysis of silicate rocks. *Amer. Mineral.* **37,** 744.

Fairbairn H. W., Schlecht W. G., Stevens R. E., Dennen W. H., Ahrens L. H., and Chayes F. (1951) A co-operative investigation of precision and accuracy in chemical, spectrochemical, and modal analysis of silicate rocks. *United States Geological Survey Bulletin* No. 980.

Kolthoff I. M. and Sandell E. B. (1952) *Textbook of Quantitative Inorganic Analysis* (3rd edition), p. 425, Macmillan, New York.

Rao C. R. (1952) *Advanced Statistical Methods in Biometric Research* p. 209, Wiley, New York.

Schlecht W. G. (1953) The probable error of a chemical analysis. *United States Geological Survey Bulletin* No. 992, p. 57.

Geochimica et Cosmochimica Acta, 1957, Vol. 11, pp. 252 to 262. Pergamon Press Ltd., London

Measurement of Li^6, He^3, and H^3 in meteorites and its relation to cosmic radiation

E. L. Fireman and D. Schwarzer
Brookhaven National Laboratory, Upton, New York

(*Received* 13 *August* 1956)

Abstract—The He^3 and Li^6 contents of six iron and five stone meteorites are measured by neutron activation. Both the iron and the stone meteorites have large He^3 contents ranging from $0{\cdot}13 \times 10^{-6}$ c.c./g to 9×10^{-6} c.c./g. The stone meteorites have Li^6 contents ranging from $1{\cdot}1 \times 10^{16}$ Li^6 atoms/g to $6{\cdot}2 \times 10^{16}$ Li^6 atoms/g. The iron meteorites have less than 10^{14} Li^6 atoms/g. There is no uniform relation between the Li^6 contents of the meteorites and their He^3 contents, indicating that the He^3 contents of both the stone meteorites and the iron meteorites are due to spallation caused by high-energy cosmic rays rather than slow neutrons and that the average slow-neutron flux has been less than 1 neutron/cm² sec.

The tritium contents of the iron meteorites, Norfork (1918), Para de Minas (1934), and Charcas (1804) are measured. A tritium content of $(2{\cdot}7 \pm 0{\cdot}3) \times 10^6$ H^3 atoms/g at its time of fall is indicated for the Norfork meteorite and of $(5{\cdot}9 \pm 1{\cdot}2) \times 10^5$ H^3 atoms at its time of fall is indicated for the Para de Minas meteorite. There is less than $1{\cdot}2 \times 10^4$ H^3 atoms/g in Charcas. The tritium and helium-3 content of Norfork combine to give it a cosmic-ray age of $0{\cdot}9 \times 10^9$ years or greater. The tritium and helium-3 content of Para de Minas combine to give it a cosmic-ray age of $1{\cdot}7 \times 10^9$ years or greater. This indicates that if iron meteorites resulted from the breakup of a larger mass, the breakup occurred $0{\cdot}9 \times 10^9$ or more years ago. Small H^3 contents but negligible helium-3 contents are found in terrestrial iron samples.

The tritium content of the iron meteorites compared with that produced in iron by high-energy proton bombardment gives the average flux of cosmic rays bombarding the meteorite in extraterrestrial space. This flux as determined from the Norfork meteorite, equals the 1954 cosmic-ray flux which does not contain the low energy cutoff; the flux determined from the Para de Minas meteorite is a factor of 3 to 6 lower. This indicates that Para de Minas, which is a 112-kg meteorite, was shielded from cosmic radiation by material ablated during its passage through the atmosphere, or was irradiated by a smaller cosmic-ray flux than Norfork.

1. Introduction

This investigation was suggested to us by Professor F. L. Whipple, who together with Professor C. Frondel supplied us with our first stone meteorite samples. Later we were able to obtain samples of iron meteorites which have a lower hydrogen and water content than the stones.

That cosmic radiation may produce measurable radioactivity in meteorites is an old thought. Attempts have been made to detect radioactivity in meteorites shortly after their fall by putting them under thin-window counters and scintillators. These attempts have not been successful. Bauer (1947) suggested the possibility of chemically isolating and counting particular radioisotopes. He also suggested that the helium content of meteorites is produced by cosmic rays, rather than from natural radioactive decay. He noticed that large meteorites had small helium contents while small meteorites had large helium contents. This he explained to be the result of shielding by more ablated material for the larger meteorites.

The mechanism by which radioisotopes are produced by cosmic rays in meteorites is spallation. Spallation from iron nuclei in iron meteorites and from oxygen, iron, and silicon in stone meteorities. The production of radioisotopes by slow neutrons in meteorites is small on the basis of the lack of correlation between the Li^6 and He^3 contents of the meteorites.

* Work performed under the auspices of the US Atomic Energy Commission.

Mayne, Reasbeck, and Paneth (1953) and Dalton, Paneth, Reasbeck, and Mayne (1953) measured the He^3/He^4 ratio in iron meteorites with a mass spectrometer and found it to be as high as 31·5%, and measured He^3 contents as high as $8{\cdot}8 \times 10^{-6}$ c.c./g. This can be contrasted with He^3/He^4 ratios of $1{\cdot}3 \times 10^{-4}\%$ for atmospheric helium and $0{\cdot}5 \times 10^{-5}\%$ to $5{\cdot}0 \times 10^{-5}\%$ for well helium. The highest He^3/He^4 found in a terrestrial mineral is $1{\cdot}2 \times 10^{-3}\%$ for a spodumene sample (Aldrich and Nier, 1948). Gentner and Zähringer (1955) also measured the He^3/He^4 ratios and He^3 contents of a number of iron meteorites by mass spectrometry and found them to be in the same range as that found by Paneth's group. Our measurements on the He^3 content of the iron meteorites by activation analysis are in accord with the mass spectrometer measurements.

The H^3 production per gram in a chondrite on the basis of the measured H^3 production cross-sections (Fireman and Rowland, 1955; Fireman, 1955; Currie, Libby, and Wolfgang, 1955) is 30% greater than in an iron meteorite. If the two types of meteorites had no helium leakage, comparable ablation from their surface, and were subjected to the same integrated flux of cosmic radiation, then there should be on the average about 30% higher He^3 contents in stone meteorites than in irons. Our He^3 measurements are consistent with these assumptions.

The tritium content of meteorites gives two results. Combined with the cross-section for tritium production by high-energy protons, it gives the cosmic-ray flux at the meteorite integrated over its last twenty-five years in extraterrestrial space. The H^3 content of Norfork gives a flux of 8 particles/cm^2 sec if cosmic rays have the low-energy cutoff at 1 BeV; however, the flux would be equivalent to that striking the earth's polar region if there is no cutoff. Para de Minas gives a smaller flux. Secondly, combined with the He^3 content, it gives a cosmic-ray age for the meteorite. This is $0{\cdot}9 \times 10^9$ years for the Norfork meteorite and $1{\cdot}7 \times 10^9$ years for the Para de Minas meteorite.

A discrepancy of a factor of 10 exists between the measurement of tritium production by high-energy protons on Fe (Fireman, 1955; Currie, Libby, and Wolfgang, 1955) and that calculated on the basis of evaporation theory (Singer, 1952; Martin, 1953). This only affects the determination of the extraterrestrial flux from the tritium content and not the H^3/He^3 age. We have used the measured values for the tritium production cross-section.

2. Description and Source of Meteorites

Meteorites are named after their place of fall. Samples of six iron meteorites and five stone meteorites have been obtained for this work.

Iron meteorites

Charcas is a 780-kg medium octahedrite found in 1804 in Charcas, Mexico. Professor H. C. Urey and G. Edwards kindly gave us a 24·3-g sample.

Mount Ayliff is a 13·6-kg coarse octahedrite found in 1907 in Cape Province, S. Africa. Dr. Brian Mason kindly sold us a 11·2-g surface sample.

Norfolk is a 23-kg medium octahedrite that fell in September 1907 in Norfolk, Virginia. Dr. Brian Mason kindly sold us a 18·2-g sample.

Norfork is a 1·05-kg medium octahedrite that fell in Norfork, Arkansas in October 1918. Dr. H. H. Ninninger kindly sold us a 35·3-g surface sample.

Para de Minas is a 112-kg medium octahedrite that fell in 1934 on the Palmital Ranch

near Para de Minas, Brazil. Dr. Walter Curvello kindly gave us a 16·6-g sample taken 1·5 to 2·0 cm from the surface.

Pitts consists of four masses of total weight 3·7 kg. It is an octahedrite with silicon inclusions that fell in Wilcox County, Georgia on 20 April, 1921. Dr. E. P. Henderson kindly gave us a 24·3-g sample of the metal phase.

Stone meteorites

Bur Gheluai is a grey hypersthene chondrite. A shower of over 100 stones with total weight of about 120 kg, the largest stone being 15·4 kg, fell in Bur Gheluai, Italian Somaliland, on 16 October 1919. Professor C. Frondel gave us 19·5-g sample.

Nakhla is a diopside-olivine-achondrite. A shower of about 40 stones with total weight about 40 kg and varying in weight from 1813 g to 20 g fell in Nakla near Alexandria, Egypt on 28 June 1911. Professor C. Frondel gave us 4·1 g.

Shelburne is a polymict brecciated veined grey hypersthene chondrite. Two stones weighing about 12.7 kg and 6·0 kg fell near Shelburne, Ontario, Canada on 13 August 1904. Professor C. Frondel gave us 13·5 g.

Sioux County is a howardite meteorite. About 20 stones totalling 4·1 kg fell in Sioux County, Nebraska on 8 August 1933. Professor C. Frondel gave us 15·5 g.

St. Michel is a white hypersthene chondrite. Two stones of 7 kg and 10 kg fell in St. Michel, Finland on 12 July 1910. Professor C. Frondel gave us 23·5 g.

3. Measurement of He^3 and Li^6

Slow neutrons acting on Li^6 and He^3 give H^3 by the $Li^6(n,\alpha)H^3$ and the $He^3(n,p)H^3$ reactions. If a meteorite sample is irradiated in the slow-neutron flux of a pile, the quantity of tritium produced is a measure of the sum of Li^6 and He^3 contents of the meteorite. If the gas extracted from a meteorite is irradiated with slow neutrons, the tritium produced is a measure of the He^3 content. The deuterium present in a meteorite gives a negligible amount of tritium under slow-neutron irradiation.

A. Slow-Neutron Activation Of Meteorite Samples

A sample of about 1 g weight is cut from the iron meteorites and about 0·25 g weight is cut from stone meteorites. These sizes are chosen because they are large compared to the range of the 2·736-MeV triton from the $n + Li^6$ reaction. To check the effect of foreign material on the surface, activations were done both with surface samples and with samples of 0·5- to 1·5-cm depth for the Pitts, Norfork, and Mt. Ayliff meteorites. The surface samples, rather than showing an increased activation due to foreign Li contamination, showed a reduced activation. This indicates a loss of He^3 from the first few millimeters of the surface of the meteorite due to the surface heating in the passage of the meteorite through the atmosphere or perhaps to some type of transition effect. The effect was most noticeable in the Pitts meteorite, where the surface sample gave $0{\cdot}38 \times 10^{-6}$ c.c./g of He^3 compared to $2{\cdot}6 \times 10^{-6}$ c.c./g of He^3 for a sample taken at a depth of 0·5 cm. A similar effect was noticed in the H^3 content of Norfork, where the sample with more surface had less H^3.

The meteorite samples together with standards containing known amounts of Li^6 in Bi are wrapped in Al foil and irradiated in the pneumatic-tube facility of the Brookhaven reactor. 15-min and 60-min irradiations were carried out (see Table 1). The flux is known for gold-foil activations to be about $2{\cdot}5 \times 10^{12}$ neutrons/cm^2 sec. The flux determined by the Bi-Li standards was $2{\cdot}5 \times 10^{12}$ neutrons/cm^2

sec for the 15-min irradiation and $2{\cdot}3 \times 10^{12}$ neutrons/cm² sec for the 60-min irradiation.

The sample is placed in a crucible inside the quartz furnace, whose outside is cooled by air blowers. About 5 c.c. of hydrogen carrier is added to the furnace. Fig. 1 is a diagram of the gas-extraction and counter-filling system. Carbon crucibles are used for the iron and Li-Bi standards; molybdenum crucibles are used for the stones. An induction heater melts the sample. It was found that all the hydrogen and helium came out of the sample within the first 10 min after it is melted. The gas is pumped from the furnace by an automatic toepler pump.

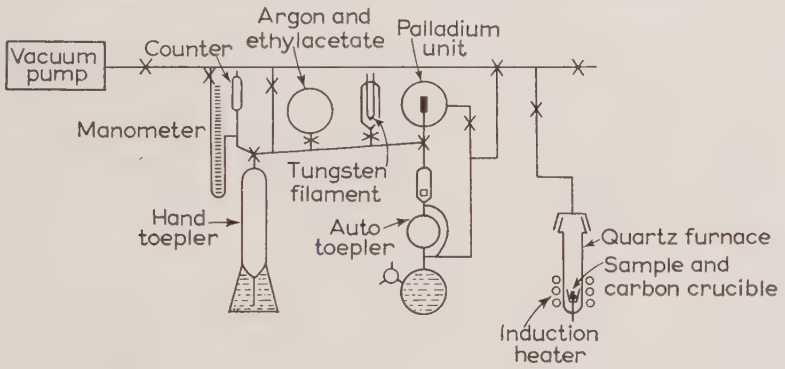

Fig. 1. Extraction and counter filling system.

The hydrogen is extracted from the gas by its passage through a Pd thimble and put into a Geiger counter and counted. The sample is remelted with 5 c.c. of additional H_2 carrier and the process is repeated to check whether any H^3 has remained in the sample, furnace, and Pd unit. The most H^3 ever found in the rerun was 10% of that found in the sample. The gas which has not passed through the Pd is put into a tungsten cracking unit, which decomposes any H_2O vapour or hydrocarbons to H_2. This H_2 is analysed for H^3. Very little H^3 or H_2 was ever found in the cracked gas. The results are summarized in Tables 1 and 3. The number of tritium decays per minute per gram meteorite sample ranged from 30 obtained in the 15-min irradiation of the Pitts surface sample to 44,000 obtained in the 60-min irradiation of Sioux County meteorite.

The neutron activation of the stone meteorites gives much more H^3 per unit flux than the activation of the gas from the stones, indicating that the bulk of the activity arises from its Li^6 content with less than 3% from its He^3 content. The Li^6 content of the stone meteorites ranges from $1{\cdot}13 \times 10^{16}$ atoms/g in Bur Gheluai to $6{\cdot}2 \times 10^{16}$ atoms/g in Sioux County (see Table 3). To check that the H^3 activity is not caused by fast neutrons, a sample of St. Michel and of Charcas were irradiated with a Cd cover. The amount of H^3 produced by fast neutrons is small and is subtracted from the slow-neutron activity. The stone samples are chips taken from near the surface of the meteorite. The Li^6 contents of the chondrites, Bur Gheluai, St. Michel, and Shelburne are lower than that of the achondrites, Sioux County and Nakhla.

The neutron activation of the iron meteorites gives the same amount of H^3 per unit flux as the activation of the gas from the irons. The tritium therefore

results from the He^3 content and not the Li^6 content. The data (see Tables 1 and 2) on the iron meteorites are consistent with an Li^6 content of 10^{14} atoms/g or less. The He^3 content of the iron meteorites ranges from $0{\cdot}38 \times 10^{-6}$ c.c./g in a surface sample of Pitts to $6{\cdot}5 \times 10^{-6}$ c.c./g in a Mt. Ayliff sample. There is variation among

Table 1. Slow-neutron activation of solid iron samples

Iron meteorites	H^3 (decays/g min)	Flux time (10^{15} neuts./cm^2)	He^3 (10^{-6} c.c./g)	Li^6 (10^{16} atoms/g)
Mt. Ayliff (0·7658 g)	236 ± 10	2·25	6·5 ± 0·3	<0·010
Mt. Ayliff (1·907 g surface)	615 ± 50	8·28	4·8 ± 0·5	
Norfolk (1·108 g surface)	145 ± 8	2·25	3·8 ± 0·24	
Norfolk (1·331 g)	708 ± 15	8·28	5·5 ± 0·13	
Norfork (1·34 g surface)	111 ± 5	2·25	2·8 ± 0·15	
Norfork (1·19 g)	790 ± 20	8·28	6·2 ± 0·17	<0·007
Para de Minas (1·58 g)	393 ± 10	2·25	2·8 ± 0·09	<0·010
Charcas (1·71 g)	116 ± 7	2·25	2·9 ± 0·2	<0·005
Charcas (1·85 g)	216 ± 5	8·28	1·3 ± 0·13	
Pitts (1·44 g surface)	30 ± 7	2·25	0·38 ± 0·21	
Pitts (1·48 g)	370 ± 12	8·28	2·6 ± 0·1	<0·004
Terrestrial Fe (1·21 g)	75 ± 6	8·28	0·10 ± 0·08	0·0015 ± 0·0007
Charcas (Cd-covered) (1·2 g)	61 ± 5	8·28		

Table 2. Slow-neutron activation of gas from iron samples

Iron meteorites	H^3 (decays/g min)	Flux time (10^{17} neuts./cm^2)	He^3 (10^{-6} c.c./g)
Mt. Ayliff (4·2 g)	91,700	7·6 ± 1·6	(8·0 ± 1·7)
Mt. Ayliff (0·7658 g)	51,200	5·5 ± 0·5	(6·2 ± 0·6)
Norfork (1·19 g)	50,000	5·5 ± 0·5	(6·1 ± 0·6)
Para de Minas (4·7 g)	29,800	7·8 ± 0·8	(2·5 ± 0·2)
Para de Minas (4·3 g)	24,400	7·6 ± 1·6	(2·2 ± 0·4)
Charcas (1·71 g)	21,700	5·5 ± 0·5	(2·6 ± 0·3)
Pitts (1·48 g)	20,200	5·5 ± 0·5	(2·4 ± 0·3)
Terrestrial Fe (7·5 g)	0 ± 300	7·6 ± 1·6	(0 ± 0·025)

the He^3 contents of different samples taken from the same meteorite. The biggest variation comes at the surface of the meteorite where there is a sharp reduction in He^3 content. A 1·4-g surface sample of Pitts gave $0{\cdot}38 \times 10^{-6}$ c.c./g while a 1·4-g sample taken at 0·5 cm depth gave $2{\cdot}6 \times 10^{-6}$ c.c./g. A 1·34-g sample of

Norfork taken from the surface and extending to about 0·5 cm in the meteorite gave $2{\cdot}8 \times 10^{-6}$ c.c./g of He^3 while a 1·2-g sample taken 1·0 to 1·5 cm from the surface gave $6{\cdot}2 \times 10^{-6}$ c.c./g. Surface samples of Norfolk and Mt. Ayliff also gave somewhat lower He^3 contents than samples 0·5 to 2·0 cm interior. The reduction of He^3 in surface material may indicate a loss of He^3 at the surface due to surface heating of the meteorite in its passage through the atmosphere. Two interior samples of Charcas had He^3 contents of $1{\cdot}3 \times 10^{-6}$ c.c./g and $2{\cdot}9 \times 10^{-6}$ c.c./g.

Table 3. Slow-neutron activation of solid stone samples

Stone meteorites	H^3 (decays/g min)	Flux time (10^{15} neuts./cm^2)	Li^6 (10^{16} atom/g)
Sioux County (0·364 g)	14,100 ± 150	2·25	6·18 ± 0·07
Sioux County (0·191 g)	44,000 ± 300	8·28	5·26 ± 0·04
Nakhla (0·1855 g)	7880 ± 140	2·25	3·33 ± 0·06
Nakhla (0·3653 g)	26,600 ± 150	8·28	3·08 ± 0·02
St. Michel (0·338 g)	3530 ± 70	2·25	1·45 ± 0·03
St. Michel (0·336 g)	12,700 ± 350	8·28	1·40 ± 0·04
Shelburne (0·286 g)	3240 ± 70	2·25	1·30 ± 0·03
Shelburne (0·350 g)	11,650 ± 320	8·28	1·33 ± 0·04
Bur Gheluai (0·218 g)	2820 ± 50	2·25	1·13 ± 0·02
St. Michel (Cd cover)	138	9·00	
Triassic Lava	78,500 ± 1000	8·28	9·38 ± 0·12

B. Slow-Neutron Activation Of Gas From Meteorites

After the hydrogen is extracted from the meteoritic gas, gas from either activated or unactivated samples can be used; it is put into an Al container of 6-in. length and 0·34-in. inside diameter. About 3·5 c.c. of gas is used. If there is less than 3·5 c.c. of meteoritic gas, tank N_2 is added to make 3·5 c.c. To this gas about 3·5 c.c. of tank H_2 carrier is added. The Al-container fillings prepared in this way have about 70-cm pressure. The filling gas is standardized so that the range of the triton from the $n + He^3$ reaction is constant. If less than 40 cm of $H_2 + N_2$ gas pressure is used, a significant number of tritons are lost in the container walls. Standard gas samples having the same amounts of H_2 and N_2 but with varying amounts of He^3 are prepared in other Al containers. These containers are irradiated together in an experimental hole facility of the Brookhaven reactor for ten days. The size of the container precludes the use of the pneumatic-tube facility. Since the containers can only be removed from the pile during a shut-down, a ten-day irradiation is required. The containers are closed with a brass valve which becomes quite radioactive. A wait of one or two days is therefore necessary before a container can be connected to the gas extraction system. This system is similar to the one shown in Fig. 1; however, no quartz furnace or induction heater is required. The irradiated gas is removed from the container and its H_2 is extracted through a Pd thimble. The amount of H_2 is

measured and then counted with a Geiger counter sealed to the line. Some activated samples required several volume dilutions before they could be counted. The counting rates varied from 2790 counts/min for the gas from the 7·5-g terrestrial Fe sample to 220,000 counts/min for the gas from the 4·2-g Mt. Ayliff sample. The H_2 plus N_2 background fillings gave 3000 $\pm$ 300 counts/min. An irradiation with a Cd-covered container gave no background counts, indicating that the background rate is caused by slow neutrons acting on the Li^6 in the container walls rather than by fast neutrons. The data are summarized in Tables 3 and 4. Comparable He^3 contents were obtained for the gas from both stone and iron meteorites. The stone meteorite Nakhla gave the highest He^3 content $(9{\cdot}0 \pm 0{\cdot}2) \times 10^{-6}$ c.c./g, while Sioux County gave the lowest He^3 content $(1{\cdot}3 \pm 0{\cdot}4) \times 10^{-7}$ c.c./g. Two gas samples from the iron meteorite, Mt. Ayliff, gave $(8{\cdot}0 \pm 1{\cdot}7) \times 10^{-6}$ c.c./g and $(6{\cdot}2 \pm 0{\cdot}6) \times 10^{-6}$ c.c./g of He^3, which agree with the solid-sample activation results. These results are also in accord with the measurements by Paneth's group. The gas from Norfork had $(6{\cdot}1 \pm 0{\cdot}6) \times 10^{-6}$ c.c./g of He^3, compared to $(6{\cdot}7 \pm 0{\cdot}2) \times 10^{-6}$ c.c./g obtained in the activation of the solid. The gas from two samples of Para de Minas had $(2{\cdot}5 \pm 0{\cdot}2) \times 10^{-6}$ c.c./g and $(2{\cdot}2 \pm 0{\cdot}2) \times 10^{-6}$ c.c./g of He^3, compared to $(2{\cdot}8 \pm 0{\cdot}1) \times 10^{-6}$ c.c./g obtained in the solid activation. As seen in Table 1, the gas from Charcas had $(2{\cdot}6 \pm 0{\cdot}3) \times 10^{-6}$ c.c./g of He^3, compared to $(2{\cdot}9 \pm 0{\cdot}2) \times 10^{-6}$ c.c./g in the solid, and the gas from Pitts had $(2{\cdot}4 \pm 0{\cdot}3) \times 10^{-6}$ c.c./g, compared to $(2{\cdot}6 \pm 0{\cdot}1) \times 10^{-6}$ c.c./g found in the solid. On the other hand, the gas from the stone meteorites gave much less H^3 activity per unit flux than did the activation of the solid stone samples. Table 3 gives the Li^6 content of the stone meteorites and Table 4 gives their He^3 content. There is no direct relation between the Li^6 content of meteorites and their He^3 content, indicating that spallation rather than slow neutrons have produced the He^3 content of meteorites. A flux of one slow neutron per cm^2 sec in the Sioux County meteorite would have produced $0{\cdot}14 \times 10^{-6}$ c.c./g of He^3 in 2×10^9 years.

4. The H^3 Measurement

In addition to the measurement of stable isotopes, it is of importance to measure some radioactive ones in meteorites. The measurement of H^3 has been suggested (Singer, 1953). Because of the short half life of H^3, one is limited to recent falls; old falls can be used for comparison purposes. Low-level counting techniques with relatively small quantities of hydrogen are required. Since iron meteorites have smaller hydrogen and water contents than stones, the first measurements were attempted with Norfork (1918), Para de Minas (1934), Charcas (1804), and a number of samples of terrestrial irons. The analysis is done with 4- to 10-g samples, so that the several runs can be made with each meteorite. After the hydrogen is counted, it is stored so that the hydrogen can be repurified and the counting repeated.

An 8·6-g sample of Norfork extending from the surface to 1-cm depth had twice as much hydrogen per gram as a 3·5-g sample cut just underneath it. The extra hydrogen is due to the presence of some terrestrial water in the surface oxide. The 8·6-g sample had $0{\cdot}034 \pm 0{\cdot}004$ H^3 decays/g min; the 3·5-g sample

had $0{\cdot}055 \pm 0{\cdot}004$ H^3 decays/g min. The Widmanstätten pattern was through both samples. The meteorite samples are cleaned before their analysis by removing most of the surface oxide with a small dental drill and by washing them in CCl_4. The sample is dried and placed in a graphite crucible that has been degassed by vacuum heating at 1800°C. The crucible is in a quartz furnace whose outside is cooled by air blowers. Fig. 1 is a diagram of the hydrogen-extraction system. It is identical to, although completely separate from, the system used to extract H_2 from irradiated samples.

The sample is first heated to 400°C for 6 hours; the evolved gas is extracted through a cold trap and forced into a Pd purifier. Very little hydrogen but quite a bit of condensable vapours evolve at this temperature. The sample is then

Table 4. Slow-neutron activation of gas from stone samples

Stone meteorites	H^3 (decays/g min)	Flux time (10^{17} neuts./cm^2)	He^3 (10^{-6} c.c./g)
Sioux County (0·191 g)	1500	$8{\cdot}0 \pm 3{\cdot}0$	$0{\cdot}13 \pm 0{\cdot}04$
Nakhla (0·1855 g)	68,300	$5{\cdot}0 \pm 1{\cdot}0$	$9{\cdot}1 \pm 1{\cdot}8$
Nakhla (0·3653 g)	65,500	$4{\cdot}9 \pm 1{\cdot}0$	$8{\cdot}9 \pm 1{\cdot}8$
St. Michel (0·338 g)	54,200	$5{\cdot}5 \pm 1{\cdot}0$	$6{\cdot}6 \pm 0{\cdot}6$
St. Michel (0·336 g)	57,000	$4{\cdot}9 \pm 1{\cdot}0$	$7{\cdot}7 \pm 0{\cdot}6$

heated to 1700°C and the gas extraction continued for 6 hours. The bulk of the noncondensable gases come off when the iron starts to boil. The hydrogen in the noncondensable gas is extracted through a Pd thimble and put into a small Geiger counter. The condensable gases are later cracked over a hot tungsten filament and then put through the same treatment. The counters are filled through the glass tube on one side sealed to the line. About 45-cm pressure of argon-ethyl acetate counting mixture is added to the hydrogen. The counter is then sealed off. Two counters were used; one had only 70% counting efficiency because of end losses, the other had 95% counting efficiency. The counters are copies of ones used by Dr. R. Davis in his neutrino experiment. The counter is placed in a low-level unit which consists of a Hg shield surrounded by a circular array of long anticoincidence Geiger counters which in turn are in a 6-in.-thick iron shield. The data given in Table 5 were taken with the counters in this unit. The data from the top of Table 5 through the 4·7-g Para de Minas sample were taken with the 70%-efficient counter, the rest of the data were taken with the 95%-efficient counter. The counter background with up to 18 cm of tank H_2 is the same as with a plain argon-ethyl acetate filling. It is $0{\cdot}10 \pm 0{\cdot}01$ counts/min. If, however, 20 cm of tank H_2 is put into the counter, its characteristics become poorer and its background goes up to $0{\cdot}13 \pm 0{\cdot}01$ counts/min.

The data given in Table 5 show an increase in the counting rates for the Norfork, Para de Minas, and terrestrial iron samples, but none for the Charcas meteorite. The highest counting rate was $0{\cdot}199 \pm 0{\cdot}009$ counts/min for the hydrogen from the noncondensable gas from the 3·5-g sample of Norfork. The

results for Norfork, Para de Minas, and Charcas are consistent with the idea of tritium in recent meteorites and none in old ones. The 8·6-g sample of Norfork had 0·034 ± 0·004 H^3 decays/g min; the 3·5-g sample of Norfork had 0·055 ± 0·004 H^3 decays/g min. The 4·3-g sample of Para de Minas had 0·022 ± 0·003 H^3 decays/g min; the 4·7-g sample of Para de Minas had 0·024 ± 0·005 H^3 decays/g min. The 11·85-g sample of Charcas had 0·0017 ± 0·0012 H^3 decays/g min, which is more than a factor of 10 smaller than that obtained for Para de Minas and more than a factor of 20 smaller than obtained for Norfork.

The H^3 counts obtained from terrestrial iron samples are puzzling. A 10·1-g

Table 5. Low-level H^3 counts

Sample	Weight (gram)	Source of H_2	Fraction of H_2 counted	Counts/min
Background				0·111 ± 0·010
Background				0·100 ± 0·004
Terrestrial Fe (nails)	7.5	cond. + noncond. + carrier H_2	63%	0·163 ± 0·011
Terrestrial Fe (reheated)	7·5	carrier H_2	100%	0·102 ± 0·008
Terrestrial Fe (hinge)	10·1	cond. + noncond.	100%	0·152 ± 0·006
Norfork (surface)	8·6	noncond.	35%	0·118 ± 0·005
Norfork (surface)	8·6	noncond.	35%	0·123 ± 0·008
Charcas	11·85	cond. + noncond.	100%	0·115 ± 0·010
Norfork (interior)	3·5	noncond.	100%	0·199 ± 0·009
Norfork (interior)	3·5	cond.	100%	0·198 ± 0·010
Background				0·110 ± 0·004
Para de Minas	4·7	cond.	100%	0·154 ± 0·010
Background				0·073 ± 0·016
Para de Minas	4·3	cond.	100%	0·161 ± 0·009
Para de Minas	4·3	noncond.	100%	0·130 ± 0·009
Background				0·110 ± 0·009
Norfork (surface)	8·6	cond.	38%	0·173 ± 0·009
Background				0·114 ± 0·010

sample from an old hinge gave 0·0073 ± 0·0009 H^3 decays/g min, which is a factor of 3 smaller than the amount of H^3 found in Para de Minas and a factor of 6 smaller than that found in Norfork. Some recent nails gave 0·019 ± 0·003 H^3 decays/g min, which is almost as much H^3 as in Para de Minas.

5. Summary and Conclusions

The helium-3 content per gram divided by the tritium decays per year per gram at the time of the meteorite fall, with a correction of about 30% for the He^3 atoms produced directly, gives a H^3-He^3 age for the meteorite. If the data for the 8·6-g and 3·5-g samples of Norfork given in Table 5 are summed and corrected for the time that elapsed from the date of fall of the meteorite to the time when the measurements were made, then 0·293 ± 0·024 H^3 decays/g min occurred in Norfork at the time of its fall. If this H^3 decay is combined with the measured He^3 content of Norfork, a tritium-helium-3 age of $1{\cdot}2 \times 10^9$ years is obtained. A 30%

correction for the He^3 produced directly (Martin, Thomson, and Wardle, 1954) reduces the age to $0{\cdot}9 \times 10^9$ years. The He^3 and H^3 results for the Para de Minas meteorite combine to give $2{\cdot}3 \times 10^9$ years for its tritium-helium-3 age. The 30% correction for direct He^3 production reduces this age to $1{\cdot}7 \times 10^9$ years. The tritium results should be regarded as upper limits until the tritium content of the terrestrial iron samples can be explained.

The H^3-He^3 age is a different type of age than a geologic age such as the K^{40}-A^{40} age. The H^3-He^3 age measures the time of meteorite exposure to cosmic rays, while the K^{40}-A^{40} age measures the time from the solidification of the meteorite. If meteorites resulted from a planetary breakup, the H^3-He^3 age is the time from the breakup while the K^{40}-A^{40} age is the time from the solidification of the original planet. The He^3-H^3 age is based on the assumption of a constant tritium content or that the flux at the meteorite integrated over 25 years is constant. This assumption can be checked by measuring radioactivities of different half-lives such as A^{39}, Cl^{36}, and Be^{10} in meteorites, since A^{39} results from the flux integrated over 500 years, Cl^{36} results from the flux integrated over 600,000 years, and Be^{10} results from the flux integrated over 5×10^6 years.

The tritium content of the iron meteorites combined with the cross-section for tritium production by high-energy protons on iron gives a measure of the flux that bombarded the meteorites. The Norfork meteorite, which has a mass of 1 kg, gives a better measure of the cosmic-ray flux in extraterrestrial space than the Para de Minas meteorite, which has a mass of 112 kg, since less material would have been ablated from its surface. The tritium production cross-section by 2·2 BeV protons on iron is 62 ± 7 mb (Fireman, 1955), by 2·05 BeV protons is 53 ± 8 mb, and by 450 MeV protons is 28 ± 5 mb (Currie, Libby, and Wolfgang, 1955). In 1954, the energy spectrum of the cosmic-ray flux bombarding the earth's polar region was found to extend down to 150 MeV or below (Neher, 1956). In 1949, the energy spectrum of cosmic rays was found to cut off at 1 BeV (Winkler, Stix, Dwight, and Sabin, 1950). In small meteorites (<5 kg mass) the low-energy cosmic rays (200 MeV to 1 BeV) have a large effect on the H^3 production, since their range equals or exceeds the dimensions of the meteorite and their H^3 production cross-section is not negligible. On the basis of the measured cross-sections, the H^3 production in small meteorites would be about 0·1 tritons/g min by the intensity of cosmic rays above 1 BeV striking the earth's poles and about 0·2 tritons/g min by those rays below 1 BeV. This sums to 0·3 tritons/g min, which is the number of tritium decays/g min obtained for Norfork at its time of fall. However, if the bombarding particles have a 1-BeV cut-off, then the flux is three times that striking the earth's polar region. The Para de Minas meteorite, which has a lower H^3 and He^3 content than Norfork, either had more material which shielded it from cosmic rays ablated from its surface or was bombarded by less flux.

The K^{40}-A^{40} age of stone meteorites has been measured to be from $1{\cdot}9 \times 10^9$ to $4{\cdot}5 \times 10^9$ years (Gerling and Pavlova, 1951; Wasserburg and Hayden, 1955; Thomson and Mayne, 1955). No similar type of age measurement has been made for iron meteorites because of their lower K contents. It would be interesting to measure the H^3-He^3 age and the K^{40}-A^{40} age in the same meteorite.

References

Aldrich L. T. and Nier A. O. (1948) *Phys. Rev.* **74,** 1590.
Bauer C. A. (1947) *Phys. Rev.* **72,** 354.
Currie L. A., Libby W. F., and Wolfgang R. F. (1955) *Phys. Rev.* **101,** 1557.
Dalton, Paneth, Reasbeck R., Thomson S. J., and Mayne K. (1953) *Nature* **173,** 1108.
Fireman E. L. and Rowland F. S. (1955) *Phys. Rev.* **97,** 1303.
Gentner W. and Zähringer J. (1955) *Naturforschung* 10c **6,** 498.
Gerling E. K. and Pavlova T. G. (1951) *Dok. Akad. Nauk. SSSR* **76,** 85.
Martin, Thomson, and Wardle (1954) *Phil. Mag.* **452,** 410.
Martin G. R. (1953) *Geochim. et Cosmochim. Acta* **3,** 288.
Mayne K. J., Reasbeck R., and Paneth F. A. (1952) *Geochim. et Cosmochim. Acta* **2,** 300.
Neher H. V. (1956) *Phys. Rev.* **103,** 228.
Singer S. F. (1952) *Nature* 728.
Singer S. F. (1953) *Phys. Rev.* **90,** 168.
Thomson S. J. and Mayne K. I. (1955) *Geochim. et Cosmochim. Acta* **7,** 169.
Wasserburg G. J. and Hayden R. J. (1955) *Phys. Rev.* **97,** 86.
Winkler J. R., Stix T., Dwight K., and Sabin R. (1950) *Phys. Rev.* **79,** 656.

Geochimica et Cosmochimica Acta, 1957, Vol. 11, pp. 263 to 278. Pergamon Press Ltd., London

The distribution of gallium, germanium, cobalt, chromium, and copper in iron and stony-iron meteorites in relation to nickel content and structure

John F. Lovering,* Walter Nichiporuk, Arthur Chodos, and Harrison Brown

Division of Geological Sciences, California Institute of Technology
Pasadena, California

(*Received* 20 *August* 1956)

Abstract—The concentrations of gallium, germanium, cobalt, chromium, and copper have been determined spectrographically in eighty-eight iron meteorites, including representatives from all structural classes, and in nine stony-iron meteorites. The analytical procedures and the structural characteristics of the meteorites studied are described.

It is confirmed that concentrations of gallium in iron meteorites are "quantized" but whereas previous workers found three "gallium groups," four such groups were found in the present work. It has further been found that germanium behaves very much like gallium. Meteorites can be divided into four "germanium groups," each group corresponding to one of the gallium groups.

Compared with gallium and germanium, concentrations of cobalt and copper were found to vary over relatively narrow ranges. Chromium, on the other hand, varies over a range which is fully as great as that observed for gallium. Correlations are observed between the concentrations of cobalt and copper on the one hand, and nickel content and structure on the other, but the relationships are by no means as obvious as they are in the cases of gallium and germanium.

The metal phases of all stony-iron meteorites studied are chemically identical in every aspect with the iron meteorites of the largest "gallium-germanium group," namely that which embraces most of the medium octahedrites and which contains about 15 p.p.m. gallium and 38 p.p.m. germanium.

1. Introduction

Goldberg, Uchiyama, and Brown (1951) analysed forty-five iron meteorites for gallium using the neutron activation technique and found that the gallium levels are apparently concentrated in three well-separated regions: Region I 45–100 p.p.m.; Region II 17–22 p.p.m.; Region III 1·7–2·5 p.p.m. It was found further that this distribution can be correlated with the structures and with the nickel contents of the meteorites.

The behaviour of palladium and gold was found to be quite different from that of gallium. While the gallium concentration in general decreases with increasing nickel concentration and decreasing kamacite band width, palladium and gold concentrations increase. It was found further that for a given nickel content the meteorites belonging to gallium class II possess lower palladium and gold contents than do the meteorites belonging to gallium classes I and III.

The apparent existence of discrete groups of iron meteorites raises a number of interesting questions concerning the origin of meteorites and the relationship between meteorites and the earth. In view of this, it was deemed worthwhile to undertake a new study of the distribution of gallium in iron meteorites using an independent analytical method and a different assemblage of meteorites. At the same time the study was extended to embrace the elements germanium, chromium, and copper.

* Present address: Department of Geophysics, The Australian National University, Canberra, Australia.

Germanium and chromium have been previously studied in iron meteorites by Goldschmidt (1930), by Goldschmidt and Peters (1931, 1933a, and 1933b), and by I. and W. Noddack (1931). Farrington (1907) averaged the existing

Table 1. Germanium and chromium contents of the metal phase of iron and stony-iron meteorites as found by Goldschmidt (1930) and by Goldschmidt and Peters (1931, 1933a, and 1933b)

Meteorite	Type	Ge (p.p.m.)	Cr (p.p.m.)
Canyon Diablo	Og	1000	500
Cape York	Om	100	
Coahuila	H	500	500
Corrizatillo	Om	500	100–500
Cranbourne	Og	100–1000	
Russel Gulch	Of	100–500	500
Santa Catharina	D_1	0	
Toluca	Om	100–500	100
Brenham	P	100	
Estherville	M	10–100	

Table 2. Copper and germanium contents of iron meteorites as found by I. and W. Noddack (1931)

Meteorite	Type	Cu (p.p.m.)	Ge (p.p.m.)
Canyon Diablo	Og	100	180
Gibeon	Of	450	300
Toluca	Om	150	100

Table 3. Average germanium, chromium, and copper contents of iron meteorites as determined by previous workers

Element	Farrington (1907)	I. and W. Noddack (1930)	Goldschmidt and Peters (1933a, 1933b)
Germanium (p.p.m.)		240	500
Chromium (p.p.m.)	100	240	300
Copper (p.p.m.)	200	305	

analyses for chromium and copper, and I. and W. Noddack (1930, 1931) studied the distribution of copper in a number of meteorites. The results of the earlier workers are shown in Tables 1, 2, and 3.

More recently YAVNEL' (1954) studied the distribution of a number of elements in the Sikhote-Alin meteorite. The concentration ranges and average values observed by him are shown in Table 4.

Table 4. Concentrations of nickel, cobalt, germanium, and copper in the Sikhote-Alin meteorite according to YAVNEL' (1954)

Element	Nickel	Cobalt	Germanium	Copper
Range of concentrations	3·80–7·58%	0·44–0·62%	100–250 p.p.m.	70–790 p.p.m.
Average concentration	5·68 ± 0·68%	0·49–0·04%	140 ± 30 p.p.m.	300 ± 170 p.p.m.

2. Analytical Methods

1. *Sampling*

Samples were obtained by drilling the cleaned surfaces of the meteorites with a tungsten carbide drill $\frac{1}{8}$ in. in diameter. Drilling was performed in as random a manner as possible, care being taken to avoid inclusions of troilite, cohenite and schreibersite. In order to avoid silicate contamination when drilling the metal phase of stony-iron meteorites, only those metallic areas were chosen which measured at least 4 mm. across.

Six samples ranging in weight from 90 to 150 mg. were obtained from each meteorite, three for nickel analysis, and three for spectrographic analysis. In sections of small surface area drillings were made as close to each other as one centimetre or less and in those of large surface area the drillings were as far apart as 10 to 35 cm. A spectrographic check for possible contamination introduced by the drill tip showed that of all elements with which we were concerned, only copper was present at as high a level as 2 p.p.m.

2. *Sample treatment*

The samples were brought into solution in 100-ml pyrex breakers which prior to their use had been thoroughly washed and kept for an hour in hot concentrated nitric acid. The samples were brought into solution in six-normal nitric acid. The acid was obtained by diluting concentrated nitric acid, which has been distilled under vacum in a quartz still, with quadruply distilled water. If there was a noticeable residue, the volume of the solution was reduced, concentrated nitric acid was added and the solution was allowed to boil gently for about an hour until the residue disappeared or was very small. 100 p.p.m. of indium and 500 p.p.m. of palladium as nitric acid solutions were then added as internal standards. The solutions were evaporated to about 10-ml then transferred to small Vycor crucibles in which they were evaporated to dryness. The samples were then ignited at 400°C for 15 min.

3. *Preparation of standards*

All metals and oxides used in this work were "Specpure" grade obtained from Johnson, Matthey and Co., Ltd. Two series of standards were prepared: one containing gallium in concentrations ranging from 1 to 100 p.p.m., with 100 p.p.m. of indium as an internal standard; another containing cobalt from 0·1 to 1·0%, chromium from 1 to 700 p.p.m., copper from 50 to 700 p.p.m., and germanium from 1 to 700 p.p.m., with 500 p.p.m. palladium as an internal standard. In both series, the investigated elements were present in a matrix made up of 91% iron and 9% nickel. The standard solutions were converted to oxides in the same manner as the samples of meteorites, thus assuring close physical and chemical resemblance of both samples and standards.

4. *Nickel*

Nickel was determined in all meteorites by the method utilized by Henderson (1941). The results reported here are directly comparable with all of those determined by Henderson and also those reported by Goldberg, Uchiyama, and Brown (1951). Nickel analyses were made on three samples from each meteorite.

5. *Spectrographic equipment*

All other elements were determined spectrographically using a Jarrell-Ash 3·4 m Stigmatic Grating spectrograph supplied with a 6-in. diameter 15-thousand-lines-per-inch grating. The grating gives a linear dispersion of 5·2 Å/mm in the first order of the visible spectrum. Regular graphite electrodes were used together with a d.c. arc source.

6. *Spectrographic methods*

Gallium. In order to obtain a sensitivity of 1 p.p.m. for gallium in a matrix of iron and nickel oxides, it was necessary to resolve Ga 4032·98 Å from Fe 4032·63 Å plus Mn 4033·07 Å and reduce background from cyanogen. This was accomplished by use of a 10 micron slit, a 3 ampere d.c. arc, and selective volatilization of gallium and indium from the matrix as well as the addition of a quantity of sodium. (Ahrens (1954) suggested the use of indium and palladium as internal standards in silicate analysis. Moving plate studies indicated their suitability in this application.) The standards and samples were ground with a mixture of 10% sodium carbonate and 90% quartz. For the range 1 to 10 p.p.m. of gallium, the proportions were 2 parts of sample to 3 parts of sodium carbonate in quartz and for the range 10 to 100 p.p.m., one part of the sample was mixed with 4 parts of sodium carbonate in quartz. Sodium is very volatile and acts as a carrier for both gallium and indium as well as cooling the arc and suppressing background due to cyanogen. Quartz serves as a diluent, as an intermediate between the volatiles and the matrix, and as a flux to form a bead with the matrix. A 25-mg sample was used in a deep graphite anode. The 90 seconds exposure was started with the appearance of the sodium flame. The sample was not completely consumed. The Eastman Kodak III-O plate was developed for 4 minutes at 20°C in DK-50 developer. The intensity ratio of Ga 4032·98 Å to In 3256·09 Å was used as it was found to give the same results as the ratio using In 4511·32 Å. The standard deviation of the method was determined from a large number of replicates of different samples and is 9%.

Cobalt, chromium, copper, and germanium. For these elements sensitivity and matrix interferences were no problem. Graphite powder was used as a diluent to reduce selective volatilization and give good burning control. One part of sample was mixed with 4 parts of graphite using ether as a contact medium. For greater sensitivity for chromium and germanium in the range of 1 to 10 p.p.m., the proportion of sample to graphite was changed to 1 : 2. The sample weight was 20 mg. A 5-ampere d.c. arc was used, and exposure time was 90 seconds. The sample was not completely consumed. Palladium 3242·70 Å was used as the internal standard line with Ge 2651·18 Å, Ge 3039·06 Å, Co 3044·00 Å, Cr 4254·35 Å, and Cu 3273·96 Å. The standard deviations are 9% for germanium, 12% for copper and chromium, and 5% for cobalt.

7. *Precision and accuracy*

Goldberg, Uchiyama and Brown (1951) found that the standard deviation of the method for nickel analysis used by them and also used here was about 0·5% when applied to a carefully controlled series of runs on the Canyon Diablo meteorite. It is likely that the nickel results reported here have about the same degree of reproducibility. Of course, from time to time substantially greater differences will be found between one run and another arising in part from the inhomogenity of the samples as well as from contamination of the samples with schreibersite and cohenite.

Some additional information concerning the accuracy of the nickel determinations was obtained from the analysis of a synthetic solution containing 89·40% iron, 9·80% nickel, and

0·80% cobalt. Three aliquots of this solution were analysed by precipitation with ammonium acetate instead of ammonium hydroxide. On the average recovery amounted to 101·6% of the nickel present in the sample. Thus it seems that small amounts of undesirable constituents might frequently accompany nickel in the precipitate and give rise to results which, although internally comparable, are consisently somewhat too high.

In order to obtain some indication regarding the accuracy of the spectrographic methods, a comparison was made of the cobalt and gallium results on several meteorites with the results obtained by Goldberg, Uchiyama, and Brown (1951). In addition, several meteorites were submitted to E. B. Sandell and H. Onishi of the University of Minnesota for gallium analysis.

Table 5. Cobalt and gallium contents of iron meteorites as determined by different methods of analysis

			Cobalt %		Gallium (p.p.m.)		
	Name	Type	Spectrographic	Chemical	Spectrographic	Neutron activation Goldberg *et. al.* (1951)	Photometry Sandell and Onishi
1	Admire	P	0·50		18	21·4	
2	Altonah	Of	0·42	0·44	1·7	2·31	2·8, 2·6
3	Arispe	Og	0·48	0·49	51	55·6	
4	Bear Creek	Om	0·51	0·67	15	17·5	
5	Bristol	Off	0·44	0·49	2	2·41	
6	Canyon Diablo	Og	0·49	0·50	74	76·3	87
7	Carlton	Of	0·50		10	13	
8	Coahuila	H	0·45	0·53	54	64·5	
9	Duchesne	Of	0·38		2·2		2·6
10	Edmonton	Off-Of	0·57	0·73	22	24·7	
11	Goose Lake	Om	0·52	0·69	57	75·1	
12	Henbury	Om	0·49	0·70	60	17·2	71, 80, 70
13	Huizopa	Of	0·38	0·67	2·8	2·49	
14	Indian Valley	H	0·45	0·50	56	62·9	
15	Maria Elena	Of	0·40	0·53	2	1·76	
16	Perryville	D anom.	0·54	0·68	19	37·9	36, 43, 42
17	Pinon	D_1	0·59	0·87	2·9	2·39	
18	Sacramento Mtns.	Om	0·48	0·55	19	20·4	
19	Sandia Mtns.	Hbc	0·49	0·53	53	56·5	
20	Spearman	Om	0·58	0·56	19	21·4	24
21	Springwater	P	0·60		15	17·9	
22	Tazewell	Off	0·60	0·70	3·2	5·20	
23	Toluca	Om	0·45	0·53	61	55·2	

The analyses were made using a sensitive colour and fluorescence reaction of gallium with rhodamine B as described by Onishi (1955). The comparisons presented in Table 5 show that cobalt determined spectrographically is consistently lower relative to cobalt determined gravimetrically as sulphate by about 17%. As for gallium, it is clear that the spectrographic method yields values which are lowest compared with those obtained by the neutron activation and the fluorescence analysis method. The neutron activation results represent roughly an average of the two extremes. The more serious discrepancy is the case of the Henbury and Perryville meteorites which were investigated in more detail. The results obtained definitely discount the possibility of experimental error, and indicate strongly that mislabelling of the specimens

in our possession occurred either during the present or previous work. A part of the collection used in this work was moved from Chicago to Pasadena in 1952, and it is possible that the meteorites in question were mislabelled at that time.

In order to obtain a check on the germanium results by an independent method, the samples were submitted to S. A. Wardani of the Scripps Institution of Oceanography, who analysed them by measuring the absorbance of the phenylfluorene complex. The results are shown in Table 6 from which it can be seen that the spectrographic results are lower than the colorimetric results by an average of 30%.*

Table 6. Germanium results obtained by two different methods

Name	Type	Germanium	
		This work	S. A. Wardani (1956)
Canyon Diablo	Og	283	353
Duchesne	Of	<1	0·8
Edmonton	Off-Of	26	38.6
Henbury	Om	209	275
Magura	Og	345	519
Tlacotepec	D_1	<1	0·5
Toluca	Om	170	270

3. Measurement of Kamacite Band-widths

The measurement of the widths of kamacite bands may yield widely different results, depending on whether the plane of the examined section is parallel to the cubic, octahedral, or dodecahedral face of an octahedron, representing in a single crystal of taenite the planes of kamacite. In this work the thickness of the kamacite bands has been measured as a function of the angles between the system of Widmanstatten bands. These angles determine the orientation of the section plane with respect to the structure octahedron. The measurements were made with the aid of angle data published by Belayev (1923).

In this work the mean apparent band widths of sixty-three octahedrites were determined. At least six measurements were made on each system of bands, and the mean of these values was then calculated. Bands wider than twice the width of the smallest bands measured were discarded. This procedure resulted in exclusion of band-widths larger than 2·3 mm. For a few octahedrites, the band widths were taken from the literature when the description appeared to be adequate.

The results expressed as a logarithmic frequency-distribution curve are shown in Fig. 1. The three frequency maxima and the two minima which are clearly evident suggest that with respect to band-widths there are three major groups of octahedrites: a group possessing band-widths narrower than about 0·5 mm,

* *Note added in proof:* We have learned that A. A. Smales of the Atomic Energy Research Establishment at Harwell has recently determined the concentrations of chromium, copper and germanium in several iron meteorites supplied by us, using the neutron activation method. His results are in substantial agreement with the results reported here.

an intermediate group covering band-widths 0·5 to about 2 mm, and a group possessing band-widths greater than about 2 mm. As we shall see later, these three groups which are defined solely on the basis of structure can be correlated with groups of meteorites which are defined solely on the basis of chemical composition.

As is well known, the system of band-width classification which was defined by Brezina (1885) and which has been generally used since, is arbitrary and

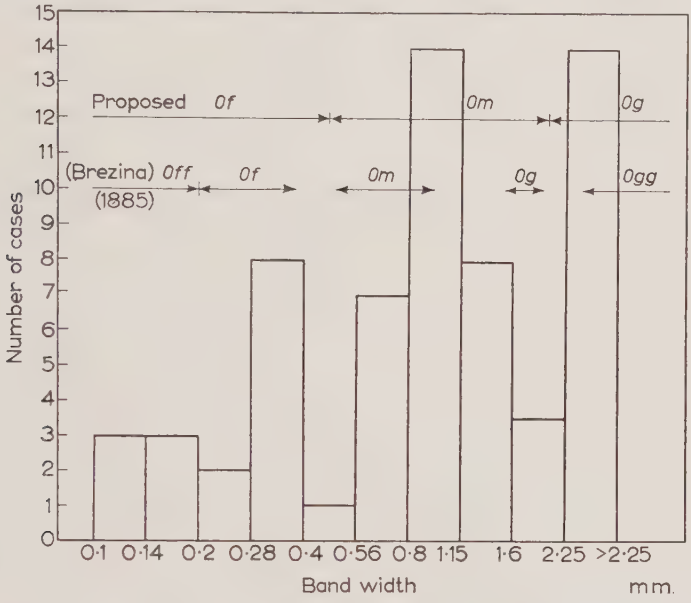

Fig. 1. Distribution of mean apparent band width in octahedrites.

the boundaries between classes are without physical basis. The present work suggests that the division of octahedrites on the basis of structure into only

Table 7. Classification of octahedrites

Type	Kamacite band widths in mm	
	Brezina (1885)	Proposed
Coarsest octahedrites (Ogg)	2·5	—
Coarse octahedrites (Og)	1·5–2·5	>2·0
Medium octahedrites (Om)	0·5–1·0	0·5–2·0
Fine octahedrites (Of)	0·15–0·4	0·05–0·5
Finest octahedrites (Off)	0·05–0·10	—

three groups represents a more natural division, and one which, from many points of view, is more convenient.

Table 8. Content of nickel, cobalt, chromium, copper, gallium, and germanium in iron meteorites

	Name	Type		Ni %	Co %	Cr p.p.m.	Cu p.p.m.	Ga p.p.m.	Ge p.p.m.
		Prior	This Work						
1	Altonah	Of	Of	8·56	0·42	45	132	1·7	<1
2	Arispe	Ogg	Og	6·77*	0·48	46	110	51	233
3	Arltunga	Dm	D (anom)	10·08	0·63	73	307	30	68
4	Ballinoo	Off	Of	10·06	0·54	59	253	44	91
5	Basedow Range†	?	Om	7·42	0·48	88	187	15	30
6	Bear Creek	Of	Om	10·14*	0·51	1·2	154	15	25
7	Bendego	Og	Og	6·8*	0·44	32	174	47	203
8	Bingara No. 2	D_2	H	5·75	0·54	33	118	66	170
	Bingara No. 3	D_2	H		0·46	55	107	46	126
	Bingara No. 4	D_2	H	5·66	0·45	53	139	45	143
9	Bischtübe	Og	Og	6·52	0·42	23	112	50	157
10	Bugaldi	Of	Of	8·99	0·48	44	95	<2	<1
11	Boxhole	Om	Om	7·72	0·50	62	133	13	31
12	Bristol	Off		8·15*	0·44	111	333	<2	<1
13	Canyon Diablo	Og	Og	7·18*	0·49	7·4	157	74	283
14	Carlton	Of	Of	12·68*	0·50	3·8	199	10	19
15	Casas Grandes	Om	Om	7·73	0·48	51	157	17	30
16	Coahuila	H	H	5·65	0·45	44	122	54	152
17	Coolac	Og	Og	6·95	0·53	4·6	158	93	335
18	Coopertown	Om	Om	9·12*	0·49	49	113	17	32
19	Cowra	Off	D_1	13·72	0·70	40	193	82	15
20	Coya Norte	H	H	5·5*	0·51	48	123	56	144
21	Cranbourne No. 9	Og	Og	7·18	0·48	4·0	119	79	262
	Cranbourne No. 10	Og	Og	7·05	0·51		194	80	343
22	Cuernavaca	Of	Of	8·76*	0·59	3·3	120	13	32
23	Deep Springs	D_1		13·44*	0·68	182	205	<2	<1
24	Delegate	Om-Og	Om	9·34	0·58	<5	102	19	48
25	Descubridora	Om		9·07*	0·56	75	148	13	49
26	Duchesne	Of	Of	9·12*	0·38	10	127	2·2	<1
27	Edmonton	Off-Of		12·66*	0·57	1·7	396	22	26
28	Forsyth County	D_2	D_2	5·55*	0·47	51	123	57	162
29	Four Corners	Obc		9·57*	0·54	2·6	248	48	141
30	Gibeon	Of	Of	7·96	0·39	200	185	2·0	<1
31	Gladstone	Ogg	Og	6·74	0·51	5·3	148	93	410
32	Glenormiston	Ombc (?)	Ob	7·12	0·52	<1	187	13	73
33	Goose Lake	Om-Og	Om	8·46*	0·52	17	390	57	221
34	Gundaring	Og-Ogg	Om	8·32	0·61	48	156	19	38
						<1			
35	Henbury	Om	Om	7·66*	0·49	(15)	186	60	209
36	Hex River	H	H	5·68*	0·47	30	105	45	143
37	Huizopa	Of	Of	7·81	0·38	233	135	2·8	<1
38	Indian Valley	D_2bc-H	H	5·64*	0·45	42	108	56	160
39	Kyancutta	Om	Om	8·28	0·59	27	231	19	42
40	Magura	Og	Og	7·08*	0·46	5·2	123	82	345
41	Maria Elena	Of		7·71*	0·40	392	140	<2	<1
42	Misteca	Om	Om	8·21*	0·55	61	146	17	41
43	Moonbi	Of	Om-Of (anom)	7·99	0·43	350	201	6·0	<1
44	Mooranoppin	Ogg	Og	6·91	0·50	<1	175	79	396
45	Mount Dooling	Om	Og	6·41	0·48	28	166	61	193
46	Mount Edith	Om	Om	9·40	0·55	<1	147	15	33
47	Mount Magnet	Off	D_1	14·72	0·54	<1	162	6·4	<1
48	Mount Stirling	Og	Og	6·93	0·55	7·2	225	63	409

Table 8 (*continued*)

	Name	Type		Ni %	Co %	Cr p.p.m.	Cu p.p.m.	Ga p.p.m.	Ge p.p.m.
		Prior	This Work						
49	Mount Tabby (2)	O	Og	6·82	0·51	44	125	50	202
50	Mungindi No. 1	Off	Of	12·18	0·56	5·8	285	10	24
	Mungindi No. 2	Off	Of	12·36	0·56	3·7	230	13	23
51	Murnpeowie	granular metabolite	Og	6·47	0·47	187	157	42	76
52	Murphy	H	H	5·52*	0·45	46	116	40	145
53	Narrabura	Off	Om-Of (anom)	10·22	0·59	<1	157	8·2	29
54	Negrillos	H	H	5·32*	0·46	80	113	55	136
55	N'Goureyma	Obc		9·26*	0·56	80		<2	<1
56	Nocoleche	Om	Og	6·42	0·47	101	124	43	134
57	Osseo	Ogg	Og	6·51*	0·47	17	125	82	313
58	Perryville	Off (?)	D (anom)	8·88*	0·54	97	285	19	77
59	Pinon	D_1	D_1	16·58*	0·59	112	37	2·9	<1
60	Providence	Og	Om	10·30*	0·50	21	120	19	33
61	Rio Loa	H	H	5·70*	0·56	36	189	47	228
62	Roebourne	Om	Om	8·04	0·56	44	190	15	49
63	Roper River	?	Om	9·91	0·58	4·9	168	15	32
64	Sacramento Mnts.	Om	Om	8·10*	0·48	22	165	19	29
65	San Angelo	Om		7·86*	0·53	100	181	8·7	39
66	Sandia Mnts.	Hbc	H	5·94*	0·49	25	123	53	143
67	Santa Rosa	D_2-Obc	Og	6·52*	0·48	60	121	49	167
68	Sao Juliao de Moreira	Ogg	Og	6·02*	0·47	1·5	79	35	73
69	Scottsville	H	H	5·33*	0·47	43	113	58	132
70	South Byron	D_1		13·47*	0·92	21	370	13	51
71	Spearman	Om	Om	8·39*	0·58	28	176	19	53
72	Tawallah Valley	D_1	D_1	18·21	0·69	54	<30	1·0	<1
73	Tazewell	Off		16·69*	0·60	<1	400	3·2	<1
74	Temora	Ogg	Og	6·66	0·45	2·6	112	93	355
75	Thunda	Om	Om	8·27	0·51	2·5	145	13	39
76	Tieraco Creek	Of-Om	Of	10·55	0·60	<1	110	13	23
77	Tlacotepec	D_1	D_1	16·23*	0·74	168	<30	<2	<1
78	Toluca	Om	Om	8·31*	0·45	4·9	125	61	170
79	Tucson	D		9·07*	0·46	2360	134	<2	<1
80	Uwet	H	H	5·70	0·47	28	134	43	164
81	Wallapai	Of		9·12*	0·73	22	253	74	76
82	Wedderburn†	?	D_1	22·2	0·63	<1	580	1·8	<1
83	Weekeroo	Ogb	Ob	7·51	0·44	<1	168	32	60
84	Willamette	Om	Om	8·30*	0·45	51	112	17	29
85	Wonyulgunna	Om	Om	9·05	0·51	1·2	118	13	34
86	Yarroweyah	D_2	D_2	5·70	0·48	67	144	48	154
87	Yenberrie	Og	Og	6·97	0·49	2·6	132	88	344
88	Youndegin	Og	Og	6·92	0·49	2·5	155	88	322

* Previous work.
† Not described in literature.

The proposed classification for octahedrites is compared with that of Brezina in Table 7. It will be noted that the proposed Of class embraces all of Brezina's Of and Off. The proposed Om class embraces all of Brezina's Om and some of his Og. The proposed Og class embraces the balance of Brezina's Og and all of his Ogg.

The etched surfaces of the metal phases of the stony-iron meteorites investigated in this study show structures which depend upon the size of the surface area. Although it was not possible to draw a clear distinction between the small and large surface areas, it appeared certain that the areas measuring 3 mm across or less, are very abundant. The patterns brought out by etching show zonal arrangement of the structural components, the outlines of each being roughly parallel to the boundaries of the metal areas. The arrangement is as follows: (1) grey border of kamacite adjoining the silicate (0·5 mm or more); (2) a very thin zone of silvery taenite; (3) a usually large, dark grey, core of dense plessite.

The pallasites which have metal areas two or more centimetres across (e.g. Newport) or which grade into octahedrites (e.g. Brenham and Glorieta Mountain) show structures that are essentially similar to those possessed by medium octahedrites. The plessite occurs in the form of trapeze-like or rectangular elongated areas (the Newport pallasite) bounded by a thin border of taenite, and which are scattered on the background of a medium Widmanstätten structure.

Table 9. Content of nickel, cobalt, chromium, copper, gallium, and germanium in the metal phase of stony-iron meteorites

Name	Type	Ni %	Co %	Cr p.p.m.	Cu p.p.m.	Ga p.p.m.	Ge p.p.m.
1. Admire	P	12·45	0·50	8·3	233	18	34
2. Albin	P	10·43	0·57	4·5	223	23	30
3. Bendock	P	9·20	0·58	<1	143	16	40
4. Brenham	P-O	10·98	0·60	<1	168	19	63
5. Glorieta Mtn.	Om-P	11·79*	0·54	2·7	217	12	18
6. Imilac	P	11·32	0·47	<1	190	19	41
7. Newport	P	10·83	0·58	<1	240	17	29
8. Pinnaroo	M	9·50	0·51	52	200	19	60
9. Springwater	P	13·16	0·60	<1	174	15	38

* Previous work.

Zavaritskii and Kvasha (1952) while studying the structure of the Pallas Iron, observed metal sites which show either concentric or the usual octahedral arrangement of the structural components. In the concentric arrangement the thickness of the olivine-adjacent border of kamacite is of the order of tenths of a millimetre, and that of the plessite-surrounding rim of taenite is of the order of hundredths of a millimetre. In the usual octahedral arrangement the width of the kamacite bands is from 0·01 to 0·02 mm, although in some metallic sites the structure becomes still finer, and slowly grades into plessite with micro-octahedral or even submicroscopic cryptocrystalline (felsitic) structure.

4. Results and Correlations

The concentrations of nickel, cobalt, gallium, germanium, chromium, and copper in eighty-eight iron meteorites, together with the observed structures

are given in Table 8. The corresponding concentrations in the metal phase of nine stony-iron meteorites are given in Table 9.

Uniformity of individual iron meteorites

Goldberg, Uchiyama and Brown (1951) showed that individual iron meteorites have compositions which appear to be quite uniform, and that variations within a single meteorite are small when compared with variations among meteorites. More recently, Yavnel' (1954) conducted an extensive investigation of the uniformity of the Sikhote-Alin hexahedrite, which fell in 1947. He made quantitative spectrographic determinations of nickel, cobalt, copper, and germanium in sixty samples obtained from a single specimen of the meteorite, and he further made determinations in triplicate of the same elements in specimens representing twenty different sites within the elliptical area of the dispersion of the shower. His results are shown in Table 10 from which it can be seen that the averages and the errors as expressed by the standard deviations are practically identical in both cases. Yavnel' concludes that the investigated elements are distributed fairly uniformly throughout the Sikhote-Alin meteorite, and that differences between individual samples lie generally within the limits of experimental error.

In this work, three samples were taken from each iron meteorite at points situated at various distances from each other. In most cases, the variations between samples were found to be less than 10%, and in only one case (chromium in the Sandia Mountains hexahedrite) was the variation as large as 20%. When we take into account the fact that errors were contributed by the chemical and

Table 10. Variations in the composition of the Sikhote-Alin meteorite according to Yavnel' (1954)

	Ni (%)	Co (%)	Cu (p.p.m.)	Ge (p.p.m.)
Average of 60 samples from one specimen	5·68 ± 0·68	0·49 ± 0·04	300 ± 170	140 ± 30
Observed range	4·32–7·58	0·44–0·62	70–790	100–250
Average of 20 samples from 20 specimens	5·63 ± 0·68	0·49 ± 0·03	350 ± 200	130 ± 30
Observed range	4·74–8·04	0·44–0·56	70–880	100–220

spectrographic procedures, we must conclude that the chemical compositions of individual iron meteorites are quite uniform, provided that the samples are sufficiently large to give representative portions of both kamacite and taenite.

Gallium and germanium groups

The gallium contents of iron meteorites are plotted against the nickel contents in Fig. 2. It can be seen that the observation of Goldberg, Uchiyama, and Brown (1951) to the effect that gallium levels are concentrated in several well-separated regions, is fully confirmed. We have found further, that the previous authors' gallium Group I, the meteorites of which they listed as having concentrations of gallium ranging from 45 to 100 p.p.m. is in reality a mixture of two

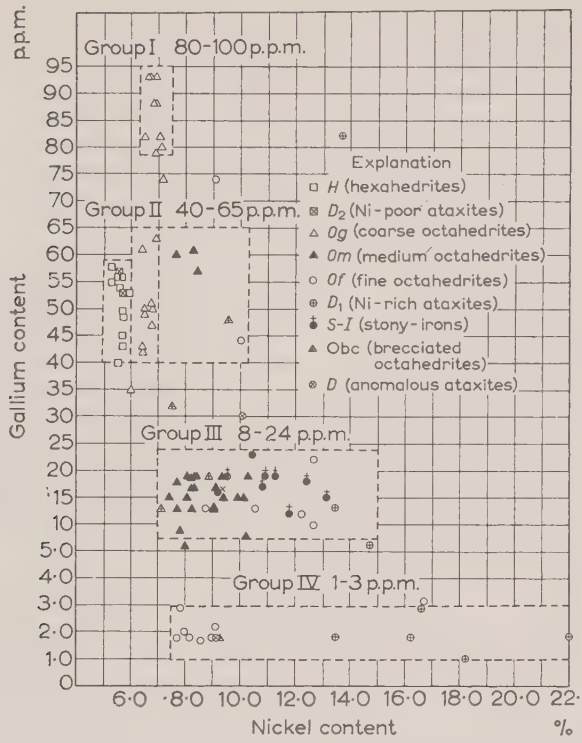

Fig. 2. Variation of gallium content of meteorites with nickel content.

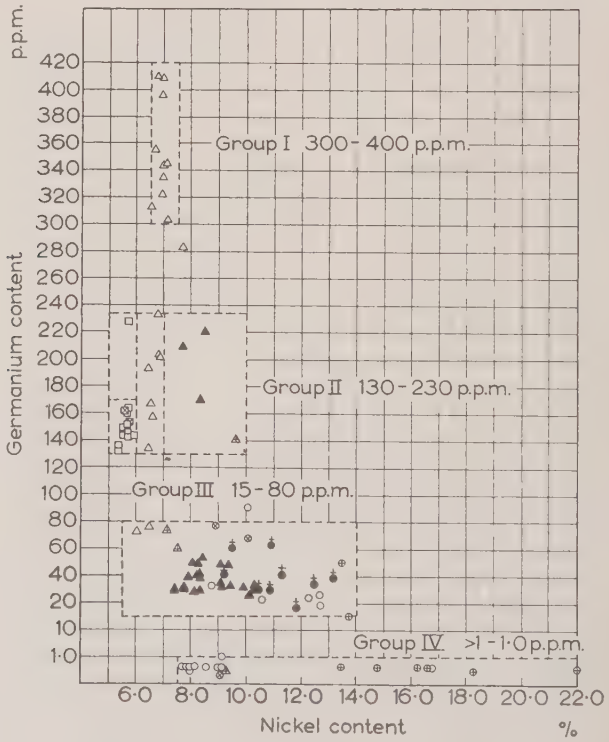

Fig. 3. Variation of germanium content of meteorites with nickel content.

distinct groups. The meteorites of the first group possess gallium concentrations ranging between 80 and 100 p.p.m. and those of the second possess concentrations ranging between about 40 and 65 p.p.m.

It is also apparent from the present work, that iron meteorites fall into separate groups on the basis of their germanium contents, as shown in Fig. 3, and that the gallium and germanium groups correspond exactly with each other

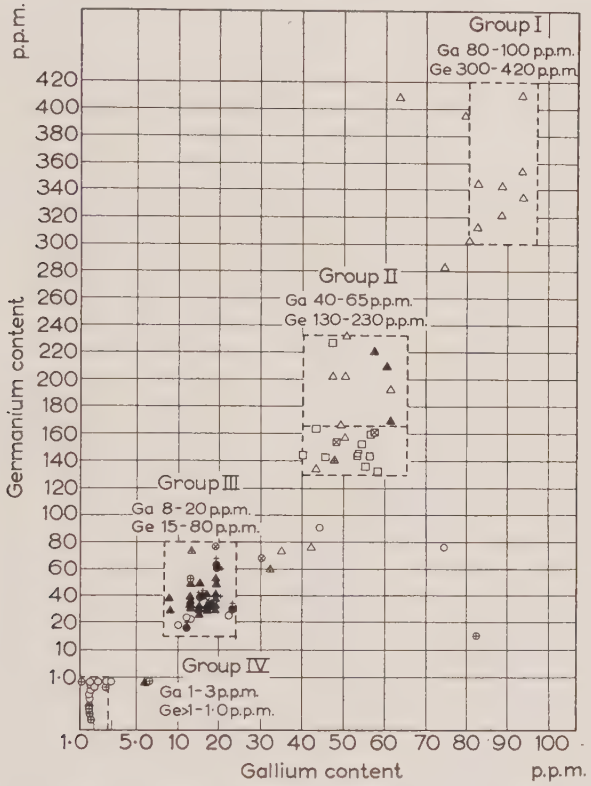

Fig. 4. Relation between gallium and germanium contents of meteorites.

This can be seen clearly in Fig. 4, where germanium concentrations are plotted against gallium concentrations.

The ranges of concentration associated with each of the groups are as follows:

	Ga (p.p.m.)	Ge (p.p.m.)
Group I	80–100	300–420
Group II	40–65	130–320
Group III	8–24	15–80
Group IV	1–3	<1–1

Of the eighty-eight iron meteorites studied, eleven are anomalous in that they do not belong to any of the above groups.

It is of interest that the ratio of germanium to gallium decreases from 4:1 for the meteorites of Group I to 3:1 for those of Group II, to 2:3 for those of Group III, and to ≤ 1 for those of Group IV.

When the structure of the meteorites belonging to each of the gallium-germanium groups are examined, it is found that without exception the meteorites of Group I possess kamacite bands which are wider than 2 mm, and thus by our proposed classification are coarse octahedrites. The remaining coarse octahedrites belong to Group II as do all hexahedrites and nickel-poor ataxites. Only three medium octahedrites belong to Group II while the balance amounting to more than 90% belong to Group III. The meteorites of fine structure are about evenly divided between Groups III and IV, while Group IV contains only meteorites of fine structure together with the nickel-rich ataxites.

It should be noted that it is possible for meteorites to possess identical nickel contents and to belong to different gallium-germanium groups. It is also possible for meteorites to possess identical nickel contents and markedly different structures.

Cobalt, chromium, and copper

When compared with gallium and germanium, concentrations of cobalt vary over a very narrow range. The cobalt contents of most meteorites appear to lie in the range of 0·38 to 0·75%. In general, the concentration of cobalt increases with increasing nickel concentration. There appears to be some relationship between cobalt concentration and structure, but aside from this, there does not appear to be any clear-cut relationship between cobalt concentrations and the gallium-germanium groups.

Chromium exists primarily in the silicate and sulphide phases of meteorites with the result that concentrations of the element in the metal phase are generally small. Unlike cobalt, concentrations of chromium vary over a wide range. Several of the high chromium values found in this work probably resulted from the presence of minute silicate or sulphide inclusions in the samples, but those values which fell below about 110 p.p.m. probably represent true variations in the concentration of chromium in the metal phase. The chromium content appears to be independent of the nickel content and there is no obvious relationship between chromium concentration and either structure or gallium-germanium groups.

Copper varies generally over a narrow range from about 100 to 260 p.p.m. There appears to be very little relation between copper concentration and nickel concentration, but some dependence upon structure is evident. The hexahedrites the nickel-poor ataxites and the coarse octahedrites, for example, possess relatively low concentrations of copper, while the fine octahedrites and nickel-rich ataxites possess relatively high concentration of the element. It is notable, however, that three meteorites (Piñon, Tlacotepec, and Tawallah Valley) possess only about 30 p.p.m. There does not appear to be a clear-cut relationship between copper concentrations and the gallium-germanium groups.

Stony-iron meteorites

GOLDBERG, UCHIYAMA, and BROWN (1951) observed that the Admire and Springwater pallasites possess nearly identical gallium contents and are similar

in nearly all respects to the large group of medium octahedrites belonging to our gallium-germanium Group III. This work confirms the earlier observations on Admire and Springwater and demonstrates further that the metal phases of most stony irons appear to possess nearly identical chemical compositions. Further, it appears that the metal phases of stony-iron meteorites are indistinguishable chemically from the meteorites of Group III.

This rather clear link between stony-iron meteorites and one particular group of irons leads us to suspect that perhaps other groups of stony meteorites may likewise be linked chemically to particular groups of iron meteorites. Were this true, it would profoundly affect our thinking concerning the origin of these extra-terrestrial objects.

5. Summary

A summary of the results is given in Table 11. The observations clearly demonstrate that there are four distinct groups of iron meteorites which differ in their contents of gallium, germanium, and to some extent of chromium, but cannot be distinguished on the basis of their contents of cobalt and copper.

Table 11 also shows the average concentrations of each of the elements studied

Table 11. Summary of results

Ga-Ge group	Number of meteorites	$\frac{Ga}{Ge}$	Range and average of concentrations (p.p.m.)				
			Ga	Ge	Co	Cr	Cu
I	9	4·1	80 — 100	300 — 420	0·45 — 0·52	>1 — 5·3	112 — 175
			86 ± 6	347 ± 25	0·49 ± 0·02	4·9 ± 0·8	143 ± 17
II	24	3·1	40 — 65	130 — 230	0·42 — 0·56	2·6 — 101	105 — 248
			52 ± 4	168 ± 11	0·48 ± 0·02	40 ± 6	136 ± 11
III	29	2·3	8 — 24	15 — 80	0·45 — 0·60	>1 — 100	102 — 257
			15 ± 1	38 ± 3	0·52 ± 0·03	30 ± 4	141 ± 14
IV	15	≧1	1 — 3	>1 — 1	0·38 — 0·74	>1 — 112	95 — 205
			≃ 2	≃ 1	0·52 ± 0·03	49 ± 5	144 ± 13
Anomalous	11	1·9	6 — 82	>1 — 410	0·43 — 0·73	>1 — 73	157 — 253
			45 ± 3	105 ± 12	0·54 ± 0·02	24 ± 2	197 ± 15
Weighted average			34 ± 2·5	107 ± 8	0·51 ± 0·02	37 ± 4	152 ± 14
Stony-irons	9	2·2	12 — 23	18 — 60	0·47 — 0·60	>1 — 8·3	143 — 240
			18 ± 2	39 ± 3	0·55 ± 0·02	≃2·5 ± 0·5	200 ± 18

in iron meteorites weighted according to the observed frequency of each meteorite type. The average concentration of 37 p.p.m. chromium is lower by a factor of three than the values of 100 p.p.m. reported by Goldschmidt (1954). The average of 0·51% cobalt agrees well with the average of 0·58% derived from the analyses of thirty-one iron meteorites by Goldberg, Uchiyama, and Brown (1951) and with the average of 0·55% reported by Noddack and Noddack (1930). The weighted average of 34 p.p.m. gallium is in good agreement with the 39 p.p.m. derived from the neutron activation results of Goldberg, Uchiyama, and Brown

(1951), but is higher by a factor of 3 as compared with the value of 13 p.p.m. reported by Noddack and Noddack (1930). The germanium average of 107 p.p.m. is lower by a factor of three than the revised value of 300 p.p.m. given by Goldschmidt (1954).

Acknowledgements—We acknowledge the generosity and whole-hearted co-operation of E. P. Henderson of the United States National Museum who made available samples of a number of the meteorites used in this study. Samples of many of the Australian meteorites were obtained thanks to the generous co-operation of the Australian Museum (R. O. Chalmers). We are greatly indebted to E. B. Sandell and H. Onishi of the University of Minnesota for chemically analysing several meteorites for gallium and to S. A. Wardani of the Scripps Institute of Oceanography for chemically analysing several meteorites for germanium.

We acknowledge further the help and numerous suggestions given us by our colleagues in the geochemical group at the California Institute of Technology.

The greater part of this research was made possible by a grant given to one of us (H. B.) by the John Simon Guggenheim Memorial Foundation. A part of the research was done under Atomic Energy Commission Contract No. AT(11-1)-208.

References

Ahrens L. H. (1934) Quantitative spectrochemical analysis of silicates.
Belayev N. T. (1923) *J. Inst. Metals* **29,** 237–406.
Brezina A. (1885) *Jahrb. k.k. Geol. Reichsanstalt.* **35,** 151–276.
Farrington O. C. (1907) *Field Columb. Mus. Geol. Ser. Publ.* 120.
Goldberg E., Uchiyama A., and Brown H. (1951) *Geochim. et Cosmochim. Acta* **2,** 1–25.
Goldschmidt V. M. (1930) *Z. Phys. Chem. Abt. A,* **146,** 404–405.
Goldschmidt V. M. (1954) *Geochemistry* (Edit. by A. Muir) Oxford.
Goldschmidt V. M. and Peters Cl. (1933a) *Nachr. Ges. Wiss. Göttingen, Math.-Phys. Kl.,* 165–183.
Goldschmidt V. M. and Peters Cl. (1933a) *Nachr. Ges. Wiss. Göttingen, Math.-Phys. Kl.,* 141–166.
Goldschmidt V. M. and Peters Cl. (1933b) *Nachr. Ges. Wiss. Göttingen, Math.-Phys. Kl.,* 278–287.
Henderson E. P. (1941) *Amer. J. Sci.* 239, 372.
Noddack I. and W. (1930) *Naturwiss.* **18,** 757.
Noddack I. and W. (1931) *Z. Phys. Chem. Abt. A* **154,** 207–244.
Onishi H. (1955) *Anal. Chem.* **27,** 832.
Yavnel' A. A. (1954) *Meteoritika, issue XI,* 107–116.
Zavaritskii A. N. and Kvasha L. G. (1952) *Meteority SSSR* pp. 79 and 80.

Geochimica et Cosmochimica Acta, 1957, Vol. 11, pp. 279 to 309. Pergamon Press Ltd., London

Untersuchungen zur geochemischen Verteilung des Zirkoniums in der Lithosphäre

Heinz Degenhardt
Mineralogisch-Petrographisches Institut der Universität, Göttingen

(*Received* 10 *August* 1956)

Inhaltsverzeichnis

Einleitung 279
1. Methode 280
2. Der Zirkoniumgehalt von gesteinsbildenden Mineralien 281
3. Die Verteilung des Zirkoniums in den Eruptivgesteinen 287
(1) Die Streuung der Zirkoniumwerte innerhalb zweier Granitaufschlüsse . . 293
4. Das Zirkonium in den Sedimentgesteinen 294
(1) Zwei Verwitterungsprofile über Granit 294
(2) Verwitterungsbildungen und Tonminerale 296
(3) Der Zirkoniumgehalt von Wässern, einigen chemischen und biogenen Sedimenten 298
(4) Sedimentäre Erze 300
(5) Kieselgesteine 300
(6) Pelite 301
(7) Psammite und Psephite 302
(8) Karbonatgesteine 303
5. Der Zirkoniumgehalt der kristallinen Schiefer 305
6. Der mittlere Zirkoniumgehalt der Lithosphäre 305
Zusammenfassung 307
Literaturverzeichnis 308

Abstract—287 minerals and rocks were analysed for zirconium by a colorimetric method quoted below. The analyses of minerals indicate that practically all rock-forming minerals contain small quantities of zirconium. Among the main constituents of rocks pyroxenes and amphiboles are preferred hosts for zirconium. They contain more than 100 p.p.m. Zr. Zirconium is concentrated in rutile, sphene, magnetite, ilmenite, and apatite, most of which contain several 1000 p.p.m. The greatest concentration of zirconium was found in aegirines with up to 0·5% Zr.

The geochemical distribution of zirconium in igneous rocks is characterized by a preference for late (acid to intermediate) products of magmatic fractionation. Alkalic rocks, on the average, contain about twice as much zirconium as rocks of calcalkalic character: alkalic syenites 680 g Zr/t–syenites 310 g Zr/t essexites 200 g Zr/t–gabbros 110 g Zr/t. There is no difference in zirconium content between plutonic rocks and their effusive equivalents. In basic and ultrabasic igneous rocks, which contain the lowest amounts of zirconium among the analysed rocks, zirconium mainly enters pyroxenes and ore minerals.

The average zirconium content of the lithosphere, calculated from the analysed igneous rocks according to their relative abundances amounts to 156 g Zr/t. On the average, sedimentary rocks contain about the same amount of zirconium as igneous rocks. A slight solubility of $ZrSiO_4$ was found. Solutions of bicarbonate of calcium proved to be the most effective solvents. The observations explain the corrosion of $ZrSiO_4$ crystals in laterites. Whereas the amount of zirconium in clays and shales is fairly constant, there is a wide range of variation in sandstones and especially in quartzites. The entire zirconium content of calcareous rocks is contained in the residue insoluble in HCl. The zirconium content of metamorphic rocks is about equal to the amount in the primary rocks.

Einleitung

Das Zirkonium ist durch seinen steigenden Gebrauch in der Technik in den Vordergrund der Betrachtungen gerückt. Auch seine geochemische Bedeutung

macht es in vieler Hinsicht aktuell. Das sehr weit verbreitete Zirkoniumsilikat Zirkon kann durch seinen Thorium- und Urangehalt der Hauptträger der Radioaktivität in den Gesteinen sein. Man kann deshalb den Zirkon auch als Ausgangsmaterial für Altersbestimmungen verwenden.

In den Gesteinen wurde das Zirkonium wegen der Schwierigkeiten, die es dem Analytiker bei der chemischen Analyse bereitete, oft nicht bestimmt. Die geochemischen Betrachtungen der alten Analysen stützen sich beim Zirkonium auf die nicht sehr zuverlässigen Daten, welche die Phosphatmethode lieferte. Erst durch die Anwendung der Emissionsspektralanalyse und der Röntgenspektroskopie konnten brauchbare Ergebnisse erzielt werden. Trotzdem sind noch zahlreiche Lücken zu schließen. Aufgabe dieser Arbeit ist es, die Verteilung des Zirkoniums in den gesteinsbildenden Mineralien zu untersuchen und besonders die noch fehlenden Zr-Werte für Sedimente zu ergänzen.

Der erste Zirkoniumwert für die Lithosphäre wurde von Clarke und Washington im Jahre 1924 mit 300 g/t angegeben. Dieser Wert wurde als arithmetischer Mittelwert aus etwa 631 Gesteinsanalysen erhalten. Im Jahre 1934 veröffentlichten G. v. Hevesy und K. Würstlin 40 auf röntgenspektroskopischem Wege gefundene Zirkoniumwerte hauptsächlich von Durchschnittsmischungen von 1184 Gesteinsproben. Alle neueren Literaturangaben für den Zirkoniumwert der Lithosphäre stützen sich auf diese Arbeit. Darin wird der Zr-Gehalt der gesamten Eruptivgesteine mit 250 g Zr/t, derjenige von tonigen Sedimenten mit 140 g Zr/t angegeben. Psammite und Kalke fehlen. Auffallend ist die große Diskrepanz zwischen Eruptivgesteinen und Sedimenten.

Die Untersuchungen, welche V. M. Goldschmidt und H. Bauer (1938) über die Verteilung des Zirkoniums in Göttingen begannen, wurden nicht abgeschlossen. V. M. Goldschmidt stützt sich bei seinem für die Lithosphäre angeführten Zirkoniumwert von 220 g Zr/t auf die Untersuchungen von v. Hevesy (1934).

1. Methode

Die Bestimmung des Zirkoniums in Gesteinen und Mineralien verlangt von einem Verfahren nicht nur Genauigkeit in einem großen Konzentrationsbereich, sondern auch eine genügende Empfindlichkeit. Der Zirkoniumgehalt kann einerseits bis auf einige Prozente steigen, während er andererseits oft unter 10^{-3}% liegt.

Grundsätzlich mußte eine Wahl zwischen Emissionsspektralanalyse, Röntgenspektralanalyse und chemischen Methoden getroffen werden. In der Spektralanalyse besteht besonders für das Zirkonium eine Schwierigkeit darin, daß es sehr schwer verdampft. Dieser Umstand kann der Bildung von ZrO_2 zugeschrieben werden. Außerdem bildet sich im Kohlebogen ZrC, welches eine noch größere Stabilität besitzt.

Gegenüber der Spektralanalyse ist das Zirkonium auf röntgenspektroskopischen Wege leichter anregbar. Hevesy u. Würstlin (1934), welche sich der Sekundärstrahlspektroskopie bedienen, geben ihre Analysenwerte bis auf 10^{-3}% an. Demnach erreicht dieses Verfahren nicht die verlangte untere Erfassungsgrenze von 10^{-4}%. Eine neue Aperatur für röntgenspektroskopische Messungen stand nicht zur Verfügung. Eingehende Versuche haben gezeigt, daß ein kolorimetrisches Verfahren am zweckmäßigsten ist.

Für den Nachweis kleiner Zr-Mengen in Silikaten wurde die kolorimetrische Bestimmung mit Alizarin-S herangezogen. Gesteine und Mineralien werden mit einem $NaOH$-Na_2O_2-Gemisch aufgeschlossen. Der Aufschluß muß wiederholt werden, um die störende Kieselsäure restlos in Lösung zu bringen. Nach Fällung der Hydroxyde mit Ammoniak, Lösen derselben und Reduktion des dreiwertigen Eisens erhält man die zu kolorimetrierende Lösung. Die durch den Hafniumgehalt der Gesteinsprobe hervorgerufene Störung ist sehr klein und liegt innerhalb der Fehlergrenze. Die untere Erfassungsgrenze des Zr-Gehaltes liegt bei $2 \cdot 10^{4}\%$. Der mittlere Fehler zweier Einzelmessungen beträgt etwa $3 \cdot 10^{-4}\%$. Von jeder Mineral-und Gesteinsprobe wurden zwei Analysen ausgeführt.—Kleine Mengen Zirkonium lassen sich durch einen Niederschlag von Titandioxydhydrat quantitativ anreichern, was für die Spurenbestimmung von Zirkonium in Gewässern von Bedeutung ist. Die ausführliche Beschreibung der Methode siehe unter H. Degenhardt (1956).

2. Der Zirkoniumgehalt von gesteinsbildenden Mineralien

Es ist bekannt, daß ein großer Teil des in den Gesteinen vorhandenen Zirkoniums im Zirkon ($ZrSiO_4$) gebunden ist. Von Interesse ist es deshalb festzustellen, in welchem Umfange sich noch Zirkonium in anderen Mineralen findet. Man muß unterscheiden zwischen Mineralen, welche Zirkonmikrolithe beherbergen, und Mineralen, deren Kationen durch Zirkonium ersetzbar sind. Besonders submikroskopische Einschlüsse machen diese Unterscheidung schwer. Werden in Mineralen mit Zr-Gehalten von mehr als 100 g/t. keine Einschlüsse gefunden, so ist mit einiger Wahrscheinlichkeit anzunehmen, daß es sich um einen echten Ionenersatz handelt.

Das Zirkonium tritt ausschließlich nur positiv vierwertig auf und hat nach V. M. Goldschmidt einen Ionenradius von 0·87 Å. Nach seiner Raumbeanspruchung steht das Zirkonium an der oberen Grenze derjenigen Kationen, welche in 6-Koordination vorkommen. Im Zirkon besitzt es 8-fache Koordination.

Die zur Analyse verwendeten Mineralien stammen aus monomineralischen Anreicherungen, Lagerstätten und Gesteinen. Die Trennung der einzelnen Gesteinsgemengteile mit Hilfe von Schwereflüssigkeiten wurde vermieden. Besonders bei den schwereren Fraktionen $>3\ g \cdot cm^{-3}$ ist keine saubere Trennung der einzelnen Komponenten mehr möglich. Deshalb wurden die einzelnen Mineralkörner mit Hilfe einer Lupe, bzw. unter dem Stereomikroskop aus dem zerkleinerten Gestein herausgelesen. Alle analysierten Kristalle wurden, soweit es möglich war, optisch auf Einschlüsse und Verwachsungen untersucht. Gefundene Einschlüsse wurden in der Tabelle hinter dem betreffenden Mineral vermerkt.

SiO_4-*Gerüststrukturen*	g Zr/t
(1) Orthoklas—S. Piera auf Elba	14
(2) Orthoklas—Tröstau b. Wunsiedel, Fichtelgeb.	15
(3) Sanidin,—Drachenfels Siebengeb., Bonn	45
(4) Albit—Tümmelbachtal, Prägraten Osttirol	16
(5) Albit—Wurmberg-Granit, Braunlage, Harz	23
(6) Albit—Radautal b. Harzburg	39
(7) Oligoklas—Ytterby, Schweden	12

	g Zr/t
(8) Labradorfels—Aurlandsfjord, Norwegen	15
(9) Leucit—Vesuv, Eruption v. 1855	11
(10) Nephelin—Katzenbuckel, Odenwald	50
(11) Eläolith—Laven, Langesund-Fjord, Norwegen	5
(12) Sodalith—Monte Somma, Vesuv	575
(13) Lasurit—Badakschan, Afghanistan	60
(14) Natrolith—Langesund, Norwegen	15
SiO_4-*Schichtstrukturen*	
(15) Muskovit—Pegmatitbruch, Spittal, Kärnten	18
(16) Muskovit—aus grobkörn. Granit, Aabelvik, Arendal, Norwegen	52
(17) Biotit—aus pegm. Mischgneis, Haslach, Schwarzwald	33
(18) Biotit—aus Eklogit, Selje, Nordfjord	35
(19) Biotit—Arendal, Norwegen	56
(20) Biotit—aus Hornblendegranit, Teufelsberg, Odenwald, (Zirkon-Einschlüsse)	112
(21) Biotit—aus Königskopf-Granit, Harz (Zirkon-Einschlüsse)	463
SiO_4-*Kettenstrukturen*	
(22) Diopsid—Schwarzenstein, Tirol	27
(23) Diallag—Prato, Florenz	39
(24) Diallag—aus Gabbro, Oberhalbstein, Graubünden	120
(25) Pyroxen—aus Basalt, Firmerich, Eifel	12
(26) Pyroxen—Mussa Alp, Piemont (Kluftmineral)	34
(27) Pyroxen—aus Basalt, Paschkopele, Böhmen	50
(28) Pyroxen—Monti Rossi, Aetna	120
(29) Pyroxen—aus Phonolithtuff, Hegau	123
(30) Pyroxen—aus Feldspatbasalt, Naurod, Wiesbaden	133
(31) Jadeit—Schwarzenberg	27
(32) Omphazit—aus Eklogit, Selje, Nordfjord	30
(33) Ägirin—Eikarholmen, Norwegen	1500
(34) Ägirin—Barkevikscheeren, Brevik, Norwegen	3700
(35) Ägirin—Caldas de Monchique, Portugal	5750
(36) Bronzit—Peterlestein, Kupferberg, Bayern	18
(37) Hypersthen—Paulsinsel, Küste von Labrador	19
(38) Nephrit—Westküste, Neuseeland	34
(39) Hornblende—Apatitgrube, Kragerö	26
(40) Hornblende—aus Amphibolandesit, Stenzelberg, Siebengebirge	110
(41) Hornblende—aus Hornblendegranit, Teufelsberg, Odenwald	113
(42) Basaltische Hornblende—Leitmeritz, Böhmen	140
(43) Arfvedsonit—Arendal	50
(44) Gastaldit—Aostal, Piemont	121
(45) Glaukophanit—Mocchie, Susatal, Italien	54
(46) Glaukophan—Piemont	302
(47) Barkevikit—Barkevikscheeren bei Brevik, Norwegen (mit Wöhlerit-einschlüssen)	2150
(48) Sillimanit—Chester, Pennsylvanien	5
SiO_4-*Inselstrukturen*	
(49) Olivinknolle—aus Melilith-Basalt, Westberg b. Hofgeismar	40
(50) Olivinknolle—aus Basalt, Hirzstein, Kassel	43
(51) Olivinfels—Mysäter, Kjölsdal, Nordfjord, Oslo	40
(52) Eisentongranat—Haibach b. Aschaffenburg Bayern	28
(53) Granat—aus Eklogit, Selje, Nordfjord	29
(54) Pyrop—Kapnik, Ungarn	38
(55) Pyrop—Meronitz bei Bilin, Böhmen	43

	g Zr/t
(56) Eisentongranat—Simplon	139
(57) Sphen—Zillertal	200
(58) Keilhauit—(Yttrotitanit), Tortveit, Norwegen	900
(59) Titanit—Ilmengebirge, Ural	1500
(60) Titanit—Chibina-Gebirge, UdSSR	2000
(61) Benitoit—San Benito River, Californien	320
(62) Turmalin—Alabaschka, Ural	11
(63) Turmalin—Tangen, Kragerö	18
(64) Disthen—aus Paragonit, St Gotthard	2
SiO_4-Gruppenstrukturen	
(65) Trüber Aquamarin—Frysaa	2
(66) Beryll—Hühnerkobel b. Rabenstein, Bodenmais, Bayr. Wald	18
Oxyde	
(67) Magnetit—Kirunavaara, Lappland	34
(68) Magnetit—aus Diorit, Elvas, Portug.	69
(69) Magnetit—aus Phonolithtuff, Hegau	73
(70) Chromit—Jugoslawien	42
(71) Titanomagnetit—aus Basalt, Bramburg I. Sohle, b. Göttingen	119
(72) Titanomagnetit—aus Basalt, Backenberg	418
(73) Ilmenit—Chester, Massachusetts	155
(74) Ilmenit—aus Basalt, Scheidsberg b. Remagen	200
(75) Ilmenit—Snarum	213
(76) Iserin—Iserwiese	550
(77) Rosenquarz—Minas Geraes, Rio Jequitinhonha	11
(78) Rosenquarz—Hühnerkobel b. Bodenmais	10
(79) Rutil—Binn, Schweiz	1700
(80) Rutil—Arendal, Norwegen	1750
(81) Zinnstein—Zinnwald	213
(82) Zinnstein—aus Kryolith, Grönland	550
(83) Columbit—Anneröd, Norwegen	3000
Sonstige Minerale	
(84) Wolframit—Arizona	23
(85) Apatit—Ehrenfriedersdorf, Sachsen	60
(86) Apatit—Katzenbuckel, Michelsberg	100
(87) Cerapatit—Frederiksvärn, Norwegen	100
(88) Kryolith—Ivigtut, Westgrönland	15
(89) Baryt—Iberg, Harz	2

Von den Analysendaten 1–13 weisen insbesondere die Natronfeldspäte und die Natronfeldspatvertreter höhere Zirkoniumwerte auf, jedoch ist der durchschnittliche Zr-Gehalt der Feldspäte mit 30 g/t gering. Einige spektralanalytisch gefundene Durchschnittswerte für Feldspäte sollen anschließend zitiert werden. R. A. Higazy (1953) findet in 16 Perthiten kein Zirkonium, allerdings ist die untere Nachweisbarkeitsgrenze für das angegebene spektralanalytische Verfahren 20 g Zr/t Nur in einem Perthit wurden 330 g Zr/t nachgewiesen; diese größere Zr-Menge stammt von Zirkoneinschlüssen. S. R. Nockolds und R. L. Mitchell (1948) finden in 9 Plagioklassen von Gesteinen aus West-Schottland durchschnittlich 68 g Zr/t.

Auffallend hoch ist der Zirkoniumgehalt des Sodaliths (575 g/t), welcher auf einem Auswürfling der Somma aufgewachsen war. Der analysierte Kristall war

farblos, durchsichtig, frei von Eisen und zeigte keine Einschlüsse. Nach C. Hintze (1897) wird z.B. im Sodalith von Laven ein geringer Molybdängehalt gefunden. Ionenradius von $Mo^{+4} = 0{\cdot}68$ Å. Es ist möglich, daß bei höherer Bildungstemperatur und genügendem Überschuß an Zirkonium in der Schmelze für die Besetzung der Lücken des Tetraedergerüstes auch das Zr^{+4} eintreten kann.

Sämtliche analysierten Minerale der Glimmergruppe wurden auf Zirkoneinschlüsse untersucht. Die einschlußfreien Glimmer zeigen einen Zirkoniumgehalt von 18–56 g/t. Die höheren Zr-Werte der Biotite aus dem Hornblendegranit und dem Königskopf-Granit stammen von Zirkoneinschlüssen. In die Glimmer scheint mit durchschnittlich 40 g/t etwa die gleiche geringe Menge Zirkonium einzutreten, wie in die Feldspäte. Minerale mit Zirkoneinschlüssen scheiden für die Mittelwertbildung aus. Es liegen aus jüngster Gegenwart zahlreiche spektralanalytisch gefundene Zirkoniumwerte für die Glimmer vor. Nockolds und Mitchell (1948) geben für 14 Biotite, welche aus Tiefengesteinen Westschottlands stammen, einen Durchschnitt von 23 g/t an. J. R. Butler (1953) führt den in einem Biotit gefundenen Zirkoniumwert von 150 g/t auf eingeschlossene Zirkone zurück. 45 Analysen von Biotiten aus metamorphen Gesteinen werden von G. W. De Vore (1955) angegeben. Man kann aus ihnen einen mittleren Zr-Gehalt von 140 g/t errechnen. Die untersuchten Biotite wurden nicht mikroskopisch geprüft und nicht von denjenigen unterschieden, welche einschlußfrei waren.

Einen wesentlich höheren Zirkoniumgehalt als Feldspäte und Glimmer weisen Pyroxene auf. Bei der Analyse der aus Basalten stammenden Pyroxene konnte beobachtet werden, daß die eisenreicheren Glieder einen höheren Zr-Gehalt zeigen als die eisenarmen. Die größten Zr-Mengen enthalten die sehr eisenreichen Natronpyroxene. Für die Pyroxene gilt demnach die Beziehung, wonach mit wachsendem Eisengehalt auch der Zirkoniumgehalt ansteigen kann. Zwischen dem Titan- und Zirkoniumgehalt der Pyroxene konnte keine Beziehung festgestellt werden.

Der Diopsid zeigt mit 27 g Zr/t den relativ niedrigsten Wert. Der höchste Wert von etwa 0,5% Zr wird in den Natron-Eisen-Pyroxenen erreicht. Mit Zunahme des Ägirinmoleküls in der unbegrenzten Mischreihe Diopsid-Ägirin kann der Zirkoniumgehalt bis zum Ägirin ansteigen. In dem sehr verbreiteten gemeinen Pyroxen herrscht das Diopsidmolekül vor. Damit ist seine Aufnahmefähigkeit an Zirkonium begrenzt.

Beim Ägirin $NaFe(Si_2O_6)$ wird der Zusammenhang der elektrostatisch nicht abgesättigten Ketten $(Si_2O_6)^{-4}$ durch die heteropolaren Kräfte des $NaFe^{3+}$ herbeigeführt. Anscheinend kann an Stelle von $NaFe^{3+}$ ein einzelnes Zr^{+4} treten. Wenn das vierwertige Zirkonium vom dreiwertigen Eisen abgefangen wird, so tritt an Stelle des Natriums eine Lücke. Daß diese Annahme richtig ist und daß weder Na noch Al für das Abfangen des Zirkoniums in Frage kommen, zeigt der geringe Zr-Gehalt des Jadeits $NaAl(Si_2O_6)$. Auch der aufgeführte Omphazit, welcher eine Beimischung von 20–25% Jadeit zur Diopsidmolekel darstellt, enthält nur geringe Zirkoniummengen.

Der Ägirin besitzt außer seinem auffallend hohen Zirkoniumgehalt auch einen beträchtlichen Anteil an seltenen Erden. Im allgemeinen kann als Faustregel

gelten, daß dort, wo seltene Erden auftauchen, auch Zirkonium zu finden ist. Die Vergesellschaftung des Zirkoniums mit den seltenen Erden liegt in der Ionenradienähnlichkeit begründet (außer $La^{3+} = 1{,}22$ Å). Besonders angereichert sind seltene Erden im Eudialyt, Ägirin, Apatit, Titanit, Zirkon. Umgekehrt findet man dementsprechend im Ägirin, Apatit, Titanit das Zirkonium.

Neuere spektralanalytische Pyroxenanalysen liegen von De Vore, Nockolds und Mitchell vor. De Vore (1955) findet in 14 Diopsiden durchschnittlich 65 g Zr/t, Nockolds und Mitchell (1948) in 3 Pyroxenen durchschnittlich 72 g Zr/t. Der durchschnittliche Zr-Gehalt der in der Tabelle angegebenen 6 Pyroxene beträgt 77 g Zr/t. Dieser Wert stimmt gut mit den Literaturwerten überein. Eine Angabe über den Zr-Gehalt von Natronpyroxenen stammt aus dem Jahre 1927 von H. S. Washington und H. E. Merwin. Sie fanden in 13 Akmiten und Hedenbergitakmiten durchschnittlich 2800 g Zr/t und in 5 Akmiten durchschnittlich 7000 g Zr/t.

Die Hornblenden zeigen etwa denselben Zirkoniumgehalt wie die Pyroxene. Auch in den Mineralien der Amphibolgruppe sind eingeschlossene Zirkonmikrolithe zu erwarten. Da der Zirkon eine Frühausscheidung ist, wird er häufig vom Pyroxen, Amphibol und Biotit umschlossen. Der hohe Zr-Gehalt des Barkevikits stammt von kleinen Wöhleriteinschlüssen. Der Barkevikit begleitet den Ägirin in den Nephelinsyenitpegmatiten (Norwegen, Schottland, Californien). Der zu den Natronhornblenden gehörende Riebeckit kann auf Grund seines Anteils an Ägirinmolekül größere Zirkoniummengen binden. In 8 Hornblenden, welche aus Eruptivgesteinen von Westschottland stammen, fanden Nockolds und Mitchell (1948) durchschnittlich 98 g Zr/t. De Vore (1955) gibt Analysenwerte von 46 aus metamorphen Gesteinen stammenden Hornblenden an. Für sie ergibt sich ein durchschnittlicher Zirkoniumgehalt von 110 g/t. Die in vorhergehender Tabelle angeführten 9 Hornblenden (ausgenommen der Barkevikit) liegen mit einem Durchschnitt von 105 g Zr/t genau zwischen den beiden oben angeführten Literaturwerten.

Daß nur wenig Zirkonium in die basischen Mg-Fe-Silikate eintritt zeigen die Olivinanalysen. In 4 Duniten fanden W. H. Pinson, L. H. Ahrens und Mona L. Frank (1953) spektralanalytisch durchschnittlich 30–40 Zr/t. Diese Werte stimmen mit den in der Tabelle angeführten Olivinwerten gut überein. Im Olivin ist ein nur sehr kleiner Teil des in den oktaedrischen Lücken in 6- Koordination befindlichen zweiwertigen Eisens ($Fe^{2+} = 0{,}83$ Å) durch Zirkonium ersetzbar ($Zr^{+4} = 0{,}87$ Å).

Bei größeren Granaten, die besonders als derbe Massen auftreten, kann ein höherer Zirkoniumgehalt von eingeschlossenen Zirkonen stammen. Die blutrot durchscheinenden böhmischen Granate zeigen keine Einschlüsse. Bei ihnen erscheint ein geringfügiger Ersatz von Mg^{2+} durch das Zirkonium möglich. De Vore (1955) fand in 32 Granaten einen Durchschnitt von 190 g Zr/t. Er hält es für wahrscheinlich, daß der größte Anteil dieses hohen Zirkoniumwertes von den im Granat vorhandenen Zirkoneinschlüssen stammt.

Der hohe Zirkoniumgehalt des Titanits spricht für eine Vertretbarkeit des Titans durch das Zirkonium. Der Titanit $CaTiO(SiO_4)$ zeigt Isomorphie mit dem Calciumzirkoniumoxysilikat $CaZrO(SiO_4)$, während der Perowskit $CaTiO_3$ mit dem Calciumzirkonat $CaZrO_3$ isomorph ist (L. Ouvrard). In 5 Titaniten, welche

aus kaledonischen Eruptivgesteinen stammen, fanden Nockolds und Mitchell (1948) durchschnittlich 1000 g Zr/t.

Trotz der zahlreich möglichen isomorphen Vertretungen von Kationen beim Turmalin ist sein Zirkoniumgehalt sehr gering. Auch der Beryll enthält nur verschwindend kleine Mengen Zirkonium. Das deutet darauf hin, wie wenig das Zirkonium in die Minerale der Borfluor- und Berylliumpegmatite eintritt. Von 4 u.a. auch auf Zirkonium untersuchten Turmalinen konnte Butler (1954) nur in einem 55 g Zr/t spektralanalytisch nachweisen.

In den titan- und eisenfreien Aluminiumsilikaten der kristallinen Schiefer, z.B. Sillimanit, Disthen, wird nur sehr wenig Zr gefunden. Es sei darauf hingewiesen, daß es sich bei den Mineralen mit nicht bestimmbarem Zr-Gehalt meist um klare, durchsichtige, eisen- und titanfreie Kristalle handelt. Damit bestätigt sich die Vermutung, daß das Zirkonium vornehmlich in denjenigen Mineralen auftritt, in denen es vorhandenes Eisen oder Titan zum Teil ersetzen kann.

Von den Eisenoxyden weisen besonders die Titanomagnetite die höchsten Zr-Werte auf. Die Titanomagnetite wurden aus den sehr fein gemahlenen Basaltproben mit Hilfe eines Permanentmagneten isoliert und optisch untersucht. Es handelte sich praktisch um reine Konzentrate. Beim reinen Magnetit (Ferroferrispinell) ist mit einem Ersatz des zweiwertigen Eisens und beim Ilmenit außerdem mit einem Ersatz des Titans durch das Zirkonium zu rechnen. In 5 aus verschiedenen metamorphen Gesteinen isolierten Magnetitkonzentraten fand De Vore (1955) u.a. für Zr einen Durchschnitt von 255 g/t.

Mit dem Zirkon sind isomorph der Thorit und der Xenotim (Ytterspat), welche bis zu 3% ZrO_2 enthalten können. Weiterhin besteht eine kristallchemische Verwandtschaft zwischen dem Zirkon, dem Mossit und Tapiolith. V. M. Goldschmidt (1926) bezeichnete sie wegen einer gewissen polymeren Isomorphie in Bezug zur Rutilzelle als "Polyrutile". Verwandtschaft mit dem Zirkon zeigen auch die Oxyde des Titans, Zinns und Niob als sog. Monorutile. Besonders in den letztgenannten Oxyden werden erhebliche Mengen Zirkonium gefunden. Außer den hier angegebenen Werten sind auch in der Literatur vereinzelte Angaben zu finden. A. F. Frederickson (1948) fand im Brookit Zirkonium und nahm an, das Zr^{+4} daß das Ti^{+4} ersetzt. Obwohl der Ionenradius von Ti^{+4} mit 0,64 Å von demjenigen des Zirkoniums mit 0,87 Å schon recht verschieden ist, so spricht doch die enge chemische Verwandtschaft der beiden Elemente für diese Annahme.

Unter den hier für Zinnstein angegebenen Zr-Werten befinden sich keine Maximalwerte. Nach Angaben von H. Schröcke (1955) können im Zinnstein Zr-Gehalte bis 1000 g/t auftreten.

Wie im Zirkon einerseits fast immer einige Prozente Phosphorsäure anzutreffen sind, so wird andererseits im Apatit häufig Zirkonium gefunden. Im Apatit ist ein Teil des Ca^{+2} (1,06 Å) durch das Zirkonium nebst seltenen Erden ersetzbar. Nach Literaturangaben können in manchen Apatiten noch größere Zirkoniummengen gefunden werden. Nockolds und Mitchell (1948) geben einige Werte über 1000 g Zr/t an. Die Autoren führen diese höheren Werte auf Zirkoneinschlüsse zurück.

Über das Verhalten des Zirkoniums im Verlaufe der magmatischen Differentation kann auf Grund der Erkenntnisse von V. M. Goldschmidt (1923), verbunden

mit den bisherigen Ergebnissen der Zirkoniumanalysen, folgendes ausgesagt werden: Vom ursprünglichen Magma geht das Zirkonium in die Silikatschmelze. Zu den ersten Kristallisationsprodukten der Silikatschmelze gehören Olivin, Magnetit mit Chromit und Ilmenit. In den Olivin tritt das Zirkonium nur in geringen Mengen ein (40 g Zr/t), im Magnetit und Ilmenit können etwas größere Zr-Mengen bis zu etwa 400 g Zr/t eingebaut werden. Noch vor der Hauptkristallisation beginnt die Ausscheidung von Apatit und Zirkon. Der Apatit, welcher dem Magma schon relativ frühzeitig durch Einbau kleine Mengen seltener Erden entzieht, nimmt gelegentlich auch größere Mengen Zirkonium auf. Während der Hauptkristallisation werden die schon früher ausgeschiedenen Apatite und Zirkonmikrolithe teilweise von Pyroxenen, Amphibolen und Glimmern umschlossen. Ein Teil des noch in der Schmelze vorhandenen Zirkoniums wird nur in kleinen Mengen in die Feldspäte und Glimmer eingebaut (30–40 g Zr/t), während bis zu 140 g Zr/t von den Pyroxenen und Amphibolen aufgenommen wird. In der Restschmelze befindet sich noch die Hauptmenge des Zirkoniums.

Hier bilden sich:

(a) bei noch vorhandener freier Kieselsäure, vermutlich unter Mitwirkung von Mineralisatoren (analog der Zirkonsynthese), Ausscheidungen von Zirkoniumsilikat;
(b) bei Anwesenheit von Titan und seltenen Erden Zr-Ti-Ce-Silikate oder Titanit mit beträchtlichen Gehalten an Zirkonium und seltenen Erden;
(c) bei Na-Fe-Überschuß Zirkonium führende Natrium-Eisen-Pyroxene mit Zr-Gehalten bis zu etwa $\frac{1}{2}$%.

Zusammenfassend kann gesagt werden, daß das Zirkonium nicht nur an die Zirkoniumminerale Zirkon, Katapleit, Eudialyt, Wöhlerit, Astrophyllit usw. gebunden ist, sondern daß es in vielen gesteinsbildenden Mineralen gefunden wird, in denen es vornehmlich das Eisen oder das Titan in kleinen Mengen ersetzen kann.

Zr-Gehalte $> 0{,}01$% Zr werden gefunden:

(a) Von den Hauptgemengteilen in Pyroxenen und Amphibolen.
(b) Von den akzessorischen Gemengteilen im Titanit, Rutil, Magnetit (Titanomagnetit), Ilmenit, Apatit.

3. Die Verteilung des Zirkoniums in den Eruptivgesteinen

Nachdem wir einen Überblick über die Zr-Gehalte der gesteinsbildenden Minerale gewonnen haben, sollen die einzelnen Gesteine in der Reihenfolge sauer-basisch besprochen werden.

Das zur Untersuchung verwendete Material stammt aus der Sammlung des mineralogischen Institutes in Göttingen. Die Zusammensetzung der Durchschnittsproben wird in den Arbeiten von Noll (1933) und von v. Engelhardt (1936) aufgeführt. Bei den von diesen Autoren hergestellten Durchschnittsproben wurden die einzelnen Gesteinsproben verschiedener Gesteinsmassive in gleichen Anteilen zugemischt. Durch anomale Bestandteile können evtl. Verfälschungen des Durchschnittswertes hervorgerufen werden, deshalb sind die Analysenergebnisse der Einzelproben für geochemische Betrachtungen wertvoller.

	g Zr/t
(90) Lithionitgranit—Eibenstock, Sachsen	27
(91) Granit—Andlau-Süd, Vogesen	100
(92) Granit—Natzviller, Vogesen	126
(93) Hornblendegranit—Teufelsberg, Odenwald	145
(94) Granit—Westerly, Rhode Island USA(G-1)	162
(95) Granit—Königskopf, Harz Durchschnitt aus 3 Proben	175
(96) Granit—Wurmberg, Harz. Durchschnitt aus 6 Proben	180
(97) Granit—Schierke, Harz	194
(98) Granit—Grimstad, Norwegen	250
(99) Granit—Eklara, Gujarat, Indien	380
(100) Pantellerit—Pantelleria	1070
(101) Porphyr—Strehlen	104
(102) Liparit—Eisenbach,Ungarn	154
(103) Obsidian—Lipari	153
(104) 8 Obsidiane—(Durchschnittsmischung von v. Engelhardt 1936)	268
(105) Syenit—Zischewig b. Dresden	275
(106) Trachyt—Drachenfels, Siebengeb.	355
(107) 22 Nephelinsyenite—(Durchschnittsmischung von v. Engelhardt 1936)	675
(108) Nephelinsyenit—Minas Geraes	750
(109) Tinguait—Serra de Tingua, Rio de Janeiro	510
(110) Keratophyr—Hüttenrode, Harz	720
(111) Riebeckit-Trachyt—Berkum, Siebengeb.	305
(112) Nephelinphonolith—Kletscherberg, böhm. Mittelgeb.	590
(113) 10 böhm. Phonolithe—(Durchschnittsmischung von v. Engelhardt 1936)	655
(114) Diorit—Gisna-Brücke, Opdal, Norwegen	35
(115) Diorit—Neuntelstein, Vogesen	52
(116) Hornblendediorit—Schriesheim b. Heidelberg	76
(117) Diorit—Teiskola, Teisko, Finnland	108
(118) Diorit—Reichenbach, Odenwald	111
(119) Quarzdiorit, (Tonalit)—Adamello, Südtirol	113
(120) Diorit—Leuthenberg, Bayern	132
(121) Granodiorit, (Opdalit)—Ulsberg, Norwegen	142
(122) 6 Andesite—Aegina (Durchschnittsmischg. von v. Engelhardt, 1936)	101
(123) 14 Andesite—Methana (Durchschn. Mischg. von v. Engelhardt, 1936)	118
(124) Augitandesit—Tokay, Ungarn	156
(125) Amphibolandesit—Stenzelberg, Siebengeb.	342
(126) Gabbro—Tampadel, Zobten	25
(127) Gabbro—Radautal, Harz	116
(128) Diabas—Langelsheim, Nordharz	70
(129) Diabas—Centreville, Virginia (W-1)	85
(130) Diabas—Hauptgrünsteinzug Remblinghausen, Sauerland. (Originalmaterial v. Ventzlaff)	102
(131) Diabas—Wallenstein, Wallen	129
(132) Diabas—Heringhausen, südl. Bestwig,	138
(133) Diabas—Hennetalsperre, Meschede	171
(134) Trachydoleritischer Basalt—Backenberg b. Güntersen (Orig. Material v. K. H. Wedepohl, 1954)	106
(135) Feldspat-Basalt—Druseltal b. Kassel	71
(136) Feldspatbasalt—Hoher Hagen b. Göttingen (Orig. Mat. v. Wedepohl, 1950)	128
(137) Feldspatbasalt—Unterhalb Bramburg b. Göttingen	168
(138) 9 indische Basalte—(Durchschnittsmischung von v. Engelhardt, 1936)	192
(139) Nephelinit—Roßberg b. Darmstadt	58
(140) Melilithbasalt—Hofgeismar (Originalmaterial, Ernst, 1936)	65
(141) Nosean-Basalt—Eschwege, westl. d. blauen Kuppe	116
(142) Essexit—Salem Neck, Massachusetts	200
(143) Peridotit—Lherz-Teich, Pyrenäen	49

Die Zirkoniumwerte der Granite zeigen eine große Variationsbreite. In den Alkalikalkgraniten dürfte der größte Teil des vorhandenen Zirkoniums als akzessorischer Zirkon vorliegen. Von untergeordneter Bedeutung ist der Zr-Gehalt von akzessorischem Erz, Apatit, Titanit. Jedoch können diese je nach Anteil und Zr-Gehalt mit einigen Prozenten am Gesamt-Zirkoniumgehalt des Gesteines beteiligt sein.

Wie sich in einem Granit der Zirkoniumgehalt auf die einzelnen Mineralkomponenten verteilen kann, soll am folgenden Beispiel gezeigt werden. Die Hauptgemengteile des Wurmberg-Granites wurden unter dem Stereomikroskop aus dem zerkleinerten Gestein herausgelesen und auf Zirkonium untersucht.

Wurmberg-Granit Nr. 2, Harz			150 g Zr/t
	Gew. %	Prozentualer Anteil:	
(144) Quarz	30%	32 g Zr/t	10 g Zr/t
(145) Feldspäte, (20% Oligoklas + 45% Orthoklas)	65%	35 g Zr/t	23 g Zr /t
(146) Biotit, (mit Zirkoneinschlüssen)	5%	900 g Zr/t	45 g Zr/t
			78 g Zr/t

Es werden also in den Mineralen insgesamt 78 g Zr/t gefunden, wobei berücksichtigt werden muß, daß die Zirkoneinschlüsse im Biotit erheblich an diesem Wert beteiligt sind. Der Rest von 72 g Zr/t liegt im Gestein als freier Zirkon vor.

Den höchsten Zirkoniumgehalt der Granite zeigen die Alkaligranite. Der in der Tabelle angeführte Pantellerit (1070 g Zr/t), welcher zur Familie der Alkaligranite gehört, führt 14% Ägirindiopsid. W. E. Tröger (1935) führt z.B. aus der Familie der Alkaligranite einen Rockallit (mesotyper Ägirin-Granit) mit 8700 g Zr/t an. Dieses Gestein enthält 43% Ägirin, aber keinen Zirkon. Der Ägirin, welcher größere Mengen Zirkonium führen kann, ist ein überaus verbreiteter Gemengteil der Alkaligranite. Die Anreicherung von Zirkonium speziell in den Alkaligraniten ist demnach vermutlich auf die Anwesenheit von Zirkonium führendem Ägirin, Ägirinaugit oder Ägirindiopsid zurückzuführen.

Spektralanalytisch gefundene Zr-Werte von Graniten sollen hier zitiert werden. Butler (1953) gibt für 5 Granite aus Cornwall durchschnittlich 30 g Zr/t an, Amstutz (1953) für 2 Schweizer Quarzporphyre 100 g Zr/t. Van Tongeren (1938) fand in 20 ostindischen Graniten durchschnittlich 144 g Zr/t. Aus 27 kanadischen Graniten, welche von Ahrens (1954) untersucht wurden, ergibt sich für Zirkonium ein Mittelwert von 170 g/t. Dieser Wert stimmt mit dem in dieser Arbeit gefundenen Granitdurchschnitt von 175 g/t gut überein.

Die vulkanischen Gläser, die meist kieselsäurereich sind, zeigen einen Zr-Gehalt wie etwa die Granite.

Der Zirkoniumgehalt der Tiefengesteine und deren Erguß und Gang-Äquivalente stimmt gut überein. Eine gute übereinstimmung z.B. zeigen die Nephelinsyenite und Phonolithe, die Syenite und Trachyte.

Die Nephelinsyenite einschließlich ihrer Ergußäquivalente zeigen mit durchschnittlich 680 g/t einen ungefähr doppelt so hohen Zirkoniumgehalt wie die normalen Syenite mit 310 g/t. Während in den Syeniten das Zirkonium fast ausschließlich als Zirkoniumsilikat vorliegt, kommt bei den Nephelinsyeniten noch zusätzlich das in den Natronpyroxenen getarnte Zirkonium hinzu. Alle Natronsyenite und Natronergußgesteine enthalten mehr oder weniger größere Mengen Ägirin. Der in der Tabelle angeführte Tinguait (510 g Zr/t), welcher zur Familie der Eläolithsyenite gehört, enthält z.B. 21% Ägirin und keinen Zirkon (Tröger, 1935).

Wie entscheidend der Ägirin am Zirkoniumgehalt der Alkaligesteine beteiligt sein kann, soll das nächste Beispiel zeigen. Es wurden die Hauptgemengteile des Nephelinsyenites von Caldas de Monchique untersucht.

Mineralbestand nach Tröger (1935)

Nephelinsyenit, Caldas de Monchique, Portugal			600 g Zr/t
	Gew. %	Prozentualer Anteil	
(147) Orthoklasmikroperthit	67%	24 g Zr/t	16 g Zr/t
(148) Nephelin	24%	38 g Zr/t	9 g Zr/t
(35) Ägirinaugit	7%	5750 g Zr/t	403 g Zr/t
Titanit, Zirkon, Erz, Kies, Apatit	2%	n.b.	
			428 g Zr/t

Rund 2/3 des im Gestein vorhandenen Zirkoniums ist im Ägirinaugit getarnt, während sich der Rest von 172 g Zr/t auf die Schwerminerale verteilt.

Für Phonolithe und Trachyte liegen in der Literatur Zr-Werte von Nockolds und Allen (1953) vor. 3 Phonolithe aus Polynesien enthalten durchschnittlich 600 g Zr/t. Dieser Wert stimmt gut mit dem hier gefundenen Durchschnittswert für 10 böhmische Phonolithe überein. Der durchschnittliche Zr-Gehalt von 10 Trachyten aus Alkali-Gesteinsprovinzen von Schottland, USA und Hawai beträgt 500 g Zr/t. In den böhmischen Phonolithen tritt außer dem Ägirindiopsid als Zirkonium führendes Silikat noch der Hainit (Na-Ca-Ti-Zr-Silikat) auf. Zum Teil werden auch in den Nephelinsyenit-Pegmatiten seltene Na-Ti-Zr-Silikate gefunden. Allerdings sind diese Minerale nicht so verbreitet wie der für Alkaligesteine charakteristische Ägirin.

Zusammenfassend kann gesagt werden, daß an der Anreicherung des Zirkoniums in Gesteinen der atlantischen Serie besonders die Natron-Eisen-Pyroxene beteiligt sind.

In den Dioriten ist der Zirkon nicht mehr so häufig wie in den Graniten anzutreffen. Der durchschnittliche Zr-Gehalt der Diorite ist mit 125 g Zr/t auch geringer als derjenige der Granite mit 175 g/t. Die Übergänge des Diorits zum Granit, insbesondere die Granodiorite, weisen höhere, dem Granit entsprechende Zirkoniumwerte auf. In 5 Granodioriten, welche aus Batholithen von Südkalifornien stammen, finden Nockolds und Allen (1953) durchschnittlich 140 g Zr/t.

Die Andesite als Äquivalente der Diorite weisen je nach Abstammung verschiedene Zr-Gehalte auf. In 9 Pyroxen-Andesiten von Crater Lake finden Nockolds und Allen (1953) durchschnittlich 120 g Zr/t. Die Pyroxen-Andesite leiten zu den Feldspatbasalten über. Diese genetische Beziehung macht sich auch im Zirkoniumgehalt bemerkbar. Der in den Pyroxen-Andesiten gefundene Zr-Wert von 120 g/t stimmt gut mit dem Basaltdurchschnittswert überein. Andererseits leiten die Hornblende- und Glimmer-Andesite in den Zr-Gehalten zu den Trachyten über. Van Tongeren (1938) findet in 9 ostindischen Andesiten durchschnittlich 370 g Zr/t. Dieser Wert ist dem Durchschnittswert für Trachyte ähnlich. Aus Hawai stammen 7 von Wager und Mitchell (1953) angegebene Andesitanalysen. Ihr durchschnittlicher Zr-Gehalt beträgt 900 g/t. An dem höheren Zr-Gehalt der Andesite ist wahrscheinlich außer den Pyroxenen auch die Glasbasis beteiligt.

In den Gabbros und Diabasen, in denen nur ganz selten akzessorischer Zirkon gefunden wird, tritt etwa die Hälfte des vorhandenen Zirkoniums in die Pyroxene ein. Der Rest verteilt sich auf Plagioglas, Magnetit, Apatit. Die 4 Diabase von Remblinghausen, Wallenstein, Heringhausen und Hennetalsperre stammen aus einem zusammenhängenden Grünsteinzug im Sauerland. Hier wird angedeutet, wie wenig konstant der Zirkoniumgehalt eines Gesteinskomplexes innerhalb eines kleinen Abschnittes sein kann.

Der mittlere Zirkoniumgehalt der Gabbros und seiner Ergußäquivalente beträgt 110 g/t. Fairbairn, Ahrens u. Gorfinkle (1953) bestimmten in 57 präkambrischen Diabasen aus Ontario spektralanalytisch 16 Spurenelemente. Für Zirkonium fanden sie einen Durchschnitt von 100 g/t. Dieser Literaturwert kommt dem oben angeführten Wert von 110 g/t sehr nahe. Hevesy u. Würstlin (1934) fanden in einer Durchschnittsmischung aus 82 Gabbros und ähnlichen Gesteinen einen Wert von 140 g Zr/t, der vermutlich zu hoch ist. Wager u. Mitchells (1943) Zr-Werte für die Skaergaard-Gabbros (Ostgrönland) betragen durchschnittlich 30 g/t; in die Pyroxene der dortigen Gabbros tritt das Zirkonium bis zu Mengen von 50 g/t.

Die Basalte enthalten zwar durchschnittlich nur etwa halb so viel Zirkonium wie die Granite, jedoch zeigen einige Basalte ähnlich hohe Zirkoniumgehalte wie die Granite. Auch bei diesen größeren Zr-Gehalten wird das Zirkonium restlos in die vorhandenen Minerale eingebaut. Das Zirkoniumsilikat bildet sich nur bei einem Überschuß an Kieselsäure.

In den Basalten und Alkalibasalten tritt eine Differenzierung des Zirkoniumgehaltes, wie wir sie bei den Alkali gegenüber den Kalk-Alkali-Gesteinen bisher kennengelernt haben, nicht auf. Charakteristisch für die Alkalibasalte ist das Auftreten von Feldspatvertretern. Jedoch enthält weder der Nephelinit noch der Melilithbasalt Alkalipyroxene. Die niedrigsten Zr-Gehalte zeigen der Nephelinit und der Melilithbasalt. Wie im großen Zusammenhang, so zeigt sich auch innerhalb einer Gesteinsfamilie die Tatsache, daß die kieselsäureärmsten Glieder den geringsten Zr-Gehalt aufweisen.

Das zur Alkalireihe der Basalte entsprechende Tiefengestein ist der Essexit. Er enthält Ägirinaugit und zeigt mit 200 g Zr/t etwa den doppelten Zr-Gehalt des Basaltdurchschnitts. Die selteneren Glieder Theralith, Shonkinit, Ijolith, Missourit,

die sich an den Essexit anschließen, enthalten durchweg Ägirinkomponenten, so daß auch bei ihnen ein höherer Zirkoniumgehalt zu erwarten ist.

In den Basalten tritt die Hauptmenge des Zirkoniums in die Pyroxene und Magnetite ein. Als Beispiel für die Verteilung des Zirkoniums in den Basalten soll der trachydoleritische Basalt vom Backenberg angeführt werden. Dieses Vorkommen wird in einer Arbeit von K. H. Wedepohl (1954) näher beschrieben. Mit 106 g Zr/t kommt der Zr-Gehalt dieses Basaltes dem Durchschnittswert für Basalte sehr nahe. Für die Feldspäte wird der Mittelwert von 30 g Zr/t, für die Olivine der sehr konstante Wert von 40 g Zr/t eingesetzt. Für die Pyroxene wird ein Zr-Gehalt von 120 g/t angenommen. Der Pyroxen vom Monti Rossi mit 120 g Zr/t entspricht in seiner chemischen Zusammensetzung etwa dem Pyroxen eines Feldspatbasaltes. Der Titanomagnetit wurde mit Hilfe eines Magneten isoliert und analysiert.

(142) Trachydoleritischer Basalt, Backenberg — 106 g Zr/t

Probe-Nr. 1	Gew. %	Prozentualer Anteil	
Feldspat	44%	30 g Zr/t	13 g Zr/t
Pyroxen	35%	120 g Zr/t	42 g Zr/t
Olivin (+Serpentin)	10%	40 g Zr/t	4 g Zr/t
Erz (Titanomagn.)	10%	420 g Zr/t	42 g Zr/t
Glas, Zeolith, Apatit, Biotit	1%	—	—
			101 g Zr/t

Der so aus dem Mineralbestand berechnete Gesamtzirkoniumgehalt von 101 g/t stimmt mit dem durch Analyse gefundenen Gesamtwert von 106 g Zr/t gut überein.

Aus den 8 angeführten Basalten ergibt sich ein Durchschnitt von 110 g Zr/t. Wager und Mitchell (1953) fanden in 7 Basalten aus Hawai durchschnittlich 90 g Zr/t. Aus halbquantitativen Spektralanalysen von Arealen mit Alkalivormacht liegen u.a. 20 Zr-Werte für Basalte vor (Nockolds und Allen, 1954). Ihr Durchschnitt beträgt 150 g Zr/t. Die Nephelin- und Melilith-Basalte zeigen auch hier den kleinsten Zirkoniumgehalt. 7 Basalte, welche aus Bezirken mit Kalk-Alkali-Vormacht stammen, zeigen einen durchschnittlichen Zr-Gehalt von 100 g/t. Die Basalte der Alkali-Effusive zeigen durchschnittlich einen etwas höheren Zr-Gehalt als diejenigen der Kalk-Alkali-Effusive. Diese Beobachtung läßt sich nicht aus dem Mineralbestand deuten.

Aus dem niedrigen Zr-Gehalt der Olivine kann man für olivinreiche Gesteine die Größenordnung des zu erwartenden Zirkoniumgehaltes abschätzen. Der in der Tabelle angegebene Peridotit einschließlich der später beschriebenen Eklogite enthalten durchschnittlich 45 g Zr/t. Diese Zahl stimmt gut überein mit dem von Pinson, Ahrens und Frank (1953) gefundenen Zr-Wert von 55 g/t für 13 Ultrabasite. Hevesy (1934) findet für eine Durchschnittsmischung von 22 Peridotiten, Eklogiten und Duniten 60 g Zr/t.

Über die Verteilung des Zirkoniums in den Eruptivgesteinen kann abschließend folgendes gesagt werden:

Das Zirkonium reichert sich besonders in den Alkaligesteinen an. Die Alkaligesteine enthalten durchschnittlich etwa doppelt so viel Zirkonium wie die Kalk-Alkali-Gesteine.

Das Zirkonium findet sich am weitesten verbreitet in intermediären und sauren Eruptivgesteinen. Es kristallisiert als Zirkon in denjenigen Magmen, die stark nach der Seite der Restkristallisation hin differenziert sind.

Die basischen, besonders die ultrabasischen Eruptivgesteine führen wenig Zirkonium.

(1) *Die Streuung der Zirkoniumwerte innerhalb zweier Granitaufschlüsse*

Um die Schwankungen des Zirkoniumgehaltes innerhalb eines Granites auf kurze Entfernung hin zu untersuchen, wurden aus 2 Granitbrüchen des Kerngranites aus dem Brockenmassiv, Harz, 9 Proben in Abständen von je 30 m genommen.

	g Zr/t
(149) Granit—Königskopf 1, Harz	179
(150) Granit—Königskopf 2, Harz	173
(151) Granit—Königskopf 3, Harz	175
(152) Granit—Wurmberg 1, Harz	150
(153) Granit—Wurmberg 2, Harz	182
(154) Granit—Wurmberg 3, Harz	150
(155) Granit—Wurmberg 4, Harz	210
(156) Granit—Wurmberg 5, Harz	204
(157) Granit—Wurmberg 6, Harz	192

Der Granitbruch des Wurmberges liegt nordöstlich von Braunlage (Harz) und derjenige vom Königskopf 3 km westlich des Wurmberges an der Straße von Braunlage nach Torfhaus. Die Probenahme in den Brüchen erfolgte von Westen nach Osten in der Reihenfolge der Nummern Königskopf 1–3 und Wurmberg 1–6.

Um die Handstücke genügend zu homogenisieren, wurden je 3 kg des Probenmaterials zerkleinert, gut durchmischt und in einer Achatkugelmühle gemahlen. Bei kleineren Probenahmen unter 0,5 kg treten zu starke Schwankungen im Zr-Gehalt infolge der Inhomogenität des groben Materials auf.

Der Zirkoniumgehalt des Granites vom Königskopf zeigt innerhalb des Abbaues auf einer Strecke von etwa 100 m eine auffallende Konstanz. Der durchschnittliche Zr-Gehalt des Königskopf-Granites entspricht mit 175 g/t etwa dem Granitdurchschnittswert von 27 kanadischen Graniten, welche von Ahrens (1954) spektralanalytisch untersucht wurden.

Größere Streuung im Zr-Gehalt zeigen die Proben des Wurmberges. Im westlichen Teil dieses Bruches (Proben 1–3) findet man Handstücke mit dem geringsten Zirkoniumgehalt, während im östlichen Teil (Probe 4–6) der Zirkoniumgehalt über dem Durchschnittswert des Bruches liegt. Insgesamt zeigen die 6 Proben des Wurmberges mit 180 g Zr/t einen etwas höheren Zirkoniumgehalt als der Granit vom Königskopf mit 175 g Zr/t. Die größten Abweichungen vom Durchschnittswert weisen die Wurmbergproben 1, 3, und 4 auf. Hier tritt eine maximale Abweichung von etwa $\pm 17\%$ gegenüber dem Mittelwert auf.

Zusammenfassend kann gesagt werden, daß die Streuung der Zirkoniumwerte auf kurze Entfernung nicht so beträchtlich ist, wie zwischen einzelnen Granitkomplexen verschiedener Gebiete.

4. Das Zirkonium in den Sedimentgesteinen

Über die geochemische Verteilung des Zirkoniums in den Sedimenten liegen bis zur Gegenwart nur wenige Angaben vor. Bekannt ist, daß der Zirkon nicht nur in den Eruptivgesteinen, sondern auch in den Sedimentgesteinen als weitverbreiteter mikroskopischer Gemengteil gefunden wird. Das häufige Vorkommen des Zirkons in den Sedimenten ist der Tatsache zuzuschreiben, daß der Zirkon der Verwitterung gegenüber sehr widerstandsfähig ist. Von Wichtigkeit ist es zunächst festzustellen, ob und unter welchen Bedingungen in den Sedimenten eine Mobilisation des Zirkoniums erfolgen kann. Zu diesem Zweck sollen zuerst die Verwitterungserscheinungen an Hand zweier bekannter Profile besprochen werden.

(1) *Zwei Verwitterungsprofile über Granit*

Beim ersten hier angeführten Verwitterungsprofil über Granit handelt es sich um ein von Piller (1951) petrographisch eingehend untersuchtes Profil in der Nähe von Andreasberg im Harz.

	g Zr/t	
(158) Granit "Piller 16"—stark verlehmt, erdig Bröckellehm, (aus 30 cm Tiefe)	306	↑
(159) Granit "Piller 15"—in Grus zerfallen, beginnende Verlehmung, (1 m Tiefe)	240	|
(160) Granit "Piller 17"—in Grus zerfallen, Feldspäte kaolinisiert (2 m Tiefe)	180	|
(161) Granit "Piller 14"—frischestes Gestein (5 m Tiefe)	195	Zunahme der Verwitterung

Das frischeste Gestein, die Probe 104, war der Verwitterung schon etwas ausgesetzt, es liegt in Grus eingebettet und zeigt etwa den Zirkoniumgehalt der anderen Harzgranite wie z.B. des Wurmberges und Königskopfes. Die drei höheren Lagen bestehen aus Grus, welcher mit zunehmendem Verwitterungsgrad feinkörniger wird. In der Probe 17, bei der eine beginnende Kaolinisierung der Feldspäte festzustellen ist, zeigt das Zirkonium mit 180 g/t seinen geringsten Wert. Dann aber steigt der Zr-Gehalt kontinuierlich von Probe 17 bis zur stark verlehmten, erdigen Schicht.

Am stärksten werden demnach diejenigen Zirkone korrodiert, welche sich im untersten Horizont des Verwitterungsprofils befinden (Probe 17). Dort hat sich das eindringende Regenwasser auf dem Wege durch die oberen Schichten nach unten an Natrium- und Calciumbikarbonat angereichert, so daß es hier am aggressivsten wirkt. Die Anreicherung des Zirkoniums in den oberen Schichten ist als relative Anreicherung zu betrachten. Während Feldspäte und auch dunkle Gemengteile verwittern und ein Teil ihrer Ionen weggeführt werden, bleibt der größte Teil der Zirkone nur wenig korrodiert zurück.

Anschließend soll das zweite Profil beschrieben werden. H. Köster (1955) bearbeitete 2 indische Lateritprofile. Dasjenige von Kot, Provinz Gujarat, Indien, soll hier angeführt werden.

	g Zr/t
(162) Probe Nr. 104—Oberer Konkretionshorizont Konkretionen	278
(163) Probe Nr. 103—Heller Horizont Ton	352
(164) Konkretionen	375
(165) Probe Nr. 102—Unterer Konkretionshorizont Ton	325
(166) Konkretionen	683
(167) Probe Nr. 101—kaolinisierter Granit Ton	138
(99) Probe Nr. 105—Granit von Eklara	380

Im Horizont Nr. 101 hat eine vollständige Kaolinisierung des liegenden Granites stattgefunden. Dabei wurden die Feldspäte und Hornblenden vollständig zerstört und die Quarzkörner stark korrodiert. In diesem Horizont (analog dem untersten Horizont im Pillerprofil) wird mit 138 g Zr/t. der geringste Zirkoniumgehalt gefunden. Alkalische Lösungen haben nicht nur den Quarz korrodiert, sondern auch den größten Teil des Zirkons aufgelöst. Demgegenüber hat sich das Zirkonium in den Eisenoxydkonkretionen der Probe Nr. 102 angereichert.

Der kaolinisierte Horizont Nr. 101 zeigt nicht nur den geringsten Zirkoniumgehalt, er ist auch praktisch eisenfrei. Das gesamte Eisen, welches in Verdunstungsperioden aus der kaolinisierten Schicht kolloiddispers nach oben wanderte, transportierte vermutlich auch das Zirkonium. In der Schicht der Probe Nr.102 bildete es anschließend die zirkoniumreichen Eisenoxydkonkretionen.

In einem Nachtrag zu diesem Profil im Bezug zur Stoffwanderung nimmt H. Köster (1956) für seine Berechnungen als Bezugsmineral den Quarz. Auch nach diesen Betrachtungen ändert sich die hier vertretene Anschauung über die Stoffwanderung nur wenig.

Die nun folgenden Lösungsversuche sollen zeigen, daß insbesondere bikarbonathaltige Lösungen den Zirkon zu lösen vermögen. Viel beobachtet sind Auflösungserscheinungen von Zirkonen in Lateritprofilen (Frederickson, 1948). Lösungsversuche von Zirkonen, welche von Dorothy Carrol (1953) ausgeführt wurden, sind qualitativ. Das in Lösung gegangene Zirkonium konnte quantitativ nicht erfaßt werden, weil die geringen Spuren welche mit Cupferron gefällt wurden, nicht wägbar waren. Der kolorimetrische Nachweis mit Alizarin-S war negativ, weil die nach Sandel (1950) benützte Methode nicht die genügende Empfindlichkeit besitzt.

Ein durchsichtiger, von Beimengungen freier Zirkon aus dem Ilmengebirge wurde in einer Achatschale aufs Feinste gepulvert und auf eine Korngröße von etwa 1–5 μ gebracht. Je 100 mg Zirkonpulver wurden mit 250 ml der verschiedenen unten angegebenen Lösungen in Schüttelflaschen 7 Tage lang bei 20°C geschüttelt.

Zur Herstellung der Calciumbikarbonatlösung wurde CO_2 bei Zimmertemperatur in destilliertes Wasser eingeleitet; währenddem wurde langsam eine filtrierte Lösung von Calciumhydroxyd so lange eingetropft, bis sich das an der Eintropfstelle ausfallende Calciumkarbonat nicht mehr als Hydrogenkarbonat auflöste und ausfallendes $CaCO_3$ als Bodenkörper vorhanden war. Die Lösung zeigte einen pH-Wert von 6,7.

Die Analysen wurden nach einer Vorschrift für Zirkoniumbestimmung von Wässern durchgeführt.

Lösungsmittel	Gelöstes Zirkonium	
Destilliertes Wasser	12 mg Zr/t	pH = 7
1%ige Natriumkarbonatlösung	32 mg Zr/t	pH = 11
1%ige Natriumbikarbonatlösung	36 mg Zr/t	pH = 8,7
bei 20°C gesättigte Calciumbikarbonatlösung	40 mg Zr/t	pH = 6,7
0,1 n Salzsäure	16 mg Zr/t	pH = 1
0,1 n Natronlauge	16 mg Zr/t	pH = 13

Die Ergebnisse zeigen, daß der Zirkon von den Bikarbonatlösungen am stärksten gelöst wird.

Selbst in reinem Wasser zeigt das Zirkoniumsilikat noch eine kleine Löslichkeit. Diese Tatsache wurde schon von Bouyoucos (1921) beobachtet. Wie die Lösungsversuche in Salzsäure und Natronlauge zeigen, scheint sich der Zirkon im sauren wie im basischen Medium in gleichem Maße zu lösen. Dies wird auch von Carrol (1953) vermutet. Die größere Löslichkeit des Zirkoniumsilikates in karbonathaltigen Lösungen geht mit der Erscheinung parallel, nach der die meisten Zirkoniumsalze in überschüssiger Alkalikarbonatlösung unter Komplexbildung löslich sind.

Strock und Drexler (1941), welche in den an Bikarbonat reichen Wässern der Saratoga-Quellen 0,35 mg Zr/L (= 0,35 g Zr/t) fanden, nehmen an, daß Natrium- und Calcium-Bicarbonat reiche Lösungen nicht nur beträchtliche Mengen des Zirkons zu lösen vermögen, sondern daß das Zirkonium auch als stabiles Dikarbonatzirkonylion $[ZrO(CO_3)_2]^{-2}$ in Gegenwart von CO_2 transportiert werden kann.

Außer der Tendenz zur Komplexbildung mit Alkalikarbonaten (ähnlich dem Thorium) ist das chemische Verhalten des Zirkoniums in wässrigen Lösungen gekennzeichnet durch seine Neigung zur Hydrolyse. Das vierwertige Zirkonium besitzt nur sehr schwache basische Eigenschaften, so daß seine Verbindungen bereits in recht sauren Lösungen bei pH = 3 hydrolytisch gespalten werden unter Bildung von ZrO_2=Hydrat. Da das durch Hydrolyse ausfallende ZrO_2—Hydrat sehr leicht kolloide Lösungen bildet, ist anzunehmen, daß es in karbonatfreien Gewässern in dieser Form transportiert werden kann.

(2) *Verwitterungsbildungen und Tonminerale*	g Zr/t
(168) Weißer Bauxit—Epleny, Ungarn	423
(169) Bauxit—Drnis, Dalmatien	440
(170) Bauxit—Istrien	505
(171) Bauxit—Eleusis, Griechenland	500
(172) Bauxit—Montenegro	504
(173) Bauxit—Ujbarok, Ungarn	523
(174) Bauxit—Mostar, Herzegowina	565
(175) Bauxit—Südfrankreich	623
(176) Kaolinit (Schlämmkaolin)—Tirschenreuth, Fichtelgebirge	88
(177) Kaolinit, <3,16 μ—Dobritz, Sachsen	92

	g Zr/t
(178) Kaolinit—Murfreesboro, Arkansas	1120
(179) Halloysit—Lawrence County, Missouri	13
(180) Montmorillonit H 24—Otay, Kalifornien	98
(181) Montmorillonit—Wyoming	140
(182) Montmorillonit—Gaura, Siebenbürgen	140
(183) Illit, H 36—Morris, Illinois	98
(184) Illit, H 35—Fithian, Illinois	118
(185) Glaukonit—Weenzen	120

In den Bauxiten reichert sich das Zirkonium mit einer etwa 3 fachen Konzentration gegenüber dem durchschnittlichen Zr-Gehalt der Lithosphäre an. Die Anreicherung des Zirkoniums in den Bauxiten ist ähnlich der eingangs erwähnten Anreicherung in Böden in erster Linie als relative Anreicherung zu betrachten, weil sich der Zirkon als verhältnismäßig stabiles Mineral im Verwitterungsrückstand anreichert.

Bauxite entstehen durch eine intensive stark alkalische Verwitterung besonders unter tropischen Klimaverhältnissen. Soweit bei dieser alkalischen Mobilisierung der Zirkon teilweise korrodiert und aufgelöst wird, scheidet sich das in Lösung befindliche Zirkonium mit dem Aluminiumhydroxyd gemeinsam wieder ab.

Die Primärgesteine der in der Tabelle aufgeführten Bauxite sind größtenteils nicht bekannt. Die Bauxite aus Siebenbürgen und Ungarn sind wahrscheinlich Kalkbauxite.

Um festzustellen, ob in den Bauxiten lösliches Zirkonium vorhanden ist, wurden sie 30 Min. mit heißer 2 n Salzsäure digeriert, dabei ging praktisch das gesamte Eisen in Lösung. In dieser Lösung wurden durchschnittlich etwa 35 g Zr/t gefunden. Diese Menge Zirkonium ist vermutlich an das Eisen gebunden. Der im Bauxit vorhandene Hydrargillit, Boehmit und Diaspor ist selbst in heißer Säure schwierig löslich. Das kristallisierte Aluminiumhydroxyd löst sich zum Unterschied von dem amorphen Oxydhydrat nur sehr schwer in Säuren auf.

M. Gordon u. K. J. Murata (1952) finden in 14 Bauxiten von Arkansas spektralanalytisch 1300 g Zr/t. Die hohen Zirkoniumwerte dieser Bauxite sind mit dem hohen Zirkoniumwert der Muttergesteine in Verbindung zu bringen. Die primären Gesteine dieser Bauxite sind Nephelinsyenite mit einem durchschnittlichen Zr-Gehalt von 500 g Zr/t. Auch gegenüber den Nephelinsyeniten erfolgt in den Bauxiten eine etwa 2–3 fache Anreicherung des Zirkoniums.

Von den Tonmineralen zeigt der Kaolinit von Murfreesboro, Arkansas, den höchsten Zirkoniumgehalt. Sein hoher Zirkoniumgehalt deutet auf einen entsprechend höheren Zr-Gehalt seines Muttergesteines, vermutlich eines Nephelinsyenites hin.

Der Kaolinit von Murfreesboro wurde mit 2 normaler Salzsäure 30 Min. in der Hitze digeriert, dabei wurden 78 g Zr/t lösliches Zirkonium gefunden. Da das Zirkoniumsilikat bei solch einer Säurebehandlung nicht in diesem Ausmaß gelöst wird, muß angenommen werden, daß diese gefundene Zirkoniummenge adsorbiert vorlag, während ein Teil des übrigen Zirkoniums in den mit Salzsäure unaufschließbaren Kaolinit eingebaut war. Außerdem wird noch ein Anteil des Zirkoniumgehaltes in Zirkonrelikten zu suchen sein, welche unter dem Mikroskop allerdings nur selten angetroffen wurden.

Das Primärgestein des Kaolinites aus dem Fichtelgebirge ist ein Granit, und das Muttergestein des Kaolinits aus Dobritz, Sachsen, ist ein Quarzporphyr. Dem niedrigen Zr-Gehalt dieser beiden Kaolinite entsprechend, führen die Ausgangssteine wenig Zirkon.

In der Kaolinitfraktion $< 3{,}16\ \mu$ von Dobritz sind keine Schwerminerale vorhanden. Auch hier ist anzunehmen, daß das Zirkonium wahrscheinlich das Aluminium substituiert.

Die Montmorillonite von Wyoming und Siebenbürgen weisen höhere Zr-Gehalte auf als durchschnittlich die Kaolinite; abgesehen vom Kaolinit von Murfreesboro. Im Montmorillonit von Wyoming ist kein Zirkon zu finden. Die Primärgesteine der amerikanischen Bentonite sind vermutlich vulkanische Tuffe. In Montmorilloniten, welche sich von Rhyoliten oder Trachyten ableiten, dürfte ein noch höherer Zirkoniumgehalt zu erwarten sein.

Der Montmorillonit besitzt ein hohes Adsorptionsvermögen, so daß in seinen Zwischenschichten nicht nur Wasser adsorbiert wird, sondern auch andere Stoffe und wenn anwesend, wahrscheinlich auch Zirkonium.

Die Illite zeigen als Verwitterungsreste etwa den Zirkoniumgehalt von Glimmern, welche eingeschlossene Zirkonmikrolithe enthielten. Auch der hier angegebene Glaukonit, der sich wohl auch vom Biotit ableiten läßt, zeigt einen ähnlichen Zr-Gehalt.

(3) *Der Zirkoniumgehalt von Wässern, einigen chemischen und biogenen Sedimenten*

	g Zr/t
(186) Helenenquelle—Bad Pyrmont	0,002
(187) Trinkwasser—Göttingen	0,003
(188) Quellenschlamm—Bad Ems	47
(189) Quellenschlamm—Wiesbaden	50
(190) Jüngstes Steinsalz—Reyershausen	0,2
(191) Älteres Steinsalz—Reyershausen	0,5
(192) Sylvin—Staßfurt	<0,1
(193) Sylvinit—Vienenburg/Harz Schacht II, 300 m Teufe	0,1
(194) Braunkohlenasche—Türnich, Rheinland	23
(195) Steinkohlenasche—Baesweiler, Aachen Rev.	25
(196) Yorkshire Cohles—Asche	106
(197) Edelschwein, ganzer Körper neugeboren (Orig. Material v. Goldschmidt)	<2
(198) Edelschwein, Knochen (v. Goldschmidt)	60
(199) Phosphoritknollen—ob. Flammenmergel Schlewecke	74

Das Göttinger Trinkwasser, welches mit 5,49 mval Karbonathärte beträchtliche Mengen Calciumbikarbonat führt, zeigt einen etwas größeren Zr-Gehalt als die Helenenquelle, welche als Eisensäuerling hauptsächlich Eisenkarbonat und weniger Calcium enthält. Das Quellgebiet des Göttinger Wassers liegt im Muschelkalk, so daß als Zirkoniumlieferant nur die tonigen Beimengungen im Kalk, bzw. die klastischen Sedimente des Leinetalgrabens in Frage kommen. Der Zirkoniumgehalt der Göttinger Quellen ist sehr gering gegen die von Strock (1941) gefundenen Mengen von 350 γ Zr/Liter im Wasser der Saratoga-Quellen. Das Saratoga-Wasser enthält etwa 100 mal so viel Zirkonium wie das Göttinger Trinkwasser. Wenn bicarbonathaltige Wässer längere Strecken durch zirkoniumreiches Gestein

zurücklegen, so sind sie in der Lage, größere Mengen Zirkonium zu lösen und anzureichern. Dieser Sonderfall, daß Quellwasser vom Kalkgebiet anschließend ein an Zirkonium reiches Nephelinsyenit-Gebiet durchwandert, ehe es zu Tage tritt, wird in der Natur nur selten praktisch verwirklicht.

Beim angeführten Quellenschlamm handelt es sich hauptsächlich um Ausfällungen von Eisenhydroxyden. Das ursprünglich im kohlensäurehaltigen Quellwasser beständige Eisenkarbonat fällt bald nach dem Austritt der Quelle and die Tagesoberfläche aus. Bei Anwesenheit von Sauerstoff fällt es als Eisenhydroxyd FeO(OH) aus. Das besonders in bikarbonathaltigen Wässern vorhandene Zirkonium wird mitgefällt und reichert sich somit im Eisenschlamm der Quellen an.

Die im Steinsalz und Sylvin gefundenen Zirkoniummengen sind mit durchschnittlich 200 γ Zr/1 kg Salz etwa von derselben Größenordnung wie der von H. Born (1934/35) in Salzen der norddeutschen Salzlager gefundene Bleigehalt.

Durch langsames Abkühlen einer gesättigten Natriumchloridlösung bei Gegenwart von Zirkonylchlorid wurde durch eigene Versuche gefunden, daß auch das Zirkonium in der gleichen Menge wie das Blei von Steinsalz aufgenommen wird, nämlich mit 200 γ Zr/1 kg Salz.

Beim Sylvin aus Staßfurt, bei dem kein Zirkonium gefunden wurde, handelt es sich um einen, in einem alten Kalischacht sekundär ausgeschiedenen Kristall. Es ist wahrscheinlich, daß bei der Umkristallisation die früher vorhandenen Fremdionen weggeführt wurden.

Man kann aus dem Zirkoniumgehalt der Zechsteinsalze Rückschlüsse auf den Zr-Gehalt des Zechsteinmeeres ziehen. Ein gewisser Anteil des im Meerwasser vorhandenen Zirkoniums dürfte vorher allerdings durch Bindung an kolloide Sedimente, insbesondere an Tonsedimente und an Eisenhydroxyde entfernt worden sein. Wenn man annimmt, daß die damalige Natriumchloridkonzentration der gesamten Ozeane von dem Elektrolytgehalt der heutigen Meere nicht sehr verschieden war, und mit einem Salzgehalt von rund 3% rechnet, so enthält eine Tonne Meerwasser 6 mg Zr. Das ist also doppelt so viel Zirkonium wie im Göttinger Trinkwasser, in welchem 3 mg Zr/t gefunden wurden. Damit ist das Zirkonium im Meerwasser so häufig wie etwa das Zink, Blei oder das Mangan.* Über den Zr-Gehalt des Meerwassers ist in der Literatur keine Angabe zu finden.

In der Asche von Kohlen reichert sich das Zirkonium ebenfalls an, wenn auch nicht in dem Maße, wie wir es z.B. vom Germanium, Beryllium oder Kobalt her kennen, denn das Zirkonium ist viel schwieriger in Lösung zu bringen.

Während der Zr-Gehalt der beiden rheinischen Kohlen gleich groß ist, ist derjenige der Yorkshire-Kohlen mit 106 g/t 4 mal so hoch. Im Flöz Barnsley 331, Yorkshire, fand L. Horton (1950) mit 100 g Zr/t. einen ähnlichen Zirkoniumgehalt in den Aschen dieser Kohlen.

Die mäßige Anreicherung des Zirkoniums in den Kohlen steht im Zussammenhang mit dem Pflanzenwuchs, aus dem sie entstanden sind. Demnach scheint das Zirkonium in den Pflanzen nur in geringen Spuren anwesend zu sein.

Nach Angaben von K. Pirschle (1939) konnten in rezenten Pflanzen bis zu 0.001% Zr (= 10 g Zr/t) nachgewiesen werden. H. W. Harvey (1945) zitiert

* *Nachtrag:* In reinem atlantischen Oberflächenwasser (Probenahme auf 65° 31,9′ Nordbreite und 28° 36,6′ Westlänge) wurden 4 mg Zr/t gefunden.

eine Meerestanganalyse von Beharrell, welcher im Kilo Tang 3 mg Zirkonium (= 3 g Zr/t) findet.

In den phosphorreichen Knochengerüsten der Lebewesen scheint sich das Zirkonium besonders anzureichern. Die Phosphoritknolle zeigt etwa einen ähnlichen Zirkoniumgehalt wie die Knochen des angeführten Schweines. Bei der Ausscheidung der Phosphorsäure wird das in Lösung befindliche Zirkonium als Zirkoniumphosphat ausgefällt.—Man muß vermuten, daß die Anreicherung von Zirconium in Knochen und Zähnen eine gewisse physiologische Bedeutung erlangen kann.

(4) *Sedimentäre Erze*	g Zr/t
(200) Eisenoolith, Lias γ—Echte, Northeim (Originalmaterial v. H. Harder, 1951)	24
(201) Hämatiterz, Lias γ—Markoldendorf (Originalmaterial v. H. Harder, 1951)	25
(202) Fein- und mittelkörniges Trümmererz—Gebhardshagen, Salzgitter (Originalmaterial v. H. Harder)	100
(203) Oolith, Dogger β—Bohrung Unterklausen I, Franken	335
(204) Manganknolle aus rotem Ton—*Challenger*, Expedition 19° 49′ N, 121° 43,6′ W	355

Bei den 2 Eisenerzen aus Echte und Markoldendorf handelt es sich um Originalmaterial von H. Harder (1951). Nach seinen Angaben haben sich die Erze des Lias-Meeres durch Ausflockung von Eisenhydroxydsolen gebildet. Im Küstenbereich flockt der Elektrolytgehalt des Meeres FeO(OH)- und SiO_2-Sole aus. Auch hier darf man annehmen, daß ausflockendes Eisenhydroxyd befähigt ist, das Zirkonium mitzufällen und anzureichern.

Der höhere Zirkoniumgehalt des Trümmererzes aus Gebhardshagen stammt von Schwermineralrelikten, welche in den klastischen Beimengungen vorhanden sind. Der hohe Zirkoniumgehalt des Oolithes aus dem Dogger β stammt hauptsächlich von Zirkoneinschlüssen in den Ooiden.

Nicht nur die Oxydhydrate des Eisens, sondern auch diejenigen des Mangans können Zirkonium adsorbieren. Daß es dabei zu beträchtlichen Anreicherungen von Zirkonium kommen kann, zeigt die Analyse der Manganknolle.

(5) *Kieselgesteine*	g Zr/t
(205) Kulmkieselschiefer—Wallau	16
(206) Feuerstein aus Diluvialgeschiebe—Remkersleben, Madeburg	12
(207) Kieselsinter, Geysir—Island	24
(208) Kieselsinter—Yellowstonepark	25

Die hier angegebenen Kieselgesteine enthalten wenig Zirkonium. Soweit es sich bei ihnen um Ausfällungen von Kieselsäure handelt, wird evtl. in Lösung vorhandenes Zirkonium nur zu einem kleinen Teil adsorbiert. In der seperat beschriebenen Analysenmethode wurde darauf hingewiesen, daß ausflockende Kieselsäure Zirkonium zu adsorbieren vermag.

Bei der aus heißen Lösungen ausgeschiedenen Kieselsäure der Kieselsinter scheint etwas mehr Zirkonium mobilisiert zu werden als bei der Feuersteinbildung, die bei tieferen Temperaturen stattfindet.

Auffallend ist der übereinstimmende Zirkoniumgehalt der an verschiedenen Orten gefundenen Kieselsinter.

(6) *Pelite*

	g Zr/t
(209) 36 deutsche paläoz. Tonschiefer—(Durchschnittsmischung von Noll, 1933/34)	175
(210) 14 japanische paläoz. Tonschiefer—(Durchschnitt von Minami, 1935)	163
(211) 10 japanische mesoz. Tonschiefer—(Durchschnitt von Minami, 1935)	165
(212) Devon-Schiefer Wissenbacher Schiefer—Rammelsberg, Harz	134
(213) Dachschiefer, Devon—Raumland, Rothaargebirge	110
(214) Kulmtonschiefer—Waldenburg, Schles.	164
(215) Tonschiefer, Rotliegendes—Manebacher Schichten	85
(216) Hauptlöser—älteres Kalilager, Volkenroda, Thür.	28
(217) Grauer Salzton—Volkenroda, Thür.	64
(218) Roter Salzton—Volkenroda, Thür.	77
(219) Bunte Zechsteinletten—Büdingen, Wetterau	70
(220) Kupferschiefer—Mansfeld	137
(221) Kupferschiefer—Albungen, Werra	170
(222) Röttonschiefer, Gips-führend—Eddigehausen, Göttingen	25
(223) Roter Keuperton, km—Friedland a.d. Leine	95
(224) Liaston, Lias α—Ziegelei Parensen	110
(225) Liaston, Lias ε—Dobbertin, Mecklbg.	120
(226) Brauner Ton, Dogger ß—Bohrung Friedrich IV, Franken	205
(227) Bänderschnitzenton, Dogger ß—Bohrung Pottenstein II, Franken	212
(228) Rötelton (Bolus) Dogger ß—Bohrung Eibenstock II, Franken	245
(229) Miozän-Ton, (Sarmatton)—Bohrung Zistersdorf	124
(230) Glaukonitton, Tertiär—Ülsen, Holl. Grenze	166
(231) Glaukonitton, Kreide—Salzgitter, Bohrung Jemmeritz I	270
(232) Glashafenton, Tertiär—Groß-Almerode	173
(233) Diluvialton—Papendorf, Mecklbg.	170
(234) Roter Ton—Meteorstation 250 I, oben 2. Hälfte 3 cm, vor Kap S. Roque, Südamerika	96
(235) Roter Ton—Meteorstation 282 I, oben 3,3 cm, westl. Kap Verden	157
(236) Roter Ton—Albatros, Kern 255, St. 359, 840, 7–842 cm	144

Da das Mineral Zirkon der Verwitterung gegenüber sehr widerstandsfähig ist, findet es sich als klastisches Relikt in den Produkten der mechanischen Sedimentation wieder. Dort macht es den Sortierungsvorgang in Tone und Sande mit, ohne nennenswerte Veränderungen zu erfahren.

Außer dem Zirkon können am Zr-Gehalt der klastischen Sedimente untergeordnet auch noch andere Schwermineralrelikte beteiligt sein, welche, wie eingangs gezeigt wurde, einige zehntel Prozente Zirkonium führen können; z.B. Magnetit, Ilmenit, Rutil, Titanit, Apatit. Auch der Zr-Gehalt anderer evtl. vorhandener Minerale, wie z.B. Pyroxene, Feldspäte oder Glimmer ist zu berücksichtigen.

Die Tone, bzw. Tonschiefer beteiligen sich mit rund 80% am Gesamtbestand der Sedimente. Damit dürfte der größte Anteil des gesamten Zirkoniumgehaltes der Sedimente in den Tonen und Tonschiefern zu suchen sein.

Von den 3 Durchschnittsmischungen zeigt diejenige von 36 deutschen paläozoischen Tonschiefern den höchsten Zirkoniumgehalt. Die 14 paläozoischen und 10 mesozoischen Tonschiefer zeigen übereinstimmende Zr-Werte. Diese Werte kommen dem Mittelwert für Tonschiefer sehr nahe. Die Abnahme des Zr-Gehaltes vom jüngeren Salzton über den älteren Salzton zum Hauptlöser ist auf den steigenden Anteil der Salzkomponente zurückzuführen. In den letztgenannten Salztonen findet man teilweise Salzgehalte bis zu 60%.

Die Kupferschiefer zeigen keine überdurchschnittlich hohen Zr-Werte. Das ist auch nicht zu erwarten, da sich im Kupferschiefer hauptsächlich solche Metalle anreichern, welche mit Schwefelwasserstoff schwer lösliche Sulfide bilden.

Der Zr-Gehalt des Röttonschiefers aus Eddigehausen ist niedrig, da wegen des hohen Gipsanteiles seine Tonkomponente gering ist.

Auffallend ähnlich sind die Zr-Gehalte der beiden Tone aus dem Lias und die Zr-Gehalte der 3 Tone aus dem Dogger ß. Das bedeutet, daß der Zirkonium-Gehalt für bestimmte Tonschichten charakteristisch sein kann. Umgekehrt kann also eine Zirkoniumanalyse beim Aufsuchen von bestimmten Horizonten von Nutzen sein.

Wenn der Zirkonium-Gehalt in den Tonen auf weite Strecken konstant bleibt, so deutet das auf eine gleichmäßige Sedimentation hin. Damit ist auch eine gleichmäßige Verteilung der Schwermineralmikrolithen verbunden, welche ihrerseits oft als Einschlüsse in blättchenförmigen Mineralen vorliegen. Solche extremen Schwankungen der Zr-Gehalte, wie man sie in Sanden und Sandsteinen antrifft, findet man in den Tonen nicht.

Verschiedene Tone, welche mit ihrem Zr-Gehalt beträchtlich unter dem Mittelwert liegen, sind keine normalen Tone. Bei ihnen wird die Tonkomponente durch Kalk oder Anhydrit verdrängt.

Den höchsten Zr-Wert der Tone weist der Glaukonitton von Salzgitter auf. Es ist wahrscheinlich, daß der Glaukonitanteil dieses Tones an dem hohen Zr-Gehalt beteiligt ist. Wenn sich der Glaukonit durch Umwandlung von Biotit gebildet hat, während im Biotit selbst Zirkoneinschlüsse häufig anzutreffen sind, so ist auch der höhere Zr-Gehalt des glaukonithaltigen Tones verständlich.

Der Zirkoniumgehalt der 3 Tiefseetone, ausgenommen der etwas geringere Zr-Gehalt des roten Tones der Meteorstation 250 I, kommt dem Zirkonium-mittelwert für Tone und Tonschiefer sehr nahe. In 2 roten Tiefseetonen von der *Challenger* Expedition findet Hevesy (1934) je 140 g Zr/t. E. D. Goldberg (1954) gibt für 8 pazifische Tone durchschnittlich 123 g Zr/t an.

Auch der Zirkoniumgehalt der roten Tone ist auf sedimentierte Zirkone und auf das an die Tonminerale gebundene Zirkonium zurückzuführen. Wahrscheinlich ist auch ein kleiner Teil des Zirkoniums an das in den Tonen vorhandene Eisen gebunden.

(7) *Psammite, Psephite*	g Zr/t
(237) 11 deutsche Karbonsandsteine—(Durchschnittsmschg. von v. Engelhardt, 1936)	140
(238) 23 deutsche Buntsandsteine—(Durchschnittsmschg. von v. Engelhardt, 1936)	365
(239) 11 deutsche Kreidesandsteine—(Durchschnittsmschg. von v. Engelhardt, 1936)	200
(240) Sandstein, Unterkreide—Bentheim-Nord	33
(241) Flözleerer Kohlensandstein, Karbon—Billmerich, Westfalen	45
(242) Grüner Sandstein, Dogger *β*—Bohrung, Pegnitz Franken	129
(243) Kalksandstein, Dogger *β*—Bohrung, Enzendorf Franken	140
(244) Unterer Buntsandstein—Freden, Leine	234
(245) Glaukonitsandstein Ehra (Bohrkern 800 m Teufe)	480
(246) 10 deutsche Quarzite—(Durchschnittsmischg. von v. Engelhardt, 1936)	573

	g Zr/t
(247) Quarzsand—Dörentrup, Lippe	75
(248) Quarzit—Valle, Kragerö	96
(249) Koblenzquarzit—Krebsberg b. Urbar, S.W.-Hang	273
(250) Taunusquarzit Devon—Rochusberg, Bingen	465
(251) 17 deutsche Grauwacken—(Durchschnittsmischg. von v. ENGELHARDT, 1936)	295
(252) Kulm-Grauwacke—Grube "Hülfe Gottes", Bad Grund, Harz, 432 m Teufe	80
(253) Kulm-Grauwacke—Sösetalsperre, Harz	110
(254) Tanner Grauwacke—Lauterberg, Harz	107
(255) Zechsteinkonglomerat (sandige Fazies)—Albungen	130

Während die sehr kleinen Zirkonkristalle etwa $< 10\ \mu$ in den Tonen eingebettet werden, bleiben die gröberen Zirkone in den Sanden zurück.

Von den 3 angegebenen Zr-Werten für die Durchschnittsmischungen zeigen die Karbonsandsteine den geringsten Zirkoniumgehalt. Dem niedrigen Zr-Gehalt der Karbonsandsteine stehen die etwa 4 mal so hohen Zr-Werte der 10 deutschen Quarzite gegenüber, von denen 2 aus dem Kambrium und 8 aus dem Devon stammen.

Der Glaukonitsandstein zeigt, ähnlich dem Glaukonitton von den Tonen, den höchsten Zr-Gehalt der Sandsteine. Das bestätigt die für den Glaukonit schon beim Glaukonitton gemachte Annahme, daß derselbe am hohen Zr-Gehalt beteiligt ist.

Der Zirkoniumgehalt der Sandsteine variiert von 33–480 g Zr/t. Wegen der beträchtlichen Unterschiede in den spezifischen Gewichten von Zirkon gegenüber Quarz und Feldspat verteilt sich der Zirkon in den rezenten Sanden nicht gleichmäßig, sondern reichert sich entsprechend den Strömungsverhältnissen an bestimmten Stellen an.

Mit durchschnittlich 350 g Zr/t weisen die Quarzite einen höheren Zr-Gehalt auf als die Sandsteine mit 200 g Zr/t. Auch die Zirkoniumwerte der Quarzite von verschiedenen Fundorten streuen sehr. TH. G. SAHAMA (1945), welcher Gesteine im südlichen Finnisch-Lappland auf Spurenelemente untersuchte, fand ebenfalls in den Psammiten eine starke Variation des Zr-Gehaltes. Bei 10 analysierten Quarziten pendeln die Zr-Werte zwischen 50 und 750 g/t.

Weniger große Schwankungen im Zr-Gehalt zeigen die Grauwacken. Die aus dem Harz stammenden beiden Kulm-Grauwacken und die Tanner Grauwacke zeigen ähnlichen Zr-Gehalt.

(8) *Karbonatgesteine*	g Zr/t
(256) 32 deutsche Devonkalke—(Durchschnittsmischg. v. v. ENGELHARDT, 1936)	25
(257) 45 deutsche Jurakalke—(Durchschnittsmischg. v. v. ENGELHARDT, 1936)	12
(258) 16 deutsche Kreidekalke—(Durchschnittsmischg. v. v. ENGELHARDT, 1936)	18
(259) Zechsteindolomit, Fluorit-führend—Römerstein, Bad Sachsa, Harz	16
(260) Zechsteindolomit—Scharzfeld, Harz	18
(261) Korallenoolith, Malm—Freden a.d. Leine	9
(262) Radiolarienschichten—Pfronten, Allgäu	18
(263) Solnhofener Plattenkalk, Malm—Solnhofen, Bayern	18
(264) Oolithzone aus mu—Auschnippetal, Göttingen	20
(265) Steinmergel, km—Ziegelei Friedland, Göttingen	35
(266) Trochitenkalk, mo_1—Reckershausen, Göttingen	15
(267) Ceratitenkalk, mo_2—Hainberg, Göttingen	30

	g Zr/t
(268) Ceratitenkalk, (harte Kalkband) mo_2—Diemarden, Göttingen . .	45
(269) Cenomanpläner—Kalerde, Hils	26
(270) Kalktuff, Quartär—Lenglern, Göttingen	23
(271) Muschelschale einer Arca—Strand von Gaybu, Pernambuco . .	<2
(272) Kalkalgen—Strand b. S. Carlos, Fernando Po	8
(273) Globigerinen-Schlamm—Meteorstation 240 a	10
(274) Globigerinen-Schlamm—Meteorstation 288 b	30
(275) Gipsbrekzie, Zechstein—Hundelshausen	4
(276) Basalanhydrit—Reyershausen	26

Von den Durchschnittsmischungen zeigen die paläozoischen Kalke den höchsten Zirkoniumgehalt.

Bei den Kalken mit den geringsten Zirkoniumgehalten handelt es sich um Kalke mit kleinen Rückständen. Von 10 Kalken wurden die Rückstände auf Zirkonium untersucht. Es zeigte sich, daß praktisch der gesamte Zr-Gehalt der Kalke in den Rückständen zu finden ist. Dort befindet er sich teils in Tonmineralen, teils in Zirkonrelikten. Der Zirkoniumgehalt der Kalke ist also eine Funktion seiner Rückstände. Man kann leicht abschätzen, welcher Zr-Gehalt in den Kalken zu erwarten ist. Setzt man für die Tone den mittleren Zr-Gehalt von 160 g/t ein, so enthält z. B. ein Kalk mit 10% tonigem Rückstand 16 g Zr/t. Dieser Wert kommt dem tatsächlichen Mittel der Kalke mit 19 g Zr/t sehr nahe.

Man kann aus den jeweilig höheren Zr-Werten der betreffenden Kalke ersehen, welcher Kalk die größten Rückstände aufweist. Der Ceratitenkalk von Diemarden hat mit 45 g Zr/t eine sehr hohe Tonkomponente. Diese Probe ist schon als Mergel zu bezeichnen. Sie zeigt etwa einen ähnlichen Zr-Gehalt wie der Steinmergel aus Friedland. Für die Mittelwertbildung der Kalke wurden die Mergel nicht herangezogen.

Während bei den meisten Kalken in 0,2 n HCl kein Zirkonium in Lösung ging, wurden beim Oolithkalk aus dem Auschnippetal 1 g/t lösliches Zirkonium gefunden. Dieser Kalk enthält einige Prozente Eisen. Das deutet darauf hin, daß ein Teil des Zirkoniums an Eisen gebunden sein kann. Daß ausfallendes Eisenoxydhydrat imstande ist das Zirkonium mitzufällen, wurde schon erwähnt. So muß mit zunehmender Verunreinigung des Kalkes mit Eisen auch mehr an Eisen gebundenes Zirkonium gefunden werden. Im Korallenoolith aus Freden (etwa 1% Fe_2O_3) wurden 0,5 g/t lösliches Zirkonium gefunden.

Daß in den gelösten Karbonaten (außer bei Anwesenheit von Eisen) kein Zirkonium nachgewiesen werden konnte, bedeutet, daß das reine Calciumkarbonat nicht in der Lage ist, Zirkonium zu binden.

Soweit Zirkonium in den marinen Organismen gefunden wird, stammt es wahrscheinlich vom aufgenommenen Eisen, welches seinerseits das Zirkonium vordem adsorptiv gebunden mit sich führte.

Während in der Muschelschale einer Arca kein Zirkonium zu finden ist, weisen die Kalkalgen einen Zr-Gehalt von 8 g/t auf.

Der Zr-Gehalt des Globigerinenschlammes der Meteorstation 288b, welcher zwischen den Kleinen Antillen und den Cap Verden-Inseln gefunden wurde, ist ebenso groß wie derjenige von Meteorstation 240a, welcher aus dem Guineabecken stammt. Der Zr-Gehalt des Globigerinenschlammes, welcher etwas größer

ist als z.B. derjenige der Kalkalgen, dürfte hauptsächlich von seiner tonigen Komponente und Schwermineralrelikten herzuleiten sein.

Die Gipsbrekzie zeigt den zu erwartenden niedrigen Zr-Gehalt. Der höhre Zr-Wert des Basalanhydrits stammt vom Tongehalt desselben.

5. Der zirkoniumgehalt der kristallinen schiefer

	g Zr/t
(277) Orthogneis—Muggenbrunn, Schwarzwald	91
(278) Paragneis—Muggenbrunn, Schwarzwald	165
(279) Amphibolit—Holandsfjord, Norwegen	12
(280) Aktinolithschiefer—Greiner Tirol	26
(38) Nephrit—Westküste, Neu-Seeland	34
(45) Glaukophanit—Mocchie, Susatal, Italien	54
(281) Ägirinditroitschiefer—Kjörlingholmen, Langesundfjord	2500
(282) Eklogit—Piemont	23
(283) Eklogitpegmatit—Grytingsvoog, Nordfjord	30
(284) Eklogit—Fattigau, Fichtelgebirge	68
(285) Glimmerschiefer—Ehrenfriedersdorf	59
(286) Phyllit, (phyllitisierter Rotschiefer)—Johannesburg, Weilburg	114
(287) Phyllit—Endschütz, Gera	167

Die metamorphen Gesteine zeigen etwa den Zr-Gehalt ihrer Primärgesteine. Da der Zr-Gehalt der meisten Primärgesteine auch innerhalb der verschiedenen Gesteinsfamilien und Gesteinsgruppen stärkere Schwankungen zeigen kann, so sind Vergleiche mit dem Zr-Gehalt der metamorphen Gesteine mit Vorsicht zu treffen.

Der Zirkoniumgehalt des Orthogneises aus Muggenbrunn entspricht etwa demjenigen eines Diorites. Der Paragneis vom selben Ort zeigt mit 165 g Zr/t den Zirkoniumgehalt eines normalen Tonschiefers und ist deshalb genetisch wohl von ihm herzuleiten.

Der angeführte Nephrit von Neu-Seeland ist ein feinfilziger Aktinolithfels. Er führt etwa denselben Zirkoniumgehalt wie der Aktinolithschiefer aus Tirol. Die Glieder der Strahlsteinreihe entstehen sekundär aus Olivin oder aus Diopsid. Dieser Zusammenhang drückt sich auch in dem sehr niedrigen Zr-Gehalt aller beteiligten Glieder aus.

Der Glaukophanit, der zum Teil ursprünglich aus Alkaligesteinen entstammen sollte, zeigt nicht den zu erwartenden höheren Zirkoniumgehalt. Dagegen leitet sich der Ägirinditroitschiefer mit seinem hohen Zr-Gehalt vom Nephelinsyenit ab. Die Natronpyroxene führen auch hier reichlich Zirkonium.

Die Eklogite, welche sich in vieler Hinsicht an die Amphibolite anschließen, zeigen eben so wie die Amphibolite den geringsten Zirkoniumgehalt.

Von den Phylliten zeigt besonders derjenige von Endschütz mit 167 g Zr/t den Zirkoniumgehalt eines normalen Tones bzw. Tonschiefers. Die Verwandtschaft zwischen Phyllit und Tonschiefer zeigt sich auch im übereinstimmenden Zr-Gehalt

6. Der mittlere Zirkoniumgehalt der Lithosphäre

Für die Berechnung des mittleren Zirkoniumgehaltes der Lithosphäre wurden die von Vogt (1931) angegebenen Häufigkeitszahlen für die verschiedenen Gesteinstypen benutzt; jedoch wurden für die Granite und die Granodiorite die von Goldschmidt (1933) vorgeschlagenen Berichtigungen angewendet.

Der Berechnung des Zirkoniumgehaltes in den Sedimenten liegen Häufigkeitsangaben von Goldschmidt (1933) und von v. Engelhardt (1936) zugrunde. Goldschmidt gibt die relative Verteilung von Tonschiefer + Sandstein, Kalkstein und Dolomit an und v. Engelhardt (1936) das Verhältnis Tonschiefer : Sandstein.

Gesteine	%-Anteil an d. Lithosphäre	Zr-Gehalt der Gesteinsgruppe	d. Häufigkeit entsprechend
Granite	39%	175 g Zr/t	68,2 g Zr/t
Granodiorite, Diorite	39%	140 g Zr/t	54,6 g Zr/t
Gabbros + Anorthosite	18%	110 g Zr/t	19,8 g Zt/t
Syenite	3%	310 g Zr/t	9,3 g Zr/t
Nephelinsyenite	0,5%	680 g Zr/t	3,4 g Zr/t
Alkaligabbros	0,25%	200 g Zr/t	0,5 g Zr/t
Pyroxenite + Peridotite	0,25%	45 g Zr/t	0,1 g Zr/t
	Durchschnitt der Eruptivgesteine:		156,-g Zr/t
Tonschiefer, Tone	79,6%	160 g Zr/t	127,4 g Zr/t
Sandsteine	11,9%	220 g Zr/t	26,2 g Zr/t
Kalke	8,1%	19 g Zr/t	1,5 g Zr/t
Dolomite	0,4%	17 g Zr/t	0,07 g Zr/t
	Durchschnitt: der Sedimentgesteine		155,-g Zr/t

Für die Mittelwertbildung der verschiedenen Gesteinsfamilien wurden außer den Durchschnittsmischungen auch sämtliche Einzelmessungen herangezogen. Es zeigen die Sedimente mit 155 g Zr/t gegenüber den Eruptivgesteinen mit 156 g Zr/t eine gute Übereinstimmung. Damit bestätigt sich die Vermutung, nach der sich der gesamte Zr-Gehalt der verwitterten Eruptivgesteine in den Sedimenten wiederfindet, wobei der geringe Zr-Gehalt des Meerwassers für die Bilanz nicht von Bedeutung ist.

Die eingangs erwähnte Diskrepanz des Zirkoniumwertes für die Eruptivgesteine von v. Hevesy und Würstlin (1934) von 220 g Zr/t gegenüber den Tonschiefern mit 140 g Zr/t ist vielleicht auf anomale Bestandteile in den Durchschnittsmischungen der Eruptivgesteine zurückzuführen.

Wenn man alle in dieser Arbeit für die Eruptivgesteine gefundenen Zirkoniumwerte arithmetisch mittelt, so erhält man mit 235 g Zr/t einen ähnlichen Wert wie v. Hevesy (220 g Zr/t). Berücksichtigt man dagegen die Häufigkeit der verschiedenen Gesteinstypen, so erhält man einen Wert von 156 g/t. Der von v. Hevesy gefundene Zr-Wert für Tone und Tonschiefer mit 140 g Zr/t. kommt dem hier gefundenen Lithosphärenwert sehr viel näher.

257 ostindische Gesteinsproben, welche von van Tongeren (1938) spektralanalytisch auf Spurenelemente untersucht wurden, enthielten durchschnittlich 170 g Zr/t. Dieser Wert kommt dem hier gefundenen Lithosphärenwert von 156 g/t nahe. Allerdings handelt es sich auch bei dem Durchschnittswert von van Tongeren um ein arithmetisches Mittel.

Unter Berücksichtigung der neuesten zuverlässigen Ergebnisse aus der Literatur kommt man ebenfalls zu einem Lithosphärenwert von rund 160 g Zr/t.

Ausschlaggebend für den Lithosphärenwert sind die Zr-Gehalte der Granite und Granodiorite, welche mit 78% am Aufbau der oberen Lithosphäre beteiligt sind. Wenn z.B. Ahrens (1954), in 27 kanadischen Graniten durchschnittlich 170 g Zr/t findet, die Diorite aber noch weniger Zirkonium führen, so kann der hohe Wert v. Hevesys von 220 g Zr/t nicht erreicht werden.

Zusammenfassung

Es wird eine quantitative chemische Bestimmungsmethode für Zirkonium angegeben, mit der man in Silikaten Zirkoniummengen bis zu $2 \cdot 10^{-4}$% nachweisen kann. Der mittlere Fehler beträgt bei je zwei Bestimmungen etwa $\pm 3 \cdot 10^{-4}$%. Insgesamt wurden 287 Mineral- und Gesteinsanalysen ausgeführt, wobei jede Analyse zur Kontrolle und Mittelwertbildung mindestens einmal wiederholt wurde.

Die Mineralanalysen zeigen, daß das Zirkonium außer im Zirkoniumsilikat und den selteneren Zirkoniummineralen in vielen gesteinsbildenden Mineralen in geringen Mengen vorhanden ist. In manchen Mineralen findet eine Anreicherung von Zirkonium bis zu einigen zehntel Prozenten statt, so z.B. im Rutil, Titanit, Magnetit, Ilmenit, Apatit, Zinnstein. Von den Gesteinshauptgemengteilen können besonders Pyroxene und Amphibole Zirkonium führen. Die größte Zirkoniumanreicherung bis zu etwa $\frac{1}{2}$% Zr wird in den Ägirinen gefunden. Diese bemerkenswerte Eigentümlichkeit wird mit der Zirkoniumanreicherung in den Alkaligesteinen in Verbindung gebracht.

Die Alkaligesteine enthalten durchschnittlich etwa doppelt so viel Zirkonium wie die Gesteine mit Kalk-Alkali-Vormacht: Alkalisyenite 680 g Zr/t—Syenite 310 g Zr/t; Alkaligabbros 200 g Zr/t—Gabbros 110 g Zr/t.

Die Ergebnisse der Eruptivgesteinsanalysen bestätigen die bekannte Tatsache, daß sich das Zirkonium bei der magmatischen Differentation in den Restmagmen anreichert. Die intermediären, mehr zur sauren Seite hinneigenden Gesteine weisen den Größten Zirkoniumgehalt auf, während die kieselsäureärmsten Gesteine den geringsten Zr-Gehalt zeigen.

Die jeweiligen Erguß- und Gangäquivalente zeigen mit ihren Tiefengesteinen übereinstimmenden Zirkoniumgehalt.

In den basischen und ultrabasischen Eruptivgesteinen, in denen kein akzessorischer Zirkon gefunden wird, ist die Hauptmenge des anwesenden Zirkoniums in den Pyroxenen und im Erz gebunden.

Während die Zr-Gehalte von Graniten aus verschiedenen Räumen maximal um den Faktor 2 schwanken können, zeigen sie innerhalb eines Plutons nur eine maximale Schwankung von ± 17% im Zr-Gehalt.

Die Sedimente insgesamt enthalten etwa die gleich Zirkoniummenge wie die Eruptivgesteine.

Die chemische Verwitterung des Zirkoniumsilikates hat nur örtliche Bedeutung, und nur sehr geringe Zr-Mengen wandern in das Meer ab.

Es wird eine geringe Löslichkeit von Zirkoniumsilikat in Wasser, eine etwas größere in alkalibikarbonathaltigem Wasser gefunden. So lassen sich die Korrosionserscheinungen von Zirkonen in Lateritprofilen erklären. Es werden Anreicherungs und Auslaugungshorizonte beobachtet. Das in Lösung befindliche Zirkoniüm

bildet keine sekundären Minerale, es fällt gemeinsam mit den Hydroxyden des Eisens, Mangans und Aluminiums aus und reichert sich dort an.

Während die Tone und Tonschiefer relativ konstante Zr-Gehalte aufweisen, schwankt der Zr-Gehalt in den Sandsteinen und besonders in den Quarziten sehr. Der große Dichteunterschied, verbunden mit turbulenter Strömung, bewirkt bei den gröberen Residualsedimenten eine ungleichmäßigere Verteilung der Schwerminerale.

In den Kalken befindet sich praktisch der gesamte Zr-Gehalt im salzsäureunlöslichen Rückstand.

Der Zirkoniumgehalt der kristallinen Schiefer gleicht etwa dem Zr-Gehalt der Primärgesteine.

Für den mittleren Zr-Gehalt der Lithosphäre wird unter Berücksichtigung der Häufigkeitsanteile der verschiedenen Gesteinstypen ein Wert von 156 g Zr/t gefunden.

Für die Überlassung dieser Arbeit, die freundliche und vielseitige Unterstützung, für Analysenmaterial, sowie für die zahlreichen Anregungen danke ich meinem hochverehrten Lehrer, Herrn Professor Dr. C. W. Correns, sehr.

Ferner danke ich Herrn Dr. K. H. Wedepohl für Literaturhinweise und für das zur Verfügung gestellte Analysenmaterial.

Mein Dank gilt außerdem Herrn Dozenten Dr. S. Koritnig, Frl. Dr. P. Schneiderhöhn und Herrn Dr. H. Harder für das freundlicherweise überlassene Probenmaterial.

Literaturverzeichnis

Ahrens L. H. (1954) The lognormal distribution of the elements. *Geochim. Acta* **5,** 1, 49; **6,** 2, 121.

Amstutz G. C. (1953) Geochemistry of Swiss lavas. *Geochim. Acta* **3,** 157.

Born H. (1934/35) Der Bleigehalt der Norddeutschen Salzlager und seine Beziehungen zu radioaktiven Fragen. *Chem. d. Erde* **9,** 66.

Boujoucos G. J. (1921) Rate and extent of solubility of minerals and rocks under different treatments and conditions. *Michigan. Exper. Sta. Tech. Bull.* 50.

Butler J. R. (1953/54) The geochemistry and mineralogy of rock weathering. *Geochim. et Cosmochim. Acta* **4,** 1, 157; **6,** 2, 268.

Carrol Dorothy (1953) Weatherability of Zircon. *J. Sed. Petrology* **23,** 2, 106.

Clarke R. W. und Washington H. S. (1924) The composition of the earth's crust *U.S. Geol. Survey, Prof. Paper* 127.

Degenhardt H. (1956) Die Bestimmung kleiner Zirkoniumgehalte in Gesteinen, Mineralien und Gewässern. *Z. Anal. Chem.* noch im Druck.

De Vore G. W. (1955) The role of adsorption in the fractionation and distribution of elements. *J. Geol.* **63,** 159.

De Vore G. W. (1955) Crystal growth and the distribution of elements. *J. Geol.* **63,** 471.

Engelhardt W. v. (1936) Geochemie des Barium. *Chem. d. Erde* **10,** 187.

Fairbairn H. W. (1950/1951) A cooperative investigation of precision and accuracy in chemical, spectro-chemical and modal analysis of silicate rocks. *Geological Survey Bulletin* **980,** 54.

Fairbairn H. W., Ahrens L. H., und Gorfinkle L. G. (1953) Minor element content of Ontario diabase. *Geochim. Acta* **3,** 34.

Frederickson A. F. (1948) Mode of occurrence of titanium and zirconium in laterites. *Amer. Min.* **33,** 374.

Goldberg E. D. (1954) mit Revelle, Arrhenius, Bramlette—Manuskript über pelagische Sedimente des Pazifischen Ozeans. 8 Analysenreihen Roter Tone. Neue Meerwasseranalysen. Scripps Institution of Oceanography, La Jolla (California)

Goldschmidt V. M. (1923) Geochemische Verteilungsgesetze der Element I. *Videnskapsselskapets Skrifter I. Math. Nat. Klasse* **3,** 13.

Goldschmidt V. M. (1933) Grundlagen der quantitativen Geochemie. *Fortschr. d. Min. Petr.* **17,** 112.

Goldschmidt V. M. (1934) Drei Vorträge über Geochemie. *Geologiska Föreningens I Stockholm Förhandlinger, Maj- Okt.* 397.

Goldschmidt V. M. (1937) Geochemische Verteilungsgesetze IX. *Skrif. Norske Vid. Acad. Oslo, Math. Nat. K*l. **4,** 100.

Gordon M. jr. und Murata K. J. (1952) Minor elements in Arkansas Bauxite. *Econ. Geol.* **47,** 169.

Harder H. (1951) Über den Mineralbestand und die Entstehung einiger sedimentärer Eisenerze des Lias. *Heidelberg. Beitr. Min.* **2,** 455.

Harvey H. W. (1945) *Recent Advances in the Chemistry and Biology of Sea Water* Cambridge, University Press.

Hevesy G. v. und Würstlin K. (1934) Die Häufigkeit des Zirkoniums. *Z. Anorg. Chem.* **216,** 305.

Higazy R. A. (1953) Observations on the distribution of trace elements in the perthite pegmatites of the Black Hills, South Dakota. *Amer. Min.* **38,** 172.

Horton L. und Aubrey K. V. (1950) The distribution of minor elements in vitrain. *J. Soc. Chem. Ind.* 69.

Köster H. (1955) Beitrag zur Kenntnis indischer Laterite. *Heidelberg. Beitr. Min.* **5,** 23.

Köster H. (1956) Die quantitative Berechnung von Substanzwanderungen in Verwitterungsprofilen mittels chemischer Analysen. *Heidelberg. Beitr. Min.* noch im Druck.

Minami E. (1935) Selengehalte von europäischen und japanischen Tonschiefern. *Nachr. d. Ges. Wiss. Göttingen. Math. Nat. K*l. **1,** 12.

Nockolds S. R. und Mitchell R. L. (1948) The geochemistry of some Caledonian plutonic rocks. *Trans. Roy. Soc. Edinburgh* **61,** 2, 20.

Nockolds S. R. und Allen R. (1953/54) The geochemistry of some igneous rock series. *Geochim. Acta* **4,** 1, 105; **5,** 2, 245.

Noll W. (1933/34) Geochemie des Strontium. *Chem. d. Erde.* **8,** 507.

Piller H. (1951) Über die Verwitterungsbildungen des Brockengranites. *Heidelberg. Beitr. Min.* **2,** 498.

Pirschle K. (1939) Die Bedeutung der Spurenelemente für Ernährung, Wachstum und Stoffwechsel der Pflanzen. *Ergebn. Biol.* **17,** 255–413.

Pinson W. H., Ahrens L. H., und Frank M. L. (1953) The abundances of Li, Sc, Sr, Ba and Zr in chondrites and some ultramafic rocks. *Geochim. Acta* **4,** 251.

Sahama Th. G. (1945) Spurenelemente der Gesteine im südlichen Finnisch-Lappland. *Bulletin de la Commission Géologique de Finlande Nr.* 135.

Schröcke H. (1955) Zur Geochemie erzgebirgischer Zinnerzlagerstätten. *Neues Jb. Miner. Abh.* **87,** 451.

Strock L. W. und Drexler S. (1941) Geochemical study of Saratoga mineral waters by a spectrochemical analysis of their trace elements. *J. Opt. Soc. Amer.* **31,** 167.

Tongeren van W. (1938) Contributions to the knowledge of the chemical composition of the earth's crust in the East Indian Archipelago, D.B. Contents, Uitgevers-Maatschappij, Amsterdam.

Tröger W. E. (1935) *Spezielle Petrographie der Eruptivgesteine* Berlin.

Vogt J. H. L. (1931) On the average composition of the earth's crust. *Skrifter Norske Vid. Acad. Oslo Math. Nat. K*l. 147.

Wager L. R. und Mitchell R. L. (1943) Preliminary observations on the distribution of trace elements in the rocks of the Skaergaard Intrusion, Greenland *Min. Mag.* **26,** 283.

Wagner L. R. und. Mitchell R. L. (1953) Trace elements in a suite of Hawaian lavas. *Geochim. Acta* **3,** 217.

Washington H. S. und. Merwin H. E. (1927) The acmite pyroxenes. *Amer. Min.* **12,** 6, 233.

Wedepohl K. H. (1954) Der trachydoleritische Basalt des Backenberges bei Güntersen, westl. v. Göttingen. *Heidelberg. Beitr. Min.* **4,** 229.

Geochimica et Cosmochimica Acta, 1957, Vol. 11, pp. 310 to 334. Pergamon Press Ltd., London

The system CaO—MnO—CO_2: Solid-solution and decomposition relations

Julian R. Goldsmith*

and

Donald L. Graf†

(*Received* 13 *July* 1956)

Abstract—A complete series of solid solutions between $CaCO_3$ and $MnCO_3$ (manganoan calcites and calcian rhodochrosites) exists above 550°C at CO_2 pressures sufficient to prevent decomposition. A solubility gap is observed below this temperature in the Mn-rich half of the system. The relation of the solubility gap to the ordered compound $CaMn(CO_3)_2$ is briefly described. At 400°C and below, experimentation is hampered by very slow reaction rates, both in hydrothermal runs and in dry runs using Li_2CO_3 as a flux.

The equilibrium thermal decomposition relations in the system are shown as a family of curves, including that for the reaction $MnCO_3 \rightleftharpoons MnO + CO_2$. The P, T curve for this reaction is a straight line between375° and 575° C expressed by the equation

$$\log_{10} P_{\text{lb/in.}^2} = -5740/T + 10{\cdot}014.$$

In the region 575° to 775° C, the relation is

$$\log_{10} P_{\text{lb/in.}^2} = -10{,}320/T - 11{\cdot}910 \log T + 50{\cdot}289.$$

The ΔH of this reaction ranges from 25·5 to 26·6 kcal/mole between 375° and 750°C.

An X-ray method for the determination of compositions in this system is described, and the cell constants of the hexagonal unit cell of rhodochrosite were determined to be $a_0 = 4{\cdot}7768$ Å, $c_0 = 15{\cdot}664$ Å.

Introduction

The principal rock-forming carbonate minerals lie within the system CaO—MgO—FeO—MnO—CO_2. Relatively little quantitative work has been done in this system in the past, but several recent investigations in the system CaO—MgO—CO_2 have been reported (Harker and Tuttle, 1955a, 1955b; Graf and Goldsmith, 1955; Goldsmith, Graf, and Joensuu, 1955). The present work is a further step in the evaluation of relations in the five-component system.

Experiments were performed dry at elevated temperatures and CO_2 pressures up to approximately 2,000 atmospheres, and hydrothermally at lower temperatures. In the hydrothermal experiments the water was used only as a fluid medium to promote reaction and did not act as a component of the system.

Experimental Procedure

Experiments at high temperatures and elevated CO_2 pressures, in the absence of water, were performed in cold-seal pressure vessels ("bombs") of Haynes Alloy No. 25, modified after the type described by Tuttle (1949). The initial carbonate materials were enclosed in Pt foil and placed in the bombs, and the entire system up to the CO_2 source was sealed and carefully evacuated before introducing CO_2, in order to prevent oxidation of manganese. Medical grade (USP) CO_2 was used, and pressures above tank pressure were obtained in two ways. In one type of apparatus a motor-driven hydraulic pump forced oil upward against a piston acting as a separator in a vertical pressure cylinder, the volume above the separator having been filled initially with CO_2 at tank pressure. In the second apparatus the pressure vessel was initially

* Department of Geology, University of Chicago.
† Illinois State Geological Survey, Urbana.

surrounded by dry ice in order to fill the system with liquid CO_2. High pressure was produced by subsequent heating, and the desired pressure was obtained by bleeding the system. Pressures were read directly from Bourdon-type gauges, and temperatures were measured with chromel-alumel thermocouples and were continually recorded on strip-chart instruments.

Hydrothermal experiments were performed in modified Morey-type bombs (Morey and Ingerson, 1937) of either 18-ml or 1-ml capacity. In many of these runs, CO_2 was added to the charge in the form of dry ice to prevent possible breakdown or hydration of the carbonates and to promote reaction by increasing solubilities in the system. The volume of the charge was relatively small compared to that of the bomb, and the degree of filling with distilled water varied from 50 to 80 per cent by volume. No attempt was made to control or measure total or partial pressures in these runs.

Three types of starting materials were used:

(a) Mixtures of reagent-grade $CaCO_3$ and $MnCO_3$. The carbonates were dried by heating in a stream of CO_2 before weighing, and eight mixtures between the end members were prepared. The carbonates were carefully mixed by grinding in alcohol in an agate mortar. The mixtures for some runs were pressed into pellets to provide more intimate contact for reaction.

(b) A portion of each of the above mixtures was converted to a well-crystallized homogeneous solid solution by reaction at high temperatures and CO_2 pressures (see Table 4). These solid solutions were then used as starting materials in subsequent runs.

(c) Coprecipitated Ca-Mn carbonates were prepared by pouring mixed 5N Ca and Mn chloride solutions into 5N K_2CO_3 solution. The precipitates were preserved in contact with their supernatant solution of KCl, and no attempt was made to remove KCl from these materials before using them in the hydrothermal experiments. As will be discussed in a following section, these precipitates are very fine-grained, poorly crystallized, single-phase solid solutions between calcite and rhodochrosite.

Upon completion of a run, the pressure vessels were cooled rapidly by a water spray or an air blast. The samples from hydrothermal runs using precipitates were washed to remove dissolved salts. All samples were examined by means of powder X-ray diffraction.

Determination of Composition by X-ray Diffraction

The spacings of several powder-diffraction lines were determined for the synthetic calcite-rhodochrosite solid-solution series (see (b) above). North American Philips 114·59-mm cameras with Mn-filtered Fe radiation were used for study of the backreflection region, and a Nonius quadruple-focusing camera with an effective Debye diameter of 229 mm was used in the frontreflection region. Techniques were essentially the same as those previously described for the $CaCO_3$—$MgCO_3$ series (Goldsmith, Graf, and Joensuu, 1955).

Fig. 1 is a plot of carbonate composition in mol per cent versus the spacings of two back-reflections, (521) and (633), (552).* The spacings of compositions beyond approximately 10 mol per cent $MnCO_3$ plot as excellent straight lines, and in well-crystallized materials giving sharp backreflections the compositions can be determined quite accurately. The plot of (633), (552) cannot be followed beyond 60 mol per cent $MnCO_3$ when Fe radiation is used, because 2θ approaches 180° in this range. Measured spacings on a material containing 4 mol per cent $MnCO_3$ show that the plots deviate slightly from straight lines as they approach the origin. The absolute d values of Specpure $CaCO_3$ (origin of Fig. 1) are well determined, the measured and computed values in this 2θ region agreeing to $\pm 0{\cdot}0002$Å (Goldsmith, Graf, and Joensuu, 1955).

Samples of analytical grade $MnCO_3$ from several manufacturers, as well as $MnCO_3$ directly precipitated from solutions of $MnCl_2$ and K_2CO_3, gave rather diffuse X-ray patterns. Heating these materials to 300°C or more, under CO_2 pressures sufficient to prevent decomposition,

* Conversion from indices based on the rhombohedral structure cell to those of the corresponding hexagonal cell may be carried out using the relations $h_{hex} = h_{rh} - k_{rh}$, $k_{hex} = k_{rh} - l_{rh}$, $l_{hex} = h_{rh} + k_{rh} + l_{rh}$. Winchell (1956) gives the appropriate matrices for this and related transformations. Thus, $(633)_{rh}$ and $(552)_{rh}$ transform to $(30{\cdot}12)_{hex}$ and $(03{\cdot}12)_{hex}$, respectively.

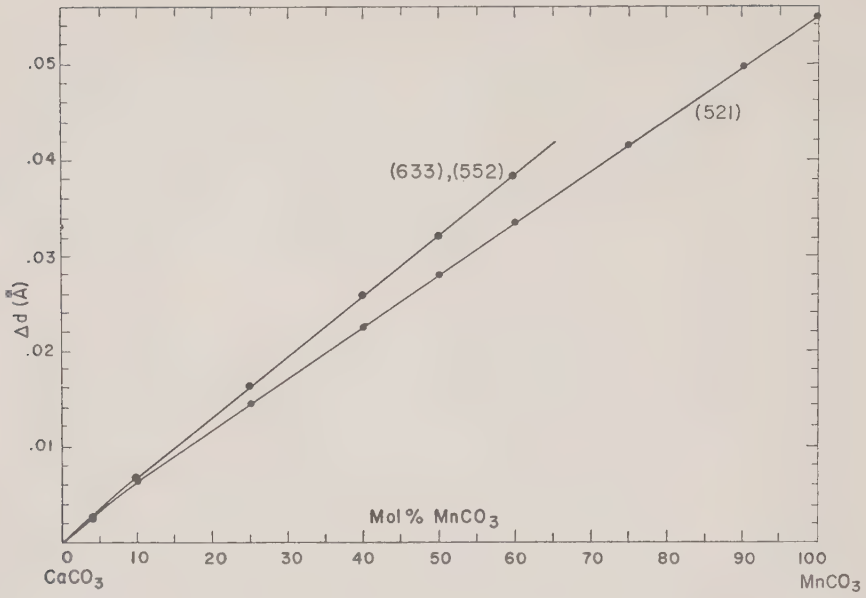

Fig. 1. Variation in $(521)_{rh}$ and $(633)_{rh}$, $(552)_{rh}$ X-ray back-reflection spacings with composition in the series $CaCO_3$—$MnCO_3$.

induced sharpening of the diffraction pattern and in addition produced a significant change in cell constants. The spacings of heated $MnCO_3$ are used here as being valid.*

Fig. 2 is a plot of composition versus spacing of $(112)_{rhombohedral}$ or $(10\bar{1}4)_{hexagonal}$ reflection. Without further data, construction of anything but a straight line through these points does not appear justified.

All measured compositions given in the following discussion were determined from the curves shown in Figs. 1 and 2.

Equilibrium Thermal Decomposition Curve of $MnCO_3$

The decomposition of $MnCO_3$, without complication due to valence change, is represented by the expression

$$MnCO_3 \leftrightharpoons MnO + CO_2 \qquad (1)$$

The P_{CO_2}, T curve for this reaction was determined in the temperature range 375 to 775°C. Fig. 3 shows this curve, plotted as log P_{CO_2} versus the reciprocal of absolute temperature ($1/T_{°K}$). The data from which the curve is drawn are contained in Table 1. The equilibrium decomposition curve of $CaCO_3$ lies to the left of the $MnCO_3$ curve in Fig. 3, i.e. $CaCO_3$ requires a higher temperature for decomposition at a given P_{CO_2} than does $MnCO_3$. Thus the P_{CO_2}, T curve for $MnCO_3$ decomposition establishes at any temperature a CO_2 value that is adequate to prevent decomposition in the system CaO—MnO—CO_2.

The data in Table 1 were determined with dried $MnCO_3$ and MnO as starting materials, the latter produced by decomposing $MnCO_3$. A small amount of

* H_2O is eliminated from these fine-grained manganous carbonates upon heating. Whether this H_2O is contained in the structure, and thus is responsible for the difference in cell size, is not known. The observed Δd between the original and heated carbonates is about 0·0035 Å for the (521) reflection. This could be misinterpreted as representing a 7 per cent $CaCO_3$ content.

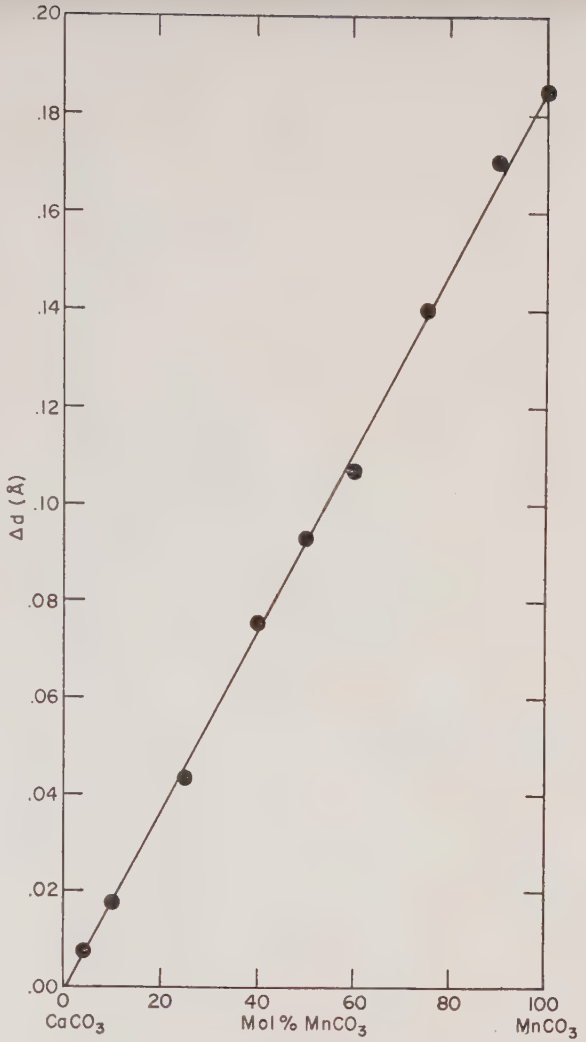

Fig. 2. Variation in $(112)_{rh}$, or $(10{\cdot}4)_{hex}$, X-ray spacing with composition in the series $CaCO_3$—$MnCO_3$.

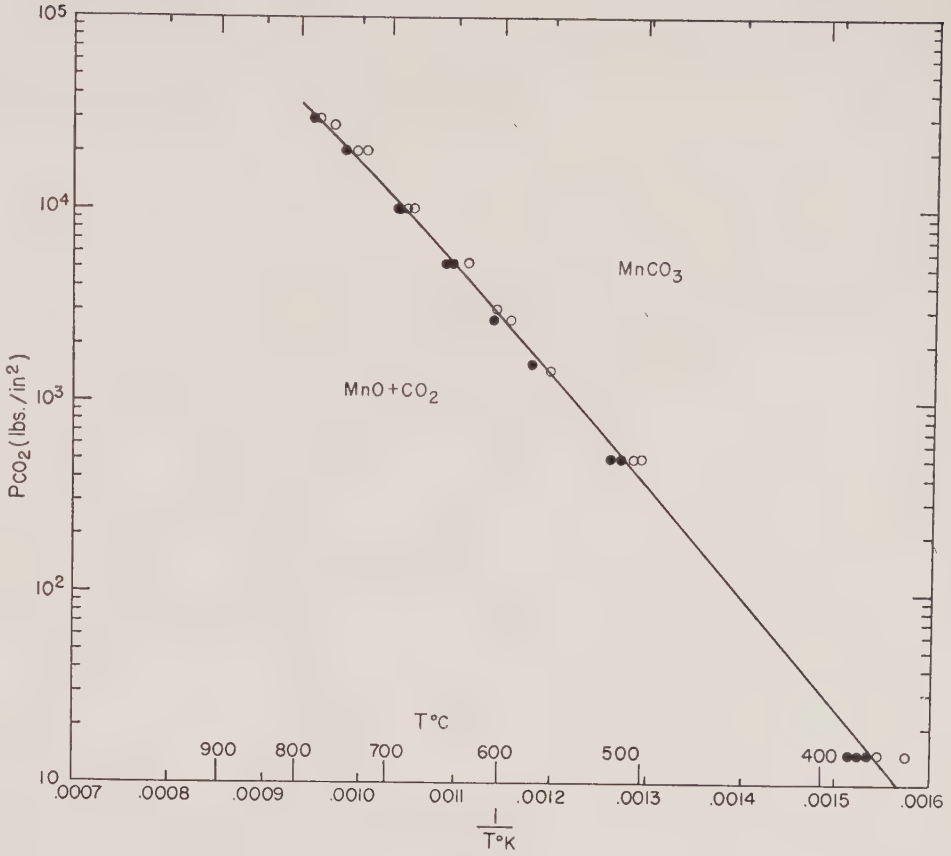

Fig. 3. Equilibrium thermal decomposition curve for the reaction $MnCO_3 \leftrightharpoons MnO + CO_2$. Open circles indicate runs in which no decomposition occurred, filled circles, runs in which some decomposition was observed.

Table 1. Equilibrium data for the reaction $MnCO_3 \rightleftharpoons MnO + CO_2$

P_{CO_2} (lb/in.^{2})	T°C	Time (hr)	Products
Runs using $MnCO_3$ as starting material*			
29,300	780	3	R, M
29,000	772	3	R
27,000	757	3·5	R
20,000	744	3	M, R
20,000	732	3	R
20,000	722	3	R
9,900	690	17	R, M
9,900	688	48	R, (M)
9,900	683	18	R
9,900	678	18	R
5,100	646	4	M, R
5,100	640	4	R, (M)
5,100	627	4	R
3,000	602	5	R
2,650	606	5	M, R
2,650	593	5	R
1,550	576	5	M, R
1,500	563	5	R
500	520	46	M, R
500	513	18	R, M
500	506	68	R
500	501	68	R
14·4	387	165	R, M
14·4	383	113	R, M
14·4	379	92	R, (M)
14·4	374	113	R
14·4	362	165	R
Runs using MnO as starting material			
29,300	780	3	M; moderate amount R by back-reaction
29,000	772	3	Mostly R; M
27,000	757	3·5	Mostly R; M
20,000	744	3	M; small amount R by back-reaction
20,000	732	3	About half R; M
20,000	722	3	About half R; M
9,900	678	18	Mostly R; M
5,100	646	4	M; small amount R by back-reaction
5,100	640	4	M; moderate amount R by back-reaction
5,100	627	4	Mostly R; M
3,000	602	5	Mostly R; M
2,650	606	5	M; small amount R by back-reaction
2,650	593	5	About half R; M
1,550	576	5	M; small amount R by back-reaction
1,550	563	5	M; small amount R
500	520	46	M; (R) by back-reaction
500	513	18	M; small amount R by back-reaction
500	506	68	M; moderate amount R
500	501	68	Mostly R; M

* $MnCO_3$ is indicated by R among the products, MnO by M. The products are arranged in approximate order of abundance. Parentheses indicate quantities near the limit of detection.

decomposition to MnO is readily detectable in the X-ray diffraction pattern. In virtually all cases, even a trace of decomposition could be visually observed, because of the strong colour contrast between the light pink $MnCO_3$ and the brilliant green MnO. Reaction (1) is readily reversible under the conditions of these experiments; MnO reacts with CO_2 to produce $MnCO_3$ in the stability field of $MnCO_3$. Thus the decomposition curve represents true equilibrium, which could be realized from either direction along both the P_{CO_2} and T axes.

The reaction $MnO + CO_2 \leftrightharpoons MnCO_3$ in fact proceeds much more rapidly than does the equivalent reaction $MgO + CO_2 \leftrightharpoons MgCO_3$ at comparable temperatures (Harker and Tuttle, 1955a; Graf and Goldsmith, 1955). The reaction velocity is great enough for a significant amount of $MnCO_3$ to form by backreaction during a temperature quench from the field where MnO is in equilibrium with CO_2, as the sample passes through the field of $MnCO_3$ stability. Thus, although a sample of MnO generally was placed in the bomb with the $MnCO_3$ in each run, the back-reaction complicates the interpretation of the data obtained. In practice it is usually possible to distinguish between background, or quench-produced, $MnCO_3$, and the larger amounts that are produced by equilibrium reaction in the field of $MnCO_3$.

It was found necessary to pump out the high-pressure system before introduction of the CO_2 to prevent the formation of higher oxides of manganese. This step is particularly important in the lower portion of the temperature range of Fig. 3. For example, iron-free bixbyite (Mn_2O_3) was produced at 628°C and 2500 lb/in.^{2} CO_2 pressure in an experiment in which preliminary evacuation was not carried out, and hausmannite (Mn_3O_4) was formed in a number of runs over a range of P_{CO_2}, T conditions. No attempt was made to determine the stability relations of the higher oxides.

Configuration of the $MnCO_3$ *decomposition curve*

The curve of Fig. 3 is essentially a straight line below approximately 600°C or 3000 lb/in.^{2} CO_2 pressure. Above these values the curve deviates increasingly in the direction of higher temperature at any given pressure. Selected values of P_{CO_2} and T read from the curve are presented in the first four columns of Table 2.

Kennedy's (1954) data on the P–V–T relations of CO_2 show that CO_2 becomes increasingly nonideal in the P–T region where the above-observed deviation takes place. The data summarized in Kennedy's Fig. 4 can be used to derive an hypothetical decomposition curve that would obtain if CO_2 were an ideal gas. A pressure "adjustment" was applied at five selected points on the curve by multiplying the pressure at the experimental curve by the appropriate value of $n = PV/RT$ as indicated from Kennedy's data.

The $MnCO_3 \leftrightharpoons MnO + CO_2$ curve of Fig. 3 is reproduced in Fig. 4. The dotted line is a straight-line prolongation of the lower portion of the curve. The five "adjusted" values are indicated by crosses. The fit of the straight line to the "adjusted" points is excellent, particularly considering the fact that the highest value was obtained by extrapolating Kennedy's data. It thus appears that within experimental error the deviation of the plot of log P_{CO_2} versus $1/T_{°K}$ from a straight line is due to the nonideal behaviour of CO_2.

Table 2. Selected thermochemical data for the reaction $MnCO_3 \rightleftharpoons MnO + CO_2$

T°C	T°K	P_{CO_2} (lb/in.^{2})	P_{CO_2} (bars)	Density of CO_2 (g/c.c.)	Molar volume (c.c.) CO_2	ΔVc.c.	ΔHkcal/mole
376	649	14·7	1·01	0·0008260*	53,300	53,300	26·2
400	673	30·5	2·10	0·001673*	26,300	26,300	25·9
450	723	120	8·28	0·006197*	7,100	7,080	25·6
500	773	385	26·6	0·01818*	2,420	2,400	26·1
				0·0182‡	2,420	2,400	26·1
550	823	1,100	75·9	0·0483‡	911	893	26·0
600	873	2,750	190	0·1122‡	392	374	26·0
650	923	6,200	428	0·2266‡	198	180	25·5
700	973	12,400	855	0·3731‡	118	100	25·6
750	1023	22,500	1,550	0·541§	81·4	63·5	$26·6_5$
777	1050	30,000	2,070				

* Interpolated from the data of MACCORMACK and SCHNEIDER (1950).
‡ Interpolated from the data of KENNEDY (1954).
§ Graphically extrapolated from the data of KENNEDY (1954).

Comparison with the dolomite decomposition curve

It was pointed out by GRAF and GOLDSMITH (1955) that the shape of the equilibrium decomposition curve of dolomite is influenced not only by the nonideality of CO_2, but also by the variable ΔH contribution from the magnesian calcites of different composition in equilibrium with dolomite at various points on the curve. The dolomite curve is reproduced in Fig. 4 for comparison with that of $MnCO_3$. The curve is nonlinear in the experimental range studied, and there is some doubt about its exact position below $P_{CO_2} = 100$ lb/in.^{2} A straight line has been roughly fitted to the portion of the curve between 100 and 1000 lb/in.^{2} and extended to higher pressures. If the CO_2 "adjustment" is applied to the experimental dolomite curve in the region where CO_2 is nonideal in the same manner as it was to the $MnCO_3$ curve, the crosses define in this region an essentially straight line which is about one third of the way from the experimental curve to the projected straight line. Thus the nonideality of CO_2 is not the only reason for the departure of the dolomite curve from a straight line. The fact that the crosses define an essentially straight line indicates that the total magnitude of other factors such as heats of mixing of the magnesian calcites, represented by the separation between the line of crosses and the projected straight line, is to a good approximation linearly proportional to $1/T_{°K}$ and log P_{CO_2}. This is so because at sufficiently low temperatures where dolomite is in equilibrium with essentially Mg-free calcite, its decomposition curve is no doubt essentially a straight line, and this straight line when projected to higher temperatures would serve the purpose of the argument in the same manner as the assumed one shown in Fig. 4. A comparison of the dolomite curve with that for magnesite ($MgCO_3$) rather than with the $MnCO_3$ curve would be desirable, but the available data for the $MgCO_3$ decomposition do not permit such an analysis.

Thermochemical values

The equation of the straight line portion of the curve between 375 and 575°C, obtained by consideration of points at $1/T_{°K}$ intervals of 0·00005, is

$$\log_{10} P_{lb/in.^2} = \frac{-5740}{T_{°K}} + 10{\cdot}014 \qquad (2)$$

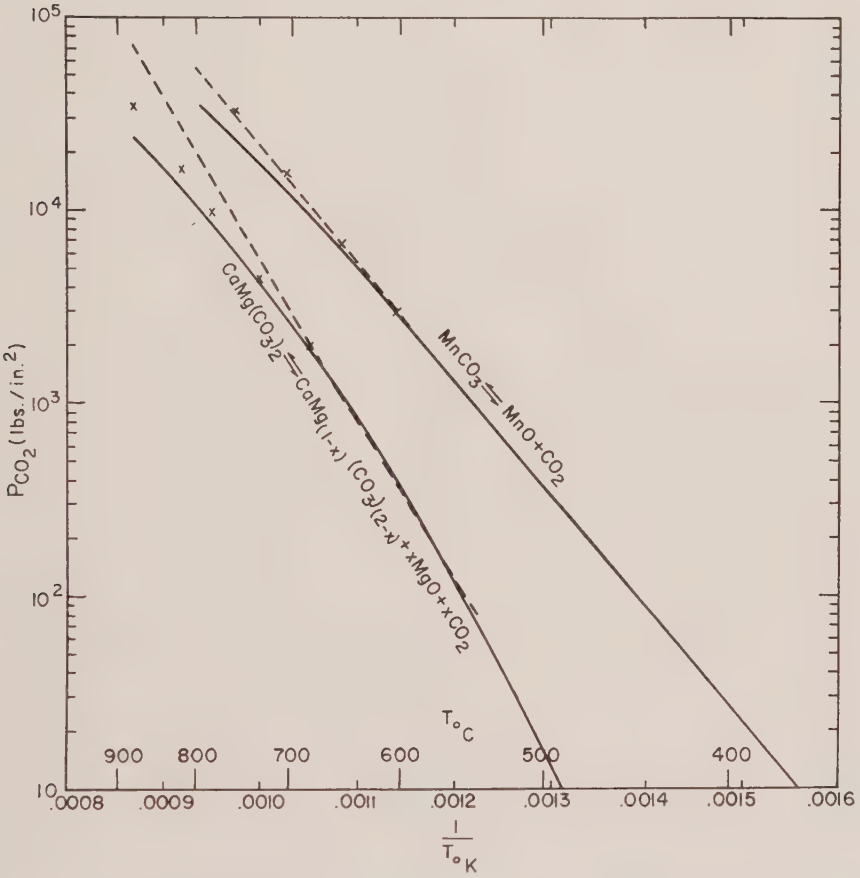

Fig. 4. Equilibrium thermal decomposition of $MnCO_3$ and $CaMg(CO_3)_2$. The respective fields of decomposition lie to the left of the curves. Crosses indicate points from the solid curve which have been adjusted for the nonideality of CO_2. Dotted lines are straight-line extensions of lower portions of curves.

Similarly, the equation of the nonlinear portion of the curve in the region 575 to 775°C, obtained by consideration of points at $1/T_{°K}$ intervals of 0·000025, is

$$\log_{10} P_{lb/in.^2} = \frac{-10{,}320}{T_{°K}} - 11{\cdot}910 \log T_{°K} + 50{\cdot}289 \qquad (3)$$

Values of P_{CO_2} obtained by calculation from equations (2) and (3) agree with those read from the curve to within ±1·5 per cent.

Conversion of equation (2) to natural logarithms produces

$$\ln P_{\text{lb/in.}^2} = \frac{-5740(2{\cdot}303)}{T_{^\circ\text{K}}} + 2{\cdot}303\ (10{\cdot}014) \tag{4}$$

and, differentiating with respect to temperature,

$$\frac{d \ln P}{dT} = \frac{5740(2{\cdot}303)}{T_{^\circ\text{K}}{}^2} \tag{5}$$

Utilizing the exact Clausius-Clapeyron equation,

$$\frac{dP}{dT} = \frac{d \ln P}{dT} \times P = P\left[\frac{5740(2{\cdot}303)}{T_{^\circ\text{K}}{}^2}\right] = \frac{\Delta H}{T_{^\circ\text{K}}\, \Delta V} \tag{6}$$

Therefore, for the straight-line portion of the curve,

$$\Delta H = \frac{13{,}220\ P\Delta V}{T_{^\circ\text{K}}} \tag{7}$$

Similarly, equation (3) yields

$$\Delta H = P\Delta V\left(\frac{23{,}770}{T_{^\circ\text{K}}} - 11{\cdot}910\right) \tag{8}$$

In order to compute ΔH values from equations (7) and (8), it is first necessary to evaluate

$$\Delta V = \text{molar volume } CO_2 + \text{molar volume MnO} - \text{molar volume } MnCO_3.$$

The molar volumes of CO_2 may be calculated easily from published data of KENNEDY (1954) and MACCORMACK and SCHNEIDER (1950), and are given in Table 2. The cell edge for MnO, $a_0 = 4{\cdot}4446 \pm 0{\cdot}0010$ Å, was obtained by measurement of the high-angle reflections in a powder X-ray diffraction diagram of a sample prepared by decomposing $MnCO_3$ at 605°C under 525 lb/in.^{2} CO_2 pressure. The cell contains Mn_4O_4. Using a value of $6{\cdot}0238 \times 10^{23}$ for Avogadro's number (STRAUMANIS, 1949), the molar volume of MnO at room temperature is 13·22 c.c. The cell constants for a sample of $MnCO_3$* recrystallized at 722°C under 20,200 lb/in.^{2} CO_2 pressure for 3 hours, $a_{\text{rh}} = 5{\cdot}9049$ Å and $\alpha = 47^\circ\ 43{\cdot}0'$ ($a_0 = 4{\cdot}7768$ Å, $c_0 = 15{\cdot}664$ Å), were obtained by extrapolation to $2\theta = 180^\circ$. Computed and measured spacings for $MnCO_3$ are given in Table 3. The $MnCO_3$ cell contains $Mn_2(CO_3)_2$, and the molar volume obtained is 31·08 c.c. To estimate the effect of thermal expansion on the molar volume of $MnCO_3$ and MnO, and thus upon ΔV, available thermal expansion data for $CaCO_3$ and MgO were used to correct the computed molar volumes. The maximum resulting change in ΔV, at temperatures covered by this study, is only 0·2 per cent, so that the correction is unnecessary. The ΔH values for selected temperatures, computed using molar volumes of the solids at room temperature, are given in the final column of Table 2.

* A spectrographic analysis by OIVA I. JOENSUU of the $MnCO_3$ gives 0·2 mol per cent $CaCO_3$, and <0·05 per cent of Mg and Fe.

Table 3. Measured and calculated X-ray diffraction spacings for rhodochrosite, $MnCO_3$

$(hkl)_{rh}$	$(hkl)_{hex}$	$\theta_{Fe K\alpha}$	$d_{measured}$	$d_{calculated}$
(110)	(012)			3·6580Å
(211)	(104)			2·8440
(222)	(006)			2·6108
(10$\bar{1}$)	(110)			2·3884
(210)	(113)			2·1720
(200)	(202)			1·9999
(220)	(024)	Front reflections not used in		1·8290
(332)	(018)	determining cell constants		1·7698
(321)	(116)			1·7622
(20$\bar{1}$)	(211)			1·5559
(21$\bar{1}$)	(122)			1·5333
(433)	(10·10)			1·4650
(310)	(214)			1·4521
(422)	(208)			1·4220
(432)	(119)			1·4066
(320)	(125)			1·3990
(11$\bar{2}$)α_1	(030)α_1	44·61	1·3783	1·3790
(11$\bar{2}$)α_2	(030)α_2	44·71	1·3787	
(444)α_1	(00·12)α_1	47·89	1·3048	1·3054
(444)α_2	(00·12)α_2	48·00	1·3052	
(421)α_1	(217)α_1	49·04	1·2818	1·2817
(442)α_1	(02·10)α_1	50·82	1·2487	1·2488
(442)α_2	(02·10)α_2	50·96	1·2488	
(431)α_1	(128)α_1	52·41	1·2216	1·2218
(431)α_2	(128)α_2	52·55	1·2218	
(330)(411)	(036)(306)			1·2193
(202)α_1	(220)α_1	54·14	1·1944	1·1942
(543)α_1	(11·12)α_1	57·695	1·1452	1·1455
(543)α_2	(11·12)α_2	57·845	1·1457	
(30$\bar{1}$)	(312)			1·1352
(532)α_1	(21·10)α_1	61·01	1·1066	1·1066
(532)α_2	(21·10)α_2	61·21	1·1068	
(32$\bar{1}$)α_1	(134)α_1	61·53	1·1011	1·1011
(32$\bar{1}$)α_2	(134)α_2	61·73	1·1013	
(420)α_1	(226)α_1	63·04	1·0860	1·0860
(420)α_2	(226)α_2	63·255	1·0862	
(554)	(01·14)			1·0801
(410)	(315)			1·0774
(542)α_1	(12·11)α_1	66·835	1·0528	1·0528
(542)α_2	(12·11)α_2	67·11	1·0528	
(22$\bar{2}$)	(042)			1·0253
(430)	(137)			1·0210
(400)α_1	(404)α_1	75·46	1·0000	0·99994
(400)α_2	(404)α_2	75·91	1·0000	
(521)α_1	(318)α_1	77·905	0·98996	0·98993
(521)α_2	(318)α_2	78·44	0·99004	
(531)	(229)			0·98472
(644)α_1	(20·14)α_1	79·595	0·98416	0·98414
(644)α_2	(20·14)α_2	80·26	0·98414	

Subsolidus Relations in the System $CaCO_3$—$MnCO_3$

We have investigated the subsolidus-equilibrium relations in the system $CaCO_3$—$MnCO_3$ at CO_2 pressures sufficient to prevent carbonate dissociation, using both dry and hydrothermal techniques. All data relative to this system are contained in Table 4. A complete series of well-crystallized solid solutions was synthesized at approximately 700°C. Below 550° the solid-solution series is not continuous. Fig. 5 shows the subsolidus relations as plotted from selected data of Table 4.

Runs above 500°C on mixtures of $CaCO_3$ and $MnCO_3$ equilibrate in reasonable times, but reactions become quite slow below this temperature. The use of small quantities of Li_2CO_3 as a flux has been found to increase reaction rate without otherwise influencing the reaction. With a Li_2CO_3 flux, dry runs down to 450°C were successful. Below this temperature, equilibrium was not reached in dry runs of 35 days' duration. Hydrothermal runs were resorted to in this region, and although more extensive reaction occurred, equilibrium was difficult to attain below 450°C, particularly in the central two-thirds of the compositional range.

The relations at temperatures of 450°C and above are well enough defined for the solvus, as shown in Fig. 5, to be drawn with reasonable confidence. Mixtures in the range between 60 mol per cent and 75 mol per cent $MnCO_3$ reacted in both dry and hydrothermal runs to two carbonate solid solutions, the compositions of which are indicated by the limbs of the solvus. The development of two solid solutions in this compositional range also was observed in runs at 425° and 400°C, but results were inconsistent and it is apparent that equilibrium was not reached.* It is unfortunate that reaction rate is so slow in this important temperature region. Of interest is the fact that at higher temperatures dry reactions in the system CaO—MgO—CO_2 take place more slowly than those in the system CaO—MnO—CO_2, whereas the reverse is true in hydrothermal runs at lower temperatures.

The initial, very finely crystalline, single-phase materials were observed to unmix in only a few of the runs at 425° and 450°C in which the precipitated carbonate solid solutions used as starting materials lie in the immiscibility gap. Again, however, equilibrium was not reached, and these runs are not indicated in Fig. 5. No unmixing was observed when the well-crystallized solid solutions initially made at high temperatures were used as starting materials. These materials, when run in the region under the solvus, were found to be unchanged.

It is apparent from Fig. 5 that a complete series of solid solutions between

---

* Reaction of $CaCO_3$ and $MnCO_3$ mixtures to a homogeneous solid solution proceeds more rapidly at total compositions near either end-member than it does with compositions in the central two-thirds of the series. In addition, the perfection and size of crystalline units tends to be better for those materials. For example, several hydrothermal runs at 450° to 475°C at the composition $Ca_{10}Mn_{90}$ yielded crystals up to 1 mm in size, mixed with fine material. This is in great contrast to typical hydrothermal runs, in which only very finely crystalline material is obtained. All of the large crystals are interpenetration twins (180° rotation on the *c* axis), and it is believed that a growth mechanism involving twinning is responsible for the large crystal size.

A characteristic reaction path could be observed in most of the runs that failed to reach equilibrium. The initially pure $CaCO_3$ tends to "soak up" more and more $MnCO_3$ until the equilibrium composition is reached. X-ray photographs of a number of these runs show all gradations in composition between pure calcite and the equilibrium composition, the diffraction lines appearing as bands originating at the calcite spacing. In other cases the nonequilibrium product is more homogeneous, with relatively sharp diffraction lines having spacings between those of calcite and the equilibrium product, irrespective of initial composition.

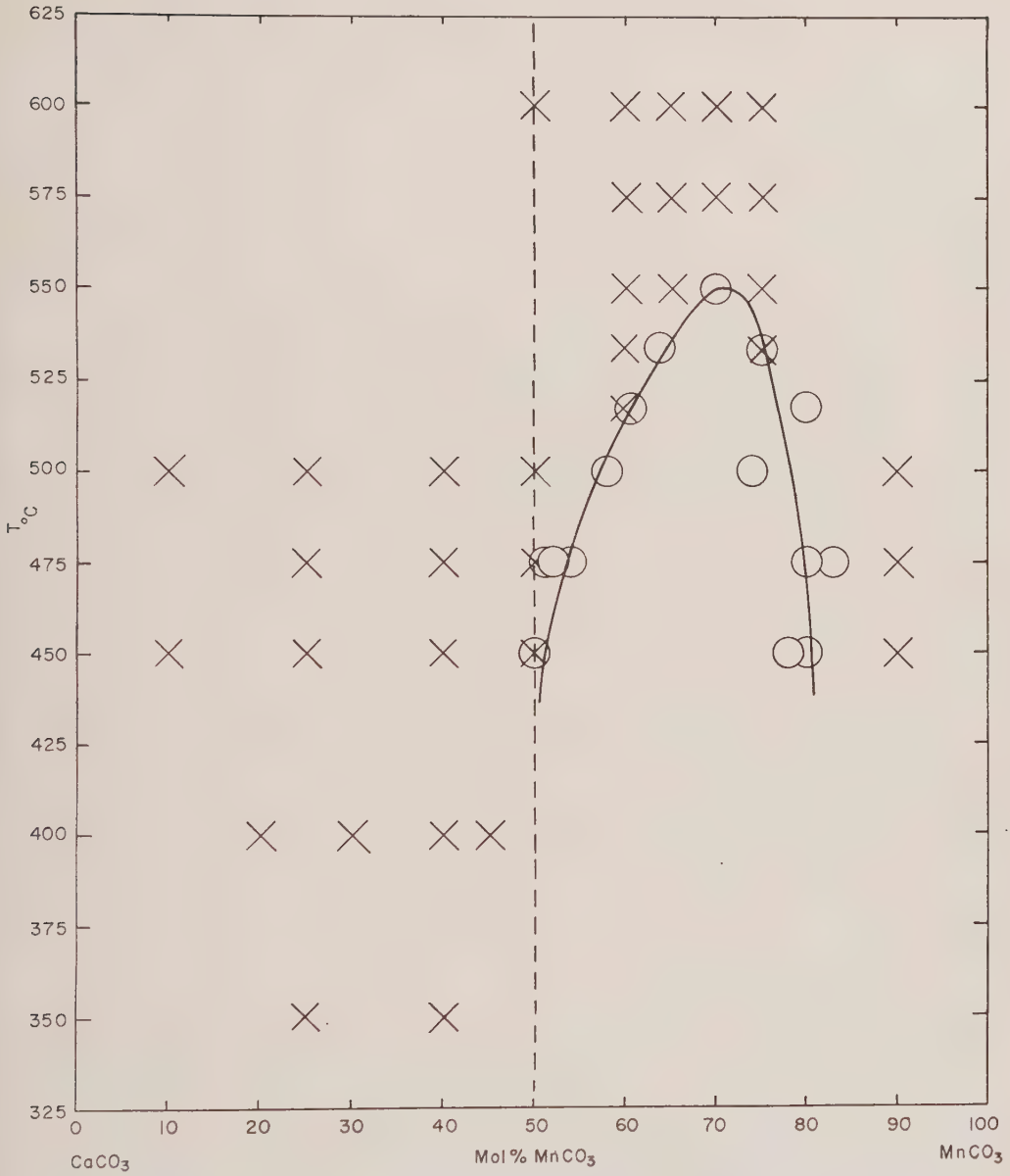

Fig. 5. Subsolidus relations in the system $CaCO_3$—$MnCO_3$. Crosses indicate points at which homogeneous solid solutions were obtained. Circles give the results of experiments in which two-phase carbonate equilibrium was obtained. Dotted vertical line indicates the $Ca_{50}Mn_{50}$ mol per cent composition.

Table 4. Dry and hydrothermal experiments in the subsolidus region of the system $CaCO_3$—$MnCO_3$

Starting materials	T°C	P_{CO_2} (lb/in.^{2})	Time (hr)	Products*
96% $CaCO_3$ + 4% $MnCO_3$	734	14,000	23	$Ca_{96}Mn_4$ solid soln.
90% $CaCO_3$ + 10% $MnCO_3$	708	14,400	23	$Ca_{90}Mn_{10}$ solid soln.
75% $CaCO_3$ + 25% $MnCO_3$	710	14,300	22	$Ca_{75}Mn_{25}$ solid soln.
60% $CaCO_3$ + 40% $MnCO_3$	708	14,400	23	$Ca_{60}Mn_{40}$ solid soln.
50% $CaCO_3$ + 50% $MnCO_3$	713	19,800	22	$Ca_{50}Mn_{50}$ solid soln.
40% $CaCO_3$ + 60% $MnCO_3$	706	17,700	23	$Ca_{40}Mn_{60}$ solid soln.
25% $CaCO_3$ + 75% $MnCO_3$	710	14,300	22	$Ca_{25}Mn_{75}$ solid soln.
10% $CaCO_3$ + 90% $MnCO_3$	706	17,700	23	$Ca_{10}Mn_{90}$ solid soln.
50% $CaCO_3$ + 50% $MnCO_3$	600	16,600	94	$Ca_{50}Mn_{50}$ solid soln.
40% $CaCO_3$ + 60% $MnCO_3$, Li_2CO_3	600	8,000	504	$Ca_{40}Mn_{60}$ solid soln.
35% $CaCO_3$ + 65% $MnCO_3$, $\frac{1}{2}Li_2CO_3$	600	8,000	504	$Ca_{35}Mn_{65}$ solid soln.
25% $CaCO_3$ + 75% $MnCO_3$, $\frac{1}{2}Li_2CO_3$	600	8,000	504	$Ca_{25}Mn_{75}$ solid soln.
25% $CaCO_3$ + 75% $MnCO_3$	600	16,600	94	$Ca_{25}Mn_{75}$ solid soln.
40% $CaCO_3$ + 60% $MnCO_3$, Li_2CO_3	575	8,000	504	$Ca_{40}Mn_{60}$ solid soln.
35% $CaCO_3$ + 65% $MnCO_3$, Li_2CO_3	575	8,000	504	$Ca_{35}Mn_{65}$ solid soln.
30% $CaCO_3$ + 70% $MnCO_3$, Li_2CO_3	575	8,000	504	$Ca_{30}Mn_{70}$ solid soln.
25% $CaCO_3$ + 75% $MnCO_3$, Li_2CO_3	575	8,000	504	$Ca_{25}Mn_{75}$ solid soln.
40% $CaCO_3$ + 60% $MnCO_3$, Li_2CO_3	550	8,000	504	$Ca_{40}Mn_{60}$ solid soln.
35% $CaCO_3$ + 65% $MnCO_3$, Li_2CO_3	550	8,000	504	$Ca_{35}Mn_{65}$ solid soln.
30% $CaCO_3$ + 70% $MnCO_3$, Li_2CO_3	550	8,000	504	Broadened reflections centered at ~$Ca_{30}Mn_{70}$ solid soln.
25% $CaCO_3$ + 75% $MnCO_3$, Li_2CO_3	550	8,000	504	$Ca_{25}Mn_{75}$ solid soln.
40% $CaCO_3$ + 60% $MnCO_3$, Li_2CO_3	532	950	528	$Ca_{40}Mn_{60}$ solid soln.
33% $CaCO_3$ + 67% $MnCO_3$, Li_2CO_3	532	950	528	$Ca_{36}Mn_{64}$ solid soln., $Ca_{25}Mn_{75}$ solid soln.
25% $CaCO_3$ + 75% $MnCO_3$, Li_2CO_3	532	950	528	$Ca_{25}Mn_{75}$ solid soln.
40% $CaCO_3$ + 60% $MnCO_3$, Li_2CO_3	517	950	432	$Ca_{40}Mn_{60}$ solid soln.
33% $CaCO_3$ + 67% $MnCO_3$, Li_2CO_3	517	950	432	$Ca_{39}Mn_{61}$ solid soln., $Ca_{20}Mn_{80}$ solid soln.

90% $CaCO_3$ + 10% $MnCO_3$, Li_2CO_3	500	1,000	404	$Ca_{90}Mn_{10}$ solid soln.
75% $CaCO_3$ + 25% $MnCO_3$, Li_2CO_3	500	8,400	138	$Ca_{75}Mn_{25}$ solid soln.
75% $CaCO_3$ + 25% $MnCO_3$, Li_2CO_3	500	1,000	404	$Ca_{75}Mn_{25}$ solid soln.
60% $CaCO_3$ + 40% $MnCO_3$, Li_2CO_3	500	1,000	404	$Ca_{60}Mn_{40}$ solid soln.
50% $CaCO_3$ + 50% $MnCO_3$, Li_2CO_3	500	8,400	138	$Ca_{50}Mn_{50}$ solid soln.
50% $CaCO_3$ + 50% $MnCO_3$, Li_2CO_3	500	1,000	404	$Ca_{50}Mn_{50}$ solid soln.
40% $CaCO_3$ + 60% $MnCO_3$, Li_2CO_3	500	1,000	404	$Ca_{42}Mn_{58}$ solid soln., $Ca_{26}Mn_{74}$ solid soln.
25% $CaCO_3$ + 75% $MnCO_3$, Li_2CO_3	500	8,400	138	Broad reflections; two solid solns. being formed
25% $CaCO_3$ + 75% $MnCO_3$, Li_2CO_3	500	1,000	404	Broad reflections; two solid solns. being formed
10% $CaCO_3$ + 90% $MnCO_3$, Li_2CO_3	500	1,000	404	$Ca_{10}Mn_{90}$ solid soln.
75 % $CaCO_3$ + 25% $MnCO_3$, Li_2CO_3	475	800	764	$Ca_{75}Mn_{25}$ solid soln.
$Ca_{75}Mn_{25}$ solid soln., Li_2CO_3	475	850	840	Unchanged
60% $CaCO_3$ + 40% $MnCO_3$, Li_2CO_3	475	800	764	$Ca_{60}Mn_{40}$ solid soln.
$Ca_{60}Mn_{40}$ solid soln., Li_2CO_3	475	850	840	Unchanged
50% $CaCO_3$ + 50% $MnCO_3$, Li_2CO_3	475	800	764	$Ca_{50}Mn_{50}$ solid soln.
$Ca_{50}Mn_{50}$ solid soln., Li_2CO_3	475	850	840	Unchanged
40% $CaCO_3$ + 60% $MnCO_3$, Li_2CO_3	475	850	1008	$Ca_{48}Mn_{52}$ solid soln., $Ca_{17}Mn_{83}$ solid soln.
$Ca_{40}Mn_{60}$ solid soln., Li_2CO_3	475	850	840	Unchanged
$Ca_{40}Mn_{60}$ ppt., H_2O, CO_2	475	—	840	Poorly xld. solid soln. near $Ca_{50}Mn_{50}$, smaller amount higher Mn solid soln.
40% $CaCO_3$ + 60% $MnCO_3$ H_2O, CO_2	475	—	840	Poorly xld. ~$Ca_{45}Mn_{55}$ solid soln.
25% $CaCO_3$ + 75% $MnCO_3$, Li_2CO_3	475	850	1008	$Ca_{20}Mn_{80}$ solid soln., $Ca_{46}Mn_{54}$ solid soln.
25% $CaCO_3$ + 75% $MnCO_3$, H_2O, CO_2	475	—	840	$Ca_{20}Mn_{80}$ solid soln., $Ca_{49}Mn_{51}$ solid soln.
$Ca_{25}Mn_{75}$ solid soln., Li_2CO_3	475	850	840	Unchanged
$Ca_{25}Mn_{75}$ ppt., H_2O, CO_2	475	—	840	$Ca_{25}Mn_{75}$ solid soln.
10% $CaCO_3$ + 90% $MnCO_3$, Li_2CO_3	475	850	1008	$Ca_{10}Mn_{90}$ solid soln.
$Ca_{10}Mn_{90}$ solid soln., Li_2CO_3	475	850	840	Unchanged
$Ca_{10}Mn_{90}$ ppt., H_2O, CO_2	475	—	840	$Ca_{10}Mn_{90}$ solid soln., large twinned xls.
10% $CaCO_3$ + 90% $MnCO_3$, H_2O, CO_2	475	—	840	$Ca_{10}Mn_{90}$ solid soln.
90% $CaCO_3$ + 10% $MnCO_3$, Li_2CO_3	450	1,000	404	$Ca_{90}Mn_{10}$ solid soln., diffuse reflections, broad (444)
$Ca_{90}Mn_{10}$ ppt., H_2O, CO_2	450	—	840	Well xld. $Ca_{90}Mn_{10}$ solid soln.
75% $CaCO_3$ + 25% $MnCO_3$, Li_2CO_3	450	1,000	404	$Ca_{75}Mn_{25}$ solid soln., slightly diffuse reflections
$Ca_{75}Mn_{25}$ solid soln., Li_2CO_3	450	1,000	768	Unchanged
$Ca_{75}Mn_{25}$ ppt., H_2O, CO_2	450	—	840	Well xld. $Ca_{75}Mn_{52}$ solid soln.
$Ca_{75}Mn_{25}$ ppt., H_2O, CO_2, Li_2CO_3	450	—	1512	Well xld. $Ca_{75}Mn_{25}$ solid soln.

Table 4 (*continued*)

Starting materials	T°C	P_{CO_2} (lb/in.^{2})	Time (hr)	Products*
60% $CaCO_3$ + 40% $MnCO_3$, Li_2CO_3	450	1,000	404	$Ca_{60}Mn_{40}$ solid soln., diffuse reflections, broad (444)
$Ca_{60}Mn_{40}$ solid soln., H_2O, CO_2	450	—	864	Unchanged
$Ca_{60}Mn_{40}$ solid soln., Li_2CO_3	450	1,000	768	Unchanged
60% $CaCO_3$ + 40% $MnCO_3$, H_2O, CO_2	450	—	864	~$Ca_{60}Mn_{40}$ solid soln., C, R
$Ca_{60}Mn_{40}$ ppt., $H_{20}O$, CO_2	450	—	840	~$Ca_{60}Mn_{40}$ solid soln.
$Ca_{60}Mn_{40}$ ppt., H_2O, CO_2, Li_2CO_3	450	—	1512	$Ca_{60}Mn_{40}$ solid soln.
50% $CaCO_3$ + 50% $MnCO_3$, Li_2CO_3	450	1,000	404	$Ca_{50}Mn_{50}$ solid soln.
$Ca_{50}Mn_{50}$ solid soln., H_2O, CO_2	445	—	864	Unchanged
$Ca_{50}Mn_{50}$ solid soln., Li_2CO_3	450	1,000	768	Unchanged
50% $CaCO_3$ + 50% $MnCO_3$, H_2O, CO_2	445	—	864	~$Ca_{50\rightarrow60}Mn_{50\rightarrow40}$ solid soln., C, R
$Ca_{50}Mn_{50}$ ppt., H_2O, CO_2	450	—	816	~$Ca_{50}Mn_{50}$ solid soln., poorly developed Mn-rich solid soln.
40% $CaCO_3$ + 60% $MnCO_3$, Li_2CO_3	450	1,000	404	~$Ca_{50}Mn_{50}$ solid soln., ~$Ca_{20}Mn_{80}$ solid soln.
$Ca_{40}Mn_{60}$ solid soln., H_2O, CO_2	450	—	864	Unchanged
$Ca_{40}Mn_{60}$ solid soln., Li_2CO_3	450	1,000	768	Unchanged
40% $CaCO_3$ + 60% $MnCO_3$, H_2O, CO_2	450	—	864	C, R, $Ca_{50\rightarrow60}Mn_{50\rightarrow40}$ solid soln.
$Ca_{40}Mn_{60}$ ppt., H_2O, CO_2	450	—	816	~$Ca_{45}Mn_{55}$ solid soln., poorly developed Mn-rich solid soln.
25% $CaCO_3$ + 75% $MnCO_3$, Li_2CO_3	450	1,000	404	~$Ca_{22}Mn_{78}$ solid soln., ~$Ca_{50}Mn_{50}$ solid soln., R
$Ca_{25}Mn_{75}$ solid soln., H_2O, CO_2	445	—	864	Unchanged
25% $CaCO_3$ + 75% $MnCO_3$, H_2O, CO_2	445	—	864	R, ~$Ca_{50\rightarrow60}Mn_{50\rightarrow40}$ solid soln., C
$Ca_{25}Mn_{75}$ ppt., H_2O, CO_2	450	—	816	$Ca_{25}Mn_{75}$ solid soln.
10% $CaCO_3$ + 90% $MnCO_3$, Li_2CO_3	450	1,000	404	Very well xld. $Ca_{10}Mn_{90}$ solid soln.
$Ca_{10}Mn_{90}$ solid soln., Li_2CO_3	450	1,000	768	Unchanged
$Ca_{10}Mn_{90}$ ppt., H_2O, CO_2	450	—	816	Large twinned xls. $Ca_{10}Mn_{90}$ solid soln.
$Ca_{40}Mn_{60}$ ppt., H_2O, CO_2, Li_2CO_3	425	—	1584	~$Ca_{52}Mn_{48}$ solid soln., ~$Ca_{24}Mn_{76}$ solid soln., diffuse reflections
$Ca_{25}Mn_{75}$ ppt., H_2O, CO_2, Li_2CO_3	425	—	1584	~$Ca_{25}Mn_{75}$ solid soln., somewhat diffuse reflections
33% $Ca_{90}Mn_{10}$ ppt. + 67% $Ca_{75}Mn_{25}$ ppt. + H_2O + CO_2 + Li_2CO_3	400	—	1416	$Ca_{80}Mn_{20}$ solid soln.
$Ca_{75}Mn_{25}$ solid soln., Li_2CO_3	400	4,500	500	Unchanged
75% $CaCO_3$ + 25% $MnCO_3$, Li_2CO_3	400	5,500	52	~$Ca_{75}Mn_{25}$ solid soln., C, (R)

75% $CaCO_3$ + 25% $MnCO_3$, Li_2CO_3	400	4,500	500	C, R, Ca-rich solid soln.
$Ca_{75}Mn_{25}$ solid soln., H_2O, CO_2	400		1584	Unchanged
75% $CaCO_3$ + 25% $MnCO_3$, H_2O	400		163	~$Ca_{75}Mn_{25}$ solid soln., R, C
75% $CaCO_3$ + 25% $MnCO_3$, H_2O, CO_2	400	–	336	~$Ca_{75}Mn_{25}$ solid soln., (C)
70% $CaCO_3$ + 30% $MnCO_3$, H_2O, CO_2, Li_2CO_3	400	–	1416	$Ca_{70}Mn_{30}$ solid soln.
$Ca_{60}Mn_{40}$ solid soln., Li_2CO_3	400	1,000	840	Unchanged
60% $CaCO_3$ + 40% $MnCO_3$, Li_2CO_3	400	1,000	840	C, R, solid soln. near C
$Ca_{60}Mn_{40}$ ppt., H_2O, CO_2	400	—	1320	$Ca_{60}Mn_{40}$ solid soln.
60% $CaCO_3$ + 40% $MnCO_3$, H_2O, CO_2, Li_2CO_3	400	—	1320	$Ca_{60}Mn_{40}$ solid soln.
50% $Ca_{50}Mn_{50}$ ppt. + 50% $Ca_{60}Mn_{40}$ ppt., H_2O, CO_2, Li_2CO_3	400	—	1320	$Ca_{55}Mn_{45}$ solid soln.
55% $CaCO_3$ + 45% $MnCO_3$, H_2O, CO_2, Li_2CO_3	400	—	1320	~$Ca_{55}Mn_{45}$ solid soln., R
$Ca_{50}Mn_{50}$ solid soln., Li_2CO_3	400	4,500	540	Unchanged
50% $CaCO_3$ + 50% $MnCO_3$, Li_2CO_3	400	5,500	52	$Ca_{>50}Mn_{<50}$ solid soln., C, R
50% $CaCO_3$ + 50% $MnCO_3$, Li_2CO_3	400	4,500	540	R, range of Ca-rich solid solns.
$Ca_{50}Mn_{50}$ solid soln., H_2O, CO_2	400	—	1584	Unchanged
50% $CaCO_3$ + 50% $MnCO_3$, H_2O	400	—	163	C, R, $Ca_{<50}Mn_{>50}$ solid soln.
50% $CaCO_3$ + 50% $MnCO_3$, H_2O, CO_2	400	—	336	Ca-rich solid soln., R, (C)
50% $CaCO_3$ + 50% $MnCO_3$, H_2O, CO_2	400	—	1584	$Ca_{50\rightarrow<50}Mn_{50\rightarrow>50}$ solid soln., R, C
50% $Ca_{50}Mn_{50}$ ppt. + 50% $Ca_{40}Mn_{60}$ ppt., H_2O	400	—	380	~$Ca_{50}Mn_{50}$ solid soln., more Mn-rich solid soln.
$Ca_{40}Mn_{60}$ solid soln., Li_2CO_3	400	1,000	840	Unchanged
40% $CaCO_3$ + 60%$MnCO_3$, Li_2CO_3	400	1,000	840	R, C, solid soln. near C
33% $CaCO_3$ + 67% $MnCO_3$, H_2O, CO_2, Li_2CO_3	400	—	1488	Incomplete reaction
50% $Ca_{40}Mn_{60}$ ppt. + 50% $Ca_{25}Mn_{75}$ ppt. H_2O, CO_2, Li_2CO_3	400	—	1488	Incomplete reaction
$Ca_{25}Mn_{75}$ solid soln., Li_2CO_3	400	4,500	1584	Unchanged
25% $CaCO_3$ + 75% $MnCO_3$, Li_2CO_3	400	5,500	52	R, $Ca_{>50}Mn_{<50}$ solid soln., C
25% $CaCO_3$ + 75% $MnCO_3$, Li_2CO_3	400	4,500	540	R, range of Ca-rich solid solns.
$Ca_{25}Mn_{75}$ solid soln., H_2O, CO_2	400	—	1584	Unchanged
25% $CaCO_3$ + 75% $MnCO_3$, H_2O	400	—	163	R, C, $Ca_{<50}Mn_{>50}$ solid soln.
25% $CaCO_3$ + 75% $MnCO_3$, H_2O, CO_2	400	—	336	$Ca_{75}Mn_{25}$ solid soln., (R), (C)
25% $CaCO_3$ + 75% $MnCO_3$, H_2O, CO_2	400	—	1584	~$Ca_{55}Mn_{45}$ solid soln., ~$Ca_{13}Mn_{87}$ solid soln.
$Ca_{10}Mn_{90}$ solid soln., Li_2CO_3	400	1,000	840	Unchanged
10% $CaCO_3$ + 90% $MnCO_3$, Li_2CO_3	400	1,000	840	R, C, solid soln. near C
75% $CaCO_3$ + 25% $MnCO_3$, H_2O, CO_2, Li_2CO_3	350	—	2448	$Ca_{75}Mn_{25}$ solid soln.
$Ca_{75}Mn_{25}$ ppt., H_2O, CO_2, Li_2CO_3	350	—	2448	$Ca_{75}Mn_{25}$ solid soln.
60% $CaCO_3$ + 40% $MnCO_3$, H_2O, CO_2, Li_2CO_3	350	—	2448	~$Ca_{60}Mn_{40}$ solid soln., (R)
$Ca_{60}Mn_{40}$ ppt., H_2O, CO_2, Li_2CO_3	350	—	2448	$Ca_{60}Mn_{40}$ solid soln.

Table 4 (*continued*)

Starting materials	T°C	P_{CO_2} (lb/in.^{2})	Time (hr)	Products*
33% $CaCO_3$ + 67% $MnCO_3$, H_2O, CO_2, Li_2CO_3	350	—	2448	~$Ca_{50}Mn_{50}$ solid soln., R (not at equilibrium)
50% $Ca_{25}Mn_{75}$ ppt. + 50% $Ca_{40}Mn_{60}$ ppt., H_2O, CO_2, Li_2CO_3	350	—	2448	Incomplete reaction
$Ca_{75}Mn_{25}$ solid soln., Li_2CO_3	300	1,000	540	Unchanged
75% $CaCO_3$ + 25% $MnCO_3$, Li_2CO_3	300	1,000	540	Little or no reaction
$Ca_{50}Mn_{50}$ solid soln., Li_2CO_3	300	1,000	500	Unchanged
50% $CaCO_3$ + 50% $MnCO_3$, Li_2CO_3	300	1,000	500	Little or no reaction
$Ca_{50}Mn_{50}$ solid soln., H_2O, CO_2	300	—	158	No reaction
50% $Ca_{50}Mn_{50}$ ppt. + 50% $Ca_{40}Mn_{60}$ ppt., H_2O, CO_2	300	—	500	$Ca_{50}Mn_{50}$ solid soln., tailing off to more Mn-rich solid soln.
$Ca_{25}Mn_{75}$ solid soln., Li_2CO_3	300	1,000	500	Unchanged
25% $CaCO_3$ + 75% $MnCO_3$, Li_2CO_3	300	1,000	500	Little or no reaction
$Ca_{50}Mn_{50}$ ppt., H_2O	250	—	15	Unchanged $Ca_{50}Mn_{50}$ solid soln.
$Ca_{50}Mn_{50}$ ppt., H_2O	250	—	50	Unchanged $Ca_{50}Mn_{50}$ solid soln.
$Ca_{50}Mn_{50}$ ppt., H_2O, CO_2	250	—	15	Unchanged $Ca_{50}Mn_{50}$ solid soln.
$Ca_{50}Mn_{50}$ ppt., H_2O	143	—	69	Unchanged $Ca_{50}Mn_{50}$ solid soln.
$Ca_{50}Mn_{50}$ ppt., H_2O	143	—	504	Unchanged $Ca_{50}Mn_{50}$ solid soln.
$Ca_{90}Mn_{10}$ ppt., H_2O	25	—	1008	$Ca_{90}Mn_{10}$ solid soln.
$Ca_{75}Mn_{25}$ ppt., H_2O	25	—	1008	$Ca_{75}Mn_{25}$ solid soln.
$Ca_{60}Mn_{40}$ ppt., H_2O	25	—	1008	$Ca_{60}Mn_{40}$ solid soln.
$Ca_{50}Mn_{50}$ ppt., H_2O	25	—	1008	$Ca_{50}Mn_{50}$ solid soln.
$Ca_{40}Mn_{60}$ ppt., H_2O	25	—	1008	$Ca_{40}Mn_{60}$ solid soln.
$Ca_{25}Mn_{75}$ ppt., H_2O	25	—	1008	$Ca_{25}Mn_{75}$ solid soln.
$Ca_{10}Mn_{90}$ ppt., H_2O	25	—	1008	$Ca_{10}Mn_{90}$ solid soln.

* "C" and "R" among the products indicate, respectively, calcite and rhodochrosite. Parentheses denote quantities near the limit of detection. All compositions are given in mol per cent.

calcite and rhodochrosite exists above approximately 550°C. The left limb of the solvus rapidly approaches the 1 : 1 $CaCO_3 : MnCO_3$ composition as temperature decreases; the relation of this limb of the curve to the order-disorder behaviour of CaMn carbonate with this composition will be discussed subsequently. The right limb of the solvus is at approximately 80 mol per cent $MnCO_3$ at 450°C, but the slope of its downward extension is not yet known. The experimentally determined gap agrees reasonably well with an observed frequency distribution of CaMn carbonates from Franklin, N.J. (Frondel and Bauer, 1955).

A complete series of solid solutions was directly precipitated at room temperature. At least those compositions lying below the solvus of Fig. 5 obviously must be metastable. These poorly crystallized solid-solutions remained unchanged, in contact with their supernatant liquid, for at least six months.

Vegard (1947) mixed together concentrated solutions of $NaHCO_3$ and CO_2-saturated solutions containing $CaCl_2$ and $MnCl_2$ in various proportions. The precipitated calcites contained a maximum of 15 mol per cent $MnCO_3$ and the rhodochrosites, up to 25 mol per cent $CaCO_3$. These results differ from those obtained in our room-temperature experiments. However, the composition of precipitates obtained in such experiments, where metastability is a factor, would be expected to vary according to the experimental conditions.

Kutnahorite, $CaMn(CO_3)_2$

The ordered dolomite-like compound kutnahorite, $CaMn(CO_3)_2$, has been described from three localities by Frondel and Bauer (1955). We have done a considerable amount of experimental work, to be reported in a forthcoming publication, on both natural and synthetic materials of this composition, and several points are pertinent to the present discussion.

The ordering reflections that distinguish the mineral kutnahorite from a disordered solid solution of the same composition are weak and cannot always be detected with confidence in powder-diffraction diagrams. Single-crystal X-ray photographs of these materials can readily be interpreted. Unfortunately, virtually all synthetic products are too fine grained for single-crystal work. We have not observed ordering reflections in any of the synthetic products, including the 1 : 1 Ca : Mn solid solutions that were produced at room temperature as well as at higher temperatures.

The fact that the left limb of the solvus approaches the 1 : 1 Ca : Mn composition suggests rather strongly that the 1 : 1 composition has a high degree of cation order below approximately 450° C. It is unlikely that this limb of the solvus, which defines a phase at or near the 1 : 1 composition in equilibrium with a more Mn-rich carbonate, would occur in this position if one were dealing entirely with completely disordered solid solutions. The question of short-range vs. long-range cation order in materials near the 1 : 1 Ca : Mn composition will be discussed in a separate publication.

The ordered compound dolomite, $CaMg(CO_3)_2$, is readily produced in the laboratory at these temperatures of 400°C and above (Graf and Goldsmith, 1956). It might be expected that the 1 : 1 composition in the system $CaCO_3$—$MnCO_3$ would have less tendency to form as an ordered compound because of the smaller

difference in ionic size of Ca and Mn as compared to Ca and Mg (see, for example, FRONDEL and BAUER, 1955; GOLDSMITH, 1953).

Comparison with the System $CaCO_3$—$MgCO_3$

Solid solution is considerably more extensive at comparable temperatures in the system $CaCO_3$—$MnCO_3$ than in the system $CaCO_3$—$MgCO_3$. In the latter system at 850°C, approximately one-fourth of the Ca in calcite is replaceable by Mg, and the solid solubility in the Mg-rich half of the system is very slight (HARKER and TUTTLE, 1955b; GRAF and GOLDSMITH, 1955). Both systems show greater solid solubility at any given temperature in the Ca-rich compositions than in those compositions with more than 50 per cent of the smaller cation. If the $CaCO_3$—$MnCO_3$ system as here determined is indicative of the general appearance of the $CaCO_3$—$MgCO_3$ system at higher temperatures, then one might assume that in the Ca-rich half of the $CaCO_3$—$MnCO_3$ system an immiscibility gap exists having a maximum temperature well below that observed in the Mn-rich region. Indeed, such a gap is a thermodynamic necessity at some temperature above absolute zero, but it may exist below those temperatures at which it can be realized experimentally.

In the $CaCO_3$—$MgCO_3$ system at moderate to low temperatures, and with bulk compositions of less than 50 per cent $MgCO_3$, a calcite containing only a small amount of Mg is in equilibrium with dolomite. This is not true of the $CaCO_3$—$MnCO_3$ system, at least in the temperature range studied. At these temperatures single-phase carbonates are stable until the region beyond 50 mol per cent $MnCO_3$ is reached. This relation is one factor that would reduce the frequency of occurrence of the 1 : 1 Ca : Mn composition in the system as a whole, compared to the frequency of occurrence of dolomite in the $CaCO_3$—$MgCO_3$ system.

EQUILIBRIUM THERMAL DECOMPOSITION RELATIONS IN THE SYSTEM CaO—MnO—CO_2

GRAF and GOLDSMITH showed earlier (1955, p. 117) that the thermal decomposition of a magnesian calcite can be expressed as

$$CaMg_x(CO_3)_{(1+x)} \leftrightharpoons CaMg_{(x-y)}(CO_3)_{(1+x-y)} + yMgO + yCO_2 \qquad (9)$$

and that the reaction is dependent on both T and P_{CO_2}.

In like fashion, the generalized thermal decomposition of solid solutions in the system CaO—MnO—CO_2 can be expressed as

$$CaMn_x(CO_3)_{(1+x)} \leftrightharpoons CaMn_{(x-y)}(CO_3)_{(1+x-y)} + yMnO + yCO_2. \qquad (10)$$

Thus, in addition to the decomposition curve of pure $MnCO_3$ (Fig. 3), a family of curves must exist, each representing the P_{CO_2}, T relations for a specific Ca Mn carbonate solid solution and analogous to those in the system CaO—MgO—CO_2 (GRAF and GOLDSMITH, 1955, Fig. 5). These relations have been elucidated, and the data shown in Table 5, and plotted in Fig. 6.* For example, the curve in Fig. 6

* The cell size of MnO produced by decomposition of the CaMn carbonates was not observed to vary within the temperature range of these experiments. At these temperatures it thus appears that there is little or no solid solution of CaO in MnO.

labelled "20" represents the equilibrium thermal decomposition (P_{CO_2}, T) curve for a CaMn carbonate solid solution containing 20 mol per cent $MnCO_3$ (i.e. $Ca_{0.8}Mn_{0.2}CO_3$). At any (P_{CO_2}, T) on the 20 per cent curve a maximum of 20 mol per cent $MnCO_3$ is stable in the structure, and a decrease in P_{CO_2} or an increase in T will produce some MnO and CO_2 and a carbonate correspondingly poorer in $MnCO_3$.

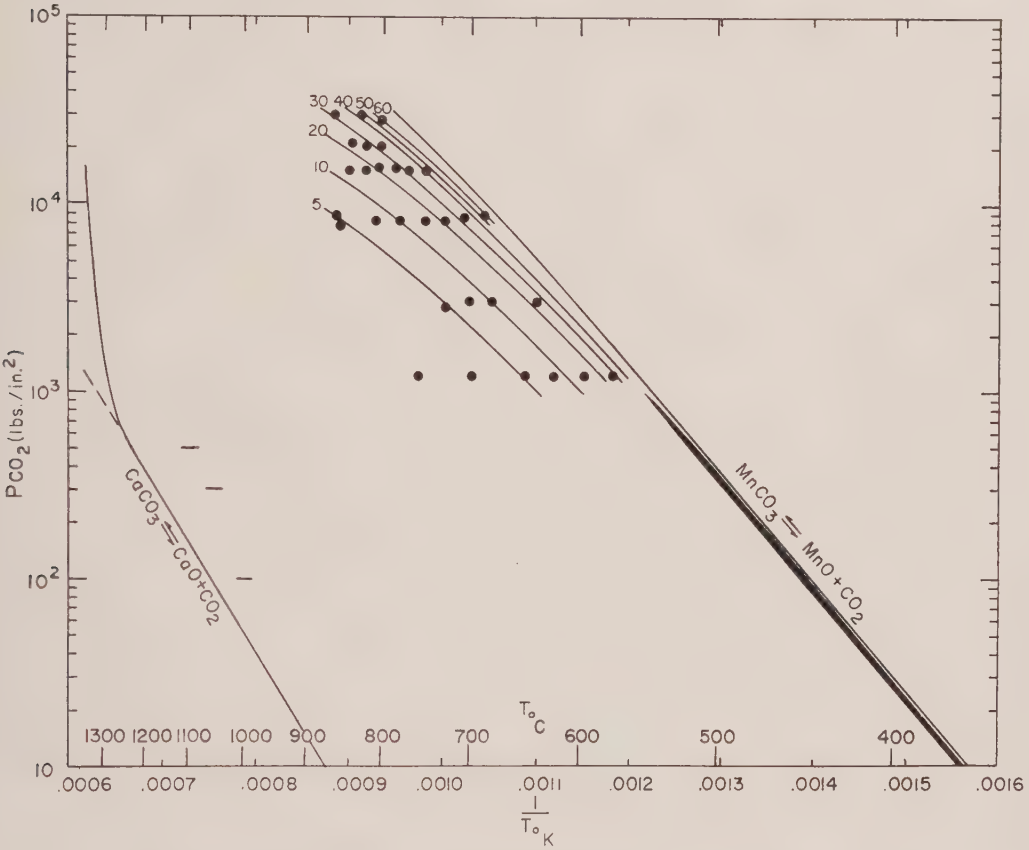

Fig. 6. Equilibrium thermal decomposition relations in the system CaO—MnO—CO_2. The curve for the reaction $MnCO_3 \rightleftharpoons MnO + CO_2$ is reproduced from Fig. 3. The numbers associated with the family of curves give the mol per cent Mn carbonate substitution stable in the calcite structure. Decomposition relations of $CaCO_3$ are shown at the left of the diagram. The narrow dark field is the region in which decomposition relations are complicated by unmixing (see text).

The data in Table 5 were obtained from runs using both solid solutions and mixtures of $CaCO_3$ and $MnCO_3$. Thus equilibrium was approached from two directions—by decomposition according to equation (10) of a solid solution initially richer in $MnCO_3$ than the equilibrium product, and by synthesis according to the reaction

$$CaCO_3 + (x + y)\,MnCO_3 \rightleftharpoons CaMn_x(CO_3)_{(1+x)} + yMnO + yCO_2. \qquad (11)$$

In addition, a variety of initial compositions were used in some experiments, and

Table 5. Runs evaluating the decomposition relations in the system CaO—MnO—CO_2. M indicates MnO among the products. Carbonate solid solution compositions are given in mol per cent

Starting materials	P_{CO_2} (lb/in.^{2})	T°C	Time (hr)	Products
50% $CaCO_3$ + 50% $MnCO_3$	30,000	856	24	$Ca_{73}Mn_{27}$ solid soln., M
$Ca_{60}Mn_{40}$ solid soln.	30,000	856	24	$Ca_{74}Mn_{26}$ solid soln., M
75% $CaCO_3$ + 25% $MnCO_3$	30,000	856	24	$Ca_{75}Mn_{25}$ solid soln.
75% $CaCO_3$ + 25% $MnCO_3$	29,400	824	43	$Ca_{75}Mn_{25}$ solid soln.
50% $CaCO_3$ + 50% $MnCO_3$	29,400	824	43	$Ca_{56}Mn_{44}$ solid soln., M
$Ca_{60}Mn_{40}$ solid soln.	29,400	824	43	Unchanged
25% $CaCO_3$ + 75% $MnCO_3$	29,400	824	43	$Ca_{56}Mn_{44}$ solid soln., M
75% $CaCO_3$ + 25% $MnCO_3$	28,300	796	41	$Ca_{75}Mn_{25}$ solid soln.
50% $CaCO_3$ + 50% $MnCO_3$	28,300	796	41	$Ca_{50}Mn_{50}$ solid soln.
25% $CaCO_3$ + 75% $MnCO_3$	28,300	796	41	$Ca_{39}Mn_{61}$ solid soln., M
$Ca_{75}Mn_{25}$ solid soln.	21,200	832	16	$Ca_{77}Mn_{23}$ solid soln., M
$Ca_{60}Mn_{40}$ solid soln.	21,200	832	16	$Ca_{79}Mn_{21}$ solid soln., M
$Ca_{90}Mn_{10}$ solid soln.	20,200	815	17	Unchanged
$Ca_{75}Mn_{25}$ solid soln.	20,200	815	17	Unchanged
$Ca_{60}Mn_{40}$ solid soln.	20,200	815	17	$Ca_{75}Mn_{25}$ solid soln., M
$Ca_{40}Mn_{60}$ solid soln.	20,100	798	48	$Ca_{69}Mn_{31}$ solid soln., M
25% $CaCO_3$ + 75% $MnCO_3$	20,100	798	48	$Ca_{69}Mn_{31}$ solid soln., M
75% $CaCO_3$ + 25% $MnCO_3$	15,400	799	48	$Ca_{82}Mn_{18}$ solid soln., M
60% $CaCO_3$ + 40% $MnCO_3$	15,400	799	48	$Ca_{82}Mn_{18}$ solid soln., M
$Ca_{60}Mn_{40}$ solid soln.	15,400	799	48	$Ca_{83}Mn_{17}$ solid soln., M
60% $CaCO_3$ + 40% $MnCO_3$	15,400	780	48	$Ca_{69}Mn_{31}$ solid soln., M
$Ca_{60}Mn_{40}$ solid soln.	15,200	764	15	$Ca_{66}Mn_{34}$ solid soln., M
$Ca_{75}Mn_{25}$ solid soln.	15,200	814	14	$Ca_{83}Mn_{17}$ solid soln., M
75% $CaCO_3$ + 25% $MnCO_3$	14,900	838	50	$Ca_{90}Mn_{10}$ solid soln., M
$Ca_{75}Mn_{25}$ solid soln.	14,900	838	50	$Ca_{89}Mn_{11}$ solid soln., M
60% $CaCO_3$ + 40% $MnCO_3$	14,900	838	50	$Ca_{89}Mn_{11}$ solid soln., M
25% $CaCO_3$ + 75% $MnCO_3$	14,900	746	50	$Ca_{56}Mn_{44}$ solid soln., M
60% $CaCO_3$ + 40% $MnCO_3$	8,500	853	66	$Ca_{96}Mn_4$ solid soln., M
$Ca_{40}Mn_{60}$ solid soln.	8,500	853	66	$Ca_{96}Mn_4$ solid soln., M
$Ca_{40}Mn_{60}$ solid soln.	8,500	683	66	Unchanged
25% $CaCO_3$ + 75% $MnCO_3$	8,500	683	66	$Ca_{27}Mn_{73}$ solid soln., M
25% $CaCO_3$ + 75% $MnCO_3$	8,400	703	72	$Ca_{63}Mn_{37}$ solid soln., M
$Ca_{40}Mn_{60}$ solid soln.	8,400	703	72	$Ca_{64}Mn_{36}$ solid soln., M
$Ca_{50}Mn_{50}$ solid soln.	8,000	774	70	$Ca_{92}Mn_8$ solid soln., M
50% $CaCO_3$ + 50% $MnCO_3$	8,000	774	70	$Ca_{92}Mn_8$ solid soln., M
$Ca_{50}Mn_{50}$ solid soln.	8,000	745	57	$Ca_{82}Mn_{18}$ solid soln., M
50% $CaCO_3$ + 50% $MnCO_3$	8,000	745	57	$Ca_{82}Mn_{18}$ solid soln., M
$Ca_{50}Mn_{50}$ solid soln.	8,000	724	70	$Ca_{72}Mn_{28}$ solid soln., M
50% $CaCO_3$ + 50% $MnCO_3$	8,000	724	70	$Ca_{76}Mn_{24}$ solid soln., M
$Ca_{60}Mn_{40}$ solid soln.	7,800	800	12	$Ca_{93}Mn_7$ solid soln., M
90% $CaCO_3$ + 10% $MnCO_3$	7,800	800	12	$Ca_{92}Mn_8$ solid soln., M
75% $CaCO_3$ + 25% $MnCO_3$	7,800	800	12	$Ca_{92}Mn_8$ solid soln., M
$Ca_{90}Mn_{10}$ solid soln.	7,600	850	41	$Ca_{95}Mn_5$ solid soln., M
75% $CaCO_3$ + 25% $MnCO_3$	7,600	850	41	$Ca_{96}Mn_4$ solid soln., M

Table 5 (*continued*)

Starting materials	P_{CO_2} (lb/in.^{2})	T°C	Time (hr)	Products
75% $CaCO_3$ + 25% $MnCO_3$	2,900	702	46	$Ca_{93}Mn_7$ solid soln., M
$Ca_{40}Mn_{60}$ solid soln.	2,900	676	70	$Ca_{91}Mn_9$ solid soln., M
75% $CaCO_3$ + 25% $MnCO_3$	2,900	676	70	$Ca_{92}Mn_8$ solid soln., M
$Ca_{40}Mn_{60}$ solid soln.	2,900	638	46	$Ca_{76}Mn_{24}$ solid soln., M
60% $CaCO_3$ + 40% $MnCO_3$	2,900	638	46	$Ca_{76}Mn_{24}$ solid soln., M
$Ca_{40}Mn_{60}$ solid soln.	2,600	724	43	$Ca_{94}Mn_6$ solid soln., M
60% $CaCO_3$ + 40% $MnCO_3$	2,600	724	43	$Ca_{94}Mn_6$ solid soln., M
75% $CaCO_3$ + 25% $MnCO_3$	1,200	753	111	$Ca_{98}Mn_2$ solid soln., M
$Ca_{75}Mn_{25}$ solid soln.	1,200	697	142	$Ca_{97}Mn_3$ solid soln., M
$Ca_{75}Mn_{25}$ solid soln.	1,200	645	119	$Ca_{94}Mn_6$ solid soln., M
$Ca_{25}Mn_{75}$ solid soln.	1,200	620	137	$Ca_{92}Mn_8$ solid soln., M
$Ca_{25}Mn_{75}$ solid soln.	1,200	596	114	$Ca_{84}Mn_{16}$ solid soln., M
$Ca_{25}Mn_{75}$ solid soln.	1,200	572	142	$Ca_{74}Mn_{26}$ solid soln., M

yielded the same final product at the same P_{CO_2} and T. The equilibrium solid solution along any curve of Fig. 6 is dependent only on P_{CO_2} and T, and not on total composition, assuming that the total percentage of $MnCO_3$ in the system is equal to or greater than the particular equilibrium value. It was difficult to establish the very Mn-rich curves because of the strong tendency toward back reaction in this region.

The data of Table 5 were smoothed by plotting temperature versus composition along six constant pressure lines before the curves in Fig. 6 were drawn. The decomposition curve of pure $CaCO_3$ is drawn in Fig. 6 from the data of Smyth and Adams (1923). Three more recently determined points for the decomposition (Harker and Tuttle, 1955a) also are plotted, and fall at significantly lower temperatures. There is a very large temperature and pressure region throughout which a rather small amount of $MnCO_3$ in solid solution is stable.

Relation of the immiscibility gap to decomposition

The existence under the solvus of two phases in equilibrium at a given temperature complicates the decomposition relations. The region so affected is shown as a dark band in Fig. 6. The components of the compositions in equilibrium on the solvus must have the same activities and, therefore, the same vapour pressure of CO_2. The coexisting phases on the solvus thus must have the same equilibrium decomposition pressure.

An enlarged schematic representation of the region in which decomposition relations are complicated by unmixing is presented in Fig. 7. The curves representing decomposition pressures for those compositions that coexist on the solvus must join at the appropriate temperature. The locus of all such junctions is shown as a heavy line in Fig. 7, and represents the P_{CO_2}, T curve for all points on the solvus. It should be emphasized that the drawing is highly schematic, and that

curvatures of the lines shown here have been distorted for ease of representation. Likewise the specific compositions mentioned in the discussion of Fig. 7 which follows have been arbitrarily chosen rather than experimentally observed.

Let us consider what would happen during isobaric cooling, or in a system with a very large CO_2 volume in which CO_2 pressure is essentially constant. Depending upon initial composition, there are three general cases to be treated. To illustrate the first case, in which the total composition lies in the two-phase region, assume a composition of 70 mol per cent $MnCO_3$, 30 per cent $CaCO_3$. At point T of Fig. 7 a

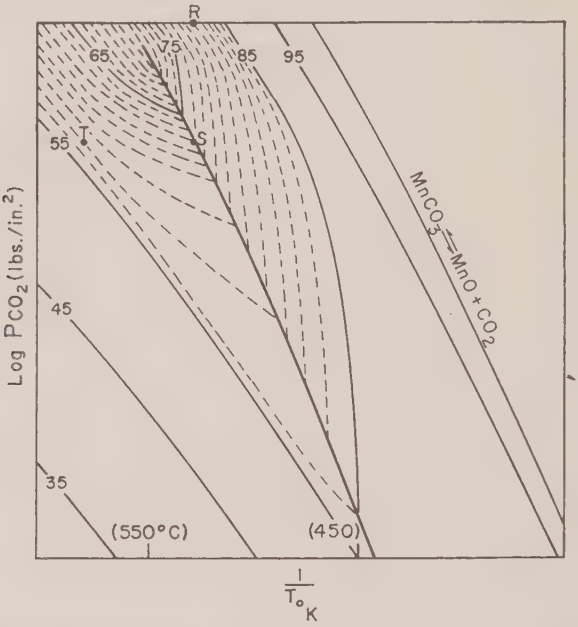

Fig. 7. Enlarged schematic drawing of the region shown in Fig. 6, in which decomposition relations are complicated by unmixing (see text). The numbers associated with the family of curves give the mol per cent Mn carbonate substitution stable in the calcite structure.

solid solution of composition $Ca_{0.43}Mn_{0.57}CO_3$ is in equilibrium with MnO and CO_2. As cooling at constant CO_2 pressure proceeds from T to S, the solid solution increases in Mn content by taking up MnO and CO_2 until at S it is $Ca_{0.38}Mn_{0.62}CO_3$. At this point the unique P,T curve related to the solvus is reached, and the composition $Ca_{0.24}Mn_{0.76}CO_3$ becomes stable in equilibrium with $Ca_{0.38}Mn_{0.62}CO_3$. Four phases are now present (two carbonates, MnO, and CO_2), and with three components the system is univariant. If the CO_2 pressure is assumed to be held constant, then temperature must also remain fixed under equilibrium conditions, until a phase disappears. In this case all of the MnO will be used up by reaction with the carbonates and CO_2, concurrently with the readjustment of the relative amounts of the two phases, the compositions of which remain as above. When all the MnO is depleted, Fig. 7 is no longer applicable; the normal solvus relationships prevail, and continued cooling produces change in composition of the two carbonates down the limbs of the solvus.

For the second case, consider a total composition of 90 per cent $MnCO_3$, 10 per cent $CaCO_3$. The final product will be a single carbonate of this composition, as seen by the location of the solvus in Fig. 5.* If one starts at point T (Fig. 7) as in the previous case, conditions will be the same up to and including those at point S, except that more MnO will be present. The same four phases will be present, and P and therefore T will remain constant at point S until one phase disappears. In this case the carbonate phase poorer in Mn will in the presence of excess MnO take up MnO and CO_2 until it is all converted to the same composition as the more Mn-rich carbonate. The development of a single carbonate phase produces another degree of freedom that permits a continuation of the cooling process to the right of point S, with attendant incorporation of MnO and CO_2 in the one carbonate until it attains the composition $Ca_{0.10}Mn_{0.90}CO_3$, and the reaction is completed.

In the third case the total composition lies on the Ca-rich side of the solvus (i.e. less than 50 per cent $MnCO_3$), and thus to the left or below point T of Fig. 7. The final product will be a single carbonate of the same composition as the total composition. The two-phase region is never reached, and the decomposition relations are not complicated by unmixing.

Now consider what would happen if CO_2 were lost very slowly from the system under isothermal conditions. At point R a solid solution of the composition $Ca_{0.20}Mn_{0.80}CO_3$ is stable. During the decrease in CO_2 pressure in going from R to S, decomposition continuously occurs until at point S the composition $Ca_{0.24}Mn_{0.76}CO_3$ is in equilibrium with CO_2 and MnO. At this point unmixing should begin, with a solid solution of the composition $Ca_{0.38}Mn_{0.62}CO_3$ coexisting with $Ca_{0.24}Mn_{0.76}CO_3$, MnO, and CO_2. Four phases are now present, and under equilibrium conditions the system would normally be univariant, but invariant under the isothermal condition imposed. CO_2 and MnO are produced continuously during the decomposition until only the more Ca-rich solid solution remains. At this point further decomposition along the downward extension of RS takes place.

In a truly closed system without an infinitely large volume of CO_2, the incorporation of CO_2 in the carbonates during cooling would result in the downward movement of CO_2 pressure along the heavy line below S (Fig. 7).

If equilibrium unmixing does not occur, these relations do not hold, and the decomposition relations would be controlled by the metastable extensions of the appropriate decomposition curves.

At lower temperatures, a gap in the $CaCO_3$-rich side of the phase diagram may be expected to appear in the decomposition diagram, to the left of the one discussed.

The 50 mol per cent decomposition curve of Figs. 6 and 7 is that for the disordered solid solution. It is likely that ordering takes place under equilibrium conditions at some lower temperature or temperature range. If so, the ordered compound would have a lower vapour pressure of CO_2 at any temperature than would the disordered form. Thus a shift of the 50 per cent curve to the left at lower temperatures should take place. Inasmuch as the left limb of the solvus approaches the 50 per cent composition, it might be expected that the heavy line of Fig. 7 would extend farther to the left at lower temperatures in response to the ordering of $CaMn(CO_3)_2$.

* The fact that the solvus may be encountered at lower temperatures is not considered here.

Acknowledgements—We wish to thank W. F. Bradley and John C. Jamieson for critical discussions of portions of the paper.

References

Frondel C. and Bauer L. H. (1955) Kutnahorite: a manganese dolomite, $CaMn(CO_3)_2$. *Amer. Min.* **40,** 748–760.

Goldsmith J. R. (1953) A "simplexity principle" and its relation to "ease" of crystallization. *J. Geol.* **61,** 439–451.

Goldsmith J. R., Graf D. L., and Joensuu O. I. (1955) The occurrence of magnesian calcites in nature. *Geochim. et Cosmochim. Acta* **7,** 212–230.

Graf D. L. and Goldsmith J. R. (1955) Dolomite-magnesian calcite relations at elevated temperatures and CO_2 pressures. *Geochim. et Cosmochim. Acta* **7,** 109–128.

Graf D. L. and Goldsmith J. R. (1956) Some hydrothermal syntheses of dolomite and protodolomite. *J. Geol.* **64,** 173–186.

Harker R. I. and Tuttle O. F. (1955a) Studies in the system CaO—MgO—CO_2: Part 1, The thermal dissociation of calcite, dolomite, and magnesite. *Amer. J. Sci.* **253,** 209–224.

Harker R. I. and Tuttle O. F. (1955b) Studies in the system CaO—MgO—CO_2: Part 2, Limits of solid solution along the binary join, $CaCO_3$—$MgCO_3$. *Amer. J. Sci.* **253,** 274–282.

Kennedy G. C. (1954) Pressure-volume-temperature relations in CO_2 at elevated temperatures and pressures. *Amer. J. Sci.* **252,** 225–241.

MacCormack K. E. and Schneider W. G. (1950) Compressibility of gases at high temperatures. IV. Carbon dioxide in the temperature range 0–600° C., and pressures up to 50 atmospheres. *J. Chem. Phys.* **18,** 1269–1272.

Morey G. W. and Ingerson E. (1937) A bomb for use in hydrothermal experiments. *Amer. Min.* **22,** 1121–1122.

Smyth F. H. and Adams L. H. (1923) The system calcium oxide—carbon dioxide. *J. Amer. Chem. Soc.* **45,** 1167–1184.

Straumanis M. E. (1949) The experimental determination of the soundness of crystals from X-ray and density measurements. *Acta Cryst.* **2,** 82–84.

Tuttle O. F. (1949) Two pressure vessels for silicate-water studies. *Geol. Soc. Amer. Bull.* **60,** 1727–1729.

Vegard L. (1947) Investigations into the structure and properties of solid matter with the help of X-rays. *Skrifter Utgitt av Det Norske Videnskaps-Akademi Oslo: I. Mat.-Naturw. Klasse,* No. 2.

Winchell H. (1956) The unit cells of calcite. *Amer. J. Sci.* **254,** 65–70.

Geochimica et Cosmochimica Acta, 1957, Vol. 11, pp. 335 to 347. Pergamon Press Ltd., London

The distribution of nickel in the Lambertville diabase

Thomas W. Storm* and Heinrich D. Holland

Abstract—The concentration of nickel in plagioclase, pyroxene, and magnetite in the diabase sill exposed south of Lambertville, N.J., has been determined colorimetrically. It was found that almost all of the nickel is contained in the pyroxene and magnetite, and that the concentration of nickel in these fractions decreases markedly toward the top of the sill. These observations agree with those on the distribution of nickel in the Nipissing diabase at Cobalt, Ontario, and in the Skaergaard intrusion of East Greenland. On the basis of the observed nickel concentration in chill border samples it can be concluded that the presence of nickel mineralization associated with the Nipissing diabase is not caused by an abnormal nickel concentration in the initial magma.

Introduction

In a classic paper Wager and Mitchell (1951) have discussed the distribution of the minor elements during the crystallization of the Skaergaard intrusion of East Greenland. The present work deals with the distribution of one of the elements considered by them in a rock unit probably of similar origin, the Lambertville diabase of New Jersey. An attempt has been made to provide a basis for comparison of the behaviour of nickel during the crystallization of a diabase and of a layered intrusive, and to provide new data on the problem of the origin of Ni—Co—Ag mineralization which is in some areas closely associated with diabasic intrusive rocks.

The Geology and Petrology of the Lambertville Diabase

The Lambertville diabase, a tabular intrusion approximately 1800 feet thick where exposed south of Lambertville, N.J., along New Jersey Highway No. 29 on the east side of the Delaware River (see Fig. 1) is one of a number of Triassic diabase sills and dikes which are found in southern New York State, New Jersey, and Pennsylvania. The sills are generally concordant with the enclosing Triassic redbeds, are probably genetically related to each other and to Triassic lava flows and volcanic necks which are found in the same region.

The most completely described diabase of this group is the Palisades sill exposed along the west bank of the Hudson River (Walker, 1940). There contact metamorphism has consisted mainly of the baking of the enclosing Triassic Brunswick shale. The lower portion of the sill shows a layering ascribed by Walker (1940) to crystal settling during solidification of the magma. A similar, but less pronounced stratification has been observed in the Lambertville diabase and has been similarly interpreted by Jacobeen (1949).

The mineralogy of the two sills is similar. As can be seen from Table 1 compiled from Rosiwal analyses of thin sections (Jacobeen, 1949, checked by H. H. Hess), the major components of the sill are plagioclase and pyroxene, the minor components magnetite, quartz, biotite, chlorite, amphibole, olivine, serpentine,

* This paper is a condensation of the senior thesis submitted by Mr. Storm to the Department of Geology, Princeton University.

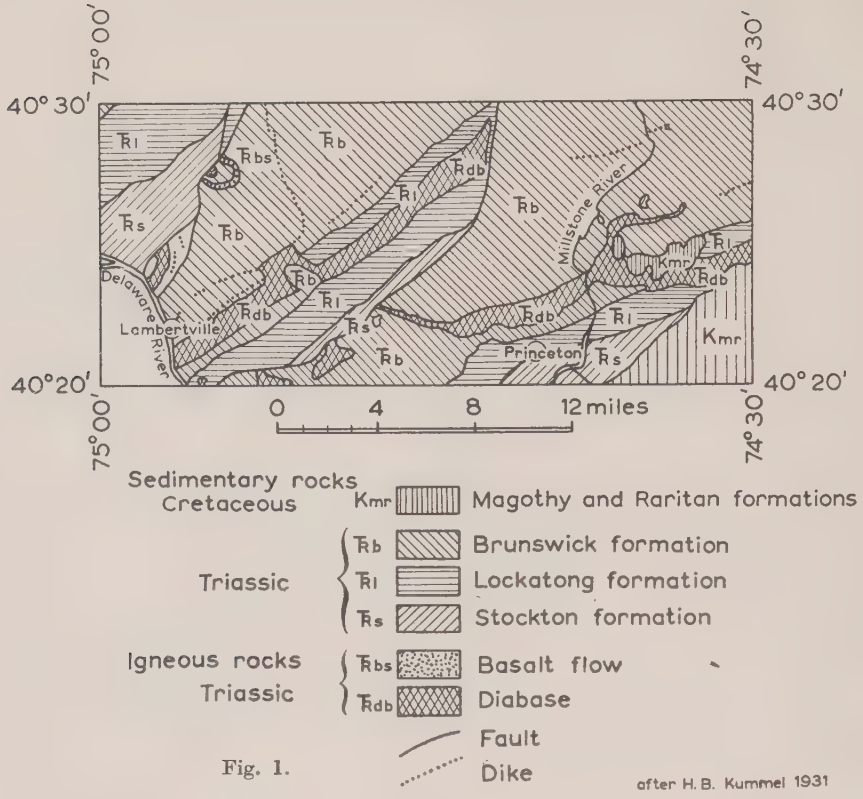

Fig. 1.

Table 1. Minerals of the pyroxene group present in samples of Lambertville diabase (after JACOBEEN, 1949)

Sample No.	
24	Augite, pigeonite (altered in core)
22	Augite, pigeonite
20	Augite, pigeonite
19	Augite, pigeonite
18	Augite, pigeonite
17	Augite, pigeonite (?)
16	Augite, pigeonite (?)
15	Pigeonite, augite
14	Pigeonite, augite
13	Pigeonite, augite
12	Pigeonite, augite; pigeonite cores rimmed by augite
11	Pigeonite (altered), augite
10	Augite, pigeonite, pigeonite inverted to hypersthene
9	Augite, pigeonite, pigeonite inverted to hypersthene
7	Augite, pigeonite, pigeonite inverted to hypersthene
6	Augite, pigeonite inverted to hypersthene
5	Hypersthene, augite pigeonite inverted to hypersthene
4	Much hypersthene, augite
3	Abundant augite, hypersthene
2	Augite, hypersthene rimming olivine

apatite, and stilpnomelane. Of these, olivine is restricted to a zone near the base of the sill, which apparently corresponds to the "olivine ledge" of the Palisades sill. The plagioclase varies in composition from approximately An60 near the base to approximately An35 near the top of the sill. The variations in the nature of the pyroxenes is shown in Table 1 (JACOBEEN, 1949). Augite is present throughout the sill, whereas hypersthene and hypersthene inverted from pigeonite are present only in the lower half and pigeonite not inverted to hypersthene only on the upper half of the sill. The diameter of the feldspar and pyroxene grains is between 0·1 and 0·7 mm in most of the sill, reaching its maximum value in the pegmatitic zone in the upper third of the diabase. Alteration of the plagioclase as shown by cloudiness of the grains in thin section is fairly common, particularly in the pegmatitic zone of the sill and is believed to have been effected during the later stage of cooling of the sill.

Preparation of Samples

Unweathered samples collected from the exposure of the Lambertville diabase south of Lambertville, NJ were trimmed, crushed in a steel mortar, and sieved to retain the grains of 120 to 200 mesh size. This fraction was repeatedly washed with water to remove very small particles adhering to the grains, and was dried in an electric oven at ca. 100°C. Magnetite, probably titaniferous, was removed from the dried sample with a hand magnet, and the "light" and "dark" fractions were separated by means of a Franz magnetic-separator. A plagioclase concentrate of greater than 99% purity was obtained in this manner. The dark fraction contained the pyroxenes and minor amounts of serpentine, chlorite, biotite, and olivine which were not removed and are included in the Ni analyses reported below for the pyroxene fraction.

Analytical Technique

Samples were reduced in an automatic grinder equipped with a tungsten-carbide mortar and pestle. After removal of the moisture by drying at ca. 100°C, 250 mg of the powdered sample were weighed into a platinum dish. 2 ml of distilled water, 0·5 ml of 70% perchloric acid, and 2·5 ml of hydrofluoric acid were added, and the mixture was permitted to evaporate almost to dryness. 2 ml of hydrofluoric acid were then added, and the mixture was taken to dryness. The residue was taken up in 0·5 ml of perchloric acid and again evaporated to dryness. The residue was brought into solution with hydrochloric acid, and the Ni was extracted, oxidized, and complexed with dimethyglyoxime as described by SANDELL (1950). The volume of the wine-red nickelic dimethylglyoxime was brought up to 25 ml, and the transmittance of the solution was measured at a wave-length of 460 mμ in a Beckman DU spectrophotometer. Standard Ni solutions were prepared with $NiCl_2 \cdot 6H_2O$, and the working curve shown in Fig. 2 was constructed. A recheck of this curve revealed no instrumental drift during the duration of the experiments.

As a test for the absence of contamination in the sample preparation precedure, 250 mg of quartz were analysed as described above. No Ni was detected in the final solution.

The efficiency of the extraction of Ni into chloroform and from chloroform into an aqueous solution was tested by comparing the transmittance of solutions containing known amounts of Ni which had been passed through the extraction procedure with that of solutions which had not been subjected to the chloroform extraction. It was thus found that the loss of Ni during the chloroform extraction is less than 3% of the total amount of Ni present in the solution.

Spiked and unspiked portions of five pyroxene samples were analysed to check the overall loss of Ni during the analytical procedure. The results are shown in Table 3, which indicates that the average loss of Ni during the analysis is approximately 3·5%. All analyses reported below have been corrected for this loss.

Duplicate analyses were run on a number of samples: the results are shown in Table 4.

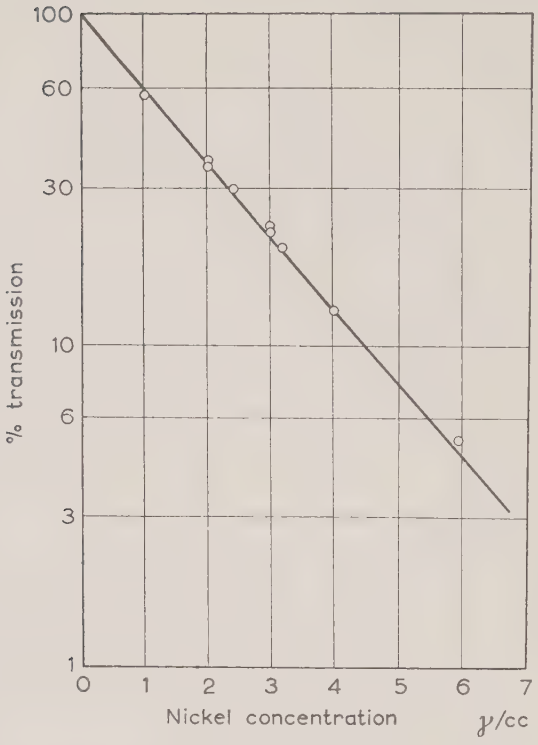

Fig. 2.

As a further check on the procedure the Ni content of diabase samples analysed spectrographically under the supervision of J. E. Hawley, Queen's University, Kingston, Ontario, was determined and found to agree reasonably well with that of the earlier determination as shown in Table 5.

Analytical Results

In Table 6 the observed Ni content of the feldspar fraction, the pyroxene fraction, and the magnetite fraction of samples of Lambertville diabase have been complied. The Ni content of the feldspar fraction is consistently very low, a maximum of 10 p.p.m. having been recorded near the base of the sill. Pyroxenes and magnetite both contain appreciable quantities of Ni. The metal preferentially enters the magnetite structure, the ratio of the concentration of Ni in the two phases being approximately 2·3 in the early crystals and rising to approximately 10 in the upper part of the sill.

Discussion of the Analytical Data

The observed concentration of Ni in samples of the diabase is a function of the Ni content of the initial magma and of the course of crystallization of the sill. An attempt is here made to interpret the latter in terms of the analytical data reported above.

In Figs. 3 and 4 the Ni content of pyroxene and magnetite has been plotted as a function of the present elevation above the base of the sill. There is a generally

Table 2. Mineralogical composition of diabase samples, based on Rosiwal analyses by JACOBEEN (1949). Length of thin-section traverses 40 mm. Concentrations reported in weight per cent

Sample No.	Plagioclase	Pyroxene	Ilmenite and magnetite	Quartz	Biotite	Chlorite	Amphibole	Olivine	Serpentine
24	48	41	4·2	4·0	0·6	2·1	0	0	0
22	36	49	10·0	2·4	0·5	0·9	0·8	0	0
20	41	42	1·9	9·6	0·7	1·4	3·4	0	0
19	52	28	9·0	4·8	2·2	3·2	0	0	0
18	40	49	0	9·4	0	1·2	0·5	0	0
17	42	42	0·4	12·1	0·2	1·9	1·1	0	0
16	61	29	1·1	6·4	1·2	0·7	0·6	0	0
15	49	40	8·7	1·2	0·7	0·2	0·2	0	0
14	44	49	5·4	1·4	0·2	0·2	0	0	0
13	33	42	15·9	0	0·6	2·9	7·1	0	0
12	62	27	3·9	0·7	0·5	2·6	3·3	0	0
11	65	30	0	1·5	0·5	0·7	1·7	0	0
10	48	46	3·1	0	0·2	0	2·7	0	0
9	34	61	2·5	1·0	0·8	0	0·5	0	0
7	51	42	2·9	0·9	2·0	0	1·8	0	0
6	47	46	3·4	1·2	0·2	0	2·9	0	0·1
5	31	61	0	1·6	3·1	0·2	1·0	0	2·3
4	36	59	0·4	0	0·7	3·4	0	0	0
3	30	59	3·3	1·0	5·4	0	0	1·0	0
2	37	55	4·9	0	1·2	1·5	0	0	0

Table 3. Comparison of the observed Ni content of spiked and unspiked samples of pyroxene and magnetite

Sample No.	Material	Amountof Ni added (γ/g)	Amount of Ni found minus amount of Ni added (p.p.m.)
24	magnetite	0	93
		200	87
7	pyroxene	0	152
		240	142
6	pyroxene	0	162
		240	151
5	pyroxene	0	156
		200	150
4	pyroxene	0	232, 224
		240	240, 226

Table 4. Comparison of duplicate analyses

Sample No.	Material	Ni content (p.p.m.)
22	pyroxene	8, 9
15	pyroxene	91, 93
10	pyroxene	150, 146
4	pyroxene	224, 232
1	whole rock	45, 48, 46, 44

Table 5. Comparison of spectrographic and colorimetric analyses of samples of Nipissing diabase, Cobalt, Ontario

Sample No.	Ni content	
	spectrographic	colorimetric
Y83	138 ± 4 p.p.m.	123 p.p.m.
Y331	303 ± 23	284
Y345	145 ± 9	130

Table 6. The nickel content of the plagioclase, pyroxene, and magnetite fractions of samples of Lambertville diabase

Sample No.	Height above base of sill (feet)	Nickel concentration (p.p.m.)		
		Plagioclase fraction	Pyroxene fraction	Magnetite fraction
24	1590	<10	9	96
22	1588		8	101
20	1464		19	116
19	1434		23	116
18	1416		25	116
17	1296		77	135
16	1202		89	157
15	1113	<10	94	
14	1069		100	194
13	864		102	230
12	803		108	241
11	751		123	276
10	621		155	364
9	567		156	368
7	484		157	376
6	415		168	383
5	320		161	
4	120		240	
3	59	<10	157	
2	22	10	147	

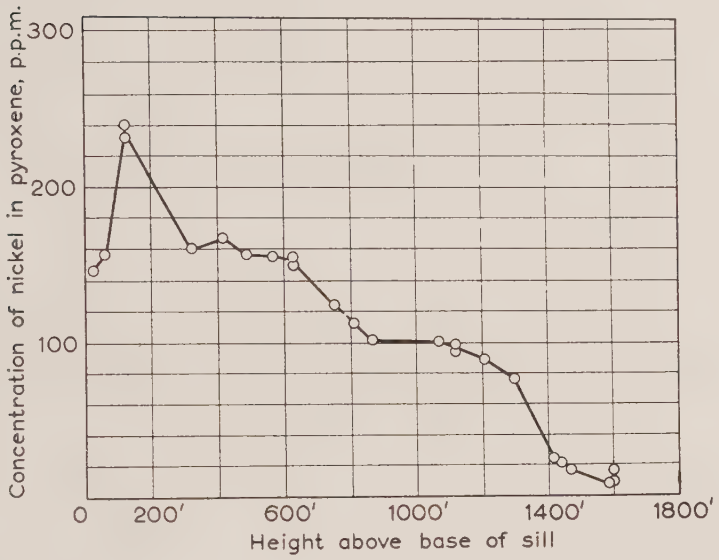
Concentration of nickel in pyroxene, p.p.m.
300
200
100
0
200′
600′
1000′
1400′
1800′
Height above base of sill

Fig. 3.

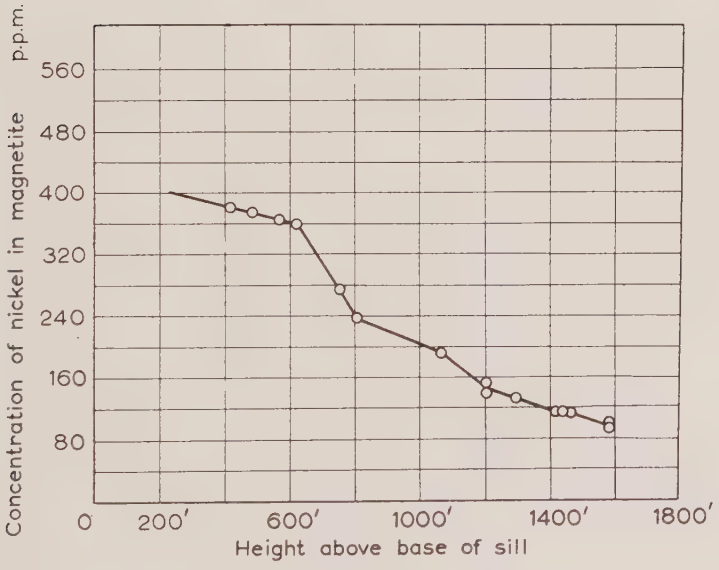
Concentration of nickel in magnetite p.p.m.
560
480
400
320
240
160
80
0
200′
600′
1000′
1400′
1800′
Height above base of sill

Fig. 4.

smooth decrease in the Ni content of both minerals with height above the base of the sill except for the single peak in Fig. 3. It is of interest to inquire whether this decrease is due to an impoverishment of Ni in the melt during crystallization or whether appreciable variations in the distribution factor of Ni between pyroxenes and melt and between magnetite and melt are responsible for the observed trends. A decision on this point can be reached only after the Ni content of the melt from which each fraction crystallized has been determined. This can be calculated if the Ni content of the magma at the start of crystallization is known, provided that it can be assumed that no lateral movement of crystals or liquid occurred during the cooling of the sill, and if the relationship between crystals and melt during solidification is known.

The concentration of an element in a basaltic magma has traditionally been taken to be equal to the concentration of this element in the chill border of the intrusive to which it has given rise. Whether or not this is a valid assumption depends on the uniformity of the composition of the magma which has crystallized to form a given sill or dike, the relationship of the composition of the sample of chill border to the composition of the magma from which it crystallized, and on the absence of later alteration which may have affected the composition of the chill border.

The validity of the assumption for the case studied here can be checked by comparing the average Ni content of the diabase computed from the Ni content of diabase samples from different parts of the sill with the Ni content of chill-border samples. In Table 7 are shown the contributions of pyroxene and magnetite to the Ni content of the rocks at various levels in the diabase. The percentage of pyroxene has here been taken to include also the percentage of biotite, chlorite, amphibole, olivine, and serpentine shown in Table 2. The values for the Ni content of magnetite in samples from the basal part of the sill for which no analyses are available has been calculated assuming a ratio of 2·3 for the concentration of Ni in magnetite and pyroxene in these samples. The value for this ratio is derived from the average of that in samples 6, 7, 9, and 10. The Ni concentration in the magnetite of sample 15 was computed from the observed Ni content of the pyroxene in this sample, and assuming that the ratio of the Ni content of magnetite and pyroxene is the average of that in samples 14 and 16. The contribution of the feldspar has been neglected.

The computed Ni content of the diabase samples is plotted as a function of the height of the samples above the base of the sill in Fig. 5. On the basis of these data it can be shown that the average Ni content in the rocks of the section sampled is about 63 p.p.m., a number appreciably greater than that for the Ni content of the chill border: 46 p.p.m. To the average must be attached an uncertainty due to errors in the modal analysis of the samples, the analytical errors, and the computation of the average with the data at hand. The combined magnitude of these uncertainties is difficult to evaluate. If the difference between the Ni content of the chill border and the average Ni content of the initial magma as computed above is real, the cause is probably to be sought in a lack of validity of the assumptions regarding the relationship of the composition of chill borders to that of the magmas from which they are derived, or in a lateral movement

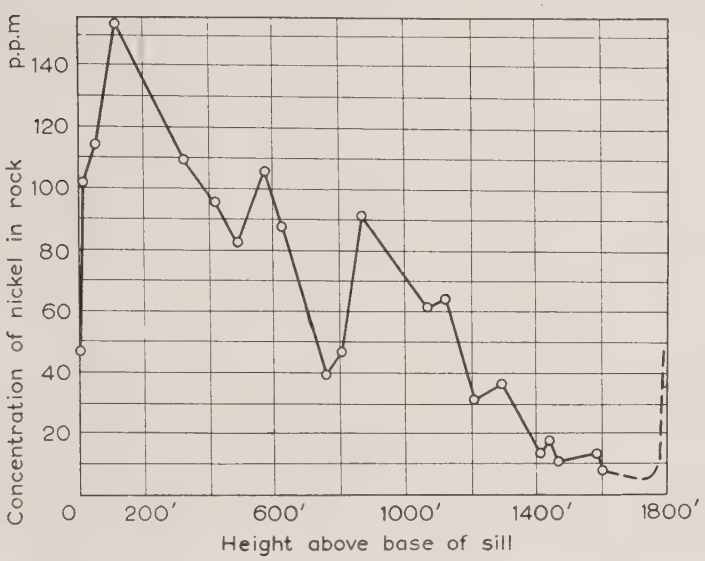

Fig. 5.

Table 7. The nickel content of samples of Lambertville diabase

No.	Pyroxene			Magnetite			Computed Ni content	Measured Ni content
	p.p.m. Ni	wt. %	p.p.m. Ni × wt. %	p.p.m. Ni	wt. %	p.p.m. Ni × wt. %		
24	9	44·2	4	96	4·2	4	8	<10
22	8	38·0	3	101	10·0	10	13	
20	19	47·1	9	116	1·9	2	11	
19	23	33·8	8	116	9·0	10	18	
18	25	50·8	12	116	0	0	12	
17	77	45·4	35	135	0·4	1	36	
16	89	31·9	28	157	1·1	2	30	
15	94	40·7	48	[175]	8·7	[15]	[63]	40
14	100	49·7	50	194	5·4	10	60	
13	102	52·3	53	230	15·9	37	90	
12	108	33·2	36	241	3·9	10	46	
11	123	33·2	41	276	0	0	41	
10	155	48·9	76	364	3·1	11	87	
9	156	62·2	96	368	2·5	9	105	
7	157	45·5	71	376	2·9	11	82	
6	168	49·0	82	383	3·4	13	95	92
5	161	67·7	109	[360]	0	[0]	[109]	
4	240	63·6	152	[540]	0·4	[2]	[154]	138
3	157	65·7	103	[352]	3·3	[11]	[114]	
2	147	58·1	86	[330]	4·9	[17]	[102]	
1	—	—	—	—	—	—	—	46

of crystals and liquid during the cooling of the diabase sheet, such as has been suggested by Hriskevich (1952).

Approximate values for the distribution factors of Ni between the liquid and crystals of titaniferous magnetite, pyroxene, and feldspar can be obtained with the data presented above. For this purpose let us assume that the Ni concentration in the magma at the time of intrusion was 63 p.p.m. and that no lateral movement of liquid or crystals occured during the solidification process in the area sampled. The concentration X_m of Ni in the magma after a fraction, f, of the sill has crystallized will then be

$$X_m = \frac{63 - \int_0^f X_s \, df}{1 - f} \tag{1}$$

where X_s is the concentration of Ni in the solids which have crystallized. The values of X_m calculated in this way are shown in Fig. 6. An alternative method of calculation would assume a concentration of 46 p.p.m. for the initial concentration of Ni in the magma, that is, equal to the Ni content of the chill border, and to introduce a correction factor for possible lateral movement of liquid or crystals during the crystallization of the magma. The uncertainties inherent in this approach are, however such that the formulation used above appears preferable.

Following Wager and Mitchell (1951) and Holland and Kulp (1949) we can define a distribution factor, F, of Ni between melt and crystal, as the ratio of the concentration X_c of Ni in the crystal to the concentration X_m of Ni in the melt from which the crystal grew

$$F = X_c / X_m \tag{2}$$

In order to calculate F for a given mineral at a given horizon in the sill it is necessary to know the appropriate value of X_m. This will be equal to the value shown for the particular horizon in Fig. 6 provided the melt was homogeneous and provided that the assumptions made in deriving X_m are valid. In Table 8 the F values for the pyroxene and magnetite fractions computed in this way have been compiled. The F values for plagioclase are on the order of 0·1.

The Distribution of Nickel in Other Basic Intrusives

The conclusions reached on the distribution of Ni in the Lambertville diabase agree satisfactorily with those reached by Wager and Mitchell (1951) on the distribution of Ni in the rocks of the Skaergaard intrusion of East Greenland and with those reached by Hriskevich (1952) on the distribution of Ni in the Nipissing diabase of Cobalt, Ontario. In the former the Ni content decreases rapidly toward the top of the intrusive; this decrease is related to the large value of the distribution factor of Ni in the pyroxenes, olivine, and magnetite as shown in Table 9. These figures agree very well with the data for the Lambertville shown in Table 8, suggesting that the mechanism for the removal of Ni from the liquid was similar in the two intrusives.

A rapid decrease of Ni content toward the top of the intrusive was also noted by Hriskevich (1952), whose data are reproduced in Fig. 7. It is therefore

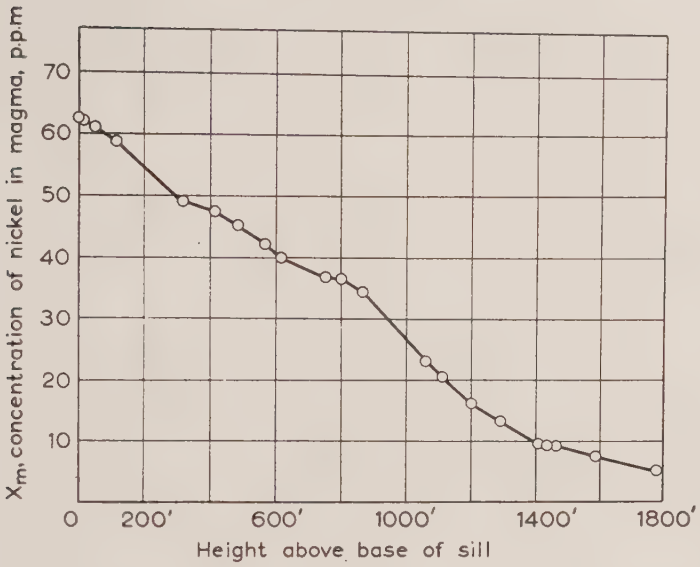

Fig. 6.

Table 8. Values for the distribution factor, F, of Ni in pyroxene and magnetite in the Lambertville diabase

Sample No.	Pyroxene	Magnetite
24	4.7	50
22	4·2	53
20	5·8	35
19	6·4	32
18	6·6	30
17	12·8	22·5
16	11·0	19·4
15	8·7	
14	8·1	15·7
13	4·9	11·0
21	4·8	10·7
11	5·3	12·0
10	5·9	13·8
9	5·5	13·0
7	5·0	12·0
6	5·1	11·6
5	4·6	
4	5·5	
3	3·4	
2	3·1	

Table 9. Estimated distribution factors, F, of Ni in minerals of the Skaergaard intrusion, East Greenland (WAGER and MITCHELL, 1951)

Mineral	A	B	C	D
Plagioclase	0·06	0·05		
Pyroxene	1·2	4·0	5·0	
Magnetite		15		10
Olivine	12	9·5		10

NOTE: those values thought by WAGER and MITCHELL to be misleading have been deleted in this table

A: Gabbro picrites of the northern border group
B: Hypersthene olivine gabbros—the lowest exposed layered rocks—occuring from 0–900 m in the layered series on the arbitrary height scale
C: Olivine free gabbros (the "Middle Gabbros") occuring from 900–1400 m in the layered series
D: Hortonolite ferrogabbros, 1400–2000 m in the layered series

probable that in diabase sills and layered intrusives as a whole these relationships obtain for the major portion of the intrusive. It is however, of interest to note that this similarity of behaviour apparently does not extend to the final stages of consolidation of diabases, since Ni mineralization is associated with the Nipissing diabase and not with the Lambertville diabase or Skaergaard intrusive. The part of the Ni mineralization in the Nipissing diabase found in aplite dikes is almost certainly a late stage differentiate of the Nipissing magma as shown by HRISKEVICH (1952); this suggests that Ni may be concentrated in the final liquid of a diabasic magma. Table 10 shows the Ni content inferred from

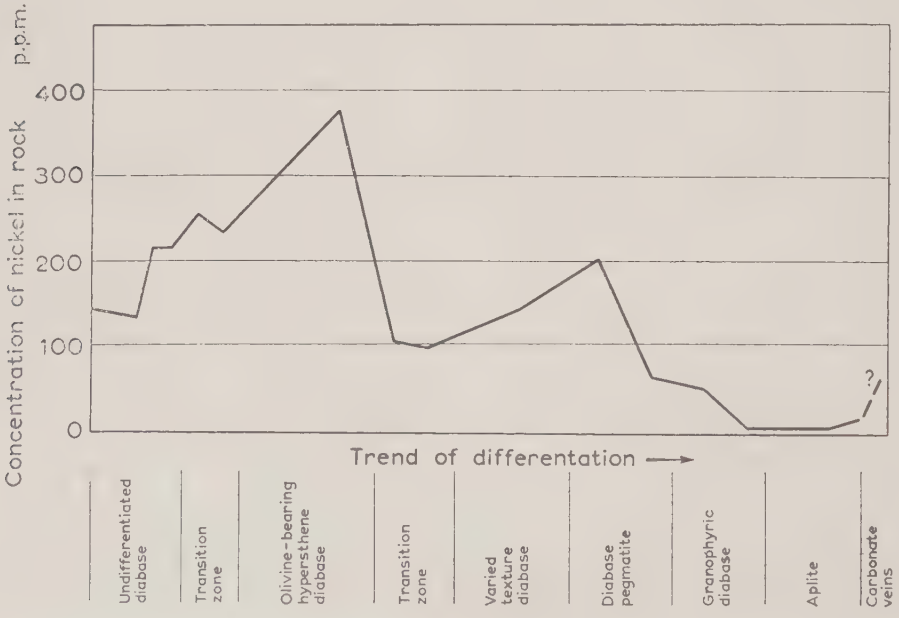

Fig. 7.

Table 10. The nickel content of the magmas at the start of crystallization as inferred from the composition of chill border samples

Lambertville	46 ± 5
Nipissing	130 ± 15
Skaergaard	170 ± 30

analyses of chill border samples of the magmas which gave rise to the three intrusives. It follows from these data that the Ni mineralization in aplites at Cobalt is not due to an abnormal concentration of Ni in the original Nipissing magma, but is related either to the concentration of other components, and/or to the course of the differentiation of the magma during the crystallization of the sill.

Acknowledgements—The authors gratefully acknowledge the assistance of Professors A. F. Buddington and H. H. Hess in the preparation of this manuscript.

References

Holland H. D. and Kulp J. L. (1949) The distribution of accessory elements in pegmatites, I. Theory. *Amer. Min.* **34,** 35–60.

Hriskevich M. E. (1952) Petrology of the Nipissing diabase sheet of the Cobalt area, Ontario. Unpublished Ph.D. thesis, Department of Geology, Princeton University.

Jacobeen F. H. jr. (1949) Differentiation of Lambertville diabase. Unpublished Bachelor's thesis, Department of Geology, Princeton University.

Sandell E. B. (1950) *Colorimetric Determination of Traces of Metals* (2nd Ed.) Interscience.

Wager L. R. and Mitchell R. L. (1951) The distribution of trace elements during strong fractionation of basic magma—a further study of the Skaergaard intrusion, East Greenland. *Geochim. Acta* **1,** 129–208.

Walker F. (1940) Differentiation of the Palisades diabase, New Jersey. *Bull. Geol. Soc. Amer.* **51,** 1059–1106.

BOOKS RECEIVED

L. H. Ahrens, K. Rankama, and S. K. Runcorn (Edited by). *Physics and Chemistry of the Earth, Series I.* pp. 317 (Pergamon Press, London 1956) 55s.

D. P. Krynine and W. R. Judd. *Principles of Engineering Geology and Geotechnics.* pp. 730 (McGraw-Hill, London 1957) £3 15s. ($10.00.)

ANNOUNCEMENT

Journal of the Geochemical Society

Arrangements have been completed for the designation of *Geochimica et Cosmochimica Acta* as the official Journal of the Geochemical Society (see front cover). This is looked on as being decidedly advantageous to both parties, with neither abrogating or usurping any of the functions or rights of the other; a co-operative agreement to advance still more effectively the science of Geochemistry.

Members of the Society are not required to subscribe to the Journal, but may do so at the special rate of $10 per year. Neither are they required, of course, to publish their papers in *Geochimica Acta*, but they are invited to submit such of their manuscripts as fall within the subject interest of the Journal for consideration. *Geochimica et Cosmochimica Acta* will continue to accept contributions from non-members and these will be received on equal grounds with those from members of the Geochemical Society.

N.B. Individuals who are not members of the Geochemical Society but who occasionally publish papers in the Journal will also be entitled to claim the special subscription rate of $10 *per annum*.

FILED IN STACKS
SEP 8 1961
Sep 64

Annals of the International Geophysical Year

The Annals of the International Geophysical Year will contain the central records of the entire enterprise and will appear as a connected and interrelated series of Annals. The journal will indicate the inception, planning, preparation, and programmes. In due course it will also include reports on progress and results of the International Geophysical Year.

VOLUME I
Introductory Volume to International Geophysical Year

VOLUME II
Reports of Proceedings of International Geophysical Year

VOLUME III
Instruction Manual for Ionospheric Studies in the International Geophysical Year

Published by Volume or in parts—£6 ($17) per Volume
AVERAGING 400 pp. per Volume
FIRST ISSUE (Part 1, Vol. 3) TO BE PUBLISHED IN MAY
Write for fully descriptive leaflet

PERGAMON PRESS
LONDON - - NEW YORK - - PARIS
4 & 5 Fitzroy Square, London W.1 122 East 55th Street, New York 22, N.Y.
24 Rue des Écoles, Paris Ve

CSAGI

SPECIAL COMMITTEE FOR THE INTERNATIONAL GEOPHYSICAL YEAR

BUREAU:

President:
Professor S. CHAPMAN

Vice-President:
Dr. L. V. BERKNER

Members:
Professor V. V. BELOUSSOV
Professor J. COULOMB

Secretary-General:
Dr. M. NICOLET

ADVISORY COMMITTEE ON PUBLICATION:
Dr. D. C. MARTIN (*Chairman*)
Dr. W. W. ATWOOD
Father J. O. CARDUS
Professor V. V. BELOUSSOV
Professor G. LACLAVÈRE
Dr. M. NICOLET

EDITORIAL ADVISORY BOARD:
Dr. A. H. SHAPLEY (*World Days*)
Professor J. VAN MEIGHEM (*Meteorology*)
Dr. V. LAURSEN (*Geomagnetism*)
Professor S. CHAPMAN (*Aurora and Airglow*)
Dr. W. J. G. BEYNON (*Ionosphere*)
Dr. Y. ÖHMAN (*Solar Activity*)
Dr. J. A. SIMPSON (*Cosmic Rays*)
Professor A. DANJON (*Longitude and Latitude*)
Sir JAMES WORDIE (*Glaciology*)
Professor G. LACLAVÈRE (*Oceanography*)
Dr. L. V. BERKNER (*Rockets and Satellites*)
Professor V. V. BELOUSSOV (*Seismology*)
Father P. LEJAY (*Gravity Measurement*)
Dr. M. NICOLET (*Nuclear Radiation*)

GENERAL EDITOR:
SIR HAROLD SPENCER JONES